

UNIVERSITY OF BELGRADE

Gordana D. Stanojević - Vitaliano

**NEW CLATHRIN NANOTECHNOLOGY
FOR TRANSPORT OF LARGE
PROTEIN MOLECULES
TO THE CENTRAL NERVOUS SYSTEM**

Doctoral Dissertation

Belgrade, 2015

УНИВЕРЗИТЕТ У БЕОГРАДУ

Гордана Станојевић – Виталиано

**НОВА НАНОТЕХНОЛОГИЈА НА БАЗИ
КЛАТРИНА ЗА ПРЕНОС ВЕЛИКИХ
ПРОТЕИНСКИХ МОЛЕКУЛА У
ЦЕНТРАЛНИ НЕРВНИ СИСТЕМ**

Докторска дисертација

Београд, 2015.

Mentors:

1. Prof. Dr. Slobodan Malobabić,
Faculty of Medicine,
University of Belgrade,
Belgrade, Serbia
2. Prof. Dr. Dejan Raković,
Faculty of Electrical Engineering,
University of Belgrade,
Belgrade, Serbia

Committee Members:

3. Academician Ljubisav Rakić,
Serbian Academy of Sciences and Arts,
Belgrade, Serbia
4. Dr. Nenad Ignjatović, Scientific Advisor,
Institute of Technical Sciences,
Serbian Academy of Sciences and Arts,
Belgrade, Serbia
5. Dr. Zoran Marković, Scientific Advisor,
The Vinca Institute of Nuclear Sciences,
University of Belgrade,
Belgrade, Serbia

ABSTRACT

Antibodies (Abs) have great promise for detection and treatment of central nervous system (CNS) disorders. However, the blood-brain barrier (BBB) is a major impediment to effective delivery. Only 0.1% of plasma Abs enter the CNS naturally via diffusion through a compromised BBB or via BBB saturation and CNS concentrations may still be insufficient for therapeutic efficacy. Moreover, Abs may take days to diffuse only a few millimeters and intracellular targets are not easily accessible to Abs. Thus, new, efficient, and noninvasive strategies are required for transporting large molecules like Abs into the CNS and inside targeted cells. Here we tested the hypothesis that clathrin, a coat protein naturally used to transport molecules across biological barriers and within cells, could serve as a nanoplatform for high-efficiency delivery of antibodies and imaging agents to the CNS.

Clathrin triskelia (17.7 nm in size) were modified to carry 81 gadolinium chelates or 25 fluorescent tags. Nanoplatforms were characterized by size, structure, protein concentration, chelate and gadolinium contents and nanoparticle relaxivity was evaluated at 0.47 T. Clathrin triskelia exhibited ionic relaxivity of $16 \text{ mM}^{-1}\text{s}^{-1}$, and molecular relaxivity of $1166 \text{ mM}^{-1}\text{s}^{-1}$. A series of studies were conducted to ascertain whether fluorescent-tagged clathrin nanoplatforms could cross the blood brain barrier. Clathrin nanoplatforms were able to cross or bypass the BBB without enhancements following intraperitoneal and intranasal administration in rats.

To demonstrate specific targeting clathrin triskelia were modified with dopamine-3-receptor-antibody (D3R-Ab), as there are no small-molecule ligands that bind exclusively to D3 receptors. One molecule of D3R-Ab was attached per clathrin triskelion and antibody remained intact and immunoreactive after the nanoparticle preparation. Low doses ($64 \mu\text{g}/\text{kg}$) of nanoparticles ($42.3 \pm 14.8 \text{ nm}$) were delivered intranasally in rats. Three hours later intact D3R-Ab-triskelia nanoparticles were found in D3R-brain regions inside neurons, with the highest concentration detected in islands of Calleja /ventral pallidum (2753 ng/g or $17.2\% \text{ ID/g}$) and nucleus accumbens (1028 ng/g). High nanoprobe concentrations (1062 ng/g) were also found in hippocampal cells that have high concentrations of D3-receptors in the cytoplasm, but low expression of D3-receptors on the cell membrane. Low concentrations were detected in the cerebellum (84 ng/g .) Nanoprobes were not detected in regions lacking D3 receptors. D3R-Abs delivered without clathrin intranasally did not enter the brain.

Our results demonstrate that engineered clathrin nanoparticles enabled D3R-Abs to effectively bypass an intact BBB intranasally, and to concentrate in targeted cells within specific brain regions, using 300 times lower doses than reported in previous BBB technologies studies. Also, clathrin-nanoplatfoms enabled D3-receptor antibodies to target the 3rd intracellular *G protein-coupled receptor* (GPCR) loop *in vivo*, and to label receptors in the cell membrane and cytoplasm. Hence, clathrin appears to provide a highly efficient nanoplatfom for delivery of antibodies to the CNS and inside targeted cells. This nanotechnology strategy may lead to development of new CNS theranostics for imaging of molecular changes in brain disorders, for monitoring disease progression and recovery, and for efficiently treating CNS disorders through targeted delivery of specific antibodies.

Keywords: Nanotechnology, Clathrin nanoparticles, CNS antibody delivery, Dopamine 3 receptor imaging

Scientific Fields: Medicine, Bioengineering, Neuroscience

РЕЗИМЕ

Различите дијагностичке методе и терапије на бази антитела се тренутно развијају за дијагностику и лечење обољења централног нервног система (ЦНС). Међутим крвно-мождана баријера (КМБ) представља непремостиву препреку када је у питању транспорт дијагностичких и терапеутских макромолекула у ЦНС. Само 0,1% антитела прелази из крвних капилара у мождано ткиво, и то дифузијом преко оштећене КМБ, или сатурацијом КМБ, и концентрација антитела не достиже терапеутски ниво у ЦНСу. Дифузија антитела кроз интерстицијални ЦНС простор је веома спора. Треба им неколико дана да пређу само 2 до 3 милиметра и интрацелуларне структуре им нису доступне. Нова нанотехнологија која не ремети физиолошке процесе у мозгу и која ефективно прелази КМБ је неопходна за транспорт антитела у ЦНС и унутар ћелија мозга. Основни циљ рада је да се развије и тестира нова нанотехнологија за ефикаснији транспорт антитела и контраста у ЦНС. Наноплатформа је базирана на клатрину који природно транспортује молекуле кроз биолошке мембране или унутар ћелија.

Клатрин протеин (величине 17,7 нм) је модификован за пренос 81 молекула гадолинијума или 25 флуоресцентних молекула. Утврђена је величина и структура наночестица и концентрација протеина и гадолинијума у наночестицама. Релаксивитет наночестице је измерен у 0,47 Т магнетном пољу. Јонски релаксивитет је износио 16 $\text{mM}^{-1}\text{s}^{-1}$ док је молекуларни релаксивитет износио 1166 $\text{mM}^{-1}\text{s}^{-1}$. Истраживања на животињама су спроведена да би се потврдио пренос флуоресцентних наночестица преко КМБ. Наночестице, које су дате пацовима интраперитонелним или назалним путем, су успеле да прођу КМБ.

Да би утврдили специфичитет наночестица за допаминске ћелије мозга, један молекул допаминског-3 антитела је повезан са клатрином. Тренутно не постоје мали молекули лиганди који имају афинитет искључиво према Д3 рецепторима. Антитело је показало афинитет искључиво према Д3 рецептору после припремања наночестица. Наночестице (величине 42,3 нм) су дате пацовима у носним капима (64 $\mu\text{g}/\text{kg}$). Три сата касније Д3 наночестице су нађене у Д3 регионима мозга. Највеће концентрације су измерене у вентралном палидуму и острвима Calleja (2753 ng/g или 17,2% ИД/г), нуклеусу акумбенсу (1028 ng/g) и хипокампусу (1062 ng/g). Хипокампадне ћелије имају више Д3 рецептора у цитоплазми него у ћелијској мембрани. Ниске концентрације Д3 антитела су нађене у малом мозгу (84 ng/g). Наночестице нису нађене у регионима мозга који не садрже Д3 рецепторе.

Резултати су показали да су клатринске наночестице омогућиле да се антитела транспортују у специфичне ДЗ регионе мозга. У поређењу са претходним нанотехнолошким студијама, у овом истраживању су коришћене 300 пута мање дозе антитела. Клатринске наночестице су омогућиле ефикасан пренос антитела у ћелије мозга, њихову реакцију са трећом петљом Г-протеин-спрегнутог рецептора унутар ћелија и детекцију ДЗ рецептора у цитоплазми и мембрани ћелије. Клатрин је ефикасна наноплатформа за пренос антитела у ЦНС и унутар ћелија. Ова нанотехнологија ће омогућити развој тераностика за снимање и праћење молекуларних промена у мозгу и за ефикасно лечење болести мозга антителима која су специфична за одређене врсте ЦНС рецептора.

Кључне речи: нанотехнологија, клатринске наночестице, транспорт антитела у ЦНС, детекција допаминског рецептора ДЗ.

Научне области: медицина, биоинжињерство, неуронаука

Table of Contents

1. Introduction	11
1.1 Therapeutic Antibodies	11
1.2 Dopamine 3 Receptor Antibody	13
1.3 Blood-Brain Barrier	21
1.3.1 Endothelial Cells and Tight Junctions	21
1.3.2 Pericytes	24
1.3.3 Astrocytes	25
1.4 Transport Across the Blood-Brain Barrier	27
1.5 Paracellular Delivery and BBB Disruption	31
1.5.1 BBB Disruption by Chemicals	31
1.5.2 BBB Disruption by Radiation Therapy	33
1.5.3 BBB Disruption by Electrical Stimulation	33
1.5.4 BBB Disruption by Ultrasound	34
1.6 Transcellular Delivery of Cationized or Fusion Proteins	36
1.6.1 Cationized Proteins	36
1.6.2 Fusion Proteins	38
1.7 Cell Mediated Delivery	41
1.8 Bypassing the BBB	41
1.8.1 Convection-Enhanced Delivery	41
1.8.2 Intrathecal Injection	43
1.8.3 Intranasal Delivery	44
1.9 Nanoparticle Delivery	49
1.10 Clathrin Nanoplatform	54
2. Research Aims	61

3. Methods	63
3.1 Materials	63
3.2 Isolation and Characterization of Clathrin Triskelia	66
3.2.1 Isolation of Clathrin Coated Vesicles	66
3.2.2 Isolation of Clathrin Triskelia	71
3.2.3 Characterization of Clathrin Triskelia	71
3.2.4 Chelation of Clathrin Triskelia	73
3.2.5 Preparation of Gd-DTPA-Triskelia	76
3.2.6 T_1 Relaxivity of Gd- DTPA-Triskelia	76
3.2.7 Preparation of Fluorescent FITC-Triskelia	77
3.2.8 Administration of FITC-Triskelia in Rats	77
3.2.9 Transcardial Perfusion with 4% Paraformaldehyde	78
3.2.10 Biodistribution of Fluorescent Clathrin Triskelia	79
3.3 Characterization of Dopamine-3 Receptor Antibody Triskelia	79
3.3.1 Crosslinking of Triskelia with D3R-Antibodies	79
3.3.2 D3R-Ab-Triskelia Immunoreactivity	82
3.3.3 D3R-Ab- Triskelia Immunohistochemistry	82
3.3.4 D3RAB- Triskelia Fluorescent Immunohistochemistry	84
3.3.5. Quantitative Determination of D3RAB-Triskelia in Brains	84
3.3.6 Toxicity Studies	88
3.3.7 Statistical Analyses	89
4. Results	90
4.1. Characterization of Clathrin Triskelia	90
4.1.1. Structure of Clathrin Nanoplatfoms	90
4.1.2. Size of Clathrin Nanoplatfoms	91
4.1.3. Chelate Ligand to Clathrin Protein Molar Ratio	92
4.1.4. Nanoparticle Relaxivity and Gd Measurements	94
4.1.5. Qualitative Determination of Triskelia Transport to the CNS	95

4.2. Characterization of Triskelia with Attached D3R-Antibodies	98
4.2.1. Structure and Size of D3RAb-Triskelia	98
4.2.2. Immunoreactivity of D3RAb-Triskelia	100
4.3. Detection of D3RAb-Triskelia in D3R Brain Regions	101
4.3.1. Qualitative Detection of D3RAb-Triskelia in the CNS	101
4.3.2. Qualitative Detection of Fluorescent D3RAb-Triskelia	103
4.3.3. Quantitative Detection of D3RAb-Triskelia in the CNS	105
4.4. Toxicity of D3RAb-Triskelia	107
5. Discussion	108
6. Conclusion	116
7. References	117
8. Biography	151

1. INTRODUCTION

1.1. Therapeutic Antibodies

Antibodies (Abs) have recently been developed for treatment of different central nervous system (CNS) disorders, including: neurodegenerative disorders (e.g., Alzheimer Dementia (AD), Parkinson's (PD) and Huntington's disease (HD)), neuroinflammatory diseases (e.g., multiple sclerosis (MS), amyotrophic lateral sclerosis (ALS)), stroke, traumatic brain injury (TBI), brain cancer, drug addiction, depression, etc. Antibodies can be modified with small molecule drugs, proteins, cytokines, contrast agents, and radiolabels to improve their diagnostic and therapeutic efficacy (Fig. 1). Multidrug strategies have been shown to be effective in treatment of cancer (Ahmed and Cheung 2014) and two FDA approved antibody-drug conjugates (ADCs) are currently on the market and with over 20 candidates in clinical trials. However, from the 350 or so antibodies that were in the clinical pipeline in 2013, the FDA has approved only two antibodies for CNS diseases (Smith 2015). In 2014 alemtuzumab was approved for treatment of MS. In 2015 dinutuximab was approved for treatment of neuroblastoma in children. This is in addition to two previously approved Abs: bevacizumab for treatment of glioblastoma multiforme (GBM) and natalizumab for MS.

Except for dinutuximab that blocks the ganglioside GD2 on the surface of neuroblastoma tumor cells (Fig. 1), all other FDA approved Abs block their targets outside the CNS. For example, bevacizumab blocks the vascular growth factor receptor (VEGFR), while natalizumab blocks the cell adhesion molecule α 4-integrin on vascular endothelial cells. However, for treatment of many brain diseases it is crucial for Abs to target molecules inside the CNS. For example, trastuzumab is clinically effective against human epidermal growth factor receptor 2 (HER2) positive breast cancer, but not against brain metastasis because of its poor CNS bioavailability. This is particularly concerning because patients with HER2-overexpressing breast cancers have a significantly higher incidence of brain metastases than patients with HER2-negative breast cancers (Palmieri, Bronder et al. 2007). Moreover, trastuzumab treatment may actually promote brain metastases, due to the CNS acting as a 'safe harbor' for cancer cells (Musolino, Ciccolallo et al. 2011).

Furthermore, clinical trials of several monoclonal Abs (mAbs) against amyloid beta (A β) in AD failed, because immunotherapy did not penetrate the CNS in sufficient concentrations to target amyloid plaques (Yu and Watts 2013). It was hypothesized that Abs in peripheral circulation would accelerate the removal of the circulating A β pool and stimulate efflux of the brain A β into the peripheral circulation, but recent studies disputed this so called “sink hypothesis” (Yu and Watts 2013).

The blood brain barrier (BBB) normally protects the brain and prohibits large foreign molecules and/or toxins from entering the CNS (Pardridge and Boado 2012). This beneficial and protective function becomes a major impediment for effective delivery of macromolecular diagnostic and therapeutic agents like antibodies to the brain (Frank, Aboody et al. 2011, Lampson 2011). Large molecules, like antibodies, cannot easily enter the CNS. Only 2% of small molecule CNS drug candidates (<400 Da) can cross the blood brain barrier (BBB) (Pardridge and Boado 2012). Major obstacles for delivering antibodies to the CNS are: their large size (~150 kDa); molecular charge; and binding to heparan-sulfate proteoglycans (Frank, Aboody et al. 2011). Only 0.1% of plasma antibodies can enter the CNS naturally via diffusion through a compromised BBB (Banks, Terrell et al. 2002), or BBB saturation (Zlokovic, Skundric et al. 1990).

CNS bioavailability of antibodies increases when the BBB is disrupted with chemicals, ultrasound, electrical stimulation, or radiation therapy (Frank, Aboody et al. 2011). Radiation therapy can lower the mean blood: cerebrospinal fluid (CSF) Ab ratio from 420:1 to 76:1 in cancer patients (Stemmler, Schmitt et al. 2007). However, CNS concentrations of antibodies may still remain below the threshold for therapeutic efficacy (Frank, Aboody et al. 2011, Mehta, Brufsky et al. 2013).

Moreover, when antibodies enter the CNS their diffusion through the tortuous interstitial space is very slow (Frank, Aboody et al. 2011). For example, Abs directly injected into the brain tumors require 3 days to move 1 mm from the site of injection (Jain 1989). These findings underscore the importance of developing efficient and noninvasive strategies for more effectively transporting antibodies into the CNS and throughout brain tissue for treatment of different brain diseases.

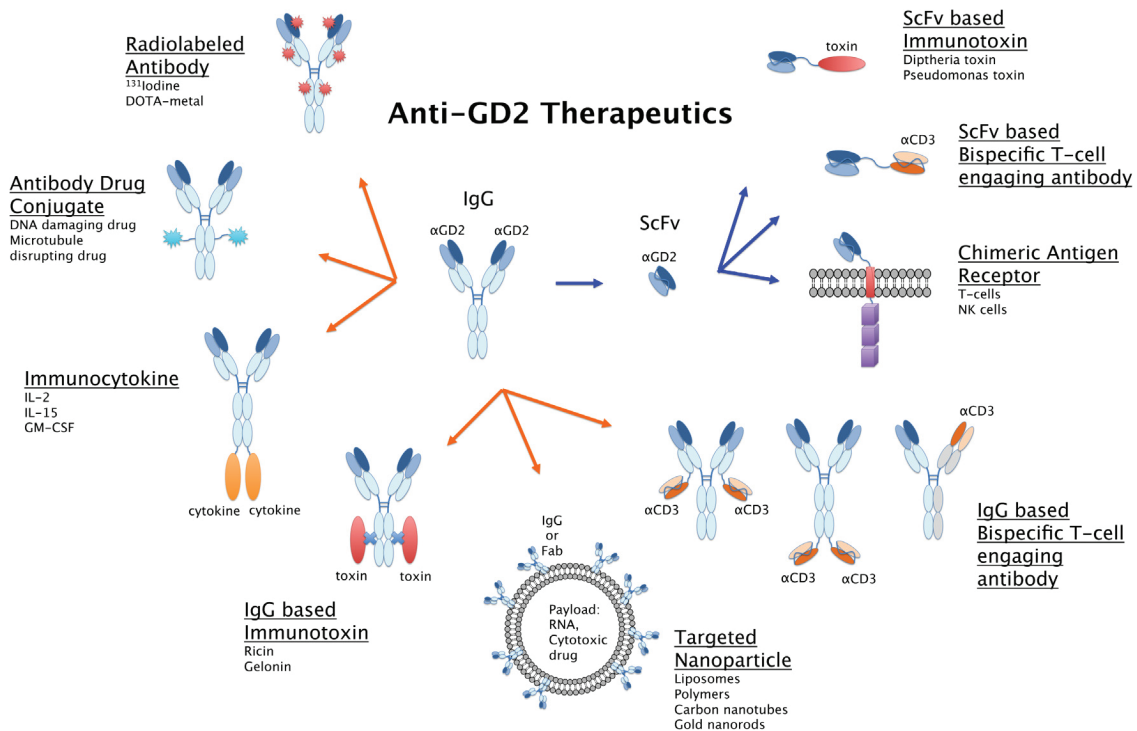


Fig. 1. Anti-GD2 therapeutics. Formats are predominantly based on full-length IgG molecules or scFv fragments. Anti-GD2 IgG templates have been used for engineering radiolabeled antibodies, antibody drug conjugates, immunocytokines, immunotoxins, targeted nanoparticles, and T-cell engaging bispecific antibodies (orange arrows). Anti-GD2 scFv fragments have been used to engineer immunotoxins, bispecific T-cell engaging antibodies, and chimeric antigen receptors for adoptive cell therapy (blue arrows) (Ahmed and Cheung 2014).

1.2. Dopamine 3 Receptor Antibody

A rapidly developing area in neuroscience is molecular-level imaging, encompassing the study of receptors, transporters, enzymes and intracellular processes. Positron emission tomography (PET) to a large degree, and single photon emission tomography (SPECT) to a lesser degree have provided important insights on receptor density in psychiatric disorders, which has helped advance our understanding of the action of psychotropic drugs. PET and SPECT imaging studies greatly contributed to our understanding of the role of dopamine (DA) in psychiatric disorders. These studies have shown that the reinforcing effects of drugs of abuse in humans are dependent on the rate of dopamine increases in the striatum, especially in the shell of the nucleus accumbens, a structure associated with the brain reward system that contains a high density of dopamine 3 receptors (Ikemoto 2007). Dopamine and dopamine 3 receptors have recently been implicated in a variety of

psychiatric disorders such as drug addiction, ADHD, schizophrenia, and mood disorders (Sokoloff, Diaz et al. 2006, Heidbreder and Newman 2010, Le Foll, Collo et al. 2014).

In 1990 Sokoloff and co-workers (Sokoloff, Giros et al. 1990) first characterized the dopamine 3 receptor (D3R). Of all dopamine receptor subtypes, D3R has the highest binding affinity to endogenous dopamine and has a restricted pattern of expression in the brain (Diaz, Levesque et al. 1995, Diaz, Pilon et al. 2000, Le Foll, Diaz et al. 2003, Le Foll, Schwartz et al. 2003). The D3 receptor has a sequence that is very similar to the D2 receptor, with a 78% identity in the trans-membrane and binding domains. The main difference in the sequence is in the 3rd intracellular cytoplasmic loop (ICL) the site of interaction with G-proteins that is important for the functional differences between the two closely related dopamine receptors (Le Foll, Wilson et al. 2014). In this study we used a rabbit anti-rat dopamine D3 receptor antibody (D3R-Ab), which recognizes the 3rd intracellular domain (amino acids 288 to 306, QPPSPGQTHGGLKRYYSIC) of the rat dopamine D3 receptor (Cat. # D3R12-A, Alpha Diagnostic International, San Antonio, TX). This antibody was selected because it targets 3rd ICL, has high affinity and selectivity for D3 receptors, and can label receptors in the plasma membrane and cytoplasm (Khan, Gutierrez et al. 1998, Wolstencroft, Simic et al. 2007). Also, we wanted to demonstrate specific targeting with nanoparticles, as D3 receptors in rats have a restricted distribution that is largely limited to mesolimbic regions. Moreover, targeting D3R brain regions for imaging and drug delivery may be of value in diagnosis and treatment of drug dependence, psychosis, and mood disorders.

In situ hybridization method has been used previously to determine the anatomical location of D3R mRNA (Fig. 2). The distribution pattern of D3 receptor mRNA in rat brain partially overlaps with that of D1 and D2 receptors, with highest D3R mRNA expression found in the nucleus accumbens (NA), olfactory tubercle (OT), islands of Calleja (IC), substantia nigra (SN) and lobes 9 and 10 of the cerebellum (CER) (Bouthenet, Souil et al. 1991, Landwehrmeyer, Mengod et al. 1993, Diaz, Levesque et al. 1995). Lower levels of D3 mRNA have been seen in mammillary bodies (MB), hypothalamus, septal area and the bed nucleus of the stria terminalis, and the diagonal band of Broca and the lateral geniculate nucleus. A similar pattern of D3R mRNA expression is seen in the human brain with the highest levels in the NA, primary visual cortex and the dentate gyrus of the hippocampus, and moderate to low expression seen in remaining cortical areas, caudate and putamen, anterior and medial thalamic nuclei, mammillary bodies, amygdala, hippocampal CA regions, lateral geniculate body, substantia nigra pars compacta, locus coeruleus and raphe nuclei (Landwehrmeyer, Mengod et al. 1993, Gonzalez and Sibley

1995, Gurevich and Joyce 1999). The presence of D3R mRNA in these regions indicates the location of the cells that make the protein, but does not necessarily mean that the protein exerts a local effect in these brain regions.

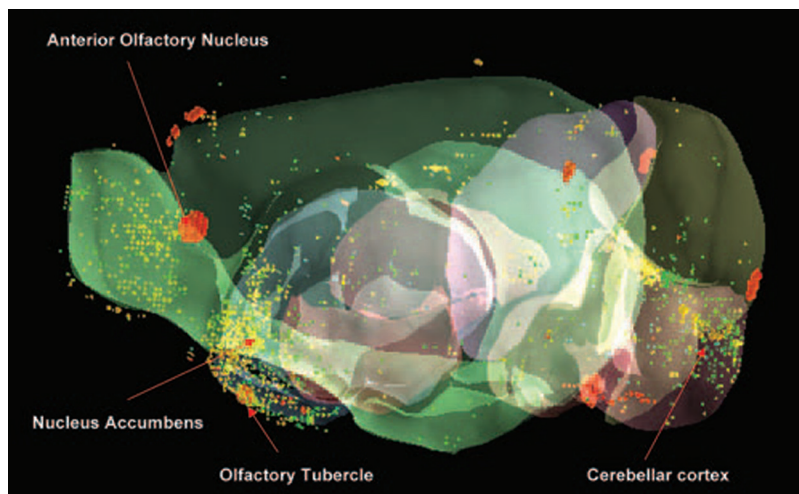


Figure 2. Three-dimensional reconstruction of the expression of the DA D3 receptor in the mouse brain (strain, C57BL/6J; age, 56 days; sex, male; technique: in situ hybridization, riboprobe RP_060412_04_A01) using the Allen Brain Atlas (Brain Explorer Version 1.4.1. Build 32, 2006–2007 Allen Institute for Brain Science) and the Anatomic Gene Expression Atlas. Highest expression/densities were observed in the ventral striatum, olfactory tubercle, lateral septum, medulla, pallidum, and thalamus (Heidbreder and Newman 2010).

Autoradiography and immunohistochemistry (IHC) have been used to map the location of D3-receptor protein. Ligands that are radiolabeled with ^3H or ^{125}I and used for autoradiography include: (+)-7-OHDPAT, trans-7-OHDPAT and [3H]-PD-128907. In rat brain the highest density of [3H]-7-OHDPAT binding sites was detected in the olfactory tubercle (OT) and islands of Calleja (IC), followed by lobes 9 and 10 of the cerebellum (CER), nucleus accumbens (NA), olfactory bulb (OB) and striatum (STR) (Levesque, Diaz et al. 1992). However, [3H]-7-OHDPAT has relatively low D3R selectivity and also binds to D2 receptors (Gonzalez and Sibley 1995). In later studies, a very similar regional pattern has been observed with the more D3-selective radioligand [3H]-PD-128907 (Akunne, Towers et al. 1995, Pugsley, Davis et al. 1995, Bancroft, Morgan et al. 1998, Levant 1998). The CNS regional density of [3H]-PD-128907 binding sites in rat brain is presented in Table 1. This CNS regional density in rodents has also been confirmed with [125I]-7-OH-PIPAT (Stanwood, Artymyshyn et al. 2000). The density of the D3R binding sites represents only a few percent of total D2-like binding sites in STR and NA (25-30 nM).

Table 1. Density of [3H]-PD128907 binding sites in rat brain

Brain region	Binding site density fmol/mg protein^a
IC	40
NAC	12
CER lobes 9 & 10	5
Hypothalamus	3.4
STR	2.3
SN & VTA	2.0
Amygdala	1.9
Frontal cortex	1.4

^a data from reference (Bancroft, Morgan et al. 1998)

IHC studies have shown a similar distribution of D3 receptors in rat brain. However, in IHC studies the D3R-Ab binding to the rat hippocampus and prefrontal cortex (Ariano and Sibley 1994, Khan, Gutierrez et al. 1998) was higher than radioligand binding reported in autoradiographic studies (Bancroft, Morgan et al. 1998, Stanwood, Artymyshyn et al. 2000). It is possible that small ligands bind only to monomeric, but not heteromeric forms of D3 receptors. Alternatively, available D3R agonists may fail to detect an additional population of D3 receptors in a low-affinity state. Overall, there was a good agreement between IHC studies and autoradiographic studies.

Discrepancies in the distributions of D3R mRNA and ligand binding have also been observed in the following brain regions: the medial geniculate nucleus, pyramidal cell layer of the hippocampus, granular layer of the dentate gyrus, and certain thalamic and amygdaloid nuclei where moderate to dense expression of D3 mRNA were observed (Bouthenet, Souil et al. 1991), but relatively little D3R-ligand binding. These discrepancies may be due to the transport of receptors to brain regions remote from producing cell bodies, or the differences in regulation of transcription and translation in different brain areas.

The binding of [3H]-7-OH-DPAT and [3H]-PD-128907 has also been examined in human brain and a similar distribution of the D3 receptor has been found (Herroelen, De Backer et al. 1994, Hall, Halldin et al. 1996, Gurevich and Joyce 1999, Piggott, Marshall et al.

1999). IHC studies have confirmed this D3R distribution (Khan, Gutierrez et al. 1998). The highest radioligand binding was seen in the IC and NA, followed by the ventral CAU, ventral PUT, with binding in the remaining areas similar to that seen in low D3-receptor expression areas, such as the cerebral and cerebellar cortices. The binding was low in the globus pallidus (3-10% of that seen in NA), which is inconsistent with PET studies where this region generates a strong in vivo binding signal with the newly developed D2/D3 agonist radiotracers.

Little is known about how D3 receptors are regulated. However, certain factors that modulate their expression have been identified. For instance, D3R expression has been shown to be upregulated in the rodent brain after use of different addictive drugs. Animal studies have revealed a selective increase in D3R expression in the brains of rodents treated with nicotine (Le Foll, Diaz et al. 2003, Le Foll, Schwartz et al. 2003), cocaine (Le Foll, Frances et al. 2002, Neisewander, Fuchs et al. 2004), morphine (Spangler, Goddard et al. 2003) and alcohol (Vengeliene, Leonardi-Essmann et al. 2006). These data suggest that D3R may play an important role in reward processing and drug addiction.

Examination of D3 receptors with PET has been limited in the past by the lack of a PET ligand with sufficient selectivity for D3 over D2 receptors. [11C]-(+)-PHNO is a novel PET D3 agonist that is applied in animal and clinical PET studies (Narendran, Slifstein et al. 2006, Graff-Guerrero, Mizrahi et al. 2009, Rabiner, Slifstein et al. 2009, Tziortzi, Searle et al. 2011). However, this ligand shows only a 20-fold higher affinity for the D₃ receptor than the D₂ receptor (Rabiner, Slifstein et al. 2009). In human brains, a significant uptake of [11C]-(+)-PHNO has been observed in regions expressing D2 and/or D3 receptors, with the highest binding seen in globus pallidus (GP) followed by ventral STR, putamen, caudate and substantia nigra (Graff-Guerrero, Willeit et al. 2008) (Fig. 3).

PET studies have found that [11C]-(+)-PHNO binds to D2 receptors in the dorsal striatum (Ginovart, Willeit et al. 2007) and to D3 receptors in the globus pallidus (Narendran, Slifstein et al. 2006). Pretreatments with D3-selective drugs (e.g., BP-897 or SB277011) significantly reduced [11C]-(+)-PHNO binding in the GP and SN in baboons (Narendran, Slifstein et al. 2006, Rabiner, Slifstein et al. 2009), while pretreatments with the D2-selective drug SV-156 significantly reduced binding in the CAU and PUT (Rabiner, Slifstein et al. 2009). Therefore, the binding of [11C]-(+)-PHNO to D2 and D3 receptors and the anatomical separation between D3-rich (GP, ventral STR and SN) and D2-rich regions (CAU and PUT) can be utilized in PET studies to simultaneously measure drug occupancy at both receptor types.

Occupancy studies with D3 antagonists (e.g., ABT-925 (Graff-Guerrero, Redden et al. 2010) and GSK598809 (Searle, Beaver et al. 2010)) have been conducted in humans by displacing [11C]-(+)-PHNO binding in D2R and D3R brain regions. Both drugs have higher receptor occupancy in the GP and SN than in the caudate and putamen, indicating specific binding to D3 receptors.

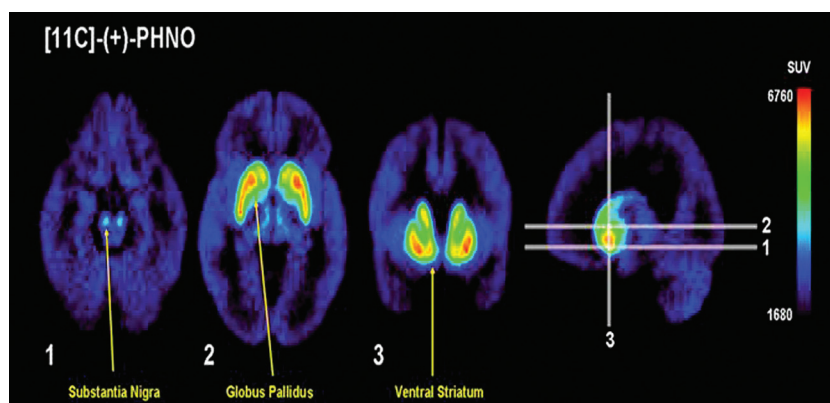


Figure 3. Imaging D3R in humans with [11C]-(+)-PHNO. PET images are from 12 healthy controls. Note the ligand preferential distribution in the substantia nigra, globus pallidus, and ventral striatum (Graff-Guerrero, Willeit et al. 2008).

Recent PET imaging studies have demonstrated upregulation of D3 receptors in drug addiction. For example, PET studies in cocaine users (Matuskey, Gallezot et al. 2014, Payer, Behzadi et al. 2014) and in methamphetamine (METH) polydrug users (Boileau, Payer et al. 2012) have shown a significant upregulation of D3 receptors. Furthermore, the priming dose of amphetamine “drug wanting” was related to increased D3 receptor levels, which supports the idea that D3 receptors may be involved in drug seeking behavior (Boileau, Payer et al. 2012). Moreover, in pathological gamblers, the [11 C]-(+)-PHNO binding in the D3-rich SN was correlated to self-reported impulsivity and severity of gambling (Boileau, Payer et al. 2013). These results suggest that increased D3 receptor levels may represent a general biomarker in addiction, and that the correlation of D3 receptor binding to impulsiveness may provide a phenotype susceptible to addiction (Le Foll, Collo et al. 2014).

Post-mortem findings from brains of cocaine overdose victims and patients with cocaine addiction revealed upregulation of D3 receptors (Staley and Mash 1996, Segal, Moraes et al. 1997). Furthermore, D3 receptors were shown to be upregulated in post-mortem brains of patients with schizophrenia, but D3 receptor levels in patients who had received

antipsychotics appeared equivalent to controls (Gurevich, Bordelon et al. 1997). In contrast, Parkinson's disease studies have found a downregulation of D3 receptors (Morissette, Goulet et al. 1998, Boileau, Guttman et al. 2009).

Similarly, studies have shown decreased D3 receptor density in brains of PD patients (Ryoo, Pierrotti et al. 1998). Therefore, human PET and post-mortem studies, and animal studies have strongly suggested abnormalities in D3 receptors in drug addiction (Sokoloff, Diaz et al. 2006, Heidbreder and Newman 2010, Le Foll, Collo et al. 2014), schizophrenia (Gross, Wicke et al. 2013) and Parkinson's disease (Joyce 2001, Joyce and Millan 2007).

Animal and human studies have also suggested that D3-selective antagonists may be of value in treatment of drug dependence, psychosis and mood disorders. Recently D3R partial agonists and antagonists have been developed as potential therapeutic agents for reducing drug seeking and relapse (Heidbreder and Newman 2010). However, a lack of selectivity for D3R has always been an obstacle to development of D3R selective drugs, as most of these ligands exhibited a partial affinity to D2R as well. New advances in medicinal chemistry have resulted in the development of drugs that have a higher selectivity to D3R than to D2R. The first selective ligand to be tested was the D3R partial agonist BP 897, which has 70-fold selectivity for D3R over D2R (Pilla, Perachon et al. 1999), followed by the development of the highly selective D3R antagonist SB 277011-A. This ligand exhibited 100-fold selectivity for D3R over D2R (Reavill, Taylor et al. 2000), had no effects on locomotor activity, and did not induce catalepsy and/or hyperprolactinemia. Other compounds have also been tested in animals that have a high potency and selectivity for D3R such as NGB 2904, PG 01037 (Heidbreder and Newman 2010, Mason, Hassan et al. 2010), but only a few have been evaluated in clinical trials.

The selective D3 antagonist GSK598809 has recently been evaluated in rodents and in human smokers using various behavioral tests to assess the reinstatement of drug-seeking behavior and the rewarding effects of contextual cues associated with nicotine intake (Mugnaini, Iavarone et al. 2013). D3 receptor occupancy of about 75% was found to be effective in blocking the conditioned place preference (CPP) for nicotine in rats. However, it only transiently attenuated craving for cigarettes in humans after an overnight abstinence. Moreover, smokers actually increased their rate of smoking, which was most likely caused by a decrease in the reinforcing effects of cigarettes. GSK598809 was also tested in obese, binge eating individuals and was found to reduce attentional bias for highly palatable food, especially in individuals who reported 'low-restrained' emotional eating (Nathan, O'Neill et al. 2012). GSK598809 also decreased the approach responses

to food cues in obese individuals and thus reduced the motivational attractiveness of food (Mogg, Bradley et al. 2012).

Buspirone, a marketed anxiolytic, was also identified as a potential candidate for treatment of drug addiction because of its high affinity for the D₃ receptor, but also for 5-HT_{1A} and D₂ and D₄. The effects of buspirone on opiate withdrawal have been studied in chronic opiate users that were under methadone treatment. Buspirone (30 mg/day) significantly reduced the Objective Opiate Withdrawal Scale score when compared to placebo (Rose, Branchey et al. 2003). Similar effects on withdrawal were also observed in cocaine users (Giannini, Loiselle et al. 1993), and a large clinical trial in chronic cocaine users is currently being conducted in the US. Therefore, a dysfunction of D₃ receptors has been implicated in different neuropsychiatric disorders, and more extensive studies on the effects of D₃ antagonists are warranted, especially given the promising preliminary results.

Efficient *in vivo* targeted imaging and drug delivery specific to D₃R cell surface molecular targets require a thorough optimization of all components of the protocol. A careful consideration of all nanotechnology aspects, including targeting antibodies, imaging agents, and nanoparticle-carriers is key to successful *in vivo* applications. Currently there is no imaging ligand with high affinity and selectivity for D₃ receptors. PET ligand [11C]-(1)-PHNO shows only 20-fold higher affinity for the D₃ receptor than for the D₂ receptor. A novel *in vivo* imaging ligand with high affinity and selectivity for the D₃ binding site and low non-specific binding to brain tissue is required. Thus, an anti-D₃RAb that has high affinity and selectivity for D₃R was selected for this study.

Currently, there is no efficient nanocarrier for psychotropic drugs that can cross an intact BBB and deliver drugs to specific brain regions. Only 2% of small-molecule psychiatric drugs can cross the BBB, and some D₃ drugs failed in clinical trials because insufficient doses were delivered to the CNS (Morgan, Van Der Graaf et al. 2012). A targeted multidrug strategy may be required for treatment of chronic CNS diseases to improve drug efficacy and minimize side effects. Antibodies have been developed for treatment of psychiatric disorders, but they could not cross an intact BBB and diffuse through the brain. Therefore a novel nanoparticle that can efficiently cross an intact BBB and diffuse through the brain is required as a CNS drug carrier (see the Section 1.10). Accordingly, our goal is to develop a new nanotechnology method for efficient and noninvasive delivery of antibodies to targeted dopamine brain regions implicated in many neuropsychiatric disorders.

1.3. Blood-Brain Barrier

The main obstacle to the development of new protein therapeutics for neuropsychiatric disorders is the presence of the BBB. The BBB separates systemic circulation from the brain and prevents entry of circulating blood cells, serum proteins, and blood-derived toxic macromolecules into the brain (Davson, Zlokovic et al. 1993). The human brain comprises over 100 billion capillaries with a total length of about 400 miles and a total surface area of about 20 m², and a median inter-capillary distance of about 50 μm (Pardridge 2005). The BBB capillaries consist of a single layer of endothelial cells (ECs); pericytes; the basal lamina; and astrocyte projections (Hawkins and Davis 2005) (Fig. 4). The BBB actively transports necessary molecules (e.g., nutrients and electrolytes) from the systemic circulation to the brain. Because of the small distance between brain capillaries, these molecules only need to diffuse a very short distance (about 25 μm) within brain parenchyma to reach neighboring neurons (Pardridge 2005).

1.3.1. Endothelial Cells and Tight Junctions

BBB endothelial cells are anatomically different from capillary endothelial cells of the periphery, and are characterized by a large number of mitochondria; presence of a few pinocytotic vesicles; lack of fenestrations; and a significant number of tight junctions (TJs). TJs are complexes of transmembrane proteins and cytoplasmic proteins linked to the actin cytoskeleton. Three different TJ-associated membrane protein groups have been described: **1)** TAMPs (TJ-associated MARVEL proteins) that include occludin, tricellulin and MarvelD3, **2)** claudins, and **3)** immunoglobulin superfamily membrane proteins JAM-A/-B/-C, coxsackie adenovirus receptor (CAR) and endothelial cell-selective adhesion molecule (ESAM) (Abbott, Patabendige et al. 2010).

TJ-associated cytoplasmic proteins include: the zonula occludens family, AF6/afadin, multi-PDZ domain protein 1 (MUPP1), membrane-associated guanylate kinase inverted (MAGI)-1, -2 and -3, PAR-3 and -6, and heterotrimeric G-proteins. TJ proteins connect brain endothelial cells together to form a physical barrier. Brain capillaries with TJs are 50-100 times tighter than the peripheral microvasculature and can significantly restrict paracellular transport (Abbott, Patabendige et al. 2010).

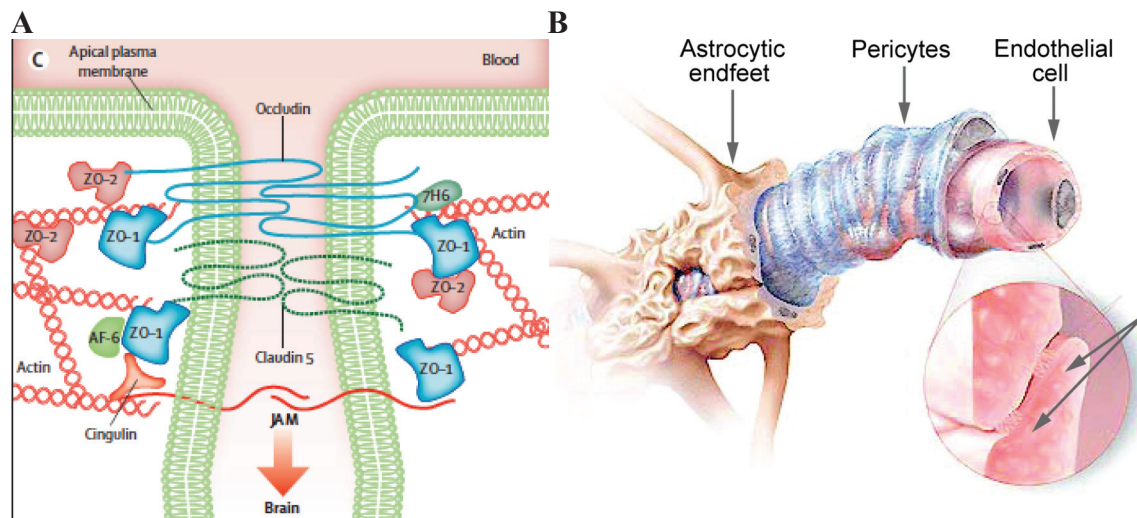


Figure 4. Blood-brain-barrier (BBB): (A) The molecular components of the tight junction (Neuwelt, Abbott et al. 2008). (B) Schematic representation of surrounding pericytes and astrocytic end-feet projecting on the endothelial cells of the cerebral capillaries that induce and maintain the BBB. In contrast, endothelial cells of peripheral capillaries do not form a tight barrier because they lack the specific input of these brain cells (Miller 2002). Illustration by C. Slayden, 2002 AAAS.

Proteins like occludin, claudin, JAMs and the ZO proteins have been shown to be responsible for TJ formation and function at the BBB, and are decreased in several CNS disorders including: stroke (Sandoval and Witt 2008), neurodegenerative disorders like AD and PD (Desai, Monahan et al. 2007), HIV (Andras, Pu et al. 2003), methamphetamine addiction (Martins, Baptista et al. 2011) etc. Tight junctions are not limited to the BBB, as they can also be found in olfactory epithelia, testis and gastrointestinal tracts. Adherens junctions (AJs) are localized below the TJs, stabilize endothelial cell-cell interactions and participate in the control of paracellular permeability. Cadherin, VE-cadherin, and associated scaffolding catenin proteins are the main constituents of AJs and play a key role in the control of CNS angiogenesis and microvascular integrity (Nico and Ribatti 2012).

Occludin (MW= 65 kDa) is a protein with 9 domains, of which four are transmembrane domains. Occludin is located at bicellular contacts and its amino acid sequence is approximately 90% conserved in mammals (Tsukita and Furuse 1998). A similar protein, tricellulin, has recently been identified in endothelial cells of the brain and retina (Mariano, Palmela et al. 2013) and at specialized tricellular contacts. TAMP proteins like occluding and tricellulin are involved in regulation of paracellular permeability. The C-terminus

domain of occludin is especially important for TJ barrier function and can interact with signaling molecules responsible for cell survival (Feldman, Mullin et al. 2005). Also, occludin is required for cytokine-mediated cell signaling (Van Itallie, Fanning et al. 2010) and for sensing redox changes in cellular barriers (Blasig, Bellmann et al. 2011).

Loss or disruption of occludin and associated TJ proteins can trigger apoptosis (Beeman, Webb et al. 2012). Moreover, mice that lack occludin can have problems not only in the CNS (e.g., calcifications), but also in many different organs (e.g., inflammation in the gastric epithelium, testicular atrophy, loss of cytoplasmic granules in salivary gland cells, and thinning of the compact bone) (Saitou, Ando-Akatsuka et al. 1997). In humans, mutations of the occludin gene cause a rare neurological disorder with a band-like calcification, simplified gyration and polymicrogyria (BLC-PMG) (O'Driscoll, Daly et al. 2010). Furthermore, patients with metastatic disease displayed significantly lower levels of occludin suggesting that the loss of occludin in tight junctions may be responsible for increased invasion and metastatic spread of breast cancer (Martins, Baptista et al. 2011).

Claudins are a family of proteins that also have four transmembrane domains (MW= 20-27 kDa), and together with occludins regulate the intercellular permeability of tight junctions (Tsukita and Furuse 1998). Human claudins consists of 26 different proteins that are widely distributed in the body (Haseloff, Dithmer et al. 2015). Claudin-5 is the most abundant claudin molecule at the BBB, and knockout mice exhibit higher permeability of the BBB for small molecular tracers (<800 Da) (Nitta, Hata et al. 2003). Other claudins have been found in much smaller concentrations at the BBB and include: claudin-1, claudin-3, and claudin-12. BBB claudins are responsible for tightening the paracellular cleft, and the loss of claudins often results in increased paracellular permeability (e.g., in MS or brain tumor vessels) (Goncalves, Ambrosio et al. 2013).

In other organs, claudins can form paracellular ion pores (e.g., claudin-2, -10, -16) or contribute to the maturation of biological barriers (claudin-6, -13). Claudins are involved in many different organ pathologies. For example, claudin-1 deficiency manifests as neonatal ichthyosis sclerosing cholangitis (NISCH) syndrome that is often associated with mental retardation (Paganelli, Stephenne et al. 2011). Moreover, deletion of claudin-5 is associated with DiGeorge/Velo-cardio-facial syndrome and high rates of schizophrenia (Sirotkin, Morrow et al. 1997). Claudin-14 mutations have been shown to cause nonsyndromic deafness (Wattenhofer, Reymond et al. 2005) while claudin-19 mutations lead to hypomagnesaemia, renal failure, and vision problems (Konrad, Schaller et al. 2006).

Junctional adhesion molecules (JAMs) belong to the immunoglobulin superfamily and have a molecular weight of about 40 kDa (Garrido-Urbani et al., 2014). JAM-A, -B, and -C are found in endothelial cells, with JAM-A highly expressed at the BBB. During early TJ biogenesis, JAMs interact directly with the cell polarity protein Par3, which is important for BBB formation. JAMs also bind to cytoplasmic proteins AF6 and ZO-1 and play a major role in maintaining the stability of TJs. For example, loss of vascular JAM-A immuno-staining in human brain tissue correlates with BBB leakiness (Padden et al., 2007). JAMs also mediate the transendothelial migration of leukocytes that is important for BBB function. In humans, mutations of JAM-C result in intracerebral hemorrhages, subependymal calcifications, and congenital cataracts (Mochida et al., 2010).

ZO proteins belong to the family of membrane associated guanylate kinases (MAGUK), and are mostly located inside the cytoplasm of endothelial cells (Bauer, Krizbai et al. 2014). ZO proteins are also found in the nucleus of epithelial cells and can regulate transcription factors (Balda and Matter 2009). ZO-1 and ZO-2 are expressed at the BBB and have been shown to be important for TJ formation. In cells lacking ZO proteins, the formation of TJ is completely disrupted (Umeda, Ikenouchi et al. 2006). ZO proteins interact directly with transmembrane proteins like occludin, claudins, and JAMs, and connect transmembrane proteins to the actin cytoskeleton. The interaction between transmembrane proteins and skeleton proteins is required for the maintenance of TJs, and dissociation of ZO-1 from the junctional complex results in increased permeability of the BBB (Hawkins and Davis 2005). Cytoplasmic proteins like cingulin, AF-6, and 7H6 also contribute to the stability and integrity of TJs (Liu, Wang et al. 2012). Deficiency of ZO-1 results in defects in angiogenesis, and also early lethality of embryos (Katsuno, Umeda et al. 2008). ZO-2 shares high sequence homology with ZO-1. It can replace ZO-1 and facilitate formation of TJs (Umeda, Matsui et al. 2004). Mouse embryos deficient in ZO-2 die early after implantation, and exhibit a decreased proliferation rate and increased apoptosis (Xu, Kausalya et al. 2008). Therefore, ZO proteins are important not only for ensuring structural integrity of the TJ, but also for integrating various signaling pathways crucial for TJ physiology.

1.3.2. Pericytes

Pericytes originate from the bone marrow pericyte progenitor cells. They cover about 30%–90% of the capillary surface and their exact function is still unclear (Dalkara and Alarcon-Martinez 2015). Pericytes have a potential to differentiate in a large number

of cell types, including glial cells and neurons (Karow 2013). They display both the mesenchymal and neural stem cell features, and are involved in CNS regenerative processes. Pericytes play a major role in angiogenesis and neovascularization and can regulate endothelial cell growth, differentiation and migration (Ribatti, Nico et al. 2011).

It has been shown that a constant collaboration between the endothelial cells, pericytes and astrocytes is required for proper functioning of the CNS neurovascular unit (Armulik, Genove et al. 2010). Pericytes connect with endothelial cells via tight junctions and paracrine signaling (Winkler, Bell et al. 2011). They exhibit contractile capabilities like vascular smooth muscle cells and regulate the capillary blood flow and BBB permeability, as well as integrity (Quaegebeur, Segura et al. 2010). During sensory stimulations (Attwell, Buchan et al. 2010) pericytes dilate capillary before arterioles in response to neurotransmitter release from the nearby active neurons. Pericyte-deficient animals do not develop proper blood vessels, and also experience BBB breakdown and leakage (Lindahl, Johansson et al. 1997), including neurodegeneration and memory problems (Bell, Winkler et al. 2010). In inflammatory conditions, pericytes act like microglia and perform different immunological functions: phagocytose toxic molecules, attract and present antigens to primed lymphocytes, produce immunomodulators (e.g., IL-1 β , IL-6, TNF α , ROS, NO and matrix metalloproteinases), and open TJs for BBB passing of immune cells. Moreover, pericytes have some features similar to fibroblasts and are able to form scar tissue after injury. The basal lamina is maintained by pericytes and encloses both the endothelial cells and pericytes. It has a thickness of approximately 30-40 nm and consists of proteins, including: laminins, collagen IV, nidogens and heparin sulfate proteoglycans (Diaz-Flores, Gutierrez et al. 2009).

1.3.3. Astrocytes

Astrocytes are ideally positioned to conduct information between blood vessels and neurons, regulate CNS blood flow, and provide trophic/metabolic support for neurons (Filosa, Morrison et al. 2015). Morphologically, astrocytes are usually star shaped and attach to the basolateral side of BBB endothelial cells with their “end-feet”, which can cover about 99% of the BBB. A single astrocyte can contact approximately 160,000 synapses, integrating neural activity with the vascular network (Bushong, Martone et al. 2002) Astrocytes have many important roles in the CNS, including: **(a)** homeostatic maintenance of extracellular ions, pH and water; **(b)** uptake and clearance of neurotransmitters such as glutamate and GABA; **(c)** supply of neurons with energy metabolites; **(d)** modulation of synapses and synaptic functions; **(e)** regulation of a local blood flow; **(f)** modulation of

inflammatory response by excreting cytokines, chemokines, and by presenting antigens; and **(g)** production of antioxidant compounds like glutathione (GSH) and superoxide dismutases (SODs) (Anderson, Ao et al. 2014).

Different types of astrocytes have been identified including: (a) protoplasmic astrocytes in the gray matter; (b) fibrous astrocytes in the white matter; (c) Bergmann glia and velate astrocytes in the cerebellum; (d) Müller cells in the retina; (e) tanycytes in the floor of the third ventricle; and (f) perivascular and marginal astrocytes forming the pial and perivascular ‘glia limitans’ (Alvarez, Katayama et al. 2013).

Astrocytes are involved in the formation of neurovascular units together with endothelial cells, pericytes and neurons. Increased neuronal activity results in vasodilatation and rapid delivery of glucose and oxygen to brain areas having increased metabolic demands. Astrocytes are most likely responsible for regulating local CNS blood flow in response to changes in neuronal activity (Filosa, Morrison et al. 2015).

Astrocytes communicate via Ca^{2+} signaling and are coupled via gap junctions that allow their signal to be spread across neural networks and blood vessels. Neuronal activity triggers an increase in intracellular Ca^{2+} in astrocytes that results in the release of vasoactive molecules, including: arachidonic acid metabolites, epoxyeicosatrienoic acids (EETs), nitric oxide (NO), glutamate, adenosine and ATP. These molecules can increase or decrease a CNS blood vessel diameter and blood flow according to the local demands. For example, glutamate release during neuronal stimulation can trigger Ca^{2+} activation in astrocytes and prostaglandin release, plus subsequent vasodilatation in arterioles (Zonta, Angulo et al. 2003). Also, during sciatic nerve stimulation, astrocytes induce upstream vasodilation of arterioles via a purinergic signaling mechanism (Xu, Mao et al. 2008). Moreover, after visual stimulation astrocytes induce changes in blood volume in the visual cortex (Schummers, Yu et al. 2008).

Astrocytes promote development and maintenance of BBB properties by releasing different growth factors, including: vascular endothelial growth factor (VEGF), glial cell line-derived neurotrophic factor (GDNF), basic fibroblast growth factor (bFGF), transforming growth factor- β (TGF- β), and angiopoetin-1 (ANG-1) (Alvarez, Katayama et al. 2013). These factors are important for the formation of tight junctions, the promotion of specialized enzyme systems and the expression of polarized transporters, including Pgp and GLUT1 (Abbott, Ronnback et al. 2006). In addition, astrocytes transport some substances across the BBB, and also contribute to homeostasis of ions, amino acids,

neurotransmitters and water at the BBB. They take up glucose via GLUT1 transporters and also produce glycogen that serves as a source of lactate for neurons (Brown and Ransom 2007).

Astrocytic end-feet express water channel aquaporin 4 (AQP4) that controls water influx at the BBB, and is dysfunctional in brain edema (Wolburg, Noell et al. 2009). KIR4.1 potassium channels co-localize with AQP4 and are also important for maintaining potassium and water balance (Simard and Nedergaard 2004). They are significantly decreased in hippocampi of patients with temporal lobe epilepsy (De Keyser, Mostert et al. 2008). Anti-KIR4.1 antibodies seem to be associated with BBB dysfunction in multiple sclerosis (MS), while anti-AQP4 antibodies are found in neuromyelitis optica (NMO) (De Keyser, Mostert et al. 2008). Neurotransmitter recycling by astrocytes can also lead to local changes in ions and water at the BBB. For example, astrocytes can also take up glutamate through Na⁺-dependent transport proteins (e.g., EAAT1 and 2) and this transport is accompanied by net uptake of ions and water (Abbott, Ronnback et al. 2006).

Astrocytes can also pump out toxins via Pgp transporters and prevent them from entering the brain (Abbott, Ronnback et al. 2006). Finally, astrocytes harbor transporters and receptors for a wide range of neurotransmitters, hormones, peptides and cytokines, which regulate their functional activity. Also, astrocytes have been implicated in the pathogenesis of many psychiatric and neurological disorders (Abbott, Ronnback et al. 2006, Sofroniew and Vinters 2010, Alvarez, Katayama et al. 2013).

1.4. Transport Across the Blood-Brain Barrier

Drug transporters that are naturally related to elements of the BBB have been successfully utilized to deliver drugs across the BBB and into the brain. There are five main transport mechanisms at the BBB: **a)** paracellular diffusion, **b)** transcellular diffusion, **c)** a carrier mediated influx and/or efflux transport, **d)** transcytosis via receptor mediated endocytosis (RME) or adsorptive-mediated endocytosis (AME), and **e)** diapedesis (Neuwelt 2004, Gabathuler 2010, Abbott 2013).

Paracellular transport involves movement of very small water-soluble molecules through the BBB tight junctions, while transcellular transport involves passive diffusion of low molecular weight (< 200 Da), highly lipophilic substances across the lipid plasma membranes of endothelial cells. Carrier-mediated transport employs different membrane bound proteins that undergo conformational changes and transport molecules down their

concentration gradient (Neuwelt 2004). Brain endothelial influx transporters supply the CNS with nutrients and include: GLUT1 glucose carrier; several amino acid carriers (including LAT1, L-system for large neutral amino acids); and transporters for nucleosides, nucleobases and other substances (Begley and Brightman 2003). Also, several organic anion (the OATP family) and cation transporters (the OCT family) are expressed on brain endothelial cells (Fig. 5).

BBB efflux transporters pump toxic molecules out of the CNS and into blood, they include: the ABC family of transporters (e.g., P-glycoprotein (Pgp); multidrug resistance-associated proteins (MRPs); the peptide transport system (PTS-1)); and anionic and cationic cyclic peptide transporters (Neuwelt 2004). Among the efflux transporters, the ABC transporters are concentrated on the luminal membrane, whereas the Na⁺-dependent transporters are generally abluminal. When molecules travel against a concentration gradient at the BBB, the required energy is provided by ATP (as in the ABC and MRP transporters), or the Na⁺ gradient created by operation of the Na⁺,K⁺-ATPase. For example, several Na⁺-dependent glutamate transporters (excitatory amino acid transporters 1–3; EAAT1–3) move glutamate out of the brain against the large opposing concentration gradient (<1 μM in ISF compared with ~100 μM in plasma) (Abbott, Ronnback et al. 2006).

Receptor-mediated endocytosis (RME) is involved in selective uptake of macromolecules like peptides and proteins. It is a highly specific type of energy dependent transport that is competitive and saturable, because it involves binding of ligands to cell surface receptors on endothelial cells, which then results in a conformational change that terminates in endocytosis of the receptor-ligand complex. Some examples of substances that undergo receptor-mediated endocytosis are: insulin, transferrin, melanotransferrin, glutathione, leptin, vasopressin, diphtheria toxin and insulin-like growth factor (IGF) I and II (Neuwelt 2004). The two main trafficking routes for BBB transcytosis appear to involve clathrin-coated vesicles (CCVs) and caveolae. However, macropinocytosis, or fluid-phase endocytosis that is independent of ligand binding, has recently also been implicated in transcytosis of some nanoparticles (Tosi, Fano et al. 2011).

Adsorptive mediated endocytosis (AME) is triggered by electrostatic interaction and induces endocytosis through the binding of positively charged molecules to the surface of the negatively charged plasma membrane of cerebral endothelial cells (Neuwelt 2004). AME has a lower affinity and higher capacity than receptor-mediated endocytosis. Cationic proteins and liposomes may undergo adsorptive endocytosis at the BBB.

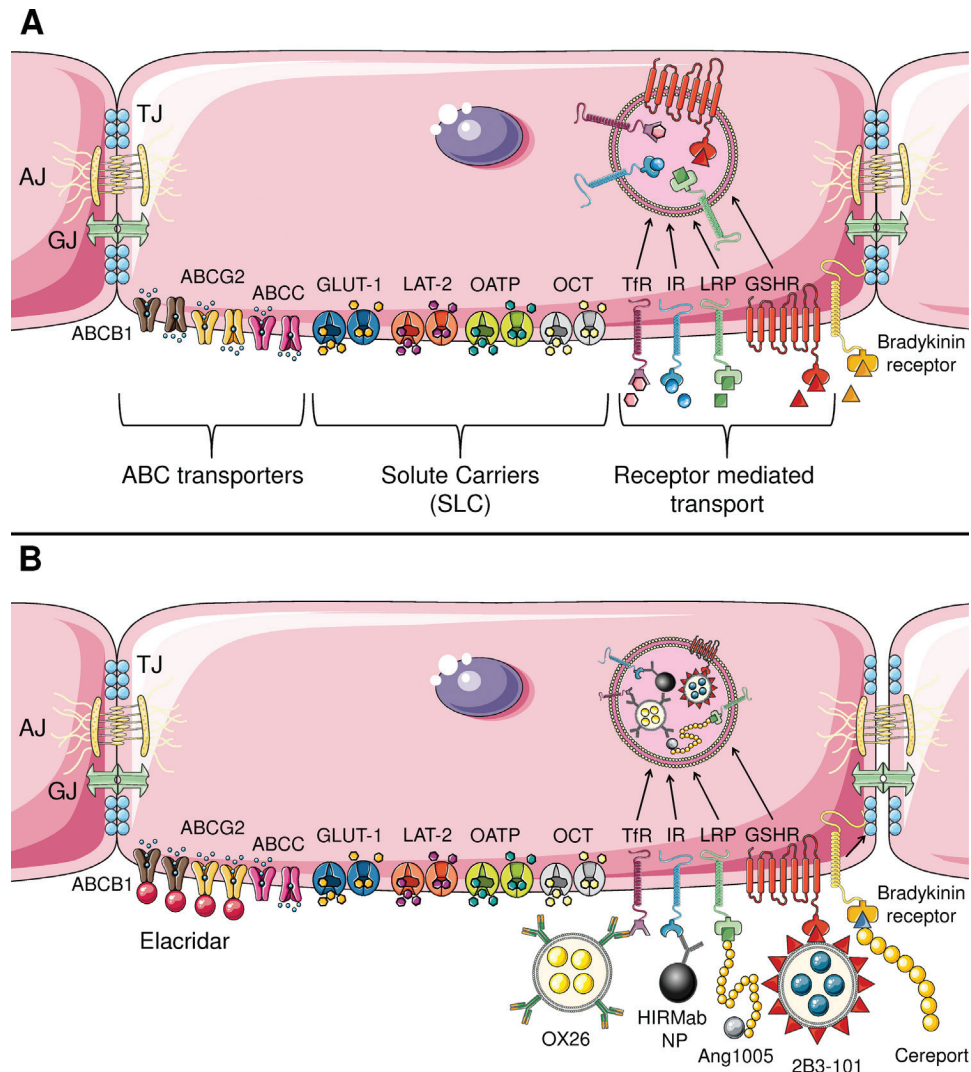


Figure 5. Therapeutic brain delivery strategies that target the physiological make-up of the BBB: (A) The BBB consists of both a physical and physiological barrier. The physical component consists of tight junctions (TJ), gap junctions (GJ) and adherens junctions (AJ) that restrict paracellular transport. The TJs are under regulation by the bradykinin receptor. The physiological barrier restricts the brain entry of harmful exogenous compounds via ATP-binding cassette (ABC) efflux transporters, and allows for efficient uptake of essential nutrients via a wide range of solute carriers (SLC), and influx transporters that can uptake glucose (GLUT-1), amino acids (LAT-2), anions (the OATP family) and cations (the OCT family). Transcytosis is mediated via a wide range of receptors including: transferrin receptor (TfR), insulin receptor (IR), LDL-receptor-related protein (LRP) and glutathione receptor (GSHR). (B) Strategies against various modalities of the intact BBB have been developed for improving therapeutic delivery to the brain. Elacridar inhibits ABCB1 and ABCG2, thereby reducing efflux and allowing increased brain penetration of small molecules. OX26, human insulin receptor mAb conjugated nanoparticles (HIRMAb NP), Ang1005 and 2B3-101 all target transcytosis pathways. Cereport targets TJ signaling through the bradykinin receptor (van Tellingen, Yetkin-Arik et al. 2015).

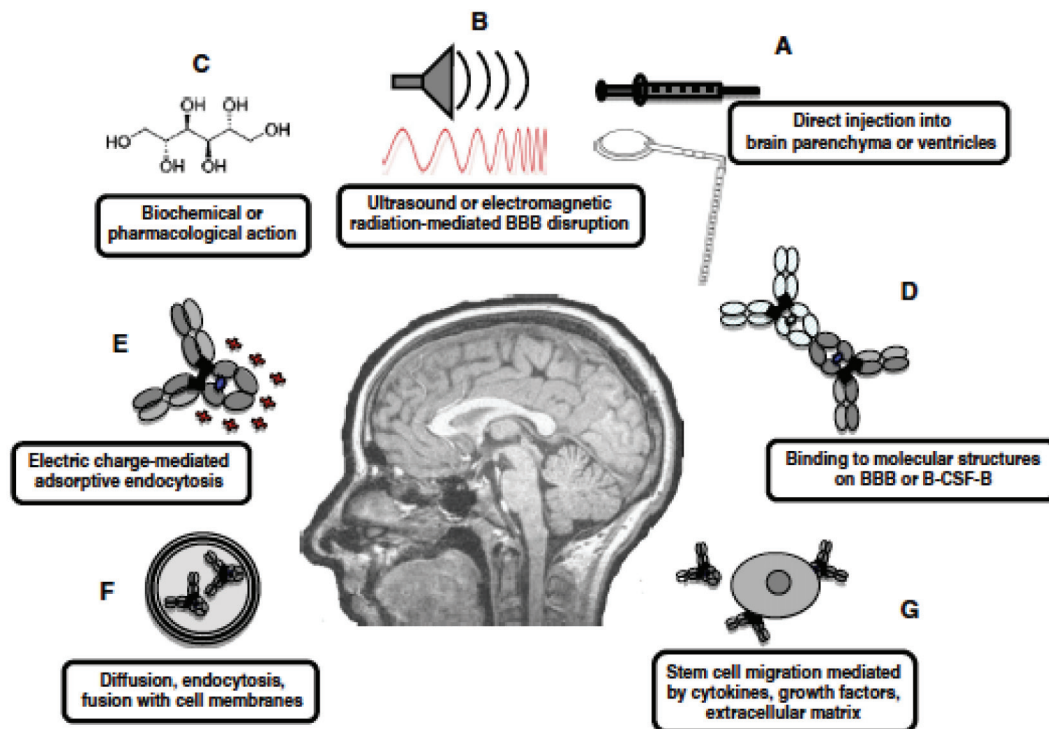


Figure 6. Current methods and underlying mechanisms of delivery of antibodies across the BBB: Methods for delivering antibodies through the BBB include direct injection (e.g., by syringe, Ommaya reservoir) (A), mechanical (e.g., ultrasound, electromagnetic radiation) (B), biochemical or pharmacological (e.g., mannitol, bradykinin) disruption of the BBB (C), ‘molecular Trojan horse’ (D), antibody cationization (E), nanoparticles (F), and stem cell-mediated antibody delivery (G). These methods are applicable for delivery of intact antibodies as well as engineered antibody fragments (e.g., Fab, scFv, minibody, diabody, triabody, tetrabody) (Frank, Aboody et al. 2011).

Finally, during inflammation activated lymphocytes and monocytes can pass the BBB via diapedesis. Chemokines activate chemokine receptors on leukocytes, which then initiate integrin activation, leukocyte attachment to the BBB endothelial cells, rolling along the vessel wall, and extravasation through the paracellular space into the CNS (Holman, Klein et al. 2011). Studies have shown that IL-17 can disrupt BBB tight junctions by inducing production of reactive oxygen species (ROS) (Huppert, Closhen et al. 2010). Furthermore, ROS can down-regulate occludin and ZO-1 tight junction proteins and open sufficient space for leukocyte extravasation (Schreibelt, Kooij et al. 2007).

Several invasive and non-invasive methods that utilize natural pathways have been developed to deliver large therapeutic molecules like antibodies across the BBB (Figure 6). The six main approaches to deliver antibodies to the brain are: **a)** disruption of the BBB, **b)** antibody cationization, **c)** conjugation of antibodies to the fusion proteins, **d)** stem cell-mediated delivery, **e)** bypassing the BBB, and **f)** nanoparticle-mediated delivery.

1.5. Paracellular Delivery and BBB Disruption

1.5.1. BBB Disruption by Chemicals

In 1940, Broman and Olsson were the first to disrupt the BBB with contrast dyes in order to deliver molecules to the brain (Kroll and Neuwelt 1998). However, in 1980 scientists first utilized hyperosmolar solutions to deliver ¹⁴Csucrose to the CNS (Rapoport, Fredericks et al. 1980). Administration of hypertonic solutions like mannitol, lactamide, arabinose, urea, or saline has been shown to disrupt the BBB. These substances can increase the permeability of the BBB by inducing osmotic shrinkage of brain endothelial cells, which leads to opening of intercellular tight junctions. Other chemicals, like vasodilators or K_{Ca} channel agonists, can also disrupt the BBB by directly increasing the permeability of TJs.

Hypertonic mannitol has been widely used in animals and humans to increase concentrations of therapeutic molecules like chemotherapeutic agents and antibodies in the brain. Compared to saline perfusion, the intracarotid hyperosmolar mannitol perfusion increased the brain to blood mAb ratio levels by 450% to 500% in the ipsilateral rat brain hemisphere (Bullard, Bourdon et al. 1984). Also, mannitol significantly enhanced brain delivery of L6 antibody in rats with small cell lung cancer xenografts (Neuwelt, Barnett et al. 1994). Similarly, after BBB disruption with mannitol, Rituximab antibody targeted CD20 protein on B-cells and effectively decreased tumor volume and improved survival in a rat model of CNS lymphoma (Muldoon, Lewin et al. 2011).

In order to improve antibody delivery in humans with relapsed primary CNS lymphoma (PCNSL) chemo-immunotherapy (e.g., Rituximab followed by carboplatin and methotrexate) was given after osmotic BBB disruption. Patients who received this treatment exhibited an excellent overall survival (Doolittle, Jahnke et al. 2007). Also, patients with recurrent malignant glioma tumors received intra-arterial cerebral infusion of the angiogenesis inhibitor bevacizumab after mannitol, and exhibited reduction in tumor area, volume and perfusion (Riina, Fraser et al. 2009, Boockvar, Tsiouris et al. 2011). In patients with melanoma brain metastasis, greater uptake of melanoma-specific

Fab antibody fragments was observed in brain hemispheres after BBB disruption with mannitol. However, no radioactive uptake was observed in the region of the tumor (Neuwelt, Specht et al. 1987). Ab-fragments did not diffuse into the tumor and over 90% of antibodies cleared from the brain within 72 h.

Vasodilators such as bradykinin and the bradykinin agonists, like labradimil or RMP-7 (Cereport®), have been shown to disrupt the BBB by increasing the permeability of tight junctions (Elliott, Hayward et al. 1996, Bidros and Vogelbaum 2009, Sarin, Kanevsky et al. 2009). Bradykinin analogs (e.g., RMP-7) were administered in conjunction with carboplatin in children with high-grade brainstem gliomas (Warren, Jakacki et al. 2006). RMP-7 produced a 2-fold increase in CNS drug concentrations (Emerich, Snodgrass et al. 1999), but the CNS concentrations were insufficient for therapeutic efficacy, and this method failed to demonstrate efficacy in Phase II and III clinical trials.

To selectively deliver drugs to brain tumors, *calcium-dependent potassium channels* (K_{Ca}) *agonists* (e.g., NS-1619) have been used to penetrate the BBB. K_{Ca} channels are highly expressed in brain tumors and brain tumor capillaries (Ningaraj, Rao et al. 2002, Ningaraj, Sankpal et al. 2009) and expression of K_{Ca} correlates with tumor growth and malignancy (Ransom and Sontheimer 2001). Targeted delivery of an antibody to the glioblastoma was significantly improved in a mouse glioblastoma xenograft model by co-administration of NS-1619 with trastuzumab. Compared to untreated controls, mice treated with NS-1619 and trastuzumab showed improved median survival (Ningaraj, Sankpal et al. 2009).

Phosphodiesterase 5 (PDE5) inhibitors, like vardenafil and sildenafil, were used effectively to increase brain-tumor barrier (BTB) permeability in gliosarcoma animal models, and to enhance anti-tumor efficacy of a chemotherapeutic agent doxorubicin (Black, Yin et al. 2008). Also, mice bearing intracranial lung cancer tumors were treated with Herceptin and vardenafil, and their survival time was significantly increased compared to the untreated controls (Hu, Ljubimova et al. 2010). Several nitric oxide donors have also increased transport of drugs to brain tumors in rats via calcium-activated potassium channels (Weyerbrock, Walbridge et al. 2003).

Integral membrane tight junction proteins like occludin, JAMs, claudin-5, and adherent junction proteins VE-cadherin and the BBB-specific cadherin-10, or AHNAK, can be used as potential targets to modulate paracellular permeability of the BBB (Deli 2009). For example, after intracarotid injection of *DeltaG*, a biologically active fragment of Zonula occludens toxin Zot, transport of several drugs across the BBB was significantly

increased (Menon, Karyekar et al. 2005). The reactive oxygen species (ROS) can also induce down-regulation of occludin and ZO-1 tight junction proteins, stimulate endothelial cell contraction and open paracellular space for leukocyte extravasation (Schreibelt, Kooij et al. 2007).

Some monoclonal antibodies that target a specific BBB antigen have also been used for BBB disruption. For example, the endothelial barrier antigen (EBA) is expressed specifically in endothelial cells of the rat BBB. By using the Ab against EBA, BBB permeability for the Evans Blue dye and MRI contrast agent ($MnCl_2$) was significantly increased (Lu, Demny et al. 2010). However, large therapeutic molecules have not been delivered with this method.

1.5.2. BBB Disruption by Radiation Therapy

Radiotherapy (RT) has been used extensively clinically for treatment of brain cancers to induce DNA damage and cell death. Studies in both animals and humans have shown that radiotherapy can disrupt the BBB and improve delivery of drugs to CNS tumors. Focused cranial RT (Baumann, Kao et al. 2013) increased drug-loaded nanocarrier (DLN) delivery into intracranial tumors in an orthotopic mouse model of GBM and significantly improved therapeutic outcomes. Tumor growth was delayed or halted, and survival was extended by >50% compared to the results obtained with either RT or the DLN alone. In clinical studies the mean blood to CSF ratio of trastuzumab dropped from 420:1 to 76:1 following radiotherapy, and was further reduced to 49:1 in patients with concurrent meningeal carcinomatosis (Stemmler, Schmitt et al. 2007).

These results indicate that CNS bioavailability of antibodies increases with radiotherapy, and concurrent use of radiation and therapeutic antibodies are being explored for CNS cancer treatment. Clinical studies with RT and bevacizumab (Barani and Larson 2015) or trastuzumab (Mustacchi, Biganzoli et al. 2015) are currently conducted in patients with brain tumors.

1.5.3. BBB Disruption by Electrical Stimulation

The BBB can be disrupted by electrical stimulation of the postganglionic parasympathetic fibers of the sphenopalatine ganglion. It has been shown that this method enhanced delivery of fluorescently-labeled anti-HER2 antibody into the cerebral cortex by 5-fold. Even though therapeutic concentrations of Abs were delivered to the brain, their diffusion

and penetration into a CNS tumor has not been demonstrated. The BBB permeability correlated inversely with molecular size of the fluorescently-labeled dextran (4–250 kDa) and decreased rapidly after cessation of electrical stimulation indicating drug delivery through the tight junctions (Yarnitsky, Gross et al. 2004, Yarnitsky, Gross et al. 2004)

1.5.4. BBB Disruption by Ultrasound

Focused low-frequency ultrasound (FUS) has been used for mechanical disruption of the BBB, because acoustic energy can be targeted to a specific brain region within a few millimeters. Studies have demonstrated that FUS may increase cerebrovascular permeability by producing shear stress in cells, by activation of signaling pathways involved in the regulation of permeability, and/or by disruption of tight junction proteins. The higher the amplitude of the acoustic pressure the larger the BBB disruption. At 0.4 MPa, approximately 50% of sonicated areas exhibited enhanced penetration of MRI contrast agent, which increased to 90% at 0.8 MPa, and 100% at 1.4 MPa (Hynynen, McDannold et al. 2005, Burgess and Hynynen 2014). However, pressure over 0.8 MPa was used to deliver a polyclonal anti-mouse dopamine D4 receptor antibody (D4RAb) and induced significant brain hemorrhaging and tissue damage (Kinoshita, McDannold et al. 2006). Moreover, CNS penetration of D4R-Abs was restricted only to the sonicated hippocampal brain area, because of limited diffusion of antibodies through brain parenchyma.

The same group (Kinoshita, McDannold et al. 2006) has later shown that therapeutic anti-HER2 antibody (trastuzumab), which targets the HER2/neu receptor and is overexpressed on ~30% of breast cancers, can distribute into the mouse cerebral cortex after transcranial sonication. After BBB disruption with 0.8 MPa, the average antibody concentration was 3,257 ng per g of tissue in the sonicated cortex. In comparison, the average CNS antibody concentration of 1,504 ng/g was achieved with 0.6 MPa. To improve trastuzumab delivery in a breast cancer brain metastases mouse model (BT474), focused ultrasound bursts were combined with circulating microbubbles (MBs). The intravenously administered MBs were used with FUS to lower the ultrasound energy required to induce BBB disruption, and to temporarily noninvasively permeabilize the BBB and brain-tumor barrier (BTB) (Park, Zhang et al. 2012). Animals in the treatment group received six weekly treatments of BTB/BBB permeabilization under MRI guidance combined with intravenous administration of trastuzumab (2 mg/kg). Seven weeks later the mean tumor volume was significantly lower in treated animals compared to untreated animals, and their median survival time was greater than 83 days (at least 32% longer than in the untreated control group).

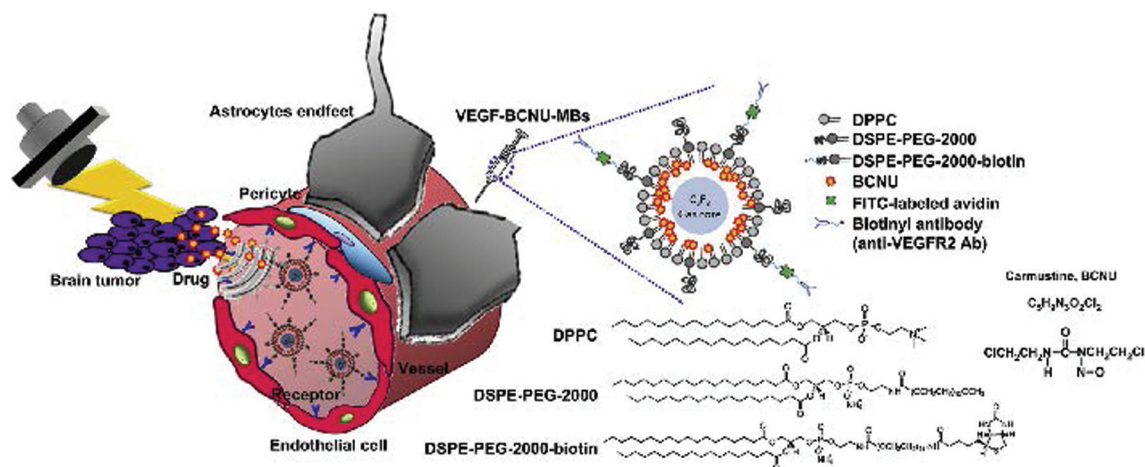


Figure 7. The concept of antibody-based and tumor vascular targeting-guided drug delivery. The VEGF-R2-targeting drug-loaded MBs (VEGF-BCNU-MBs) are administered intravenously and home to the tumor vasculature via the specific antibody. After accumulation of drug-loaded vehicles, FUS sonication is delivered to locally open the BBB to enhance local chemotherapeutic agent (BCNU) delivery (Fan, Ting et al. 2013).

FUS has also been combined with nanoparticle platforms to improve CNS cancer diagnosis and treatment. For example, gold nanoparticles were delivered to rat brain 9L gliosarcoma tumors with MRI guided FUS to enable spectral mapping of nanoparticles with surface enhanced Raman scattering (SERS)-based molecular imaging (Diaz, McVeigh et al. 2014). Nanoparticles coated with anti-epidermal growth factor receptor (EGFR) antibody or nonspecific human IgG exhibited increased uptake in tumor cells. A similar strategy has also been used to target rat glioblastoma tumors with anti-vascular endothelial growth factor receptor (VEGFR) antibody coated MBs and loaded with chemotherapy (e.g, 1,3-bis (2-chloroethyl)-1-nitrosourea, BCNU) (Fan, Ting et al. 2013). The combination of FUS exposure and VEGFR-Ab-BCNU-microbubbles (Fig. 7) opened the BBB, increased tumor-specific targeting, enhanced chemotherapeutic agent delivery, reduced liver accumulation, and improved the median survival time in a rat GBM model. Therefore, FUS shows great promise for treatment of brain cancers, but further studies are necessary to gauge the feasibility of this approach in humans.

Finally, therapeutic capabilities of FUS have also been demonstrated in animal models of Alzheimer's disease (AD). The ultrasound-mediated transient BBB disruption enabled delivery of therapeutic anti-amyloid antibodies and their co-localization with amyloid plaques in Alzheimer's mouse models (Raymond, Treat et al. 2008). Image-guided

transcranial FUS was able to enhance delivery of anti- β -amyloid antibodies to targeted brain regions and also reduce the plaque burden in a mouse model of Alzheimer's disease (Jordao, Ayala-Grosso et al. 2010). However, even with multiple treatment sessions the decrease of plaque burden was modest.

The same research group has recently shown that FUS-induced BBB disruption alone reduced the size of the plaques, most likely through the delivery of endogenous antibodies (Jordao, Thevenot et al. 2013). These studies demonstrated FUS feasibility for treatment of neurodegenerative disorders. While FUS shows promise in animal models, it has significant limitations for use in humans including acoustic signal attenuation and signal distortion emanating from the skull. Also, issues regarding safety and toxicity of repeatedly disrupting the BBB in large brain regions will need to be resolved.

Regardless of the method used to disrupt the BBB, these techniques carry significant risks. Although some studies have concluded that BBB disruption (BBBD) appears reasonably safe (Doolittle, Miner et al. 2000), several studies have reported an increased risk of seizures following BBBD (Marchi, Angelov et al. 2007). In patients who received intra-arterial hyperosmotic mannitol before chemotherapy, 25% of the procedures triggered focal motor seizures in the hemisphere contralateral to the BBB disruption. The seizures occurred within minutes of BBB disruption and up to 6 h after the procedure, and the degree of BBBD correlated with the probability of seizure development. Prophylactic anti-epileptic drugs did not prevent the occurrence of seizures. Moreover, methods that disrupt the integrity of the BBB can also increase BBB permeability to toxins and pathogens that can cause CNS infection and/or inflammation (Frank, Aboody et al. 2011). Given the reported side effects and the role of the BBB in providing protection from foreign molecules and maintaining brain homeostasis, invasive techniques seeking to disrupt this natural barrier should be used with caution and only in special circumstances, and further, might not be suitable for use in chronic neuropsychiatric disorders.

1.6. Transcellular Delivery of Cationized or Fusion Proteins

1.6.1 Cationized Proteins

Positively charged proteins have been shown to have an ability to penetrate the CNS via absorptive-mediated endocytosis (AME). The isoelectric point of proteins can be

increased by protein cationization. Cationization is a chemical treatment that causes the conversion of carboxyl groups of a protein into extended primary amino groups. A cationized protein can interact with negative charges at the luminal plasma membrane of brain endothelial cells and can undergo adsorptive mediated transcytosis through the BBB. Proteins can be cationized using various, synthetic (e.g., hexamethylenediamine) or naturally occurring (e.g., putrescine) polyamines. For example, the isoelectric point of bovine serum albumin was increased from approximately 4 to 10 by covalently attaching hexamethylenediamine, which induced a 48-fold enhancement of in vitro uptake in isolated rat brain capillaries. Furthermore, brain capillary uptake of albumin was enhanced over 11-fold in vivo (Kumagai, Eisenberg et al. 1987). Different therapeutic molecules can be attached to cationized albumin and delivered across the BBB via AME (Pardridge, Triguero et al. 1990).

By attaching hexamethylenediamine antibodies can be cationized to improve CNS delivery. Bovine brain capillaries can rapidly uptake cationized IgG molecules, but not native IgG molecules (Triguero, Buciak et al. 1989). Studies have demonstrated transcytosis of cationized IgG molecules through the BBB and into brain parenchyma. For example, cationized monoclonal antibodies that target β -amyloid protein have shown enhanced in vitro binding to isolated rat brain capillaries (Bickel, Yamada et al. 1994).

Recent studies demonstrated increased CNS uptake of polyamine-modified F(ab')₂ fragments targeted to A β plaques in a mouse model of Alzheimer's disease (Ramakrishnan, Wengenack et al. 2008). Also, cationization allowed Fab'2 fragments against tetanus toxin to be transported across the brain endothelium by AME (Girod, Fenart et al. 1999). Furthermore, cationization of monoclonal antibodies against HIV protein markedly increased their endocytosis across the BBB, and enhanced inhibition of HIV-1 replication (Pardridge, Bickel et al. 1994).

These studies have demonstrated that cationization can be an important strategy for transporting antibodies across the BBB. However, cationization can also compromise their binding affinity and alter their pharmacokinetic and pharmacodynamic properties (Herve, Ghinea et al. 2008). Chemical modification may aggregate proteins and yield heterogeneous molecular species. Also, this approach is not mediated by specific recognition of targeted BBB transporters. After intravenous injection, cationic carriers can bind nonspecifically to blood elements and endothelium in systemic vasculature, especially in the lung, and can accumulate in the liver.

1.6.2. Fusion Proteins

Noninvasive strategies have focused on identifying ways to enable drugs to penetrate an intact BBB. Insulin and transferrin receptor (TfR)-mediated endocytosis are well-characterized BBB processes that are often used to transport large molecules like antibodies (Yu and Watts 2013). Following this strategy, a monoclonal antibody (mAb) has been generated to target human insulin receptor (HIRmAb) on the BBB and shown to facilitate CNS entry of different biologicals (Pardridge and Boado 2012). HIRmAbs have served as a molecular ‘Trojan horse’ to transport several biologicals across the BBB including: glial-derived neurotrophic factor (Boado and Pardridge 2009), β -glucuronidase (Boado and Pardridge 2010), tumor necrosis factor receptor (Hui, Boado et al. 2009), and anti-A β -Ab (Boado, Lu et al. 2010) etc.

Studies have shown that brain-penetrating antibody pharmaceuticals can be developed for treatment of neurodegenerative disorders such as AD. For example, a single chain Fv (ScFv) antibody against A β peptide was bioengineered as a fusion protein with HIRmAb, and was successfully transported across primate BBB in vivo. The brain concentration was 0.3% ID per 100 g of primate brain (or about 1 nM) (Boado, Lu et al. 2010). HIR-antibody can cross-react with the primate or human insulin receptor, but not with the rat or mouse insulin receptor, limiting preclinical investigations. Therefore, a different BBB strategy has been applied in preclinical rodent studies. ScFv was fused to TfRmAb to target mouse TfR on the BBB, and its CNS concentration was 3.5 % injected dose (ID)/g of brain tissue after intravenous delivery in mice (Boado, Zhou et al. 2009). In comparison, the brain uptake of 3D6 Ab alone in the mouse cortex was equivalent to 0.07% of injected dose (ID)/gram of brain (Bard, Fox et al. 2012). In a follow up study, double transgenic PSAPP mice were treated every 3-4 days for 12 weeks by intravenous injections of TfRmAb-ScFv fusion protein, and brain A β ¹⁻⁴² concentrations were reduced by 40% (Zhou, Fu et al. 2011). Recently, PSAPP mice were treated daily with subcutaneous injections of fusion protein, and this caused a 57% and 61% reduction in amyloid plaques in the cortex and hippocampus, respectively (Sumbria, Hui et al. 2013).

A bispecific antibody has also been designed that binds to TfR and to enzyme β -secretase (BACE 1), which cleaves amyloid precursor protein into toxic amyloid- β (A β) in AD (Yu, Zhang et al. 2011). The bispecific Ab was more effective than the monospecific anti-BACE1-Ab in reducing β -amyloid in a mouse model of AD, demonstrating that BACE function was indeed inhibited. Moreover, in cynomolgus monkeys, anti-TfR-BACE Abs induced a 50% reduction in plasma A β levels after 24 hours (Yu, Atwal et al. 2014). By contrast, anti-BACE antibodies showed very little uptake into the monkey brain and had

no impact on brain A β levels.

Furthermore, the lower-affinity anti-TfR2–BACE-Ab was compared with the higher affinity anti-TfR1-BACE-Ab to assess the effect of TfR affinity on brain uptake (Bien-Ly, Yu et al. 2014). The lower-affinity Ab showed higher brain concentrations and better therapeutic properties than the higher affinity antibody, which triggered TfR degradation. Similarly, the bispecific anti-A β antibody with a monovalent binding mode to TfR facilitated transcytosis across the BBB and binding to β - amyloid plaques, whereas a bivalent binding mode Ab induced lysosome sorting and degradation of TfRs (Niewoehner, Bohrmann et al. 2014). These results clearly show that brain-penetrating antibodies can be developed for treatment of neurodegenerative disorders.

Brain-penetrating antibodies have also been used for diagnosis and treatment of brain tumors, but with limited efficacy. Different drugs have been attached to TfR antibodies or ligands for targeting tumors that overexpress TfRs, but they have been delivered directly into brain tumors (Daniels, Bernabeu et al. 2012). In one study conjugation of the murine TfR-specific mAb OX26 to the ¹¹¹In-labeled EGF-peptide allowed successful ex vivo imaging of GBM tumors expressing EGFRs in rats (Kurihara and Pardridge 1999). EGF peptide alone did not get into the brain and did not bind to the tumor (Fig. 8).

A completely different BBB strategy has been used for delivery of anti-HER2 monoclonal antibodies to brain tumors. Angiopep-2 (An2) peptide, which crosses the blood-brain barrier (BBB) by receptor-mediated transcytosis via low-density lipoprotein receptor-related protein 1 (LRP1), was conjugated to anti-HER2 mAb (Regina, Demeule et al. 2015). Modified Abs were able to penetrate the BBB and increase survival in mice with intra-cranially implanted BT-474 xenografts. Anti-HER2-mAbs have been used clinically to increase survival in patients with HER2 positive breast cancers, but they are ineffective against brain metastases due to poor brain penetration.

Using transcytosis across the BBB to deliver therapeutic molecules may be advantageous over direct intracerebral delivery, because all cells of the CNS are within approximately 40 μ m of a capillary, thereby limiting the distance the therapeutic agent would be required to diffuse (Banks 2009).

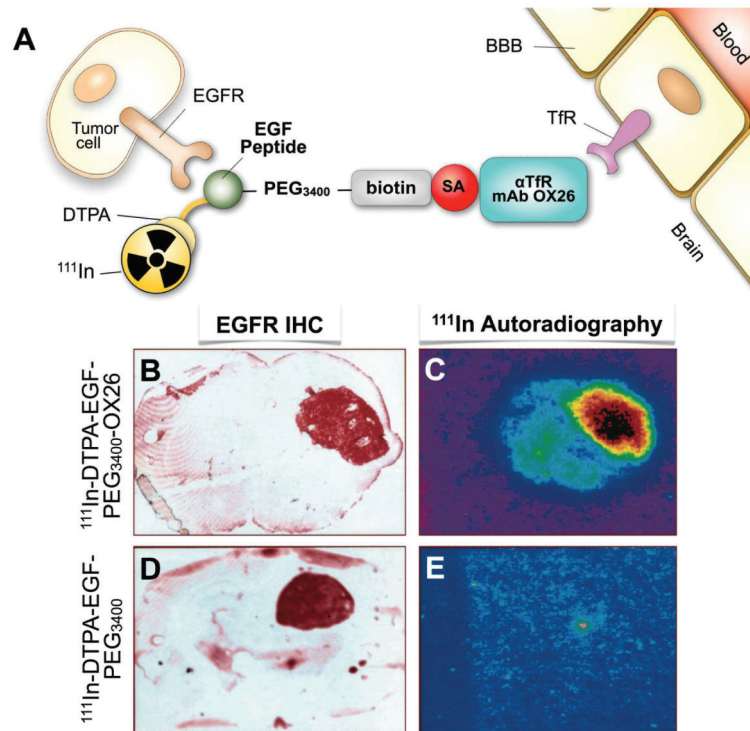


Figure 8. A Trojan Horse Technology: (A) Structure of dual targeted epidermal growth factor (EGF) chimeric peptide conjugated to rat transferrin receptor (TfR) targeted mAb OX26. The EGF is radiolabeled with ¹¹¹In. The EGF was cross-linked via PEG to the OX26 mAb. (B, D) Brain sections of U87 human glioma tumor-bearing rats were stained immunohistochemically using a mAb to the human EGF receptor (EGF-R), which demonstrates expression of the EGF-R in brain tumor specimens. (C, E) Ex vivo ¹¹¹In-autoradiography demonstrates that the brain tumor can be imaged with the EGF chimeric peptide that can undergo transport across the BBB in vivo via anti-TfR-mAb OX26. There is no imaging of the brain tumor when the non TfR-targeted EGF peptide radiopharmaceutical is administered, because the EGF does not cross the BBB alone (E) (Kurihara and Pardridge 1999).

However, there are some disadvantages: **1)** CNS delivery is limited by the number of available BBB transporters; **2)** the distribution of BBB saturable transporters is heterogeneous and CNS delivery may be limited in certain brain regions; **3)** the RME vector may interfere with CNS delivery of important molecules required for brain function; **4)** the RME-directing vector may lead to trafficking of the therapeutic cargo to lysosomes for degradation; and **5)** widespread expression of transporters on peripheral organs can limit the capability of RME for specific brain delivery and increase systemic side effects. For example, insulin receptors are prevalent in pancreatic tissue, and HIRmAb-GDNF fusion proteins induced focal pancreatic intraepithelial neoplasia lesions in primates

(Ohshima-Hosoyama, Simmons et al. 2012). Also, transferrin receptors are mostly expressed on immature red blood cells (reticulocytes) and serious dose related reductions in reticulocytes were observed in mice that received anti-TfRD/BACE1 antibodies (Couch, Yu et al. 2013). Currently there are no FDA approved bispecific antibodies for treatment of CNS diseases.

1.7. Cell-mediated Delivery

Neural stem cells (NSCs) and mesenchymal stem cells (MSC) are able to cross the BBB and target tumors within the CNS (Frank, Najbauer et al. 2010, Kean, Lin et al. 2013). NSCs can be genetically modified to produce and secrete intact IgG, cross the BBB and deliver antibodies to ectopic human breast cancer xenografts in the mouse brain (Frank, Edmiston et al. 2009). Also, MSCs modified to express a single chain antibody targeting the glioma-associated antigen EGFRvIII showed therapeutic efficacy against human glioma xenografts when implanted intracranially in mice (Balyasnikova, Ferguson et al. 2010). Further studies of stem cell-mediated antibody delivery are needed to optimize stem cell delivery across the BBB and to achieve therapeutic concentrations of antibodies within the CNS.

1.8. Bypassing the BBB

1.8.1. Convection-Enhanced Delivery

Macromolecular drugs can be administered directly into the brain tissue to bypass the BBB. For example, antibodies have been injected directly into brain tumors, but their diffusion through the tumor is very poor. Antibodies require 3 days to move 1 mm from the site of injection due to their large molecular size (Jain 1989). Therefore, antibodies cannot easily reach the regions of the tumor that are more distant from the injection site. Moreover, after the resection of glioma tumors, radio-immunoconjugates were injected into glioma resection cavities to deliver a boost of radiation (Hopkins, Chandler et al. 1998). The peak radioactive dose was delivered 0.16–0.18 cm below the cavity margin, and the mean dose at 2 cm deep was only 5.3% of the peak. Thus, direct injection of radiolabeled antibodies leads to limited diffusion into normal brain parenchyma. In order to enhance drug diffusion from the injection site and to increase the volume of distribution, pressure can be applied during CNS drug infusion using a convection-enhanced delivery (CED) method.

The CED method was successfully used in animals and humans, and was able to improve

the volume of distribution of radiolabeled macromolecules (Bobo, Laske et al. 1994, Yang, Barth et al. 2009). In a crossover study, patients with glioma tumors who received radiolabeled antibodies via CED as a first-line therapy had a slightly higher volume of distribution than the patients who received an intratumoral bolus injection first (Sampson, Akabani et al. 2006). In the Phase I and II clinical trials, patients with malignant gliomas were treated with a radiolabeled chimeric mAb (¹³¹I-Cotara) that binds to the DNA-histone H1 complex. Radiolabeled mAbs delivered via CED appear to be promising therapeutic and imaging agents (Hdeib and Sloan 2011), because scientists were able to deliver 90% to 110% of the prescribed radioactivity to the targeted brain regions. However, the number of patients was too small to reach conclusions about Cotara's clinical efficacy.

Scientists (Grossi, Ochiai et al. 2003) tested CED administration of trastuzumab in animals with HER2 overexpressing cancer cells, and demonstrated a 96% enhanced survival time in rats that received 2 mg/kg of Ab intracranially compared to rats that received the same dose intraperitoneally. Authors also demonstrated extensive diffusion of radiolabeled trastuzumab throughout the tumor mass in animals. Similarly, glioma-bearing mice were treated with bevacizumab alone or in combination with irinotecan via CED, and survived 30% longer than mice treated with the same drugs systemically (Wang, Sivakumar et al. 2015). MRI-guided CED was used to monitor delivery of therapeutic antibodies (e.g., anti-EGFRvIII or cetuximab) conjugated to iron nanoparticles in mouse models of glioma (Hadjipanayis, Machaidze et al. 2010, Kaluzova, Bouras et al. 2015). Glioma-bearing mice treated via CED with antibodies attached to iron particles survived longer than untreated mice. Furthermore, boronated polyamidoamine dendrimers were chemically linked to cetuximab and delivered via CED in EGFR gene-transfected glioma rat models. The mean survival times (MST) were longer in rats that received boron neutron capture therapy with bioconjugates than in irradiated controls (Wu, Yang et al. 2007). In the follow up study of boron neutron capture therapy the combined delivery of two antibodies (cetuximab and the anti-EGFRvIII mAb) was more effective in extending the MST in rats than delivery of a single antibody (Yang, Wu et al. 2008).

These animal and human data suggest that CED methods may improve therapeutic efficacy of intracranial antibody therapy of CNS cancer. Although some studies have concluded that CED appears safe for cancer patients, several other studies reported serious side effects (e.g., increased risk of seizures or infection) (Frank, Aboody et al. 2011). The invasive CED strategy may be effective for brain cancer patients, but may not be useful for patients with chronic neurodegenerative or neuroinflammatory CNS diseases where a noninvasive drug delivery method is required.

1.8.2. Intrathecal Injection

Macromolecules can be injected intrathecally into cerebrospinal fluid (CSF), where they can distribute throughout the CNS via CSF circulation (Proescholdt, Hutto et al. 2000). Intrathecally administered rituximab has been shown to be therapeutically effective against CNS lymphoma and leukemia and to enhance patient survival (Perissinotti and Reeves 2010). In a Phase 1 clinical trial, survival ranged from 1.1 week to more than 134 weeks, and the mean 1-hour post-dose CSF concentrations were similar to the peak therapeutic concentrations in serum after intravenous injection of rituximab. In the prospective study, 7 pediatric patients with treatment refractory B-cell acute lymphoblastic leukemia received rituximab 10 mg twice weekly for 4 weeks intrathecally. After 24 months 5 patients remained in complete remission (Jaime-Perez, Rodriguez-Romo et al. 2009). Also, intrathecal trastuzumab has been studied in treatment resistant patients with leptomeningeal carcinomatosis secondary to HER2-overexpressing metastatic breast cancer. In a systematic review/pooled analysis (Zagouri, Sergentanis et al. 2013), intrathecal administration of trastuzumab significantly enhanced patient survival. In 68.8 % of cases, a significant clinical improvement was observed and the median overall survival was 13.5 months. Clinical improvement and CSF response were associated with longer CNS progression-free survival.

Preliminary results in these clinical studies are encouraging, but further studies are required to confirm clinical efficacy of intrathecally administered Abs. Although the CSF–brain barrier appears to be more permeable than the BBB, a layer of ependymal cells significantly restricts drug penetration across this barrier. Thus, delivery of antibodies into the CSF is insufficient to guarantee the penetration through the CSF–brain barrier and diffusion throughout the CNS. Pharmacokinetics of intrathecal trastuzumab was evaluated in cynomolgus monkeys and large variations in CSF concentrations were found (Braen, Perron et al. 2010). Authors attributed these variations to uneven distribution of drug throughout the CNS and rapid transfer of trastuzumab from the CSF into serum after intrathecal administration. Clinical studies have also shown that radiolabeled drugs diffuse very slowly and unevenly from ventricles to periventricular areas and deeper into the brain (Johanson, Duncan et al. 2005). The CNS diffusion rate depends of the particle size and concentration, and large particles like antibodies have poor diffusion through the CNS (Wolak and Thorne 2013). Therefore, brain regions located further from the ventricles, such as the subcortical and rostral regions are significantly more difficult to reach by intrathecal administration (Johanson, Duncan et al. 2005). Also, efflux transporters like P-gp can quickly remove Abs that can enter the brain from the CSF.

1.8.3. Intranasal Delivery

In recent years, the intranasal route of administration has emerged as an important method for delivering macromolecules like proteins to the CNS, because intranasal drug administration is non-invasive, generally well tolerated, and because it completely bypasses the BBB. As a result, macromolecules can be transported directly from the nasal epithelium into the brain (Lochhead and Thorne 2012). The olfactory and trigeminal nerves are involved in smell and sensory perception respectively, and their terminals are exposed in the nasal cavity. Brain regions involved in olfactory perception project to the limbic areas of the brain (Fig. 9). Also, there is a direct connection between the olfactory system and the midbrain. For example, unilateral intranasal delivery of horseradish peroxidase (HRP) (Balin, Broadwell et al. 1986) resulted in ipsilateral labeling of dopamine brain regions: the ventral tegmental area (VTA), SN pars reticulata, and ventral pallidum. The anatomical connection between the dopamine regions and the olfactory system can be utilized in diagnosis and treatment of neuropsychiatric disorders, because it provides direct access for pharmaceuticals to enter the brain areas often affected by CNS disorders (e.g., schizophrenia, mood disorders, drug addiction, ADHD, PD etc.).

There are 3 main mechanisms that are involved in passing the nasal barrier: transcellular, paracellular, and axonal transport (Illum 2003). Transcellular transport through the olfactory epithelium includes passive diffusion of lipophilic molecules, and adsorptive or receptor-mediated endocytosis of macromolecules. It can result in a direct CNS transport and systemic vascular transport. Lipophilic, low molecular weight (MW) drugs, like fentanyl, can undergo fast transcellular transport via diffusion and are observed to have high bioavailability (~80%) (Illum 2003). In comparison, peptides that are often transported intranasally via endocytosis are less than 1% bioavailable (Illum 2003).

The paracellular route involves the rapid transport (< 30 min) of molecules between the intercellular junctions of olfactory epithelial cells that include: tight-junctions (TJs), adhering junctions, desmosomes, and gap-junctions (Graff and Pollack 2005). The average size of the paracellular channels is approximately 10 Å, and the molecular weight (MW) cut-off is about 1 kDa (Illum 2003). However, studies have shown that several growth factors (MW= 30-40 kDa) can undergo brain uptake via paracellular route following intranasal administration (Balin, Broadwell et al. 1986, Liu, Fawcett et al. 2001). Because of the continuous renewal of the olfactory receptor cells, the integrity of these junctions has been questioned (van Woensel, Wauthoz et al. 2013).

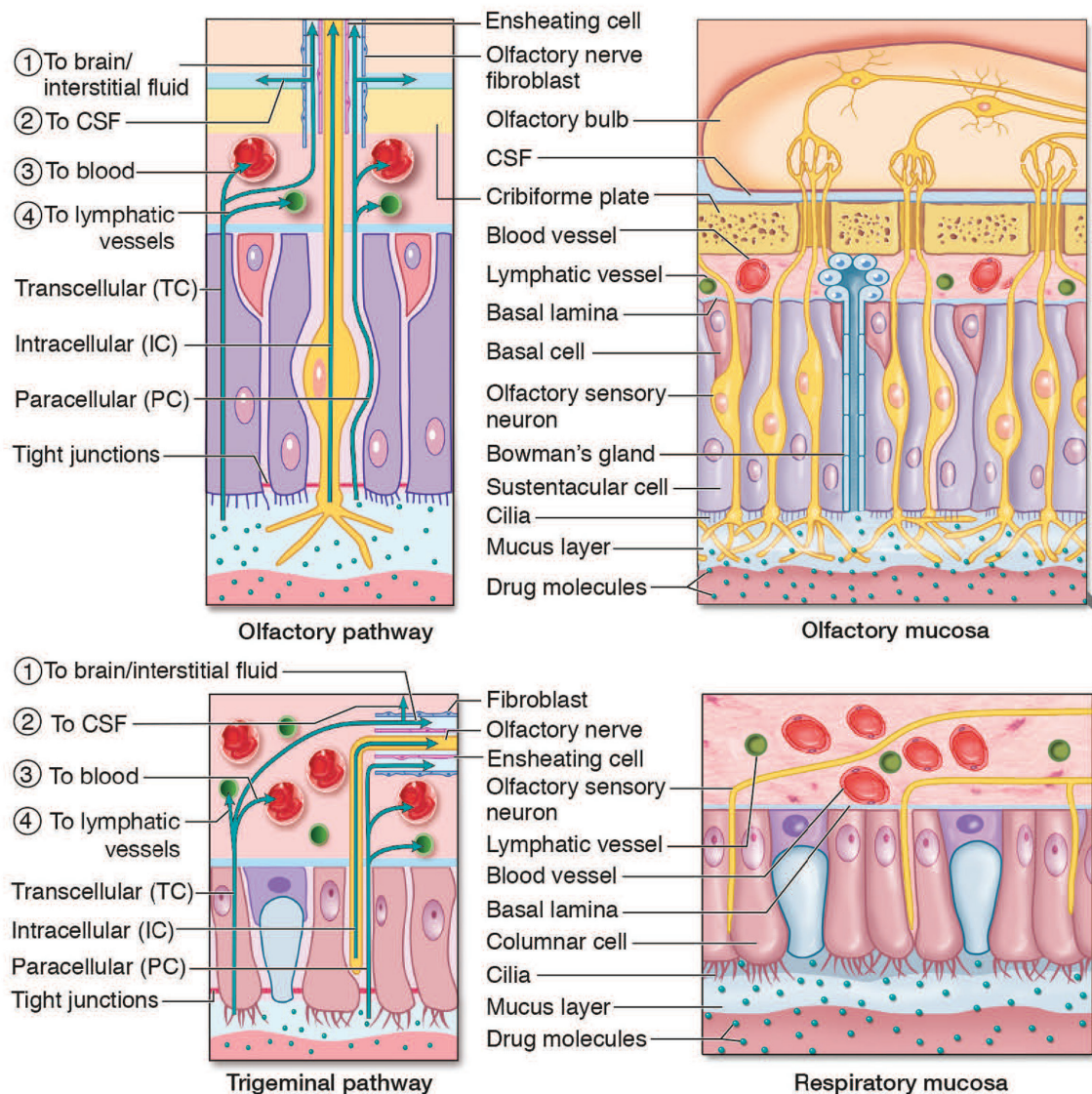


Figure 9. Potential intranasal transport routes for substances to enter the brain: The olfactory filaments penetrate the nasal mucosa of the upper part of the nose and substances may be transported inside the nerve axon (intracellular). Transport across the mucosa also occurs between the cells (paracellular) or through the cells (transcellular). After crossing the mucosa substances may follow channels surrounding the nerve bundles (perineuronal), be absorbed into submucosal blood and lymphatic vessels or move into the subarachnoid CSF where they may enter the brain interstitium via perivascular channels. The trigeminal nerve endings do not completely penetrate the mucosal surface. Substances cross the mucosa and continue along the same transport routes as described above. A part of the ophthalmic branch (V1) innervates the upper anterior nasal segment with similar projections as the olfactory nerve. The maxillary branch (V2) provides sensory and parasympathetic innervation to the majority of the respiratory mucosa and projects to the brain stem (Djupesland, Messina et al. 2014).

Macromolecules can also be taken up via endocytosis by olfactory and trigeminal neurons and transported via axons. For example, scientists (Jansson and Bjork 2002) administered a fluorescent dye intranasally and demonstrated its transport along the olfactory and trigeminal nerves. Also, wheat germ agglutinin-horseradish peroxidase (WGAHRP, MW 62 KDa) (Thorne, Emory et al. 1995) undergoes endocytosis through olfactory neurons. WGA also can be used for intranasal drug transport (Chauhan, Davis et al. 2011). However, this method of drug transport is slow (van Woensel, Wauthoz et al. 2013), can take from 24 hours to days and depends on the diameter of axons, which in humans ranges from 100 nm to 700 nm in size (Morrison and Costanzo 1992).

Several factors can affect intranasal absorption of drugs, and include: a) drug metabolism and hydrolysis, b) the p-glycoprotein efflux pump, c) the neonatal Fc receptor efflux for Ab clearance, d) nasal congestion/decongestion, e) pathological conditions like allergic or infectious rhinitis, and f) mucociliary clearance (Graff and Pollack 2005). A protective mucus layer on the nasal epithelium is recycled every 10-15 minutes in order to remove particles to the back of the throat so they can be swallowed and eliminated. This protective function can significantly limit drug absorption and increase drug elimination. Therefore, a concentrated form of the drug should be administered intranasally in a small volume of solution to prevent swallowing or leaking of the drug (Dhuria, Hanson et al. 2010).

There are several drug-related factors that also can affect intranasal transport, which include: molecular weight, molecular size, concentration and pKa of the drug, and volume and pH of the solution. Studies have shown that CNS transport following intranasal administration is greater when the molecule is unionized, has low molecular weight, small diameter, and pH between 4.5-6.5 (Dhuria, Hanson et al. 2010). Moreover, CNS diffusion of molecules through the brain extracellular space is limited by particle diameter, especially for large particles like antibodies. Scientists (Thorne and Nicholson 2006) have estimated that particles between 38-64 nm in size can be transported through the fluid-filled pores of extracellular space. Therefore, particles smaller than 65 nm are optimal for CNS transport.

Small molecule drugs that normally do not cross the BBB have been successfully delivered to the CNS intranasally (e.g., 5-fluorouracil (Sakane, Yamashita et al. 1999) and methotrexate (Wang, Jiang et al. 2003)). Several peptides have been administered intranasally to humans and exhibited therapeutic effects including: vasopressin (MW= 1100 Da), corticotropin releasing factor (MW= 21,423 Da), growth hormone releasing factor (MW= 3358 Da), insulin (MW= 6000 Da), and an analog of cholecystokinin (CCK-8) (Thorne and Frey 2001). Several growth factors, like insulin growth factor (IGF-1), nerve

grow factor (NGF), transforming growth factor beta-1 (TGF- β 1), have all demonstrated widespread CNS distribution after intranasal delivery (Thorne and Frey 2001, Thorne, Pronk et al. 2004, Ma, Ma et al. 2007, Capsoni, Covaceuszach et al. 2009).

Grow factors cannot usually penetrate the BBB and are unstable after oral or intravenous administrations, but remained fully functional in the CNS after intranasal delivery. For example, NGF reversed neurodegeneration in a mouse model of Alzheimer's disease (Capsoni, Giannotta et al. 2002, De Rosa, Garcia et al. 2005), IGF reduced the infarct size and improved symptoms in a rat model of stroke (Liu, Fawcett et al. 2001), while fibroblast growth factor (FGF) improved motor activity in a mouse model of PD (Kucherianu, Kryzhanovskii et al. 1999).

Many large particles like viruses can easily enter the human brain through the intranasal route. Therapeutic antibodies have also been delivered intranasally in animal models of stroke and AD. One hour after induction of bilateral prefrontal photothrombosis in rats, intranasal administration of anti-glutamate antibody (250 μ g/kg) improved retention of conditioned passive avoidance response (Romanova, Shakova et al. 2010). Moreover, intranasal delivery of the same Ab improved memory in rats that received injections of A β fragments (A β 25–35) into the nucleus basalis of Meynert (Gorbatov, Trekova et al. 2010). Furthermore, 5XFAD mice with A β plaques were treated intranasally twice a week for 8 weeks with NU4 antibody (20 μ g dose per mouse) (Xiao, Davis et al. 2013). This treatment improved spatial memory and reduced brain plaques in mice by about 28%. Recently, these mice have also been treated intranasally with a 6E10-Ab conjugated to the Wheat Germ Agglutinin (WGA), which resulted in about 50% reduction of small and soluble amyloid plaques, but not large and fibrillar plaques (Chauhan, Davis et al. 2011). To improve intranasal delivery, small single-chain variable fragments (scFv) (MW=26 kDA) have been used instead of large Abs (MW=150 kDA). Chronic intranasal treatment with scFv (1.5 mg/ml) reduced congophilic amyloid angiopathy (CAA) and beta-amyloid plaque numbers in the cortex of APP^{swe}/ PS1^{dE9} mice (Cattepoel, Hanenberg et al. 2011).

These data on intranasal delivery of Abs are promising. However, CNS concentrations of antibodies were not reported and pharmacokinetic studies were not performed. It is unclear whether therapeutic effects were related to amyloid or glutamate clearance via circulating antibodies in the systemic vasculature, or via Abs in the CNS. One study reported low CNS concentrations of Abs after intranasal delivery (Cooper, Ciambone et al. 2013). They demonstrated that intranasal delivery of antibodies (24 mg/kg) that were modified to avoid efflux from the CNS resulted in low rat brain concentrations (from 20

to 40 ng/g or 0.0003-0.0007 %ID/g of brain tissue) at the peak time point. Thus, further studies are required to improve delivery of therapeutic Abs to the CNS via the intranasal route, and we plan to test intranasal delivery of antibodies with and without nanoparticles.

Advantages of noninvasive nose-to-brain transport include: the potential rapid onset of action, avoidance of the systemic circulation, reduction of systemic side effects and hepatic/renal clearance, and the possibility of chronic self-administration of drug. However, intranasal administration of drugs also has disadvantages. The volume of administered drug is usually small and only drugs that are active at very low concentrations (micro molar or lower) can be administered intranasally. Frequent drug administrations can cause nasal irritation, mucosal damage, and loss of sense of smell. Moreover, intranasal transport is different in rodents compared to humans because of obvious anatomical differences between the species (Graff and Pollack 2005). In rats, a nasal cavity is small, but nasal mucosa makes up as much as 50% of the total nasal epithelium, while in humans, a nasal cavity is much larger, and nasal mucosa makes up about 8% of the total nasal epithelium. Thus, it is difficult to extrapolate preclinical animal intranasal data to humans. Despite these difficulties, CNS drugs have been FDA approved for intranasal delivery.

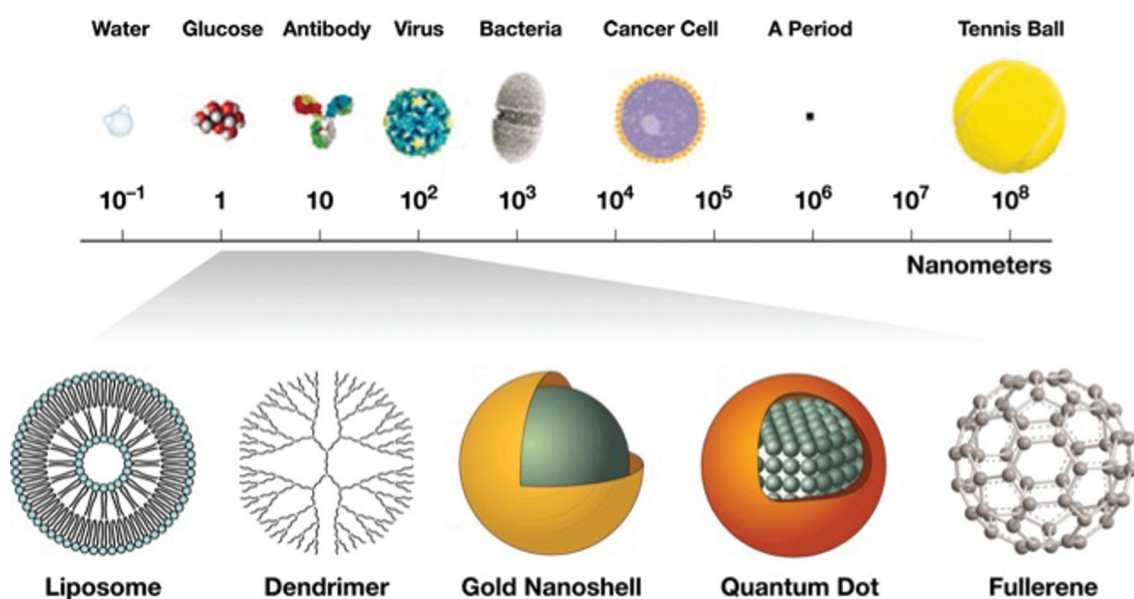


Figure 10. Nanoparticles: Nanoscale devices are 100-10,000 times smaller than human cells (Vitaliano and Vitaliano 2008).

1.9. Nanoparticle Delivery

Nanotechnology is an interdisciplinary pursuit (Rakovic and Uskokovic 2010) that involves the design, specification, synthesis and production of nanomaterials and devices whose smallest functional organization is at the nanometer scale (one billionth of a meter) (Fig. 10). Nanotechnology can provide a new noninvasive approach for diagnosis, prevention and treatment of CNS diseases by delivering CNS drugs that promote recovery and normalize function. A key milestone is to noninvasively deliver adequate concentrations of drugs across the BBB to affected neuronal cells. CNS delivery technologies are still far removed from the “magic bullet” proposed by Paul Ehrlich at the beginning of the 20th century, where a drug is precisely targeted to an exact site of action. Only 2% of small-molecule drug candidates can cross the BBB, and 100% of large molecules cannot get into the brain (Pardridge and Boado 2012). Today’s CNS nanotechnologies can only deliver from 0.5 to 3% of the injected dose (ID) of macromolecular drug per gram of brain tissue (Frank, Aboody et al. 2011).

Several types of nanoparticle platforms for CNS delivery of antibodies have been designed that include: polymers, solid lipid nanoparticles (SLNPs), liposomes, micelles, dendrimers, metallic particles, proteins etc. (see Table 2). Macromolecules cannot easily penetrate the BBB and several transport mechanisms have been used for uptake of nanoparticles by the brain across the BBB (Lockman, Mumper et al. 2002, Neuwelt, Abbott et al. 2008, Gabathuler 2010). Large molecules are usually internalized at the BBB by two different mechanisms: receptor-mediated endocytosis (RME) and adsorptive-mediated endocytosis (AME). In order to utilize these BBB processes nanoparticles have been functionalized for BBB transport with different types of molecules, including, surfactants (e.g., polysorbate 80); anti-transferrin or insulin receptor antibodies (see Figure 11); single domain antibodies; and different peptide vectors (e.g., SynB vectors, penetratin, angiopep-2, CDX, RGD or TAT peptides) (Pardridge 2007).

These various noninvasive methods for BBB passing have been used with varying degrees of success and with relatively low efficiency (Neuwelt, Abbott et al. 2008, Bhaskar, Tian et al. 2010, Kateb, Chiu et al. 2010). For example, different drugs have been delivered via liposomes (Schnyder and Huwyler 2005, Smith and Gumbleton 2006, Daniels, Bernabeu et al. 2012) by targeting transferrin receptors (e.g., daunomycin, 5-fluoruracil, doxorubicin, nerve growth factor, beta-galactosidase and luciferasa gene etc.).

Evidence also exists that polybutylcyanoacrylate (PBCA) nanoparticles coated with

polysorbate 80 cross the BBB and enhance brain entry of a number of therapeutic agents such as dalargin, loperamide, doxorubicin, NMDA, tubocurarine etc. (Kreuter 2004, Olivier 2005). The majority of nanoplatforms have been designed and tested for diagnosis and treatment of cancer, but only a few have been applied specifically in treatment of brain cancer or other brain diseases.

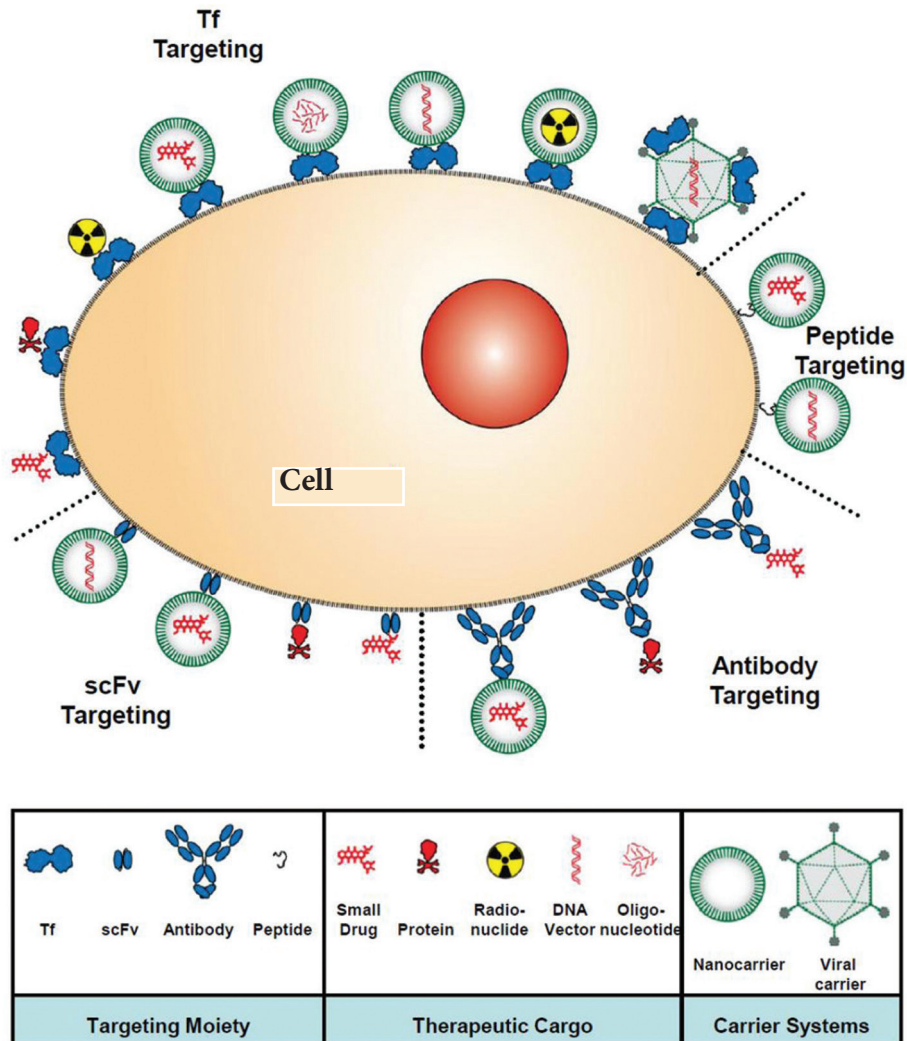


Figure 11. Strategies for transporting therapeutic agents via TfR on the BBB: The BBB transport can be mediated by the natural ligand Tf, a specific peptide, monoclonal antibodies or single chain antibody fragments specific for the extracellular domain of the TfR. The therapeutic agent can be delivered conjugated to the compound or enclosed in a nanocarrier. Targeting the TfR has been an option to deliver drugs, therapeutic proteins, oligonucleotides or radionuclides, and genes in viral vectors (Daniels, Bernabeu et al. 2012).

Nanoparticle studies of delivery of therapeutic antibodies to the CNS have mostly been conducted *in vitro* in brain tissues or BBB models. For example, liposomes have been used to deliver anti-mAbs to amyloid deposits in post mortem brain tissues (Canovi, Markoutsas et al. 2011). Also, bevacizumab modified cationic liposomes exhibited improved cellular uptake and tumor targeting *in vitro* (Kuesters and Campbell 2010). Solid lipid nanoparticles were also used to entrap bevacizumab and were able to penetrate BBB cell models and increase Ab activity by 100- to 200-fold (Battaglia, Gallarate et al. 2015).

A chitosan scaffold containing fluorouracil (5-FU) and bevacizumab was investigated in a glioblastoma cell line and was able to prevent tumor formation *in vitro* (Kutlu, Cakmak et al. 2014). Single walled carbon nanotubes (SWNTs) conjugated with anti-CD133 mAbs have demonstrated selective lysis of CD133-positive glioblastoma multiforme (GBM) cells (Wang, Chiou et al. 2011).

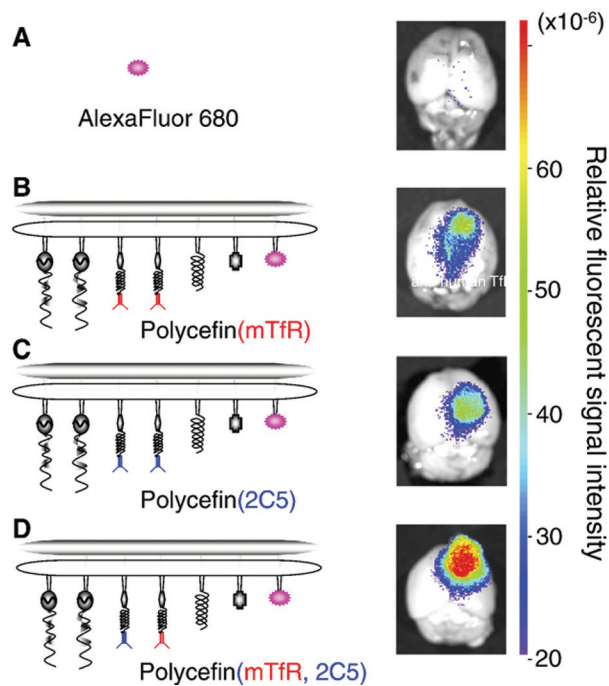


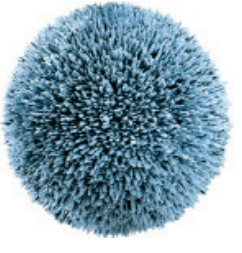
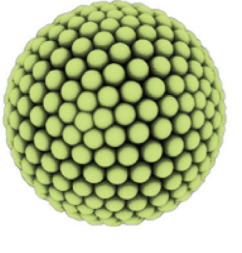
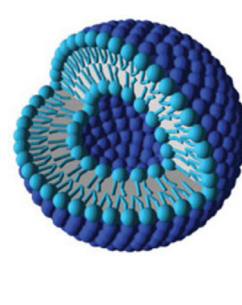
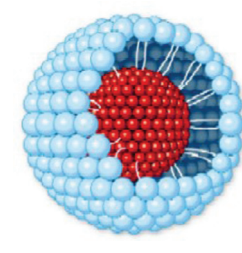
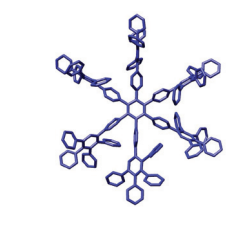
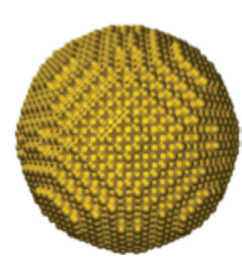
Figure 12. Tumor Imaging: Fluorescence imaging of brain from nude mice bearing human U87MGm glioma 24 h after intravenous injection of free Alexa Fluor 680 and the indicated Alexa Fluor 680-labeled Polycefin variants. Only the tumor contains fluorescent drug. The highest drug accumulation in the tumor is observed for the tandem configuration in Polycefin (mTfR, 2C5) (Fujita, Lee et al. 2007).

Only a few studies (del Burgo, Hernandez et al. 2014) have tested nanoparticle-mediated antibody delivery to the CNS in animal models (see Table 2.). The efficacy of the monoclonal anticancer antibody 2C5 conjugated to PEGylated liposomes loaded with doxorubicin has been demonstrated in an astrocytoma mouse model (Gupta and Torchilin 2007). Similarly, 2C5-Abs were conjugated to poly-(malic acid)-NPs (Polycefim) modified with anti-TfR-Abs for BBB crossing. A significantly higher accumulation of double Abs-targeted NPs has been observed in animals bearing glioma tumors in comparison to animals that received NPs targeted with a single Ab (Fujita, Lee et al. 2007) (see Fig. 12). In vivo studies (Mortensen, Jeppesen et al. 2013) have also shown a high accumulation of cetuximab-modified immunoliposomes in GBM xenografts in mice.

In vivo efficacy of anti-EGFR metallic nanoparticles in GBM tumors was demonstrated in animals treated with cetuximab-iron oxide nanoparticles (IONPs). After treatment with cetuximab-IONPs and subsequent ionizing radiation, a significant increase in overall survival was observed in nude mice implanted with human GBM xenografts (Bouras, Kaluzova et al. 2015). Also, immunoliposomes modified with EGFR-Abs (Feng, Tomizawa et al. 2009) provided an effective mean of delivering ^{10}B into CNS glioma cells for boron neutron capture therapy (BNCT).

Furthermore, cetuximab attached to a fifth-generation (G5) polyamidoamine dendrimer containing boron significantly improved survival of glioma bearing rats after BNCT (Wu, Yang et al. 2007). However, cetuximab attached to a G5-dendrimer containing the cytotoxic drug methotrexate improved tumor targeting in glioma-bearing rats, but not their survival (Wu, Barth et al. 2006). Also, gold nanoparticles containing cetuximab, panitumumab, or rituximab were not able to suppress tumor growth in EGFR-expressing H1975 tumor mouse models (Ahmed, Pan et al. 2015).

Trastuzumab modified nanoparticles have also been developed for diagnosis and treatment of metastatic HER2+ breast cancers. For example, poly-(malic acid)-NPs carrying attached MRI tracer (Gd-DOTA) were able to pass through the BBB and specifically target cancer cells for efficient imaging (Patil and Sherbet 2015). In newly developed double tumor xenogeneic mouse models of brain metastasis this method allowed differential diagnosis of HER2- and EGFR-expressing brain tumors with antibodies attached to NPs. After MRI diagnosis, breast and lung cancer brain metastases were successfully treated in mice with tumor-targeted nanoconjugates carrying molecular inhibitors of EGFR or HER2.

Table 2. CNS Nanoparticles (Vitaliano & Vitaliano 2008)	Characteristics	Antibody Tx	Target	Other Ligands	Reference
	Polymer: Synthetic (e.g. PLA, PLGA, PMLA) or natural (e.g. alginate, gelatin, chitosan) made solid carriers. Some have a fluid core. Good stability. Surface modifications for cell targeting and endocytosis at BBB. Size: 10-1000 nm	2C5 + TfR-Ab Trastuzumab or Cetuximab + TfRAB	Nucleosome TfR HER2 EGFR TfR	Alexa 680 LOEt+ AON+ Alexa 680+ Gd-DOTA	Fujita 2007 Patil 2015
	Solid Lipid NPs: Solid lipid matrices stabilized by surfactants. Lipid NCs: Surfactants surrounding an oily core. Good stability. Surface modifications for cell targeting and endocytosis at BBB. Size: 10-1000 nm	OX26 Ab and NFL-TBS.40-63 peptide	TfR or Tubulin	FcdiOH	Laine 2012
	Liposome: Spherical vesicles with an aqueous inner core enclosed by phospholipid bilayers. Easy preparation. Commercial availability. Surface modifications for cell targeting and endocytosis at BBB. Suitable for hydro- and lipophilic drugs. Size: 50-300 nm	2C5 Cetuximab Antibodies	Nucleosome EGFR EGFR	Doxo-rubicin Sodium borocaptate + Nickel	Gupta 2006 Mortensen 2013 Feng 2009
	Micelle: Hydrophobic polymer block core with a hydrophilic polymer block shell. Difficult preparation. Useful for non-water soluble drugs. Surface modifications for cell targeting and endocytosis at BBB. Size: 20-200 nm	EGF1 nanobody	EGFR	Doxo-rubicin	Talelli 2013
	Dendrimer: One or more central core from which highly branched polymeric molecules arise. Can be easily functionalized. Surface modifications for cell targeting and endocytosis at BBB. Size: 2-15 nm	Cetuximab Cetuximab	EGFR EGFR	Boron Methotrexate	Wu 2007 Wu 2006
	Metallic nanoparticle: One metallic core made of iron, gold, silver etc. Can be functionalized and used for imaging. Surface modifications for cell targeting and endocytosis at BBB. Possible CNS toxicity. Size: 2-15 nm	Cetuximab or Panitumumab or Rituximab Cetuximab Cetuximab	EGFR EGFR CD20 EGFR EGFR	Gold Iron oxide Iron oxide	Ahmed 2015 Kaluzova 2015 Bouras 2015

Protein nanoplatfoms have also shown great promise as natural element drug carriers, because they are biocompatible, non-toxic, can deliver both hydrophilic and lipophilic drug molecules, protect their cargo from degradation by plasma enzymes, and transport their load across biological membranes. Protein-based nanoplatfoms include: albumin, collagen, transferrin as well as viral nanoparticles (Manchester and Singh 2006, Maham, Tang et al. 2009). Different chemotherapy agents have been attached to albumin (Wicki, Witzigmann et al. 2015) which significantly improved their therapeutic properties, but these nanoparticles cannot cross an intact BBB. Viral vectors are often used for DNA delivery and have excellent BBB permeability, but are highly immunogenic. Each nanotechnology has its own strengths, but also respective weaknesses (Nel, Xia et al. 2006, Shvedova, Kagan et al. 2010). Stability has also been a problem, but has been improved with nanoparticle coatings (Artemov, Bhujwalla et al. 2004) such as dextran, polyethylene glycol (PEG), surfactants and by anionic modifications. PEGs have often been added to the surface of nanoparticles in order to prevent their aggregation in solution, to decrease uptake by the reticuloendothelial system, and to increase the half-life of the nanoparticle formulation. A major problem is that nanoparticles also have to be modified with different molecules to be able to cross the BBB and to penetrate neurons or other cells. Each of the nanoparticle modification strategies poses its own risks (Artemov, Bhujwalla et al. 2004). Finding an appropriate nontoxic, non-immunogenic, efficient drug carrier that can also cross an intact BBB has been challenging. Noninvasive delivery of macromolecules to the CNS is crucial for applicability of this technology to clinical neuroimaging and drug delivery. The BBB is intact in the majority of neuropsychiatric disorders, which represents a significant challenge for nanoparticle delivery.

1.10. Clathrin Nanoplatfom

There is an unmet medical need for a novel drug and contrast agent delivery system for treatment of neuropsychiatric disorders. An important advance is the use of bioengineered clathrin nanoparticles in nanomedicine. This unique nanotechnology can easily cross biological barriers (e.g., BBB) and penetrate cells. This nanotechnology provides a carrier platform with improved stability, rigidity, functionality and loading capacity relative to other nanoparticles (Vitaliano and Vitaliano 2008).

Clathrin is a ubiquitous protein found in bacteria, fungi, plants, animals and humans, and has low antigenicity. Clathrin self-assembles into a lattice-like vesicle coat on cell membranes. Clathrin coated vesicles (CCVs) were first isolated in 1976 (Pearse 1976). A clathrin coat is made up of three-legged clathrin mono-units called triskelia. Each

triskelion has three heavy chains (190 kDa) and three light chains (25-29 kDa). The clathrin heavy chain has five functionally distinct regions: the globular amino-terminal domain (β -propeller), a distal leg, a flexible curved region termed the knee, a proximal leg, and a carboxy-terminal end (hub) that mediates clathrin trimerization (see Fig. 13). Adaptor proteins interact with the clathrin heavy chain β -propeller domain via peptide-in-groove interactions (ter Haar, Harrison et al. 2000). Several clathrin box-motifs have been discovered in the β -propeller domain including: the clathrin box motif L Φ X Φ [DE] (Dell'Angelica, Klumperman et al. 1998), a variant clathrin box or DLL motif [S/D]LL (Morgan, Prasad et al. 2000) and a 'type II clathrin box' (Drake and Traub 2001) also termed the W-box motif PWDLW (Miele, Watson et al. 2004). These clathrin box motifs have been used for peptide attachments and templating of metals on clathrin vesicles (Schoen, Schoen et al. 2011). The light chain is responsible for clathrin assembly and stability of clathrin lattice, and it binds to Huntingtin-interacting protein 1 (HIP1) and HIP1-related protein (HIP1R) (Chen and Brodsky 2005).

In 1986 scientists (Vigers, Crowther et al. 1986) first demonstrated the three-dimensional structure of a clathrin coat. Clathrin triskelia can self-assemble into fullerene structures called clathrin cages (CCs) ranging from 30 nm to 100 nm in size. By combining protein crystallography (ter Haar, Musacchio et al. 1998) and cryoelectronmicroscopy (Fotin, Cheng et al. 2004) high-resolution images of clathrin coated cages have been presented. CCs can encapsulate lipid vesicles, resulting in clathrin-coated vesicles (CCVs) (Kirchhausen 2000, Brodsky, Chen et al. 2001). CCVs are naturally occurring transport vesicles responsible for receptor-mediated endocytosis at the plasma membrane, and sorting of proteins at the trans-Golgi network. Clathrin-mediated endocytosis (CME) (Figures 14 & 15) provides a pathway for internalization of extracellular molecules and signaling factors of trans-membrane receptors for the purpose of nutrition and communicating extracellular signals to intracellular targets (Conner and Schmid 2003, Kirchhausen, Boll et al. 2005, Le Roy and Wrana 2005).

CCVs have native multi-cargo capacity, and simultaneously may carry different types of cargo, like neurotransmitters, neurotrophic factors, antibodies, and hormones (Brodsky 2012, Kirchhausen, Owen et al. 2014). The rigid clathrin protein cage stabilizes its cargo and environmentally sequesters the vesicle and its contents. In secretory cells, such as neurons or neuroendocrine cells, CME is used to recycle vesicle membranes (Fig. 16). Moreover, activity-dependent trafficking of postsynaptic receptors during long-term depression (LTD) is mediated by CME. In general, the molecular machinery required for activity-induced endocytosis appears to be very similar to that used for ligand stimulated

endocytosis (Slepnev and De Camilli 2000, Royle and Lagnado 2003, Augustine, Morgan et al. 2006). The process of CME can be divided into several steps: 1) coat nucleation and assembly, 2) coated pit maturation, 3) fission, and 4) uncoating (Figures 14 & 15). A dynamic network of protein-protein and protein-lipid interactions coordinates these events. Accessory proteins assist the AP-2 and clathrin in the invagination and fission reactions or link them to the actin cytoskeleton, and include: dynamin, endophilin, amphiphysin, synaptojanin, eps15, syndapin, intersectin, auxilin, and hsc70 (Slepnev and De Camilli 2000).

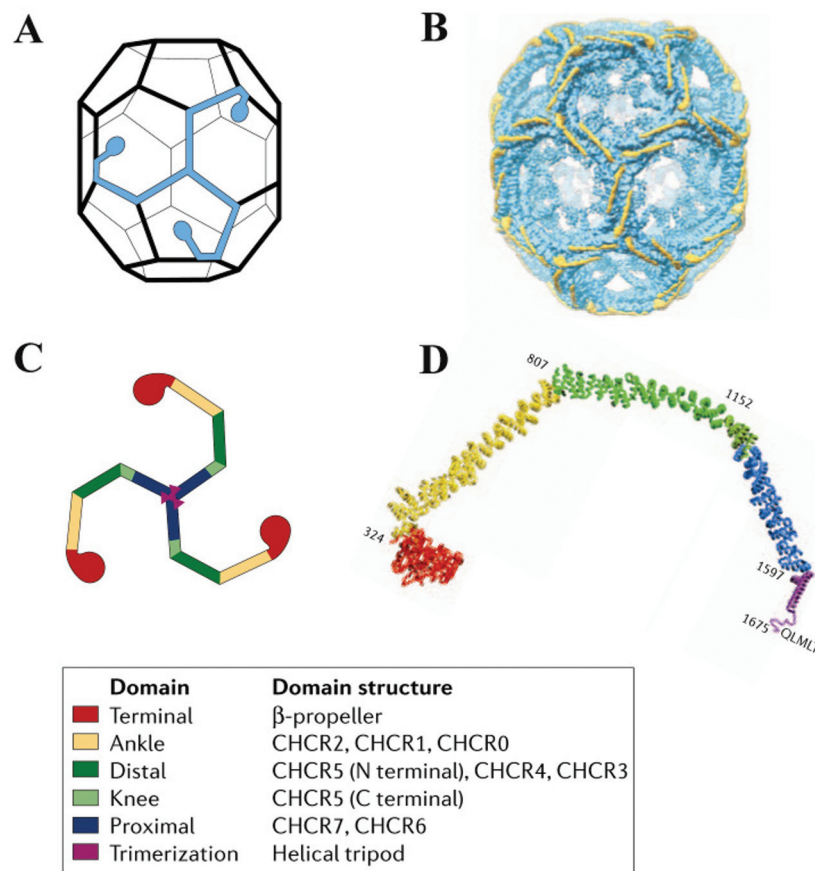


Figure 13. The architecture of clathrin: (A) Clathrin barrel with a single triskelion highlighted in blue. (B) An 8 Å reconstruction of a clathrin barrel with the light chains highlighted in yellow. (C) Schematic representation of a clathrin triskelion, which highlights the various domains using different colors (see the box). The clathrin-heavy-chain repeat (CHCR) modules that are involved in each domain are listed. (D) Single clathrin heavy chain molecule colored as in (C) (Edeling, Smith et al. 2006).

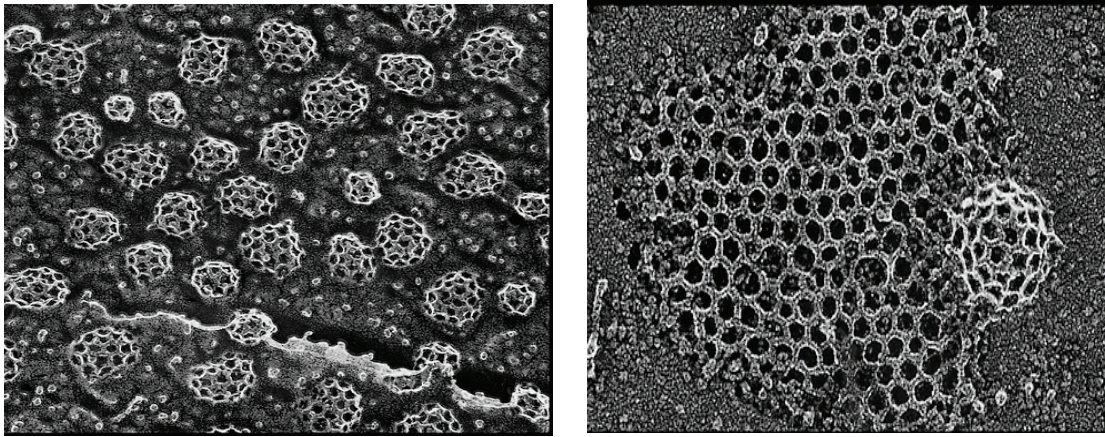


Figure 14. Clathrin lattice: Deep-etch view of a typical clathrin lattice found on the inside of cultured cells. Images are from (Heuser, Keen et al. 1987).



Figure 15: Sequential stages in clathrin-mediated endocytosis at the presynaptic terminal. Top: electron micrographs of clathrin-coated pit intermediates trapped at different stages by experimental manipulations in the lamprey reticulospinal synapse. Bottom: schematic representation of the endocytosis stages. **a)** microinjection of antibodies against endophilin followed by stimulation. **b, c)** microinjection of the SH3 domain of amphiphysin (b) or peptide PP15 (c), which corresponds to its cognate binding site in dynamin followed by stimulation. **d)** microinjection of the SH3 domain of endophilin followed by stimulation. **e, f)** dynamin-coated tubules induced by the incubation of broken synaptosomes with cytosol and GTP γ S. **g)** microinjection of the peptide PP-19, which blocks SH3-mediated interactions of endophilin (Slepnev and De Camilli 2000).

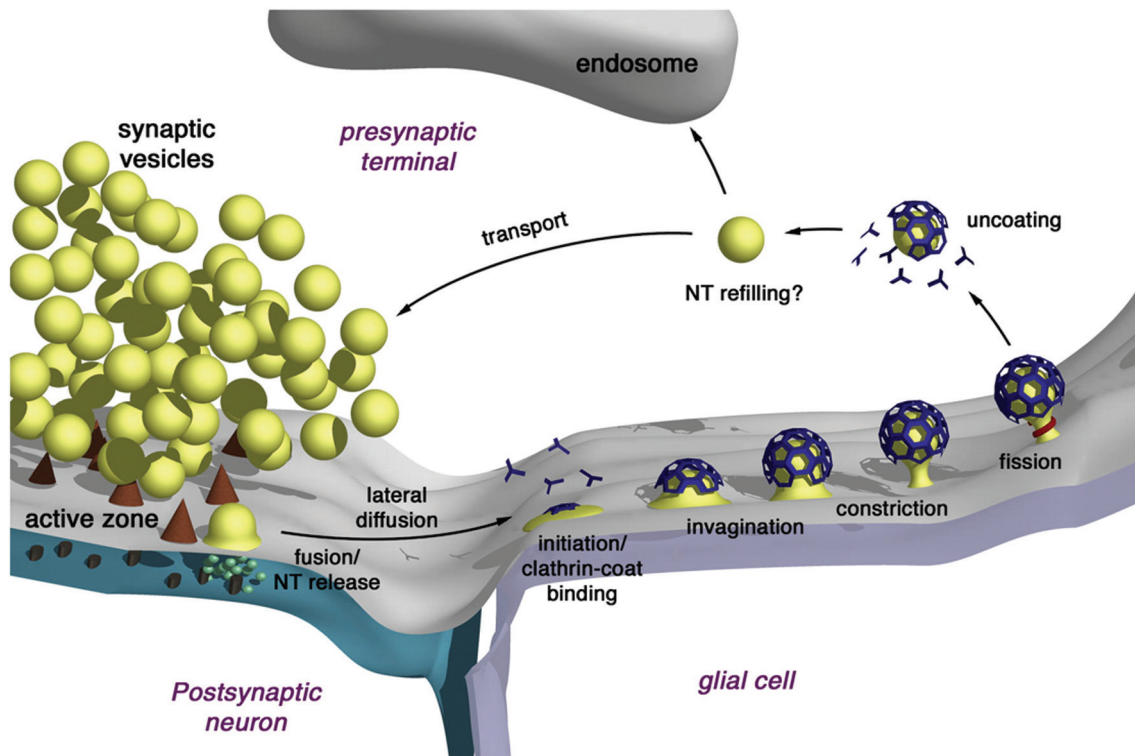


Figure 16. Model of clathrin-mediated synaptic vesicle endocytosis: Synaptic vesicles fuse with the presynaptic membrane at the active zone and release neurotransmitter into the synaptic cleft. The membrane of the fused vesicles then diffuses laterally to the areas outside the active zone where it is retrieved by CME. CCV formation involves several morphologically distinct steps, from clathrin coat binding, invagination of the coated bud, constriction and fission of the pit ‘neck’ and the subsequent stripping of the clathrin coat from the newly formed vesicle. The vesicle is then either directly transported back to the cluster of synaptic vesicles or to a primary endosomal compartment. During endocytosis and migration to the release site vesicles are refilled with transmitter (NT). Reproduced from (Shupliakov and Brodin 2010).

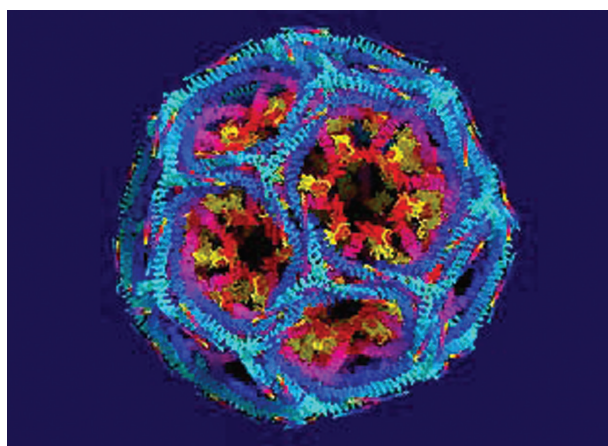
Studies have established that clathrin can be efficiently recruited onto protein-free liposomes (Takei, Haucke et al. 1998, Drake, Zhu et al. 2000, Baust, Czupalla et al. 2006). The GTP-binding protein ADP ribosylation factor (ARF) mediates assembly of clathrin-coated vesicles (CCVs) on liposomes and generates high-affinity membrane-binding sites for the AP-1 adaptor complex. The AP-1 recruits clathrin triskelia, which polymerize to form the coated vesicles. The efficacy of this process is dependent on the composition of the liposomes. Liposomes rich in PS and PI (Zhu, Traub et al. 1999) were the most efficient in binding AP-1 and recruiting clathrin triskelia. Thus, CCVs can use existing liposome technologies for drug delivery as they could be easily bioengineered and may prove cost-effective.

The clathrin lattice is about 100 fold stiffer than the typical liposomal membrane (Baba, Rauch et al. 2001). Also, the clathrin lattice has bending rigidity (285 ± 30 kBT) that is estimated to be 20 times higher than the rigidity of inner lipid vesicle (Jin, Prasad et al. 2006). Thus, clathrin coats improve stability and rigidity of the encapsulated lipid vesicle. Studies have also shown that clathrin-coated vesicles and clathrin baskets are resistant to trypsin digestion. The polygonal structure acquired by clathrin when organized into a basket or a CCV remained intact after about 1/3 of its mass was removed by digestion with trypsin (Schmid, Matsumoto et al. 1982, Zarrilli, Lippoldt et al. 1985). Clathrin triskelia are also resistant to pH changes and are able to self-assemble into clathrin cages and CCVs in pH ranges from 2 to 7 (Maezawa and Yoshimura 1990). These beneficial biophysical properties make clathrin a suitable biomaterial for design of nanoplatfoms.

Our data (Vitaliano, Vitaliano et al. 2012) indicate that non-toxic clathrin has the potential to serve as an extremely efficient CNS nanoplatfom for the following reasons: **1)** clathrin naturally crosses cell membranes, including an intact BBB (Gragera, Muniz et al. 1993), diffuses through the brain and also moves through synaptic clefts (Granseth, Odermatt et al. 2007); **2)** it actively transports substances inside the neurons (e.g., dopamine and its receptors); **3)** it plays an active role in endocytosis of CNS receptors, in cell signaling (Mills 2007), and in cell mitosis and in proliferation (Royle, Bright et al. 2005), **4)** it can be used to effectively deliver to specific brain regions different protein molecules (e.g., antibodies) by using *300 times lower doses* than reported in other BBB technologies studies and (Vitaliano and Vitaliano 2008), **5)** further, CTs can serve as robust platforms onto which multiple functional motifs can be added through genetic or chemical modifications; **6)** also, clathrin nanoplatfoms are size adjustable and can incorporate liposomes; and **7)** finally, clathrin can carry hundreds of molecules including drugs with poor solubility (e.g., calpain inhibitors) and/or drugs that cannot cross the intact BBB (e.g., antibodies) (Vitaliano, Vitaliano et al. 2012) (see Fig. 17). Dendrimers, nanogels, liposomes, solid-lipid nanoparticles and similar nanostructures maintain properties 5, 6 and 7, but not 1, 2, 3, and 4. Thus, our CT nanoplatfom (Vitaliano, Vitaliano et al. 2012) appears to be an appropriate new transport carrier for different therapeutic and diagnostic agents. We are proposing to use three innovative approaches: **1)** modify CTs for *in vivo* use; **2)** develop a new non-invasive brain delivery method for transporting and targeting Dopamine 3 antibody-nanoprobes; and **3)** test a new bio-nanotechnology method to demonstrate its feasibility for CNS antibody delivery.

The research we accomplish will enable us to develop new nanotechnology tools and techniques for targeted brain delivery of macromolecular drugs. Strategies for regional

delivery of macromolecular therapeutics in the brain are desirable, whether to prevent degeneration, induce recovery, or to be used to study regional brain structure or function. Specific targeting using low doses of drugs would have the potential to reduce side effects by limiting action at undesirable sites, which could make treatments more tolerable and may enhance efficacy of treatments and limit their toxicity.



- **Nontoxic and biodegradable**
- **No aggregation**
- **No opsonization**
- **No drug alteration**
- **Multi-cargo capacity**
- **Non-invasive BBB-passing**
- **Non-invasive Cell-passing**
- **Moves through CNS**
- **Targeted delivery**
- **Enhanced cell functions**
- **Enhanced drug functions**

Figure 17. Advantages of Clathrin Nanoparticles: Clathrin nanoparticle do not need to be modified to cross the BBB or penetrate cells. Clathrin can enhance ligand signaling and cell functions (Vitaliano and Vitaliano 2008).

Moreover, nasal delivery for noninvasively circumventing the BBB and providing dosing matched to brain-related needs would be a major clinical advance. This advance would be significant for the treatment of CNS diseases refractory to oral or injectable delivery routes, and also for enabling improved patient compliance. Psychiatric diseases involve several biochemical cell processes and signaling pathways and new multi-purpose drug nanocarriers may be required in the future to effectively treat these complex disorders. Clinical trials for treating cancer have clearly shown that multi-drug strategies are required for optimal therapeutic outcome. To date, multiple neuroprotective and psychotropic agents have not been delivered to the CNS via nanoparticles. Further, the project may lead to the development of a high-resolution, stable, molecular nanoprobe that can be used with different imaging modalities for research of molecular abnormalities in neuropsychiatric disorders. This study will provide data on the effectiveness of this new nanotechnology and build a foundation for future clinical applications. Numerous other possibilities exist for CT applications in research of neuroprotection and neuroregeneration, including assay, diagnostic, therapeutic, and prosthetic applications. Targeted, high precision dosing may also be done for genes, RNA interference and antisense gene therapeutics, as well as for other psychotropic drugs for treating brain disorders.

2. RESEARCH AIMS

AIM # 1: Develop and characterize new clathrin nanoparticles, demonstrate brain delivery in rats and determine which noninvasive method of administration is most efficacious: intranasal vs. intraperitoneal.

The goal of this AIM was to develop a new clathrin nanoplatform, which would then serve as a carrier for CNS delivery of large proteins (e.g., antibodies) and imaging agents. The intent was to develop a new nanotechnology for imaging and drug delivery that would have a high loading capacity sufficient to allow intranasal administration of antibodies and imaging agents in a 70 μ l volume of solution or less. Also, a nanoparticle loaded with Gd contrast agent should have high T1 relaxivity to permit future magnetic resonance imaging (MRI). The nanoparticle formulation should also protect the protein from proteolysis by enzymes or from phagocytosis by antigen processing cells. In addition, the ideal nanoparticle size should be less than 60 nm in order to increase nose to brain transport of antibodies and their CNS diffusion and penetration. The nanoparticle formulation should also provide sufficient physical and chemical stability in order to deliver intact antibodies to targeted brain structures.

AIM # 2: Develop and characterize clathrin nanoparticles with anti-dopamine 3 receptor antibodies and demonstrate that nanoparticle preparation does not compromise D3R antibody integrity and immunoreactivity.

The goal of this AIM was to develop clathrin nanoparticles for intranasal delivery of D3RABs, and to characterize nanoparticle formulation for particle size, loading efficiency, and protein integrity and immunoreactivity. Western Blot was performed to confirm antibody immunoreactivity in the nanoparticle preparation. The idea behind the WB test was that only an intact D3RAB would bind specifically to its receptor in brain cortical and cerebellar membranes, thereby permitting determination of whether the antibody remained immunoreactive and intact after the nanoparticle preparation process, which included the antibody PEGylation and crosslinking to clathrin nanoparticles. A blocking peptide that blocks immunoreactive sites on the antibody was used to test nanoparticle specificity for D3 receptor.

AIM # 3: Enable the new clathrin nanoparticle to bypass the BBB intranasally and deliver D3RABs to targeted D3R brain regions, and determine efficiency of delivery by comparing CNS concentrations of intranasally administered D3RABs with and without clathrin.

The goal of this AIM was to assess whether intranasally administered D3RAb-triskelia bypass the BBB and target D3R brain regions. This AIM consisted of two studies. The first study was a qualitative study to determine whether intranasally administered clathrin nanoparticles deliver D3Abs to targeted dopamine brain regions, and to assess whether there was an advantage to the clathrin nanoparticle formulation. Immunohistochemistry was used to qualitatively assess delivery and integrity of administered D3RAb-clathrin-nanoparticles in rat brains and to compare antibody vs. antibody-nanoparticle nose to brain transport. The expectation was that the intact D3R-Abs would be clearly visible only in D3R rat brain regions (e.g., islands of Calleja, ventral pallidum, nucleus accumbens etc.) after intranasal delivery of nanoparticles. In order to assess nanoparticle stability in D3R brain regions with confocal microscopy, fluorescent rhodamine-PEGs were attached to clathrin triskelia and D3R-Abs were labeled with Alexa 488 secondary antibodies. It was expected that D3RABs would co-localize with clathrin triskelia in rat brains if nanoparticles were completely intact after intranasal delivery.

The second study was a quantitative study to determine concentrations of D3RABs in different brain regions and to assess whether intranasal administration of nanoparticle formulation would provide greater CNS delivery of Abs than the intranasal administration of Abs formulation. The brains were collected 3 hours after intranasal delivery of nanoparticles, saline or Abs only. D3RAB concentrations in different brain regions were measured by ELISA and compared in animals that received Abs with clathrin vs. animals that received Abs without clathrin.

AIM # 4: Determine the toxicity of intranasally administered D3RAB-triskelia in healthy rats.

The goal of this AIM was to assess whether intranasally administered D3RAB-clathrin nanoparticle is toxic. To assess signs of toxicity, rats were examined every 30 minutes for lack of movement, ataxia, hunched posture, ruffled fur, hypothermia, dehydration, dyspnea, tachypnea, seizure and sustained rapid movement around the cage, one hour after intranasal delivery for 2 hours. Six additional rats continued to be examined every 24 h for 4 days. A 0 to 3 scale was used to evaluate each symptom (e.g., 0 = no symptom; 1 = mild; 2 = moderate; and 3 = severe symptom) and to calculate a total score. The nanoparticle toxicity was assessed by comparing the mean scores in rats that received nanoparticles versus controls. The cell damage was also assessed histologically four days after nanoparticle or saline administration by comparing different brain regions in rats that received nanoparticles vs. controls.

3. METHODS

3.1. Materials

Table 3. Materials and Reagents

ABC Vectastain elite kit (PK-6100) Vector Laboratories, Burlingame, CA.
Affinity Pure Rabbit Anti-Rat D3R IgG # 2 (D3R12-A) Alpha Diagnostic International, San Antonio, TX.
Alexa 488-goat anti-rabbit IgG antibody (A11008) 0.5ml: Invitrogen, Carlsbad, CA.
Ammonium Acetate (A1542) Sigma Aldrich, St. Louis, MO.
Amicon-Ultra-4 with 100 kDa MWCO, lab supplies, Millipore, Billerica, MA.
Arsenazo III (668-00-4): Sigma Aldrich Chemical Company, St. Louis, MO.
Biosafe stain (161-0786) Bio Rad, Hercules, CA.
Bovine serum albumin (BSA) (A3059) Sigma Aldrich, St. Louis, MO.
Bradford Quick start kit (500-020) Bio Rad, Hercules, CA.
Chloroform (288306) Sigma Aldrich Chemical Company, St. Louis, MO.
DAB substrate kit (SK-4100) Vector Laboratories, Burlingame, CA.
Dithiothreitol (DTT) (BP172-5) Fisher Scientific, Rockford, IL.
Dried milk bovine (M7409) Sigma Aldrich Chemical Company, St. Louis, MO.
Easy-Titer® IgG Assay Kits (23305) Thermo Scientific, Cambridge, MA.
ECL Western Blotting Detection Reagent, GE Healthcare, Pittsburgh, PA.
EGTA (E3889) Sigma Aldrich Chemical Company, St. Louis, MO.
Eosin-Y, Alcoholic 12372-87-1, Cancer Diagnostics, Durham, NC.
Ethyl alcohol: Sigma Aldrich, St. Louis, MO
Ficoll PM40 (17-0300-10) GE Healthcare, Pittsburgh, PA
FITC Labeling Kit (53004) Thermo Scientific, Cambridge, MA.
Fluoromount-G: Electron Microscopy Sciences, Hatfield, PA.

Gadolinium Chloride (10138-52-0) Sigma Aldrich, St. Louis, MO.
Goat anti-rabbit IgG antibody coupled to HRP (111-035-144): Jackson ImunoResearch Laboratories, West Grove, PA.
DTPA-ITC, Macrocyclics, Dallas, TX.
Heparin: Baxter Health Care Corporation, Deerfield, IL.
HEPES 7365-45-9, American Bioanalytical, Natick, MA.
Hydrogen peroxide (30%) (216763-100ML): Sigma Aldrich, St. Louis, MO.
IGEPAL CA 630 (I8896) Sigma Aldrich, St. Louis, MO.
Ketamine: Fort Dodge Animal Health (Wyeth), Madison, NJ.
Laemmli Sample Buffer (161-0737) Bio Rad, Hercules, CA.
Maleimide-PEG-NHS (MW 3500), JenKem Technology, Allen, TX.
Magnesium chloride (M9272) Sigma Aldrich, St. Louis, MO.
Mayer's Haematoxylin (517-28-2), Cancer Diagnostics, Durham, NC.
MaxiSorp® Nunc ELISA plates: Nalgene Nunc International, Rochester, NY.
Methanol (ACS) (67-56-1) Fisher Scientific, Pittsburgh, PA.
2- Methyl Butane; Sigma Aldrich Chemical Company, St. Louis, MO.
MES (145224-94-8) American Bioanalytical, Natick, MA.
MiniproteanTGX precast gels 10%, Bio Rad, Hercules, CA.
Neg-50 frozen section medium: Richard Allen Scientific, Kalamazoo, MI.
Nitric Acid (7697-37-2) Fisher Scientific, Pittsburgh, PA.
Normal goat serum (S-1000) Vector Laboratories, Burlingame, CA.
Paraformaldehyde: Sigma Aldrich Chemical Company, St. Louis, MO.
Peroxidase substrate kit DAB (SK-4100) Vector Laboratories, Burlingame, CA.
Phosphatase inhibitor cocktails (P-2850, P-5726) Sigma Aldrich, St. Louis, MO.
Phosphate buffered saline (PBS): Roche Diagnostic Corporation, Indianapolis, IN.
PMSF (P7626) Sigma Aldrich Chemical Company, St. Louis, MO.
Protease inhibitor cocktails (P-8340): Sigma Aldrich, St. Louis, MO.

Percision Plus protien all blue standards (161-0373) Bio Rad, Hercules, CA.
RIPA Lysis buffer (R0278): Sigma Aldrich Chemical Company, St. Louis, MO.
Rhodamine 110 chloride (432202) Sigma Aldrich Chemical Company, St. Louis, MO.
Sodium Acetate (127-09-3) Sigma Aldrich Chemical Company, St. Louis, MO.
Sodium azide (S2002) Sigma Aldrich Chemical Company, St. Louis, MO.
Sodium orthovanadate (S-6508) Sigma Aldrich Chemical Company, St. Louis, MO.
Sodium chloride (S9888) Sigma Aldrich Chemical Company, St. Louis, MO.
Sodium hydroxide (71690) Sigma Aldrich Chemical Company, St. Louis, MO.
Sodium carbonate (S-6139) Sigma Aldrich Chemical Company, St. Louis, MO.
Sprague-Dawley male rats: <i>Charles River Laboratories</i> , Newton, MA.
SureBlue™ TMB microwell peroxidase substrate (52-00-01): KPL, Gaithersburg, MD.
Sucrose (S0389) Sigma Aldrich Chemical Company, St. Louis, MO.
Syringe filters, 0.2 µm: Nalgene Nunc International, Rochester, NY.
TMB Stop Solution (50-85-05): KPL, Gaithersburg, MD.
Tris hydrochloride (1185-53-1) American Bioanalytical, Natick, MA.
Tris Glycine-SDS (10X) buffer (RGF-3390 KDM) Fisher Scientific, Pittsburgh, PA.
Tris Glycine (10X) blotting buffer (5089990115) Fisher Scientific, Pittsburgh, PA.
Triton X-100 (T8787) Sigma Aldrich Chemical Company, St. Louis, MO.
Tween 20 (P2287) Sigma Aldrich Chemical Company, St. Louis, MO.
Xylazine: Vetus Animal Health, Owings Mills, MD.
VectaShield Mounting medium with DAPI (H-1200) Vector Labs, Burlingame, CA.
Yttrium chloride (451363) Sigma Aldrich Chemical Company, St. Louis, MO.

The composition of the buffers was as follows: **a)** liver homogenization buffer consisted of 50 mM 2-(N-morpholino)ethanesulfonic acid (MES), 100 mM sodium chloride, 1 mM ethylene glycol tetraacetic acid (EGTA), 0.5 mM magnesium chloride, 0.02% sodium

azide, and 0.5 mM DL-dithiothreitol (DTT) (pH 6.5); **b**) triskelia “dissociation buffer”, Tris (tris(hydroxymethyl)-aminomethane) buffer, 0.5 M Tris-HCl, 3 mM dithiothreitol (DTT), the pH = 7; **c**) triskelia “chelation buffer”, HEPES [N-(2-Hydroxyethyl) piperazine-N'-ethanesulfonic acid] buffer, 0.1 M HEPES, the pH = 8.5; **d**) cages “assembly buffer”, MES [2-(N-morpholino) ethanesulfonic acid] buffer, 50 mM MES Na, 100 mM NaCl, 2 mM DTT, the pH = 6.5; **e**) phosphate buffer, 50 mM KH_2PO_4 , the pH (6.7-8.3) was adjusted with the addition of 0.1 M NaOH; **f**) 0.1 M ammonium acetate buffer, the pH (5.5-6); **g**) 0.15 M sodium acetate buffer, the pH = 4; and **h**) RIPA buffer contained 150 mM sodium chloride; 1% (v/v) Nonidet P-40; 0.5% (w/v) sodium deoxycholate; 0.1% (w/v) sodium dodecyl sulfate (SDS); 50 mM Tris base, and 10% (v/v) glycerol.

3.2. Isolation and Characterization of Clathrin Triskelia

3.2.1. Isolation of Clathrin Coated Vesicles (CCVs)

Clathrin-coated vesicles were isolated from fresh rat livers according to the published procedures (Campbell, Fine et al. 1983, Zhu, Drake et al. 2001) (Figure 18). Rat livers (330 g) were obtained from Sprague-Dawley (250 g) rats (Charles River Labs) and homogenized at 4°C in MES homogenization buffer (pH 6.5) using a Waring commercial blender. The MES buffer consisted of 50 mM 2-(N-morpholino)ethanesulfonic acid (MES), 100 mM sodium chloride, 1 mM ethylene glycol tetraacetic acid (EGTA), 0.5 mM magnesium chloride, 0.02% sodium azide, and 0.5 mM DL-dithiothreitol (DTT), and pH was adjusted to 6.5 with sodium hydroxide. The buffer volume to tissue weight ratio was 2:1. A protease inhibitor phenylmethylsulfonyl fluoride (PMSF) was added at a final concentration of 0.5 mM. The liver homogenate was first centrifuged at 11,900 rpm in a Sorvall GSA rotor for 45 min at 4°C. The resulting supernatants were decanted, pooled, and centrifuged at 40,000 rpm in a Beckman 45Ti rotor for 60 min at 4 °C. Pellets containing the coated vesicles were collected and re-suspended in a small volume of MES buffer by using a loose-fitting Dounce homogenizer. The suspension was then diluted with an equal volume of 12.5% Ficoll and 12.5% sucrose (both in MES buffer) and spun at 19,000 rpm in a Sorvall SS34 rotor for 40 min at 4°C. The supernatant was collected and diluted with 4 volumes of MES buffer, and coated vesicles pelleted for 60 min at 40,000 rpm in a Beckman 45Ti rotor. The pellet, containing crude clathrin-coated vesicles, was re-suspended in MES buffer (pH 6.5) using a Dounce homogenizer. CCVs were imaged with a Jeol 1200EX electron microscope (1200X Jeol, Tokyo, Japan). Contaminants (e.g., oval ribonucleoprotein structures or vaults) were found together with CCVs in the samples (Figure 19A). A final discontinuous sucrose gradient step (Zhu, Drake et al. 2001) was added to remove contaminating vaults (Fig. 19B).

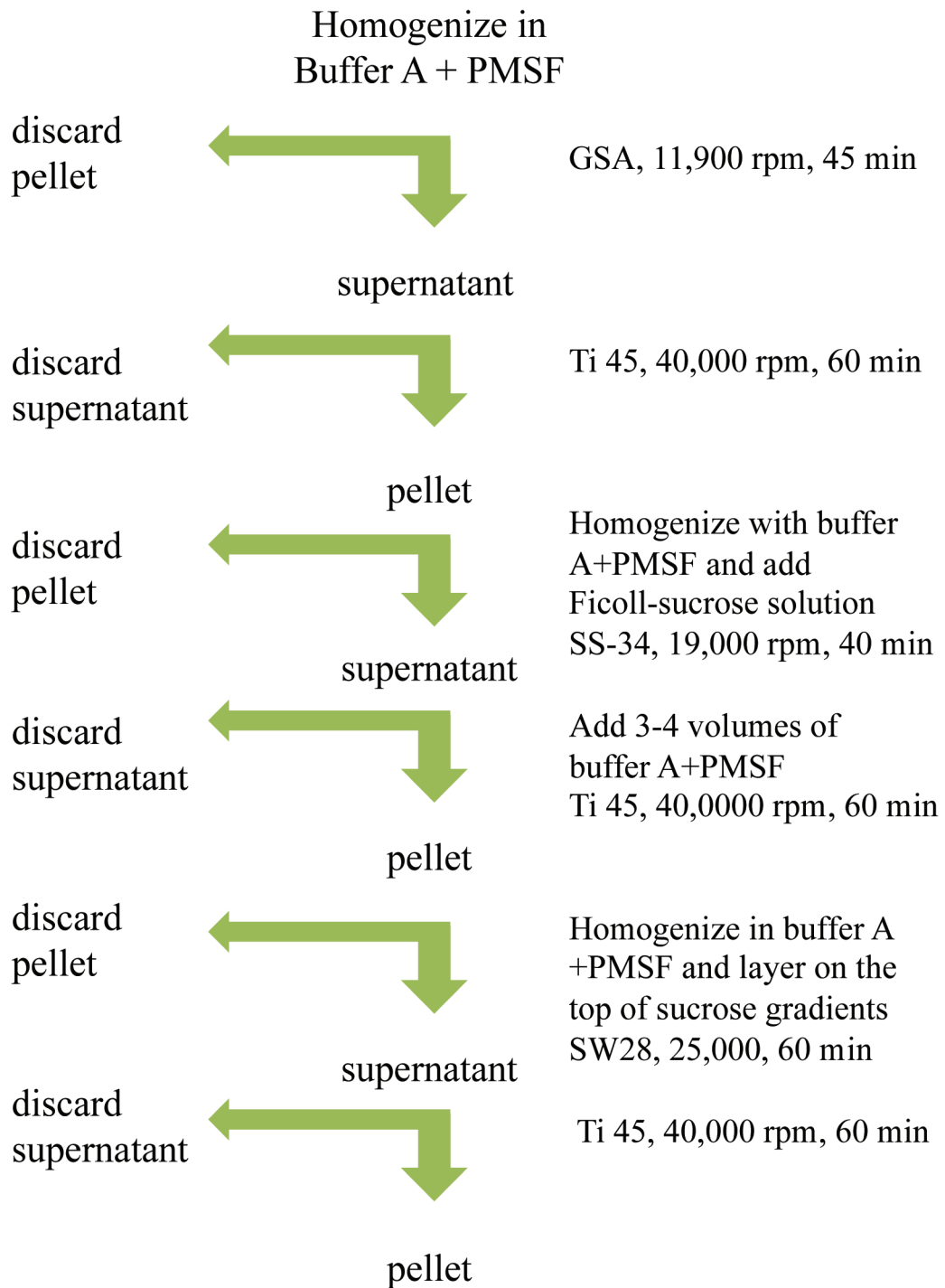


Figure 18. Purification scheme for clathrin-coated vesicles (CCVs)
(Vitaliano and Vitaliano 2008).

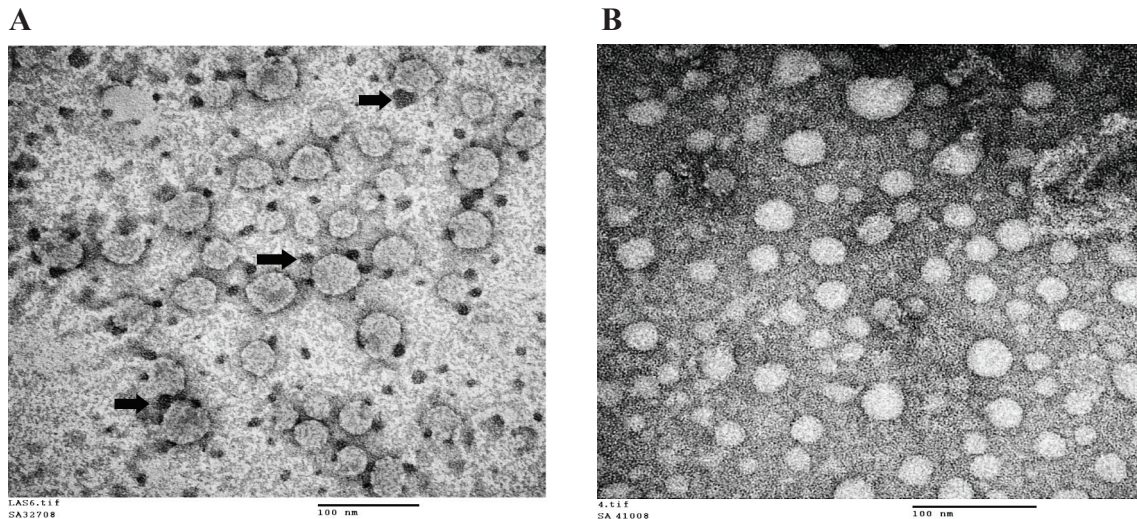


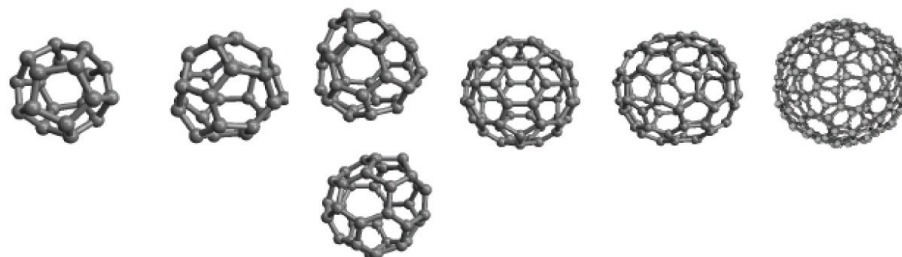
Figure 19. Images of CCVs isolated from rat livers before (A) and after (B) the purification: Vaults (black arrows) were removed with a discontinuous sucrose gradient step. The scale bar is 100 nm (Vitaliano and Vitaliano 2008).

First, sucrose gradient solutions (40%, 30%, 20%, 10% and 5%) were prepared in MES buffer. The pellet from the last step was re-suspended in MES buffer (pH 6.5) using a Dounce homogenizer. Discontinuous sucrose gradients were then prepared in SW28 tubes by layering (bottom to top) the following: 5 ml 40% sucrose, 5 ml 30% sucrose, 6 ml 20% sucrose, 8.5 ml 10% sucrose, and 8.5 ml 5% sucrose. The crude CCV preparation (4-5 ml) was laid on top of the gradient and centrifuged at 25,000 rpm (100,000 g) in an SW28 rotor for 1 hr at 4°C. Twenty-six 1.5-ml fractions were collected from the top. SDS PAGE analyses indicated that CCVs moved into the 10-30% sucrose layers while the vaults remained in the 5% sucrose layer.

The fractions containing CCVs (typically fractions 12-21 as numbered from the top of the gradient) were mixed, diluted with 3 volumes of MES buffer, and collected by centrifugation at 40,000 rpm in a Beckman 45 Ti rotor for 1 hr at 4°C. The resultant CCV pellet was re-suspended in MES buffer with a Dounce homogenizer, quickly frozen on dry ice, and stored in small aliquots at -80 °C.

In CCVs clathrin triskelia legs create a lattice of hexagonal and pentagonal faces, and isolated CCVs can exhibit a range of three-dimensional designs (see Table 4). The most frequently formed cage-like structures are built from 28, 36, and 60 triskelia, which, respectively, are a ‘mini-coat’ with tetrahedral symmetry, a ‘hexagonal barrel’ with D6 symmetry, and a ‘soccer ball’ with icosahedral symmetry (Figure 20).

Table 4. Clathrin Fullerene Structures (Vitaliano and Vitaliano 2008)



CCVs	cells	cells	cells	neurons	hepatocytes	fibroblasts
Bucky-ball-like	C_{20}	C_{28}	C_{36}	C_{60}	C_{82}	C_{140}
Hexagons	0	4	8	20	30	60
Triskelia	20	28	36	60	82	140
Heavy Chains	60	84	108	180	246	420
Diameter	40	50	60	76	90	120
Mol. Weight (MDa)	13	18	23	38	53	77

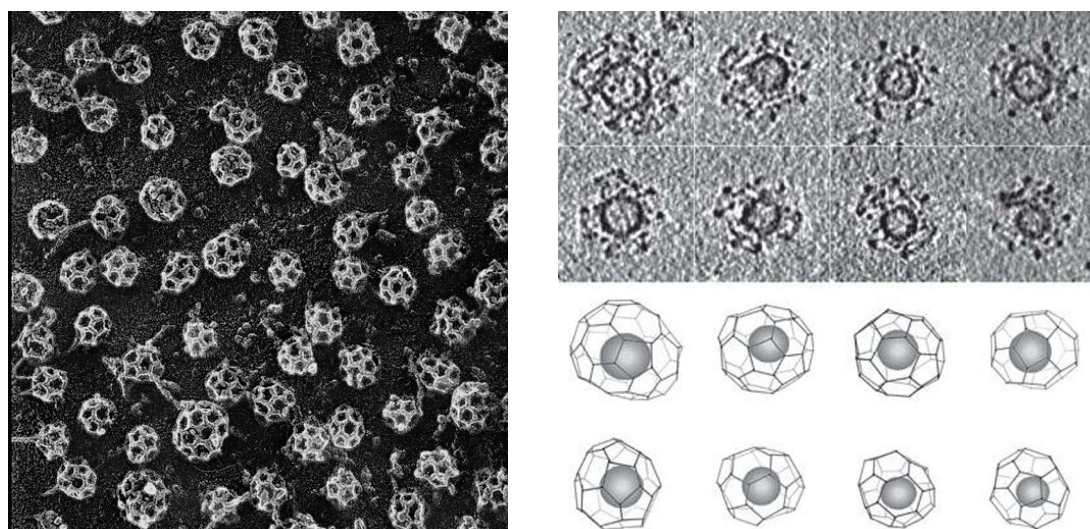


Figure 20. Images of clathrin fullerene structures: CCs image #14 from Heuser lab (Left); CCVs (Right) examined by electron cryotomography (Top) Gallery of central sections through tomograms of individual coated vesicles. (Bottom) Drawing of corresponding lattices, with position of vesicle shown (Cheng, Boll et al. 2007).

Table 5. The Major Protein Components of Clathrin Coated Vesicles (Vitaliano and Vitaliano 2008)

CCVs	Proteins	Mol Wt (KDa) (SDS-PAGE-based)
Triskelion	clathrin heavy-chain	180
	clathrin light-chain LCa	34
	clathrin light-chain LCb	32
AP-2 adaptors (plasma membrane derived)	alpha A	112
	beta 2	106
	alpha C	105
	mu 2 or AP50	50
	sigma 2 or AP17	17
AP-1 adaptors (Golgi-derived)	beta 1	110
	gamma	104
	mu 1 or AP47	47
	sigma 1 or AP20	20

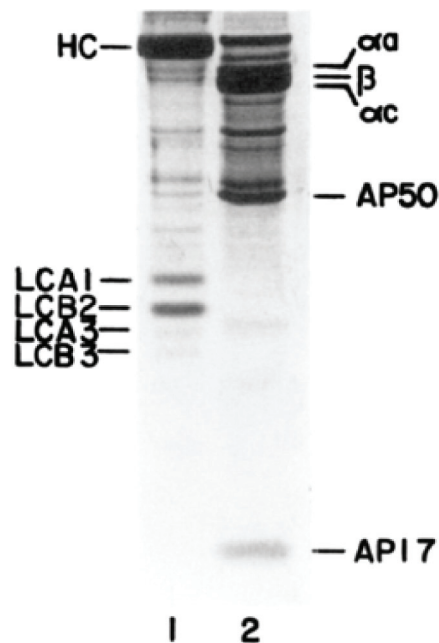


Figure 21. SDS-PAGE analysis of clathrin and its associated protein complex: Clathrin and its associated protein complex AP-2 were fractionated by SDS-13% PAGE and stained with coomassie blue (Matsui and Kirchhausen 1990).

The major protein components of CCVs were presented in Table 5 and Figure 21. AP-I complexes, found in association with clathrin-coated structures localized at the Golgi apparatus, and AP-2 complexes, associated with similar structures at the plasma membrane. Under physiological conditions, APs interact with clathrin to assemble a stable coat that forms the cytoplasmic lattices surrounding coated pits and coated vesicles. In CCVs the APs lie between the clathrin lattice and the lipid membrane of coated vesicles (Matsui and Kirchhausen 1990).

3.2.2. Isolation of Clathrin Triskelia (CTs)

Soluble clathrin coat proteins, mainly clathrin triskelia and adaptor proteins (APs) were released from purified clathrin-coated vesicles with a dissociation buffer 0.5 M tris(hydroxymethyl)-aminomethane (Tris-HCl, pH 7.4) according to published protocols (Keen, Willingham et al. 1979, Jackson 1993). The frozen clathrin-coated vesicles in MES buffer were thawed and mixed with an equal volume of 1.0 M Tris buffer (pH 7) on ice for 10 min. The soluble coat proteins are separated from the residual clathrin-coated vesicle membranes by centrifugation at 40,000 rpm for 60 min at 4 °C in a Beckman 70.1 Ti rotor. The sample was then loaded onto a 3 x 100 cm column of Sepharose CL-4B that was pre-equilibrated in 0.5 M Tris buffer (pH 7.4) containing 0.02% sodium azide and 0.5 mM DTT. After about 2 to 3 hrs, a void appeared and 5 ml fractions were collected at a flow rate of 30 ml/hour. Clathrin appears as a broad peak after the void, followed by a small peak containing adaptor proteins (AP-1 and AP-2) (Figure 22). Triskelion and adaptor peak fractions were collected separately and concentrated using Amicon-Ultra-4 ultrafiltration devices (Millipore, Billerica, MA).

3.2.3. Clathrin Triskelia Self-assembly and Characterization

To test clathrin triskelia function, clathrin cages were assembled by mixing clathrin triskelia and AP-2 proteins at a ratio of 3:1 (v/v) according to the standard method (Fotin, Cheng et al. 2004) The mixture was dialyzed against MES buffer (50 mM MES Na, pH 6.5, 100 mM NaCl, 2 mM DTT) two times for 12 hours at 4°C. The relatively high NaCl concentration in the MES buffer was used to facilitate formation of D6 barrel CCs. Aggregated protein was removed by centrifugation in an Eppendorf centrifuge at 15,000 rpm at 4°C for 10 min. Assembled cages were separated from unassembled triskelia by high-speed centrifugation at 60,000 rpm in a TLA-100.4 rotor (Beckman Coulter, US) at 4°C for 12 min, and then re-suspended in MES buffer (20 mM MES Na, pH 6.2, 2 mM DTT).

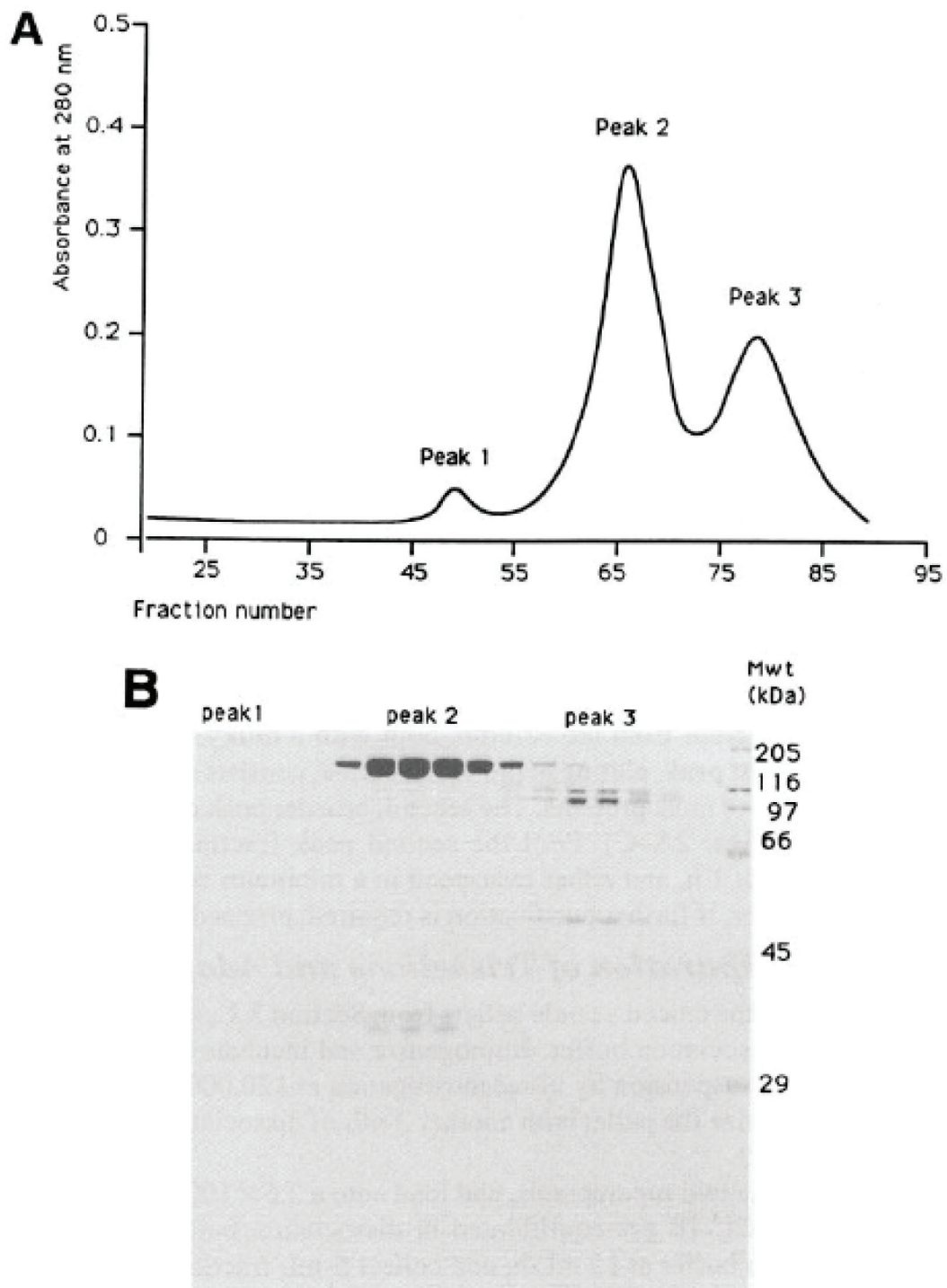


Figure 22. Gel filtration of triskelia and adaptors on Sepharose CL-4B: (A) Elution profile. (B) Analysis of peak fraction by SDS-PAGE (Jackson 1993).

To determine protein concentration by Bradford protein assay (Bio Rad, Hercules, CA) Clathrin triskelia solution was dialyzed against at least a 500-fold volume excess of phosphate buffered saline (PBS buffer, pH 7.4) for 8 hours. Clathrin triskelia were characterized by Electron Microscopy (1200X Jeol, Tokyo, Japan), SDS-PAGE (Bio Rad, Hercules, CA) and diffusion light scattering methods (550-LB, Horiba, Kyoto, Japan) using published methods (Vitaliano, Vitaliano et al. 2012).

Transmission Electron Microscopy (TEM) analysis of nanoparticle size and structure was performed on a Jeol 1200EX electron microscope (Jeol, Tokyo, Japan). About 5 μ L of protein solution (0.05 mg/ ml) was applied to carbon-coated copper grids for 3 minutes. The grids were rinsed with ddH₂O, exposed to 5 μ L of 1% solution of uranyl acetate (UA), and dried before imaging.

Dynamic Light Scattering (DLS) was performed using a LB-550 (Horiba, Kyoto, Japan) to confirm size and uniformity of nanoparticles.

Sodium dodecyl sulfate-polyacrylamide gel electrophoresis (SDS-PAGE) was performed on a Mini-Protean apparatus (Bio-Rad, Hercules, CA). Visualization of protein bands was accomplished by Coomassie Brilliant Blue staining (Bio-Rad, Hercules, CA). Commercially available standards (Bio-Rad, Hercules, CA), and NIH ImageJ software (<http://rsb.info.nih.gov/ij>) with MolWt macro (<http://www.phase-hl.com/imagej.htm>) were used for estimation of molecular weights.

3.2.4. Chelation of Clathrin Triskelia

A 120-fold molar excess of 2-(4-Isothiocyanatobenzyl)-diethylene-triamine-pentaacetic acid (DTPA-ITC, Macrocyclics, Dallas, TX) was added to triskelia (5 mg/ml) in 0.1 M HEPES [N-(2-Hydroxyethyl) piperazine-N'-ethanesulfonic acid] buffer, (pH 8.5) and incubated for 8 hours at 4°C. Chelating agent was conjugated to protein through lysine residues (Fig. 24) (Mirzadeh, Brechbiel et al. 1990).

Protein was then washed 6 times in 0.1 M ammonium acetate (pH 6) by using Amicon-Ultra-4 with 100 kDa MWCO (Millipore, Billerica, MA) according to the published method (Cooper, Sabbah et al. 2006). Protein concentration was determined by Bradford protein assay (Bio-Rad, Hercules, CA).

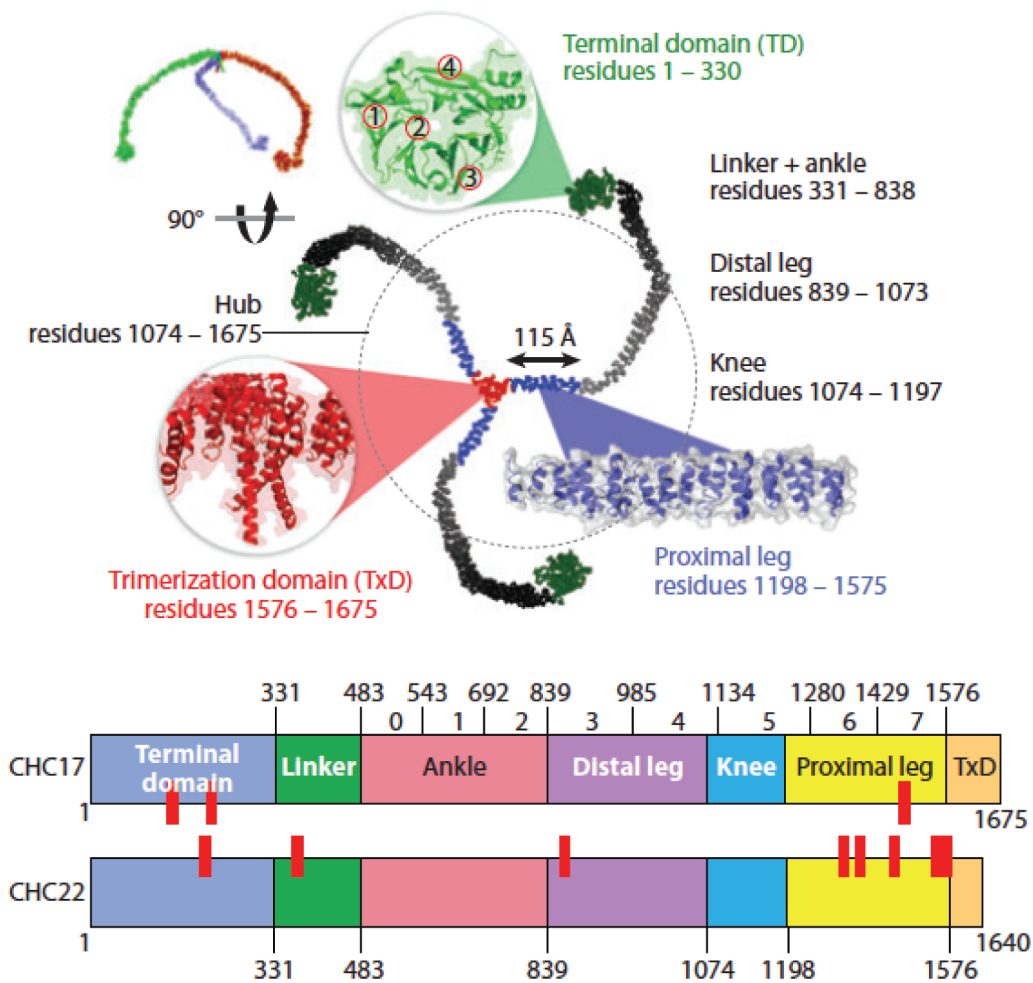


Figure 23. Structural features of clathrin heavy chains (Brodsky 2012): The domain structures and amino acid boundaries are indicated for functional domains of CHC17. The structures reproduced are from PyMol (triskelion-accession number 3IYV; trimerization domain-accession number 3LVH; terminal domain-accession number 2XZG; proximal leg-accession number 1B89) and are based on Fotin et al. (2004b), ter Haar et al. (1998), and Ybe et al. (1999). The four numbered sites on the terminal domain structure represent binding sites for interacting proteins based on Lemmon & Traub (2012). At the bottom, the predicted domain structure of CHC22 is aligned with CHC17, and the amino acid boundaries of the eight clathrin heavy chain repeats (CHCR 0–7) in CHC17 are delineated.

Ligand (DTPA-ITC) to protein molar ratio was determined by using a spectrophotometric method (Pippin, Parker et al. 1992) that was based on reaction between DTPA-ITC-protein conjugate and yttrium (Y^{3+}) complex of arsenazo III. Arsenazo III is a highly sensitive colorimetric reagent for yttrium and other metal ions. A 500 ml stock solution of the Y^{3+} -arsenazo III complex contained: 5 μ M arsenazo III, 1.6 μ M Y^{3+} and 0.15 M sodium

acetate buffer (pH 4). From 10 to 60 μL of 0.123 mM DTPA-ITC were added serially to the cuvette that contained Y^{3+} -arsenazo III complex.

Absorbance values were measured at 652 nm by using the Spectronic GENESYS 10 Bio spectrophotometer (Thermo Electron Corp., Madison, WI) and a calibration plot constructed. Then, from 20 to 80 μL of DTPA-ITC-protein conjugate were added to the Y^{3+} -arsenazo III complex, and absorbance values were recorded after 10-15 minutes at 652 nm. Unknown concentrations of DTPA-ITC were calculated by using a calibration plot and the following expression:

$$x = (y - 0.11) / -0.046$$

where x represents an unknown concentration of DTPA-ITC, and y is the sample absorbance at 652 nm. After correction for protein dilution, ligand to protein molar ratio was determined. These experiments were done in triplicate.

```
MAQILPIRFQEHLLQLQNLGINPANIGFSTLTMESDKFICIREKVGGEQAQVVIIDMNDPSN
PIRRPISADSAIMNPASKVIALKAGKTLQIFNIEMKSKMKAHTMTDDVTFWKWISLNTVA
LVTDNAVYHWSMEGESQPVKMFDRHSSLAGCQIINYRTDAKQKWLTTGISAQQNRVVGGA
MQLYSVDRKVSQPIEGHAASFAQFKMEGNAEESTLFCFAVRGQAGGKLHIEVGTPTGN
QPFPPKAVDVFFPPEAQNDFPVAMQISEKHDVVFLITKYGYIHLVDLETGTCIYMNRI SG
ETIFVTAPHEATAGIIGVNRKGQVLSVCVEEENIIPYITNVLQNPDLALRMAVRNNLAGA
EELFARKFNALFAQGNYSAAKVAANAPKGI LRTPDTIRRFQSVPAQPGQTSPLLOYFGI
LLDQGLNKYESLELCRPVLQQGRKQLEKWLKEDKLECEELGDLVKSVDPTLALSIVYL
RANVPNKVIQCFAETGQVQKIVLYAKKVGYPDWIFLLRNVMRISPDQGGQFAQMLVQDE
EPLADITQIVDVFMENLIQQCTAFLLDALKNNRPSEGPLQTRLLEMNLMHAPQVADAIL
GNQMFTHYDRAHIAQLCEKAGLLQRALEHFTDLYDIKRAVVHTHLLNPEWL VNYFGSLSV
EDSLECLRAML SANIRQNLQIWWQVASKYHEQLSTQSLIELFESFKSFEGLFYFLGSI VN
FSQDPDVHFYKIQAAACKTGQIKEVERICRESNCYDPERVKNFLKEAKLTDQLPLIIVCDR
FDFVHDLVLYLYRNSLQKYIEIYVQKVNPSRLPVVIGLLDVCSEDEVIKNLIIVVRGQF
STDELVAEVEKRNRLKLLLPWLEARIHEGCEEPATHNALAKIYIDSNNNPERFLRENPHY
DSRVVGKYCEKRDPHLACVAYERGQCDELINVCNENSLFKSLSRYLVRRKDPELWGSVL
LESNPHYRRPLIDQVVQTALSETQDPEEVSVTVKAFMTADLPNELIELEKIVLDNSVFSE
HRNLQNLILITAIKADRTRVMEYINRLDNYDAPDIANIAISNELFEEFAIFRKFVNTS
AVQVLI EHI GNLDRAEFYFAERCNEPAVWSQLAKAQLQKGMVKEAIDSYIKADDPSSYMEV
VQAANTSGNWEELVKYLQMARKKARES YVETELIFALAKTNRLAELEEFINGPNNAHIQQ
VGDRCYDEKMYDAAKLLYNNVSNFGRLASTLVHLGEYQAAVDGARKANSTRTWKEVCFAC
VDGKEFRLAQMCGLHIVVHADELEELINYQDRGYFEELITMLEAALGLERAHMGMTTEL
AILYSKFKPKQKREHLELFWSRVNI PKVLRAAEQAHLWAEVFLYDKYEEYDNAIITMMN
HPTDAWKEGQFKDIITKVANVELYYKAIQFYLEFKPLLLNDLLMVLSPRLAHTRAVNYFS
KVKQLPLVKPYLRSVQNHNNKSVNESLNNLFI TEEDYQALRTSIDAYDNFDNISLAQRLE
KHELIEFRRIAAYLFKGNRNRWKQSVELCKKDSLYKDAMQYASESKDTELAEELLQWFLQE
EKRECFGACLF TICYDLLRPDVVLETAWRHNIMDFAMPYFIQVMKEYLTKVDKLDASESLR
KEEEQATETQPIVYGGPQLMLTAGPSVAVPPQAPFGYGYTAPPYGGPQPGFGYSM
```

Figure 24. Rat Clathrin Heavy Chain (Cltc) with 1675 amino acids (FESTA format).

Lysines (K) and Cysteines (C) were used for modifications;

<http://www.uniprot.org/uniprot/P11442.fasta>

3.2.5. Preparation of Gadolinium-DTPA-Triskelia

Modifications of proteins with Gd-chelates are often performed in two different buffers (Cooper, Sabbah et al. 2006). Protein chelation is often performed in basic buffers, while metallation with gadolinium is performed in acidic buffers. To avoid modifying triskelia in acidic buffers, Gd-chelates were prepared separately in ammonium acetate buffer (pH 5.5). Acidic buffers are not optimal for triskelia, because triskelia can assemble into polyhedral cages at low pH (< 6.5) (Crowther and Pearse 1981). Based on spectrophotometric results, 81-fold molar excess of DTPA-ITC (over the amount of triskelia) was solubilised in 100 mM ammonium acetate and pH adjusted to pH 5.5 with acetic acid. Then, 0.9 equivalents of gadolinium chloride were added and reaction incubated at 37°C for 2 hours (Anderson, Isaacman et al. 2006). An aliquot of gadolinium-DTPA-ITC was assayed for free gadolinium content using arsenazo III (Gouin and Winnik 2001). Finally, clathrin triskelia in concentration of about 5 mg/ml in 0.1 M HEPES buffer (pH 8.5) were mixed with prepared Gd-DTPA-ITC for 8 hours at 4°C. Unconjugated ligand was separated from the nanoplatfroms by dialysis (two times) against a 500-fold volume excess of phosphate buffered saline (PBS) (pH 7.4) at 4°C for 24 hr. Protein concentration was determined by Bradford protein assay (Bio-Rad, Hercules, CA).

Sodium dodecyl sulfate-polyacrylamide gel electrophoresis (SDS-PAGE) was performed on a Mini-Protean apparatus (Bio-Rad, Hercules, CA). Visualization of protein bands was accomplished by Coomassie Brilliant Blue staining (Bio-Rad, Hercules, CA). Commercially available standards (Bio-Rad, Hercules, CA), and NIH ImageJ software (<http://rsb.info.nih.gov/ij>) with MolWt macro (<http://www.phase-hl.com/imagej.htm>) were used for the estimation of molecular weights. Analysis of nanoparticle size and structure was performed on a Jeol 1200 EX electron microscope (Jeol, Tokyo, Japan). DLS was performed using a LB-550 (Horiba, Kyoto, Japan) to confirm size and uniformity of nanoparticles.

3.2.6. T₁ Relaxivity of Gd-DTPA-Triskelia

In vitro relaxivity (r_1) of Gadolinium-DTPA-ITC-nanoparticles was established using a 0.47 T Bruker Minispec NMR system (Bruker, Billerica, MA) at 40°C. The longitudinal relaxation rate ($R_1 = 1/T_1$) was determined from 20 experimental time points generated by an inversion recovery pulse sequence. Longitudinal relaxivity (r_1) was calculated from the slope of linear least squares fit of $1/T_1$ as a function of Gd³⁺ concentration for different protein concentrations. Triskelia nanoplatfroms were in PBS buffer (pH 7.4), the

relaxation rate of the PBS buffer was ($R_{\text{PBS}} = 0.2317$), and protein concentration was from 717.64 nmol/L to 5,741.16 nmol/L.

The gadolinium concentration of nanoparticle solutions was measured by a relaxometric procedure according to the standard method (Datta, Hooker et al. 2008). These experiments were performed in triplicate. Briefly, a volume of 750 μL of each solution was added to 750 μL of 70% HNO_3 directly into a glass ampoule. After gentle centrifugation (1500 rpm, 3 min) ampoules were sealed and heated at 120°C for 5 days to ensure that all Gd^{3+} was solubilized as free aqua ion. Then the water proton T_1 of these solutions was measured at 20 MHz and 40°C, and Gd^{3+} concentration in starting solutions determined from a standard curve obtained using standard GdCl_3 solutions (0.0125 – 0.4 mM), and by using the following expression:

$$[\text{Gd}] = \frac{[R_1^* - R_{1B}]}{r_1} \times 2$$

where r_1 is the relaxivity ($\text{mM}^{-1}\text{s}^{-1}$) of the aqua ion under identical standard experimental conditions, R_1^* (s^{-1}) is the relaxation rate of the sample, and R_{1B} (s^{-1}) is the relaxation rate of the solution.

3.2.7. Preparation of Fluorescent FITC-Triskelia

In order to qualitatively determine brain distribution of nanoparticles, clathrin triskelia were modified with fluorescent tags. Brain distribution of clathrin triskelia was assessed in rats using fluorescent analysis of nanoparticles carrying fluorescein-isothiocyanate (FITC, Pierce, Rockford, IL) following intranasal and intraperitoneal administration. Fluorescent FITC labels were conjugated to triskelia through reactive lysine residues using a Pierce FITC Labeling Kit (Pierce, Rockford, IL). Protein was first dialyzed in BupH Borate Buffer and a 27-fold molar excess of fluorescent dye was then added to the protein and sample was incubated for 1 h at RT. Excess dye was removed by dialysis and fluorescent-tag to protein molar ratio was determined by spectrophotometric analyses using manufacturer's instructions and SDS-PAGE analyses. Dynamic light scattering was performed using a LB-550 (Horiba, Kyoto, Japan) to confirm size and uniformity of nanoparticles.

3.2.8. Administration of FITC-Triskelia in Rats

Experiments were conducted in accordance with National Institutes of Health 1996 Guide for the Care and Use of Laboratory Animals and approved by McLean Hospital's Institutional Animal Care and Use Committee (Protocol #07-6/2-21). Male Sprague

Dawley (SD) rats (250-300 g) (Charles River, MA) were housed with ad libitum food and water in constant temperature and humidity conditions on a 12 hr. light/dark cycle.

Male Sprague-Dawley (SD) rats (250-300 g) were anesthetized with a mixture of ketamine/xylazine, at a dose of 80 and 20 mg/kg, respectively, and were placed in a supine position with their noses at an upright 90° angle (Dhuria, Hanson et al. 2010). Preliminary studies demonstrated that bolus administration of volumes >8 µl per nostril resulted in respiratory distress. Therefore, the administered volume was limited to 5 µl increments, staggered every 4 min, alternating nares for a total of 35 µl per side. Administration was performed using a 10 µl Hamilton syringe fitted with a 1 cm segment of PE20 tubing (Braintree Scientific). The mouth and the opposite naris were closed during nanoparticle administration so the drops could be naturally aspirated. The total administered dose was 33.3 µg of clathrin protein in 70 µl of PBS (pH 7.4) per rat. This protein dose was chosen based on review of the literature, which indicated that 33 µg was within the range of protein doses that was used for imaging and/or provided therapeutic effects in rats after intranasal administration. For intraperitoneal administrations 124 µg of protein in 250 µl of PBS (pH 7.4) was used.

3.2.9. Transcardial Perfusion with 4% Paraformaldehyde

Animals (n = 4 per time point) were sacrificed and perfused at 30, 60 and 90 minutes following nanoparticle administration. Control animals (n = 2) that did not receive any nanoparticles were also sacrificed and perfused before starting experiments with nanoparticles. Male Sprague-Dawley (SD) rats (250-300 g) were deeply anesthetized with a bolus of sodium pentobarbital (Nembutal, 120 mg/kg). Rats were perfused transcardially with 4% paraformaldehyde before being sacrificed.

Each rat was placed in a supine position, and an incision was made below the sternum at the level of the xiphoid process. The diaphragm was then cut, and the heart was exposed. A needle was inserted into the left ventricle, and 1 ml of cold heparin (1,000 units/ml) was injected to prevent blood from clotting. The needle was removed, and a perfusion needle was then inserted into the same opening in the left ventricle. In order to allow the blood to drain freely, a cut in the right atrium was made. Each rat was infused with about 300 ml of cold PBS (pH 7.4) into the left ventricle until the color of the liver changed from maroon to a light tan, indicating that all of the blood had been flushed. At that point about 250-350 ml of freshly prepared, cold 4% paraformaldehyde in PBS was infused into the left ventricle until the rat became stiff.

Brains were then removed and submerged in 4% paraformaldehyde in PBS and post-fixed for 6-8 hours. The brains were transferred to a vial containing 30% sucrose in PBS and refrigerated for about 48-72 hours until they sunk to the bottom of the vial. Brains were embedded in OCT, quickly frozen in dry ice-cooled 2-methylbutane and stored at -80°C until use.

3.2.10. Biodistribution of Fluorescent Clathrin Triskelia

Coronal sections, 30 µm thick, were cut along the rostral to caudal axis of the brain using a cryostat. Representative sections were taken at the level of the olfactory bulb, frontal cortex, striatum, basal forebrain, hippocampus, midbrain, and posterior regions including the cerebellum. Sections were mounted on Super Frost Plus slides (Fisher Scientific, Pittsburgh, PA), dried, and coverslipped using Vectashield mounting medium (Vector Laboratories, CA). Each section was examined by fluorescence microscopy using a Zeis Axio Scope A1 photomicroscope (Zeiss, Thornwood, NY) at 40 X magnification to localize clusters of green fluorescent deposits that were either scattered throughout the neuropil or localized within cells.

3.3. Characterization of Dopamine-3-receptor-Antibody-Triskelia

3.3.1. Crosslinking of Triskelia with Dopamine-3 Receptor Antibodies

The antibody in this experiment is a rabbit anti-rat dopamine D3 receptor antibody (D3R-Ab), which recognizes the 3rd intracellular domain (amino acids 288 to 306, QPPSPGQTHGGLKRYYSIC) (Figure 25) of the rat dopamine D3 receptor (Cat. # D3R12-A, Alpha Diagnostic International, San Antonio, TX). This D3R amino acid sequence is 88% conserved in mouse and 63% in human and monkey D3R receptors. There is no significant sequence homology with other dopamine receptors (D1, D2, D4 or D5). This antibody was selected because it has high affinity and specificity for the D3 receptors, and can label receptors in the plasma membrane and cytoplasm (Khan, Gutierrez et al. 1998, Wolstencroft, Simic et al. 2007). Also, D3 receptors in rats have a restricted distribution that is largely limited to mesolimbic regions (Le Foll, Wilson et al. 2014). Moreover, research suggests that D3-selective antagonists may be of value in treatment of mood disorders, drug dependence and psychosis (Section 1.2.).

Maleimide-PEG-NHS (MW 3500, JenKem Technology, Allen, TX) was used to

crosslink the D3R-Ab to clathrin triskelia. A 10-fold molar excess of Maleimide-PEG-NHS was added to D3R-Abs (1 mg/ml) in PBS buffer (pH 7.4) and incubated for 2 hours at 23°C. PEGs were attached to the primary amines (-NH₂) of D3R-Ab lysine residues. Unconjugated PEGs were removed by ultrafiltration using Amicon-Ultra tubes with 100 kDa MWCO (Millipore, Billerica, MA).

PEGylated D3R-Abs were then incubated with clathrin protein (4.3 mg/ml) at 1:1 molar ratio overnight in PBS (pH 7.4) at 4°C. Maleimide in PEGs reacted specifically with sulfhydryl groups (-SH) of clathrin cysteine residues. Protein concentration was determined by Bradford protein assay (Bio Rad, Hercules, CA). Antibody concentration was determined by using Easy-Titer® Rabbit IgG Assay Kit (Pierce, Rockford, IL). The prepared nanoparticle solution had 0.32 mg/ml of Abs and 1.38 mg/ml of clathrin. Dynamic light scattering (550-LB, Horiba, Kyoto, Japan) were used to confirm size and uniformity of nanoparticles according to the published protocol (Vitaliano, Vitaliano et al. 2012).

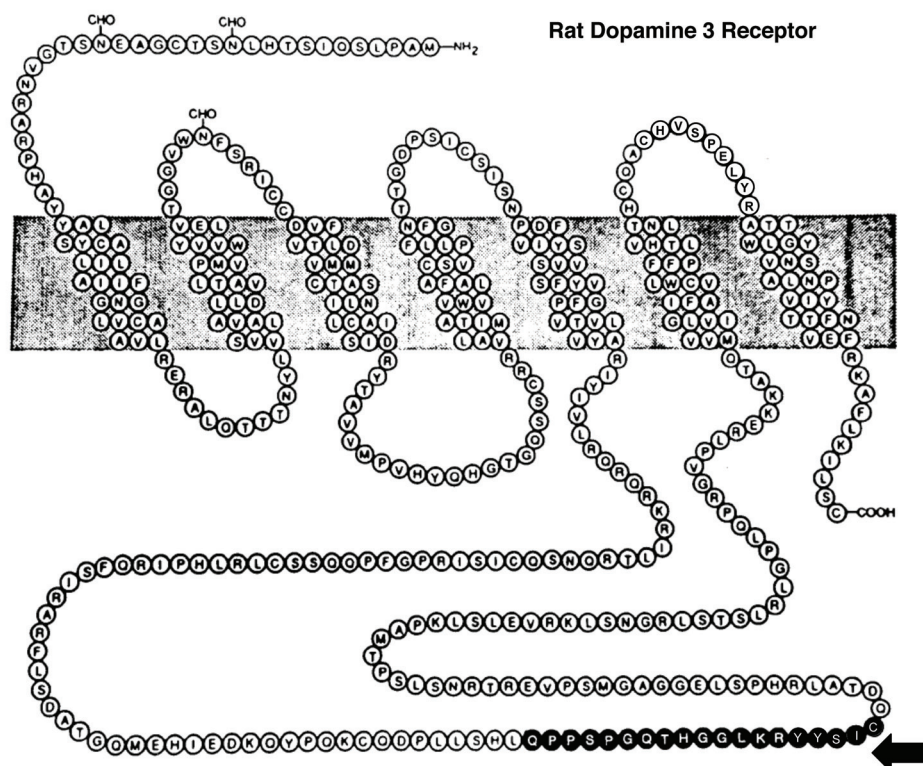


Figure 25. Diagram of the rat dopamine D3 receptor amino acid sequence: Nanoparticles were conjugated to antibodies that attach to an epitope on the third intracellular loop, outlined in black (Vitaliano and Vitaliano 2008).

For fluorescent studies, Rhodamine–PEG–Maleimide (JenKem Technology) was added to clathrin in PBS buffer (pH 7.4) and incubated for 2 hours at 23°C according to the published protocol (Vitaliano, Vitaliano et al. 2012). Unconjugated PEGs were removed by ultrafiltration using Amicon-Ultra tubes with 100 kDa MWCO (Millipore, Billerica, MA). The number of rhodamine-PEGs attached to clathrin heavy chain was estimated by using SDS PAGE.

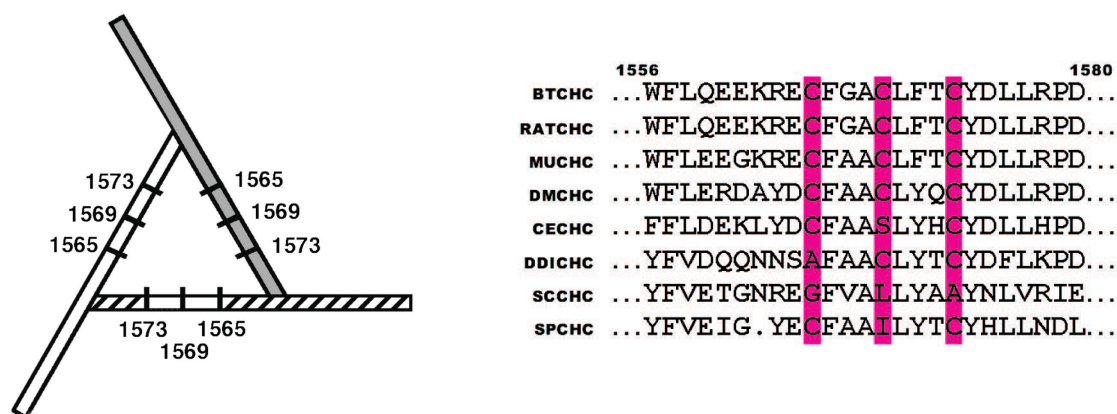


Figure 26. Clathrin cysteine residues: (A) Model of the clathrin trimerization domain showing the positions of cysteine residues. Identical clathrin heavy chain legs are shown in white, gray and stripes. The numbers refer to cysteines 1573, 1569 and 1565. (B) Sequence alignment of clathrin heavy chain residues in the trimerization domain indicating the conservation of cysteines. The numbering is based on the bovine sequence. BTCHC: bovine; RATCHC: rat; MUCHC: human muscle; DMCHC: Drosophila; CECHC: Caenorhabditiselegans; DDICHC: Dictyostelium; SCCHC: Saccharomyces cerevisiae; SPCHC: Schizo-saccharomyces pombe. The colored vertical bars indicate cysteines 1565, 1569 and 1573 (Ybe, Ruppel et al. 2003).

Each rat clathrin heavy chain has 30 cysteine residues, but only some are readily available for modifications (Vitaliano, Vitaliano et al. 2012). The maleimide in PEG chains has high specificity for the protein -SH groups of cysteines, which was utilized in the surface decoration of Clathrin triskelia with PEG chains. The trimerization region between 1550 and 1615 of each clathrin leg contains three cysteines at positions 1565, 1569 and 1573. Figure 26 presents a model of the clathrin trimerization domain that shows three-fold symmetry between heavy chain subunits (Ybe, Ruppel et al. 2003). In this model cysteines 1573, 1569 and 1565 are represented as forming a cluster of 9 cysteine residues. Sequence alignment of residues 1556–1580 from a variety of mammalian species and lower organisms indicates that cysteines 1565, 1569 and 1573 are conserved in higher

mammals (Figure 26). The three cysteines at positions 1565, 1569 and 1573 of clathrin triskelia do not participate in disulfide bonding and can be used to attach maleimide-PEG chains.

PEGs were used in this study because PEG conjugation masks the protein's surface, reduces its renal filtration, prevents the approach of antigen processing cells and reduces its degradation by proteolytic enzymes. Also, PEG conveys to molecules its physico-chemical properties and therefore modifies biodistribution and solubility of peptide and non-peptide nanoparticles. The PEG coating is highly hydrated and this layer protects against interactions with molecular and biological components in the blood stream and nonspecific binding to the tissues.

3.3.2. Immunoreactivity of D3R-Ab-Triskealia

Nanoparticle immunoreactivity was tested in-vitro by Western Blot analyses. Brain lysates from rat cortex and cerebellum were prepared in the modified radioimmunoprecipitation buffer (RIPA) (pH 8) according to the published methods (Gearhart, Middlemore et al. 2006) as described below in the Section 3.3.5. To detect dopamine D3 receptors, proteins in the supernatants were separated by sodium dodecyl sulfate–polyacrylamide gel electrophoresis (SDS-PAGE) on 10% acrylamide gels.

Proteins were then transferred to nitrocellulose membranes using a Mini Trans-Blot Cell (Bio-Rad, Hercules, CA). Blots were rinsed, blocked for 2 h in Tris buffered saline (TBS) (10 mM Tris, 150 mM NaCl, pH 8.0) containing 0.05% (w/v) Tween-20, plus 5% (w/v) dry milk, and incubated with 2.5 µg/ml of D3R-Ab-triskealia, or D3R-Abs, overnight at 4°C. Blots were again washed three times for 10 min in TBS mixed with Tween-20 (TBS-T) and incubated with a horseradish peroxidase-conjugated goat anti-rabbit IgG (1:2000, Jackson ImmunoResearch Laboratories, West Grove, PA) for 1 h at 23°C, and developed using chemiluminescence procedure (Amersham, Arlington Heights, IL). As a control for the specificity of immunoreactive bands, D3R-Ab-nanoprobes were pre-incubated with an immunizing peptide (D3RAB-CTs: D3R12-P, 1 µg: 5 µg) for 24 h at 4°C, or completely omitted.

3.3.3. D3R-Ab-Triskealia Immunohistochemistry

Brain distribution of D3Ab-triskealia nanoprobes was assessed in rats using immunohistochemistry (IHC) following intranasal administration. Male Sprague-Dawley

(SD) rats (250-300 g) (n=12) were randomized into 3 groups (D3R-Ab-nanoprobe group, D3R-Ab, or saline group) and anesthetized with ketamine/ xylazine (80/20 mg/kg). A volume of 50 μ l of D3R-Ab-triskelia PBS solution (64 μ g/kg of Abs and 277 μ g/kg of CTs), or D3R-Ab only solution (64 μ g/kg of D3R-Ab), or saline, was delivered in nose drops as described previously. Animals (n=4 per group) were sacrificed 180 minutes following nanoparticle administration.

Rats were perfused transcardially with PBS followed by 4% paraformaldehyde as described previously. Brains were removed, post-fixed, cryoprotected in three changes of 30% sucrose, and frozen in dry ice-cooled 2-methylbutane and stored at -80 °C until required. Coronal tissue sections of 30 μ m thickness were then cut throughout the entire brain using a Leica CM3050S cryostat (Leica Microsystems) and IHC was performed.

Sections were first washed 3 times for 5 min. with PBS (pH 7.4) to remove any traces of cryoprotectant and/or embedding medium (i.e., Neg-50 was used for cryostat sectioning). The endogenous peroxidase activity was quenched by incubating tissue in methanol/PBS (1:1) with 0.3% hydrogen peroxide for 30 min at room temperature (RT). Sections were then washed with PBS three times for 5 min. In order to block non-specific binding sites, sections were blocked with 10% normal goat serum (NGS) in PBS (pH 7.4) for 20 min at RT. Sections were then stained for 30 min at RT with a 1:200 dilution of goat anti-rabbit secondary antibody coupled to the biotin (Vector Laboratories, Burlingame, CA), and again washed 3 times for 5 min in PBS. Finally, sections were incubated for 30 min at RT in avidin–biotin–HRP complex (ABC reagent, Vectastain Elite; Vector Laboratories, CA).

After rinsing in PBS, peroxidase activity was detected by incubation with 3,3'-diaminobenzidine (DAB) for 4 min at RT in the presence of hydrogen peroxide using Vector Kit (Vector Laboratories, CA). The peroxidase reaction was stopped in water. Sections were then mounted on the Super Frost Plus slides (Fisher Scientific, Pittsburgh, PA), dried, dehydrated in graded ethanols, cleared in xylene, cover-slipped with permount, and examined using a Zeiss Axio Scope A1 photomicroscope (Zeiss, Thornwood, NY).

IHC was also performed with brain sections from SD rats (n=4) that received D3R-nanoparticles, but were not perfused. Their brains were quickly frozen in isopentane and fixed in acetone for 20 min at 4°C. IHC was performed as described above. There were no differences in CNS staining patterns between perfused vs. non-perfused rats.

3.3.4. D3RAb- Triskelia Fluorescent Immunohistochemistry

In vivo stability and specificity of D3R-Ab-clathrin-nanoparticles were also assessed in rats using fluorescent analysis of nanoparticles carrying rhodamine-PEGs (JenKem, Allen, TX) following intranasal administration. Rhodamine-PEGs were first attached to clathrin triskelia as described previously and according to published protocols (Vitaliano, Vitaliano et al. 2012). Unconjugated Rhodamine-PEGs were removed by ultrafiltration using Amicon-Ultra tubes with 100 kDa MWCO. PEGylated D3R-Abs were then conjugated to triskelia as described previously.

Male Sprague-Dawley (SD) rats (250-300 g) (n=12) were randomized in 4 groups and received fluorescent D3R-Ab-CTs (64 µg/kg of Abs and 277 µg/kg of CTs), or D3R-Abs (64 µg/kg), or rhodamine-PEG-CTs (277 µg/kg of CTs), or saline intranasally, and were sacrificed and perfused 3 hours after nanoparticle administration.

Brains were removed, post-fixed and cryoprotected as previously described. Coronal sections (30 µm) were taken using a cryostat at different brain levels and immuno-fluorescent studies were performed. To further assess nanoparticle stability and determine whether rhodamine labeled clathrin nanoparticle deposits in the D3R brain regions colocalized with D3RAb deposits, immuno-fluorescent studies were performed on sections from D3R brain regions.

First, sections were washed 3 times for 5 min with PBS to remove any traces of cryoprotectant and/or embedding medium. Sections were then blocked for 45 minutes in 10% normal goat serum (NGS) to block nonspecific binding sites, followed by incubation for 1 hour at room temperature with a 1:200 dilution of goat anti-rabbit IgG antibody conjugated to Alexa 488 in 1.5% NGS (Life Technologies, Grand Island, NY). The sections were washed again 3 times with PBS for 5 min each, mounted on the Super Frost Plus slides (Fisher Scientific, Pittsburgh, PA), dried, and coverslipped using Vectashield mounting medium (Vector Laboratories, CA). Processed sections were examined and photographed using a Zeis Axio Scope A1 (Zeiss, Thornwood, NY) and Leica TCS-NT laser confocal microscope (Leica Microsystems, Buffalo Grove, IL).

3.3.5. Quantitative Determination of D3R-Ab-Triskelia in the CNS

Antibody was quantified in the brain tissues by using Easy-Titer® Rabbit IgG Assay Kit (Pierce, Rockford, IL). Also, this assay was used to determine if D3RAb protein integrity

was conserved in brain tissue following intranasal administration. Male Sprague-Dawley (SD) rats (250 to 300 g) (n= 5 per group) were randomized into 3 groups (D3R-Ab-nanoprobe group, or D3R-Ab group, or saline), and anesthetized with ketamine/ xylazine (80/20 mg/kg). A volume of 50 μ l of D3R-Ab-triskelia PBS solution (64 μ g/kg of D3Ab and 277 μ g/kg of CTs), or D3R-Ab PBS solution (64 μ g/kg), or saline, was delivered in nose drops (5 μ l per drop) over a 20-minute period.

Animals were sacrificed at 180 minutes following nanoparticle administration based on our previous studies (Vitaliano, Vitaliano et al. 2012) and D4R-Ab studies (Kinoshita, McDannold et al. 2006). Brains were removed from the rat skulls within 3 minutes and were immediately frozen in dry ice-cooled 2-methylbutane. Brains were then wrapped in aluminum foils, labeled and stored at -80°C until use.

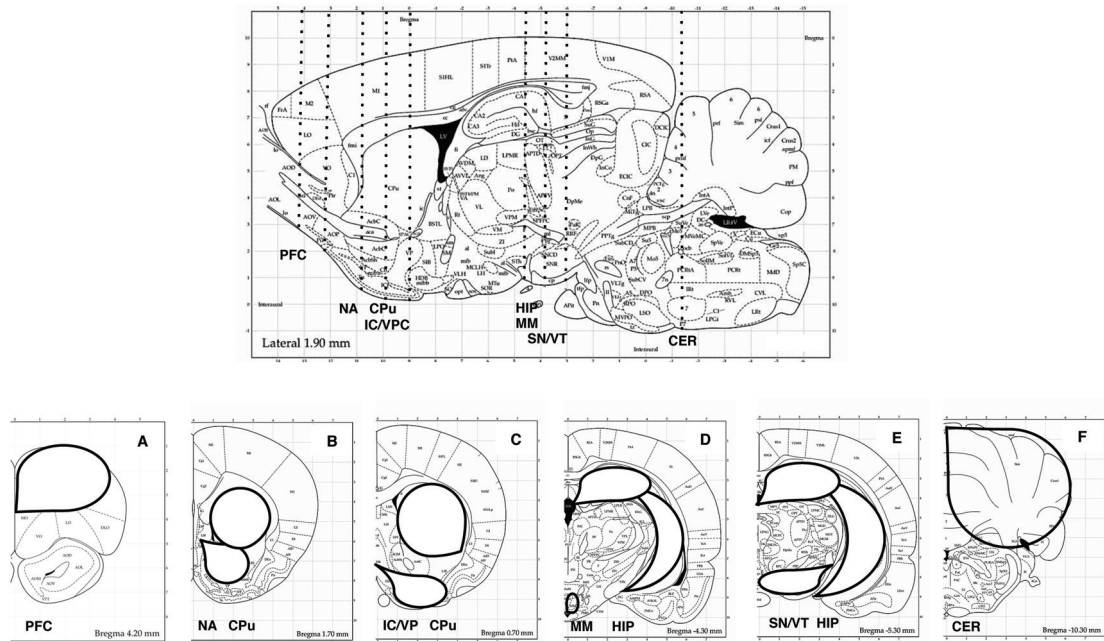


Figure 27. Brain regions used for ELISA are presented in the sagittal and coronal rat brain diagrams. Locations of coronal sections are represented as vertical dashed lines in the sagittal section of the rat brain (Paxinos and Watson 1998). Rat brain regions that were dissected from the coronal brain slices include: (A) prefrontal cortex (PFC); (B) nucleus accumbens (NA) and corpus striatum (CPu); (C) islands of Calleja (IC) and ventral pallidum (VP); (D) hippocampus (HIP) and medial mammillary bodies (MM); (E) substantia nigra (SN) and ventral tegmental area (VT) and (F) cerebellum (CER) (Vitaliano and Vitaliano 2008).

Brain regions including: prefrontal cortex (PFC), corpus striatum (CPu); nucleus accumbens (NA); islands of Calleja/ventral pallidum (IC/VP); hippocampus (HIP); medial mammillary bodies (MM); substantia nigra/ventral tegmental area (SN/VT); and cerebellum (CER) were dissected with a brain matrix (Zivic Instruments, Pittsburgh, PA) and using “The Rat Brain Atlas” by Paxinos and Watson (1998) as a guide for neuroanatomical landmarks. The prefrontal cortex as a control region with low levels of dopamine 3 receptors was dissected from the coronal brain slice that extended from about 3.2 mm to 4.2 mm anterior to bregma. Rat brain regions with high levels of dopamine 3 receptors were then dissected in the order listed below. The nucleus accumbens was dissected from a coronal brain slice that spanned 0.7 to 1.7 mm relative to bregma, while the coordinates for the corpus striatum were from 0.2 to 1.7 mm anterior to bregma. The islands of Calleja and ventral pallidum were dissected from the coronal brain slice approximately from 0.2 to 0.7 mm anterior to bregma. The medial mammillary bodies were dissected from the brain slice located from -4.30 mm to -5.30 mm posterior to bregma, while coordinates for the dorsal hippocampus were from -4.3 to -6.0 mm posterior to bregma. The substantia nigra and ventral tegmental area were dissected from the coronal brain slice that extended from about -5.3 mm to -6 mm posterior to bregma.

Tissue samples were weighed and homogenized in 10 vol of modified radioimmuno-precipitation buffer (RIPA) (pH 8) according to published methods (Gearhart, Middlemore et al. 2006) (about 10 μ l of RIPA buffer per milligram tissue). RIPA buffer contained 150 mM sodium chloride; 1% (v/v) Nonidet P-40; 0.5% (w/v) sodium deoxycholate; 0.1% (w/v) sodium dodecyl sulfate (SDS); 50 mM Tris base, and 10% (v/v) glycerol (all from Sigma–Aldrich), and was supplemented with 200 μ l of phenylmethanesulfonyl fluoride (PMSF), 100 μ l of 200 mM sodium orthovanadate, 100 μ l of protease inhibitor mixture, and 200 μ l of each phosphatase inhibitor mixtures 1 and 2 (Sigma–Aldrich) per 10 ml of ice-cold buffer. All tissue samples were then incubated on ice for 20 minutes to solubilize more proteins from the membrane components. The homogenates were then transferred into 1.5 ml polypropylene microtubes and sonicated 1 or 2 times for 5 sec. on ice using a Sonic Dismembrator (Fisher Scientific Model #100; set at level 1). These settings were selected to completely dissociate tissue, while minimizing foaming and heating, which could denature proteins.

The sonicated samples were then rocked for 1 h at 4°C on an orbital mixer (MiniMixer, RPI) in order to facilitate tissue lysis. Samples were also centrifuged at 12,000 rpm for 20 min at 4°C in the Eppendorf 5415 Micro-centrifuge, and the supernatants that contained solubilized brain proteins were collected. Total protein in brain lysates was determined using Bradford Protein Assay Kit (Bio Rad). The amount of D3R-Ab in each supernatant

sample was quantified using Easy-Titer® Rabbit IgG Assay Kit (Pierce, Rockford, IL) according to manufacturer protocol (Figures 28 & 29).

Procedure Summary

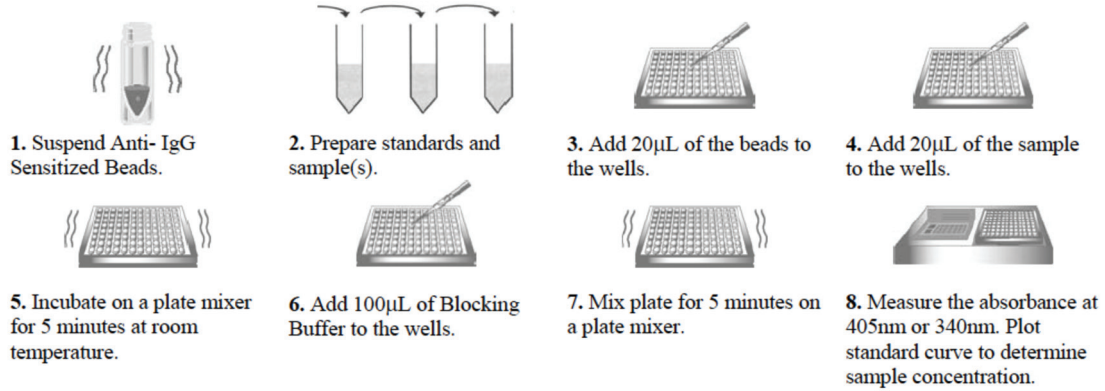


Figure 28. The Easy-Titer IgG Assay: The assay procedure uses monodispersed polystyrene beads that are coated with anti-IgG antibodies and absorb light at 340 and 405 nm. When the beads are mixed with a sample containing IgG, they aggregate, causing decreased absorption of light. The decrease in absorption is proportional to IgG concentration and a standard curve can be generated to quantify levels of IgG in tissue supernatant samples (from Thermo Scientific instructions #23305).

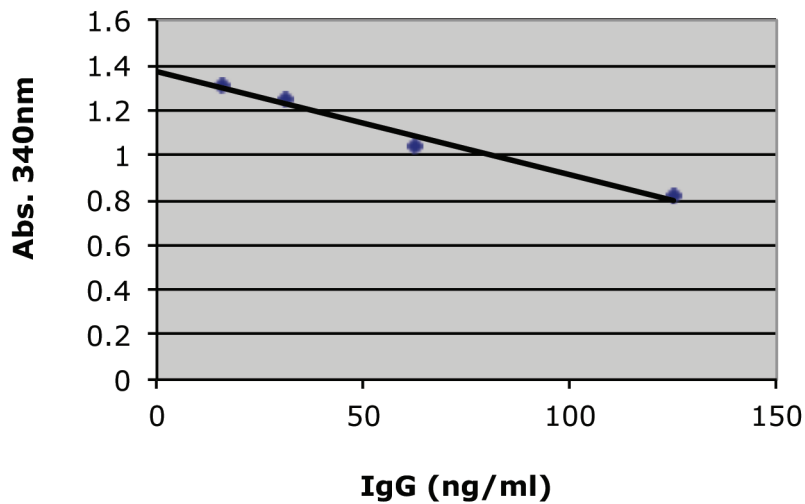


Figure 29: Standard curve for rabbit IgG. The Easy-Titer® Rabbit IgG Assay Kit was used to calculate concentrations of D3R-Abs in tissue homogenates prepared from different brain regions. Standard curve range: 7.8 ng/mL to 125 ng/ml (Vitaliano and Vitaliano 2008).

The sensitized beads were prepared and 20 μ l of beads were added to the wells of a 96-well microplate (Table 6). Prepared samples and standards were then added into the appropriate wells containing beads and mixed on a plate mixer. Finally, Blocking Buffer (100 μ l) was added to each well and a 96-well microplate was mixed for 5 min. Absorbance at 340 nm (A340) was measured with Epoch microplate reader (BioTek, VT), and converted into the D3R-Ab concentrations per manufacturer instructions. The assay had a lower limit of quantification value of 7.8 ng/ml.

Table 6. ELISA plate design used in the immunoassay

	1	2	3	4	5	6	7	8	9	10	11	12
A std	0	7.8	15.6	31.2	62.5	125	0	7.8	15.6	31.2	62.5	125
B std	0	7.8	15.6	31.2	62.5	125	0	7.8	15.6	31.2	62.5	125
C	PFC	PFC	PFC	CPu	CPu	CPu	NA	NA	NA	IC/VP	IC/VP	IC/VP
D	HIP	HIP	HIP	MB	MB	MB	SN	SN	SN	CER	CER	CER
E	PFC	PFC	PFC	CPu	CPu	CPu	NA	NA	NA	IC/VP	IC/VP	IC/VP
F	HIP	HIP	HIP	MB	MB	MB	SN	SN	SN	CER	CER	CER
G	PFC	PFC	PFC	CPu	CPu	CPu	NA	NA	NA	IC/VP	IC/VP	IC/VP
E	HIP	HIP	HIP	MB	MB	MB	SN	SN	SN	CER	CER	CER

A & B: standards (from 7.8 to 125 ng/ml);

C & D: animal #1 received D3RAb-nanoparticles;

E & F: animal #2 received D3RAb only;

G & E: control animal #3 received saline.

3.3.6. Toxicity Studies

Each rat was examined every 30 minutes for lack of movement, ataxia, hunched posture, ruffled fur, hypothermia, dehydration, dyspnea, tachypnea, seizure and sustained rapid movement around the cage, one hour after intranasal delivery for 2 hours. Six additional rats continued to be examined every 24 h for 4 days. We used a labeling system that prevented the examiner from knowing the identity of each animal. A 0 to 3 scale was used to evaluate each symptom (e.g., 0 = no symptom; 1 = mild; 2 = moderate; and 3 = severe symptom) and to calculate a total score. Histological studies were conducted in Sprague-Dawley rats (250-300 g) (n=6) four days after nanoprobe or saline administration. Rat brain tissues were processed as described, stained with hematoxylin and eosin, and compared using light microscopy.

3.3.7. Statistical Analyses

Statistical analyses were performed using Graph Pad Prism® version 5.0. Data was presented as mean ± standard error of the mean (SEM). Comparison between multiple groups of data was conducted by one-way analysis of variance (ANOVA), and Tukey's post-hoc test was used to determine the differences between individual groups. Comparisons between the two groups of data were performed by using the unpaired Student's t-test.

Table 7. Research Goals

1. Produce, characterize and test in-vivo clathrin nanoplatforms	2. Design and characterize D3RAb-CT nanoprobes	3. Evaluate CNS distribution and in-vivo stability of D3RAb-CTs	4. Measure concentrations of D3RAb-CTs in D3R rat brain regions	5. Evaluate D3RAb-CT neurotoxicity
IN: 14 rats = 2+ 4X3 IP: 14 rats = 2+ 4X3		IF: 16 rats = 4 X 4 IHC: 12 rats = 3 X 4	15 rats = 5+5+5	6 rats = 3+3
a. Isolate Clathrin Triskelia (CTs)	a. PEGylate D3R-Abs	a. Randomize animals in 4 groups: nanoprobe, D3RAb, CT or saline	a. Randomize animals in 3 groups: saline nanoprobe or D3RAb	a. Randomize animals in 2 groups: saline or nanoprobe
b. Attach MRI contrast agent (Gd-DTPA) OR fluorescent FITC	b. Attach PEG-ylated Abs OR rhodamine-PEGs to CTs	b. Anesthetize animals and perform I.N. administration	b. Anesthetize animals and perform I.N. administration	b. Anesthetize animals and perform I.N. administration
c. Determine nanoparticle size and structure	c. Determine nanoparticle size and structure	c. Collect brains 3h after I.N. delivery	c. Collect brains 3h after I.N. delivery	c. Monitor animal behavior
d. Measure Gd and CT concentrations and T1 relaxivity	d. Determine nanoparticle immunoreactivity with WB	d. Process tissue and perform IHC OR IF	d. Process tissue and perform ELISA	d. Collect brains 4 days after I.N. delivery
e. Anesthetize animals and deliver CTs		e. Visualize nanoprobes in rat brains	e. Determine Ab concentrations in the CNS	e. Determine nanoprobe toxicity
f. Collect brains & image fluorescent CTs in rat brains		f. Data analysis	f. Data analysis	f. Data analysis
EM, SDS-PAGE, DLS, Arsenazo and Bradford assays, NMR	EM, SDS-PAGE, DLS, Western Blot (WB)	Immunohistochemistry (IHC) Immunofluorescence (IF)	ELISA	Behavioral evaluation and H&E staining

4. RESULTS

4.1. Characterization of Clathrin Triskelia

The first goal was to develop a clathrin nanocarrier and test its brain penetration after intranasal and intraperitoneal delivery in rats.

4.1.1. Structure of Clathrin Nanoplatfoms

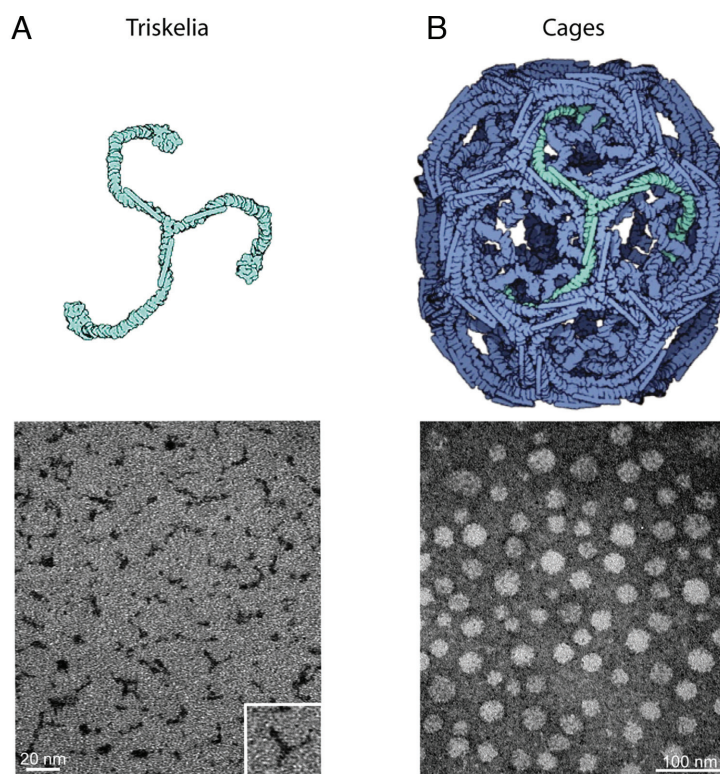


Figure 30. Structure of nanoplatfoms: (A) The first diagram represents a three-legged clathrin triskelion (light green). Transmission electron microscopy (TEM) image shows clathrin triskelia with attached Gd-DTPA-ITC negatively stained with 1% uranyl acetate. (B) The second diagram represents a clathrin cage lattice (blue) self-assembled from clathrin triskelia. The TEM image shows clathrin cages with attached Gd-DTPA-ITC negatively stained with 1% uranyl acetate. Clathrin cages formed hexagonal barrels with D6 symmetry (Vitaliano, Vitaliano et al. 2012).

Triskelia nanoplatfoms modified with Gd-DTPA MRI contrast agent were developed. This nanoplatfom utilized a clathrin triskelion (three-legged) protein complex composed of a trimer of clathrin heavy chains (CHC), each bound to a single clathrin light chain (CLC) (Fig. 30A). To test clathrin triskelion integrity and function after purification,

clathrin-cages (CCs) were self-assembled from clathrin triskelia (Fig. 30B). Functional CTs self assembled into clathrin cages in an acidic buffer (e.g., MES, pH 6.5). Electron microscopy showed a large proportion of conjugated Gd-DTPA-clathrin triskelia (Fig. 30A), and also conjugated Gd-DTPA-clathrin cages (Fig. 30B). The majority of Gd-DTPA-CCs had D6 symmetry, formed hexagonal barrels with 36 clathrin triskelia, and comprising 108 heavy chains and 108 light chains (Vitaliano, Vitaliano et al. 2012).

4.1.2. Size of Clathrin Nanoplatfoms

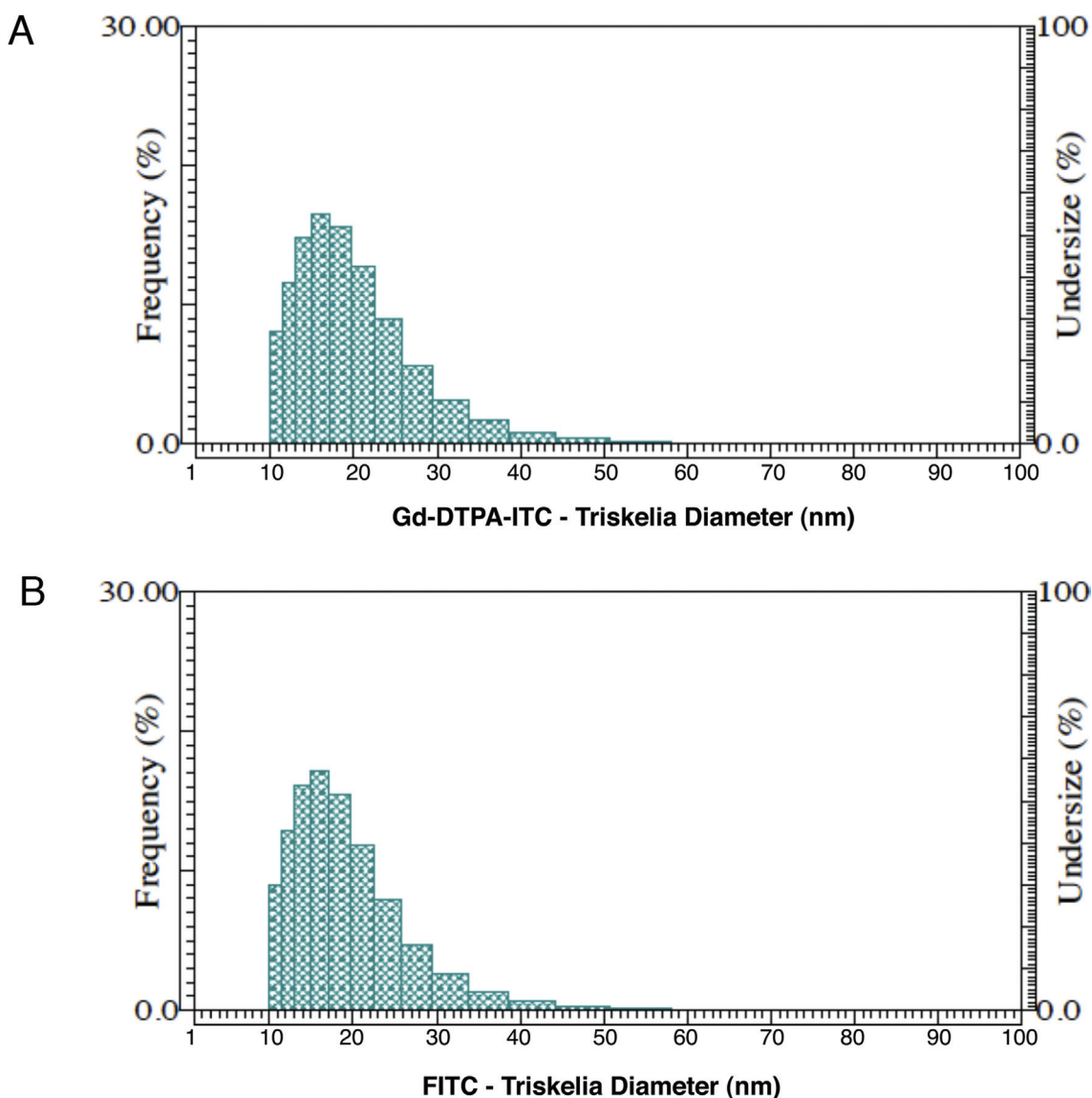


Figure 31. Size of nanoplatfoms: Dynamic light scattering (DLS) measurements indicated the mean hydrodynamic radius of (A) clathrin triskelia with Gd-DTPA contrast agents was 18.5 ± 6.5 nm and of (B) fluorescent FITC-clathrin triskelia was 17.8 ± 6.2 nm (Vitaliano, Vitaliano et al. 2012).

The mean hydrodynamic radius of clathrin triskelia with attached Gd-DTPA was 18.5 ± 6.5 nm (Figure 31A). Previous DLS studies of clathrin triskelia in solution also reported a Stokes radius of 17 to 18 nm (Yoshimura, Kameyama et al. 1991, Ferguson, Prasad et al. 2006). DLS instruments use spherical models to estimate particle sizes. However, a triskelion is not a spherical particle. A single triskelion has three legs that are bent, puckered, and positioned differently in 3-dimensional space. Electron microscopy has shown that triskelion legs can vary from 35 to 62 nm in total length after straightening (Kirchhausen, Harrison et al. 1986, Kocsis, Trus et al. 1991). High-resolution atomic force microscopy also confirmed that the legs are flexible along their entire length (Kotova, Prasad et al. 2010). Thus, there is variability in the measurements of triskelion size. The mean hydrodynamic radius of fluorescent FITC-clathrin triskelia was 17.8 ± 6.2 nm (Figure 31B). FITC-triskelia were similar in size to the GD-DTPA- triskelia.

4.1.3. Chelate Ligand to Clathrin Protein Molar Ratio

A chelating agent (DTPA-ITC) was attached to the clathrin protein, and chelate ligand to protein molar ratio (L/P) determined. Standard spectrophotometric methods were used (Pippin, Parker et al. 1992) based on the reaction between DTPA-ITC ligand protein conjugate and an yttrium (III) complex of arsenazo III. Figure 32A shows dependence of absorbance at 652 nm on DTPA-ITC molarity. Linearity of data demonstrates that Beer's law was observed over the concentration range of 0-2.0 μ M of DTPA-ITC. Absorbance at 652 nm was determined for 20-80 μ l solutions of DTPA-ITC-Clathrin-triskelia (Fig. 32B). Protein concentration was determined by Bradford protein assay. The mean DTPA-ITC: Clathrin Heavy Chain molar ratio was 27.04 ± 4.8 : 1 for triskelia (Vitaliano, Vitaliano et al. 2012).

SDS-PAGE image analyses showed changes in the molecular weight of modified clathrin heavy chains (CHCs). After modification of CHC with Gd-DTPA we found 2 peaks that indicated different molecular weights (190,988 Da and 207,532 Da) (Fig. 33A). Thus, molecular weight of triskelia CHCs increased by 10,143 Da (from 180,845 Da to 190,988 Da), and by 26,687 Da (from 180,845 Da to 207,532 Da). Thus, between 12.57 and 33.06 molecules of Gd-DTPA-ITC were attached to each CHC. Molecular weight of the fluorescent CHC increased by 3,244 Da (from 180,039 Da to 183,283 Da), indicating that 8.33 molecules of FITC (MW 389.38 Da) were attached to each CHC (Fig. 33B). These data are consistent with spectrophotometric data. Rat CHC has 1675 amino acid residues, of which 97 are lysine residues, but only some are available for conjugation with DTPA-ITC.

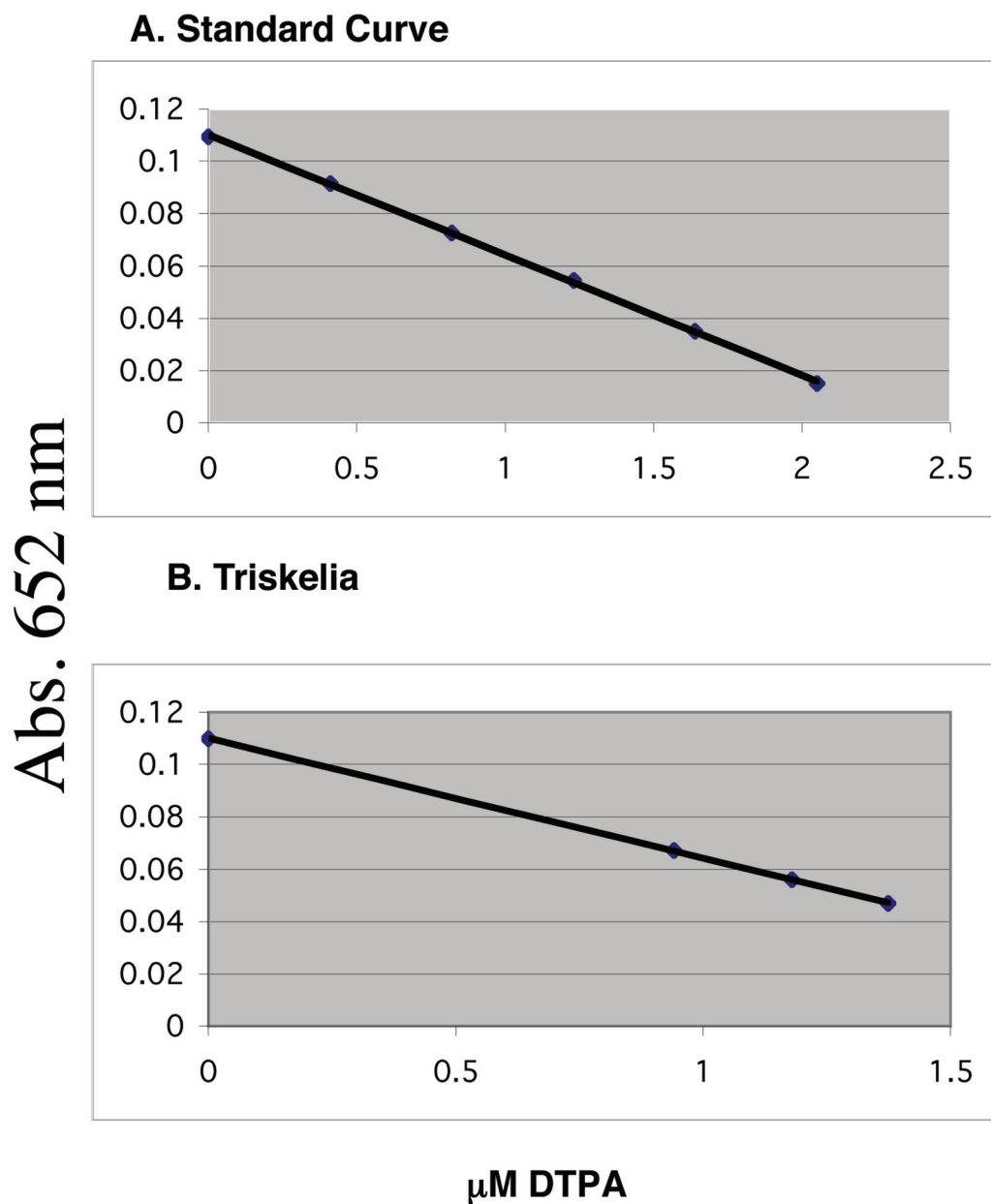


Figure 32. The spectrophotometric method for the determination of a DTPA Ligand: (A) Linear relationship between the absorbance of the yttrium complex of arsenazo III at 652 nm and the molarity of DTPA-ITC ($R^2 = 0.999$). (B) Relationship between the absorbance ($A=652$ nm) and the concentration of DTPA-ITC during a sample titration of the yttrium complex of arsenazo III with DTPA-ITC-clathrin triskelia. The mean Ligand (DTPA-ITC)/ Clathrin Heavy Chain molar ratio was $27.04 \pm 4.8: 1$ (Vitaliano, Vitaliano et al. 2012).

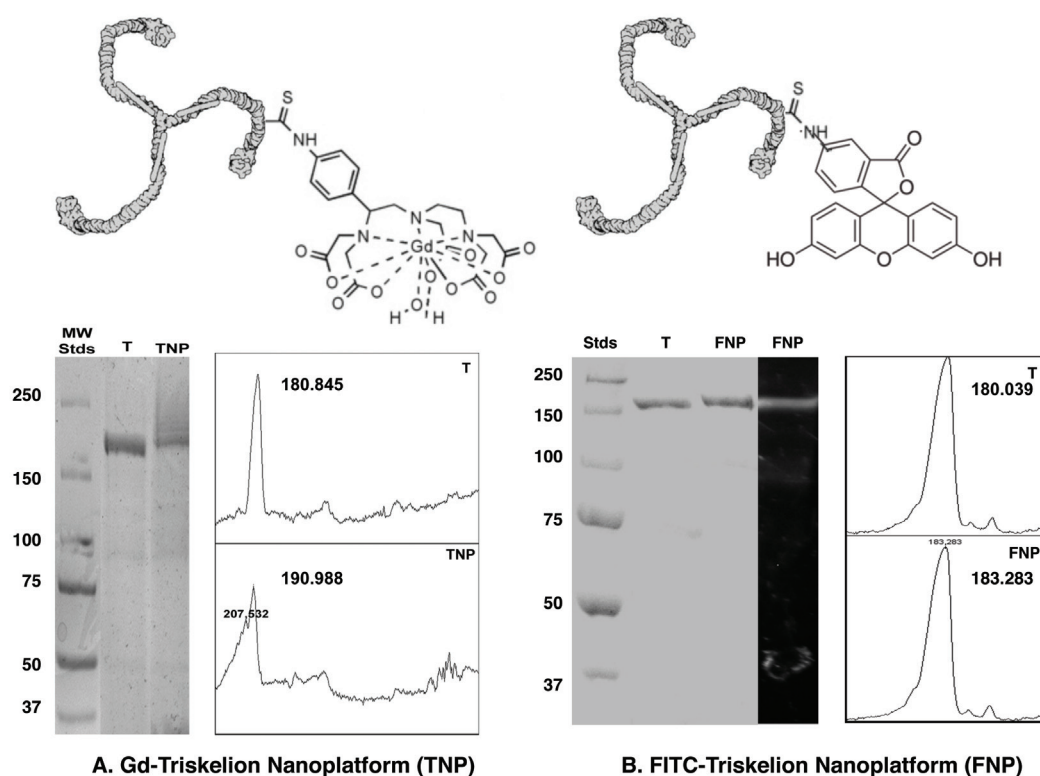


Figure 33. SDS-PAGE of the modified Clathrin-nanoplatfoms: (A) Clathrin triskelion Gd-contrast agent nanoplatfom: Line 1: Standards; Line 2: Unmodified Clathrin triskelia; Line 3: Clathrin triskelia with attached Gd-DTPA-ITC. SDS-PAGE analyses show that modified clathrin heavy chain (CHC) bands in triskelia coincide with two molecular weight markers (190,988 kDa and 207,532 kDa). Molecular weight of the triskelia CHCs increased by 10,143 and 26,687 Da. Thus, between 12.57 and 33.06 molecules of the Gd-DTPA-ITC were attached to the CHC. (B) Fluorescent Clathrin triskelion nanoplatfom: Line 1: Standards; Line 2: Unmodified Clathrin triskelia; Lines 3 and 4: Clathrin triskelia with attached fluorescent FITC labels. SDS-PAGE analyses show that modified CHC bands in fluorescent triskelia coincide with the molecular weight marker of 183,283 kDa. Molecular weight of the fluorescent CHC increased by 3,244 Da, indicating that 8.33 molecules of the FITC were attached to each CHC. Abbreviations: T=triskelia, Stds=standards, TNP= Gd-triskelion nanoplatfom, FNP= FITC-triskelion nanoplatfom (Vitaliano, Vitaliano et al. 2012).

4.1.4. Nanoparticle Relaxivity and Gd Measurements

Gadolinium concentrations and T_1 relaxivities were determined for clathrin triskelia. Gadolinium concentrations were measured by relaxometry (Datta, Hooker et al. 2008)

and spectrophotometric methods (Gouin and Winnik 2001). Spectrophotometric results indicated that 100% of added gadolinium was chelated by DTPA-ITC. The Gd to DTPA-ITC molar ratio was 0.9:1. Nuclear Magnetic Resonance (NMR) results confirmed spectrophotometric results for clathrin triskelia. The Gd concentration in 750 μ l of triskelia conjugate was 0.0689 mM according to spectrophotometric methods, and 0.0693 mM according to NMR methods. Relaxivities for each sample were calculated using T_1 data and spectrophotometrically determined gadolinium concentrations. At 0.47 T, Gd-DTPA-ITC-triskelia displayed a relaxivity of 16 $\text{mM}^{-1}\text{s}^{-1}$ per gadolinium ion (Fig. 34) and 1,166 $\text{mM}^{-1}\text{s}^{-1}$ per particle. Thus, triskelia exhibited 4 times higher ionic relaxivity and 291.5 times higher molecular relaxivity compared to Gd-DTPA (Vitaliano, Vitaliano et al. 2012).

Relaxivity of Triskelia

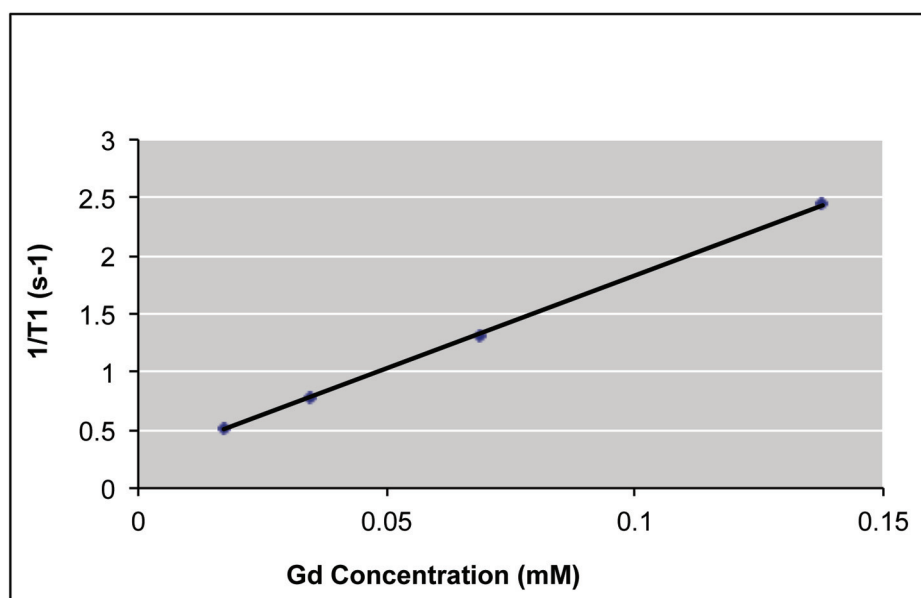


Figure 34. T_1 Relaxivity of the modified Clathrin-nanoplatfoms at 0.47 T:

Solid line ($R^2 = 0.9996$) represents a linear relationship between the relaxivity rate of the modified clathrin triskelia and Gd molarity. Triskelia nanoplatfoms had ionic relaxivity of 16 $\text{mM}^{-1}\text{s}^{-1}$. Molecular relaxivity was 1,166 $\text{mM}^{-1}\text{s}^{-1}$ (Vitaliano, Vitaliano et al. 2012).

4.1.5. Qualitative Determination of Triskelia Transport to the CNS

In order to determine whether clathrin nanoparticles could cross or bypass the BBB in rats, triskelia were modified with fluorescent tags. Fluorescent fluorescein isothiocyanate (FITC) labels were conjugated to triskelia through reactive lysine residues using a Pierce FITC Labeling Kit (Figure 33B).

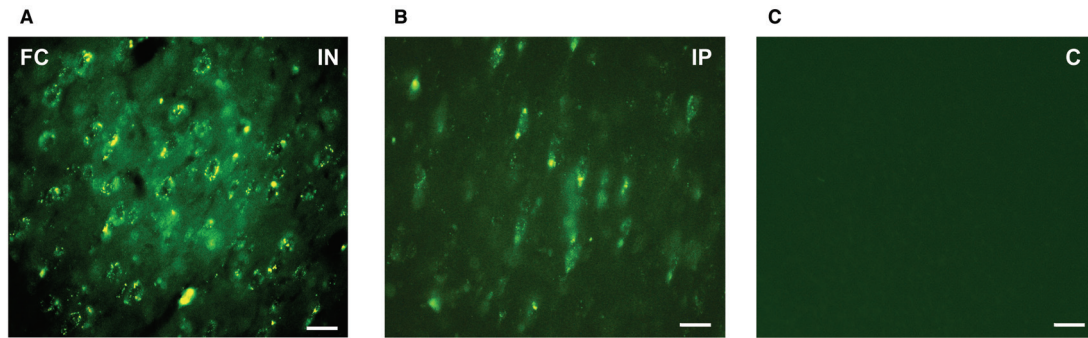


Figure 35. Delivery of clathrin nanoplatfoms to the rat frontal cortex: Ninety minutes after (A) intranasal (IN) and (B) intraperitoneal (IP) administration FITC-labeled clathrin triskelia (green) were identified in the frontal cortex (FC) in rats. Control animals (C) do not show any fluorescent patterns in the frontal cortex. The scale bar is 100 μ m.

In order to determine background levels of fluorescence in rat brains, control animals (n=2 per group) were sacrificed before intranasal and/or intraperitoneal administrations. The background fluorescence levels in the frontal cortex, stratum and substantia nigra of control animals are shown in Figures 35 & 36.

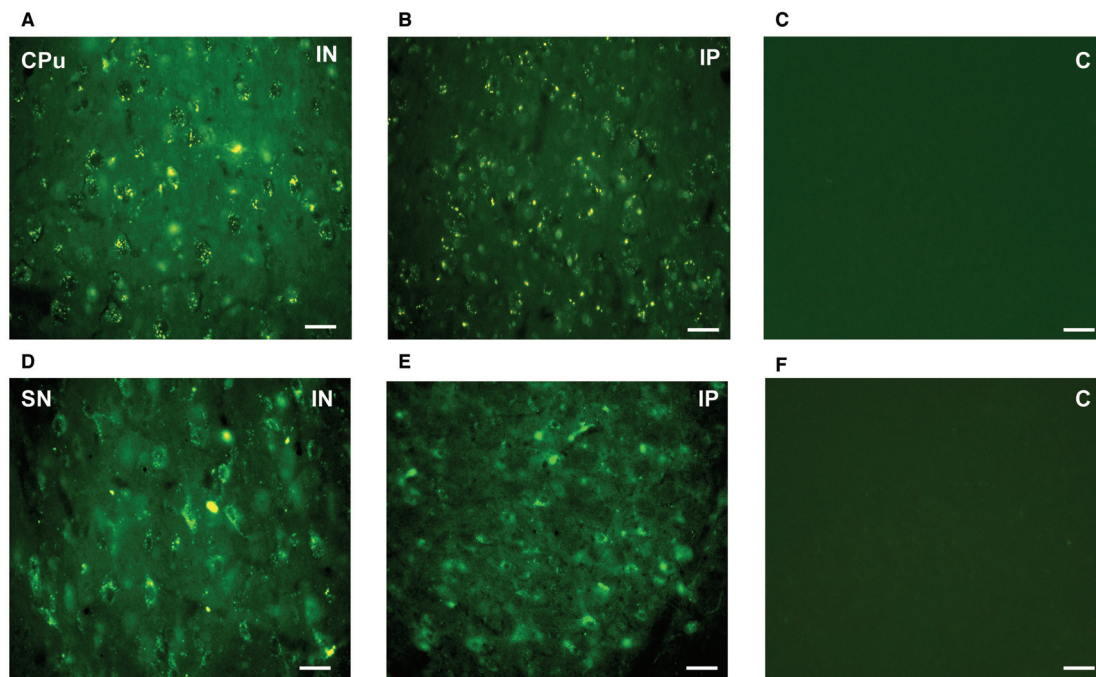


Figure 36. Delivery of clathrin nanoplatfoms to the rat corpus striatum and substantia nigra: Ninety minutes after (A & D) intranasal (IN) and (B & E) intraperitoneal (IP) administration FITC-labeled clathrin-triskelia (green) were identified in the corpus striatum (CPu) (A & B) and substantia nigra (SN) (D & E) in rats. Control animals (C & F) did not show any fluorescent patterns in the corpus striatum and substantia nigra. The scale bar is 100 μ m (Vitaliano, Vitaliano et al. 2012).

Minimal levels of auto-fluorescence were observed in brain sections from control rats and there were no areas of punctuate fluorescence in any of these sections.

Distribution of fluorescent patterns did not differ between the two routes of administration. The widespread punctate fluorescent deposits were mostly localized within discrete cellular structures (Figures 35 & 36). Since discrete fluorescent deposits were not observed in the brain regions from control animals (Figures 35 & 36), it is unlikely that the deposits observed in the FITC-triskelia treated rats were simply due to tissue auto-fluorescence. Therefore, clathrin triskelia successfully bypassed the BBB when delivered intranasally and also crossed the BBB when delivered intraperitoneally and both were widely distributed throughout the rat brain. However, higher doses of clathrin protein were used for intraperitoneal administration because liver and and/or plasma enzymes can cause protein degradation.

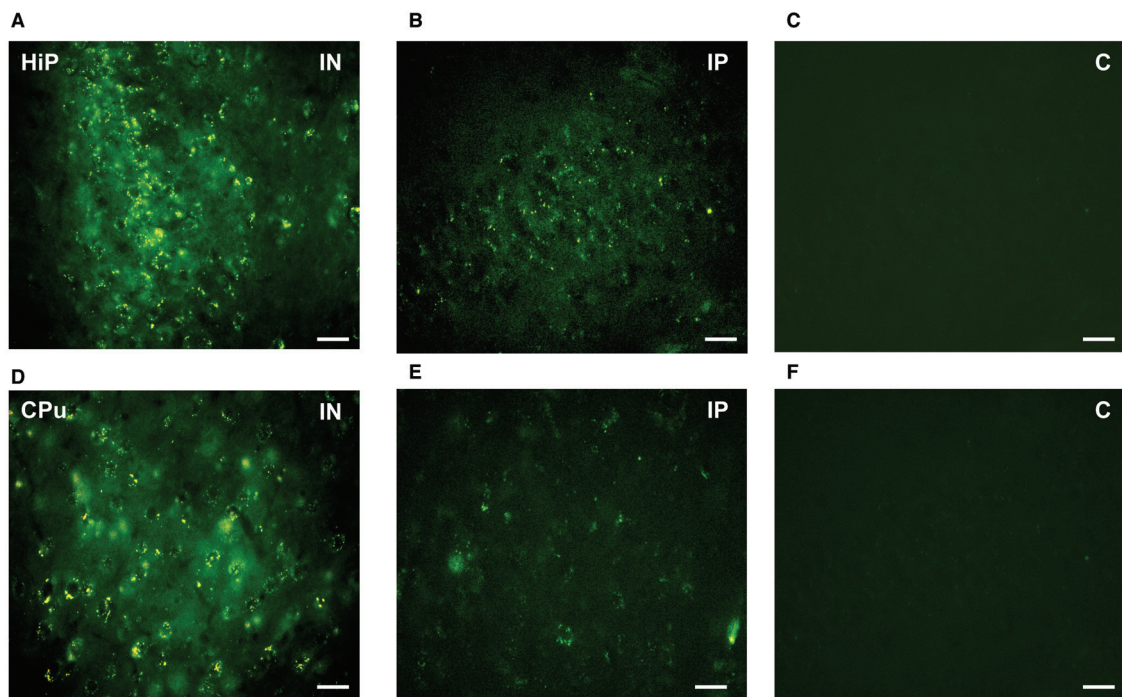


Figure 37. Delivery of clathrin nanoplatforms to the rat hippocampus and corpus striatum: Thirty minutes after (A & D) intranasal (IN) and (B & E) intraperitoneal (IP) administration FITC-labeled clathrin-triskelia (green) were identified in the hippocampus (HiP) and corpus striatum (CPu). In rats that received FITC-triskelia intraperitoneally (B & E) deposits were sparsely distributed at this time point. Control animals (C & F) did not show any fluorescent patterns in the hippocampus and corpus striatum. The scale bar is 100 μm (Vitaliano, Vitaliano et al. 2012).

Finally, multiple scattered bright fluorescent protein deposits were observed 30 minutes after intranasal administration in brain regions of animals that received FITC-triskelia intranasally (Figure 37). However, in rats that received FITC-triskelia intraperitoneally deposits were sparsely distributed and poorly visible in these brain regions 30 minutes after nanoparticle administration. For example, compare the hippocampal images for intranasal versus intraperitoneal delivery at the 30-minute time point (Figure 37). These findings suggested that intranasal delivery resulted in faster transport and/or higher uptake of the fluorescent protein in the rat brain than intraperitoneal delivery. Moreover, rapid clathrin protein transport from the nose to the brain indicated paracellular delivery of nanoparticles. This study provides the first evidence that clathrin nanoparticles can be successfully delivered intranasally or intraperitoneally into the rat brain, and that these nano-carriers (without ligands or antibodies) can distribute widely throughout the brain.

4.2. Characterization of Triskelia with Attached Dopamine 3-Abs

4.2.1. Structure and Size of D3RAB-Triskelia

The second goal was to develop and characterize a D3RAB-clathrin nanoparticle, and demonstrate that nanoparticle preparation does not compromise antibody integrity and immunoreactivity.

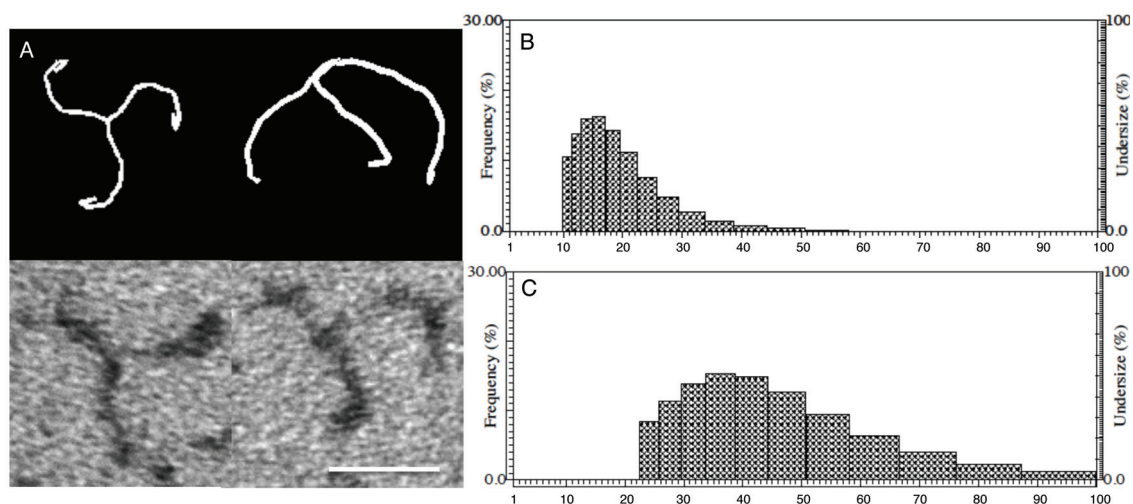


Figure 38. Clathrin nanoparticles: (A) Diagrams represent clathrin triskelia with three legs that are bent, puckered, and positioned differently in 3-dimensional space. Transmission electron microscopy (TEM) images show clathrin triskelia with attached metal (Gd) negatively stained with 1% uranyl acetate. (B) Dynamic light scattering (DLS) indicated that the mean hydrodynamic radius of unmodified clathrin triskelia was 17.7 ± 6.4 nm. (C) The mean hydrodynamic radius of D3R-Ab-triskelia was 42.3 ± 14.8 nm.

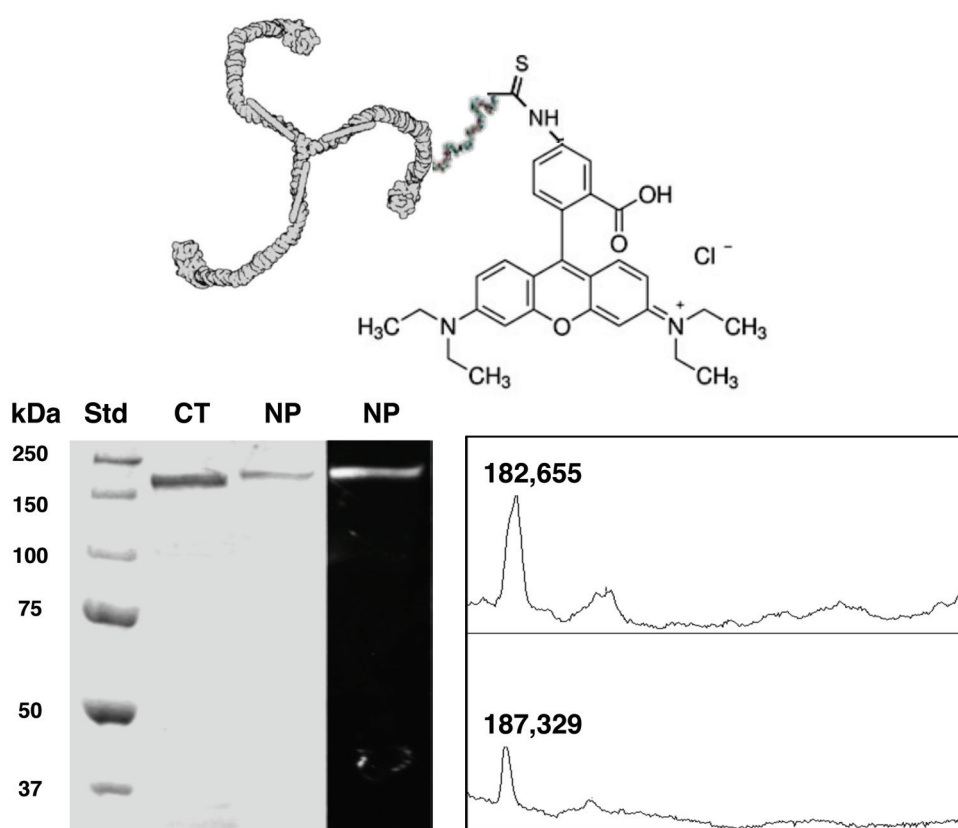


Figure 39. Clathrin triskelia rhodamine-PEG nanoplateforms: Line 1: Standards; Line 2: Unmodified Clathrin triskelia (CT); Lines 3 and 4: Clathrin nanoplateforms with attached rhodamine-PEGs (NP). SDS-PAGE analyses showed that modified clathrin heavy chain (CHC) bands coincided with the molecular weight marker of 187,329 kDa. Molecular weight of the CHC increased by 4,674 Da (from 182,655 to 187,329 Da) indicating that one molecule of the rhodamine-PEG was attached to the CHC.

Clathrin triskelia, as seen by electron microscopy and diagramed (Fig. 38A), is a three-legged protein complex composed of a trimer of clathrin heavy chains (CHC), with each CHC bound to a single clathrin light chain (CLC). The mean hydrodynamic radius of clathrin triskelia was 17.7 ± 6.4 nm (Figure 38B). Clathrin triskelia were modified with D3R-Ab-PEGs. The mean hydrodynamic radius of D3R-Ab-PEG-clathrin triskelia was 42.3 ± 14.8 nm (Fig. 38C). D3R-Ab-PEG-triskelia were about 25 nm larger than unmodified triskelia. A D3R-Ab was about 10 nm in size and PEGs were 15 nm in size. Thus, there were no free unattached antibodies in the nanoparticle solution.

Number of PEGs conjugated to clathrin cysteine residues were estimated spectrophotometrically with a rhodamine-PEG-maleimide, and confirmed by SDS PAGE

(Figure 39). The PEG maleimide group reacts specifically with protein sulfhydryl groups when the pH of the reaction mixture is about 7.4, resulting in the formation of a stable thioether linkage. Approximately one PEG molecule was attached to each triskelion CHC.

4.2.2. Immunoreactivity of D3RAb-Triskelia

Western Blot was used to determine whether D3R-Ab remained intact and functional after PEGylation and crosslinking with the clathrin protein. This test was based on the principle that only an intact D3RAb would be able to bind to its dopamine-3 receptor, thereby permitting determination of whether the protein retained its biological activity through the nanoparticle preparation process. Nanoparticle immunoreactivity was tested *in vitro* by Western Blot analyses of brain lysates from rat cortex and cerebellum. D3R-Ab-triskelia (Fig. 40) immunoreacted with two polypeptide bands with molecular sizes 49 kDa and 196 kDa respectively. These bands represent monomeric and tetrameric configurations of D3 protein receptors (Nimchinsky, Hof et al. 1997). Pre-incubation of nanoprobe with D3 synthetic peptides that blocked Ab immunoreactive sites caused the complete disappearance of immune bands (Fig. 40). Thus, D3R-Ab remained functionally intact in nanoparticle preparations and its immunoreactivity was blocked by the D3 synthetic peptide.

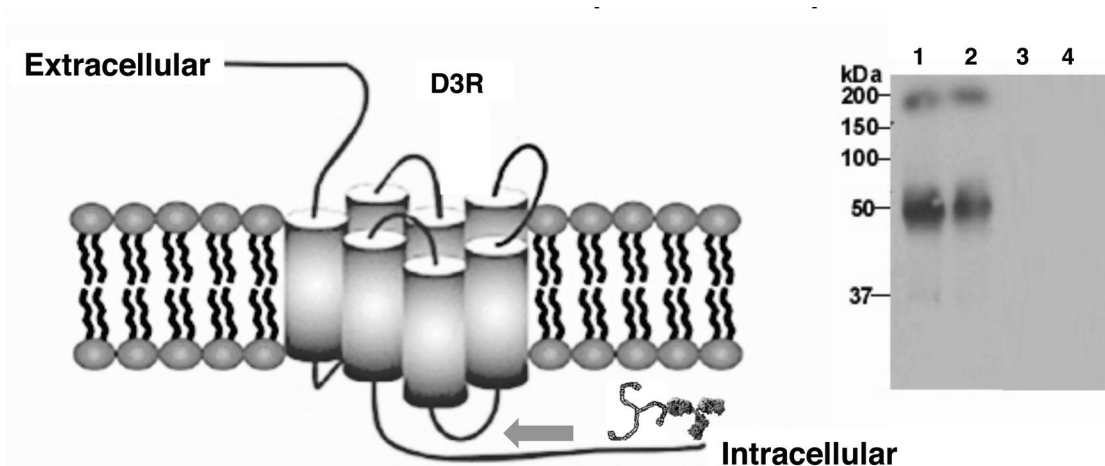


Figure 40. D3RAb-triskelion binds to the D3R: Diagram represents a D3R-Ab-triskelion, which recognizes the 3rd intracellular domain of the rat dopamine-3 receptor. Immuno-blots of membranes from the rat brain cortex (Lines 1 and 3) and cerebellum (Lines 2 and 4): D3R-Ab-triskelia immunoreacted with two polypeptide bands of expected molecular sizes (49 kDa and 196 kDa) (Lines 1 and 2). Pre-incubation of nanoprobe with D3 synthetic peptides caused the complete disappearance of immune bands (Lines 3 and 4) (Vitaliano and Vitaliano 2008).

4.3. Detection of D3RAb-Triskelia in D3R Brain Regions

The third goal was to demonstrate D3RAb-triskelia *in vivo* stability and targeted delivery to D3R brain regions both qualitatively and quantitatively.

4.3.1. Qualitative Detection of D3RAb-Triskelia in the CNS

In order to qualitatively confirm whether D3R-Ab-clathrin nanoprobe could specifically target D3R brain regions, male SD rats (250–300 g) (n=12) were randomized into 3 groups: D3R-Ab-triskelia group, D3R-Ab only group, and saline treated group. Three hours after intranasal administration rats were sacrificed and immunohistochemistry was performed.

The development of a protocol for D3Ab immunohistochemistry required several steps. First, a dilution study was conducted using varying dilutions of biotin labeled secondary goat anti-rabbit IgG (Vector labs). Based on secondary antibody dilution studies, it was concluded that a 1:200 dilution of secondary antibody resulted in the best immunohistochemical images (Figure 41). In addition, an antibody elimination control study was performed in which the anti-D3Ab primary antibody was omitted and only saline was given intranasally to rats. Primary antibody omission did not yield any staining.

Furthermore, in a set of sections the secondary antibody was omitted (no secondary control), while maintaining all other conditions in the assay, and these sections did not exhibit any staining. Subsequent D3RAb immunohistochemical assays were conducted with a 1:200 secondary antibody concentrations. Representative images of ant-D3R-Ab immunoreactivity (IR) from the nucleus accumbens, islands of Calleja, hippocampus and substantia nigra of rats are shown in Figure 41.

D3R-Abs were identified by immunohistochemistry in D3R brain regions only in rats that received D3R-Ab-triskelia, but not in animals that received D3R-Abs or saline. Thus, D3R-Ab-triskelia successfully bypassed the BBB intranasally, diffused through the brain, penetrated cells, and labeled D3 receptors in the following brain regions: olfactory tubercle, islands of Calleja, ventral pallidum, nucleus accumbens, striatum, frontal/parietal cortex, hippocampus, medial mammillary bodies, anteroventral thalamic nucleus, substantia nigra/ ventral tegmental area, and cerebellum (lobules 9 and 10).

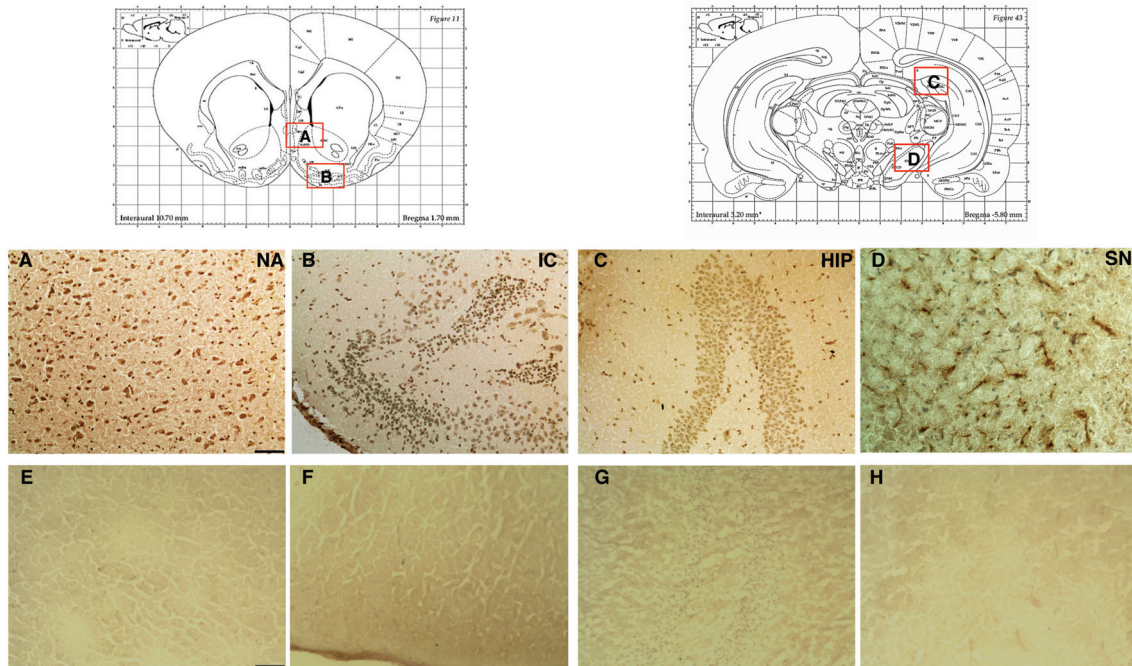


Figure 41. Nanoprobe targeted D3R rat brain regions: Three hours after intranasal administration positive signals (brown) from the anti-D3R-Ab can be detected by immunohistochemistry in D3 brain regions of perfused animals that received D3R-Ab-triskelia (upper panels), but not in animals that received only D3R-Abs (lower panels): (A, E) nucleus accumbens (NA); (B, F) islands of Calleja (IC); (C, G) hippocampus (HIP) and (D, H) substantia nigra (SN). Diagrams of coronal brain sections are from Paxinos and Watson (1998). The scale bar is 100 μ m (Vitaliano and Vitaliano 2008).

To determine whether nanoprobe distribution corresponded in perfused and non-perfused animals, D3RAb immunohistochemistry was performed on islands of Calleja, nucleus accumbens and substantia nigra sections from rats that received nanoprobe intranasally, but were not perfused with formaldehyde (Fig. 42). Animal perfusion can modify CNS penetration of nanoparticles and crosslink or mask protein targets.

As shown in Figure 42, D3R immunoreactivity was detectable in the IC, NA and SN. The pattern of labeling was similar to that observed in rats that were not perfused. Nanoprobe appeared to be concentrated in D3R brain regions with obvious cellular localization. This pattern suggests that nanoprobe distribution clearly reflects D3 receptor distribution in rat brain. Furthermore, the protein's integrity, as indicated by its recognition by a specific antibody, appeared to have been preserved throughout the process of nanoprobe preparation, uptake at the nasal epithelium, and transport in brain.

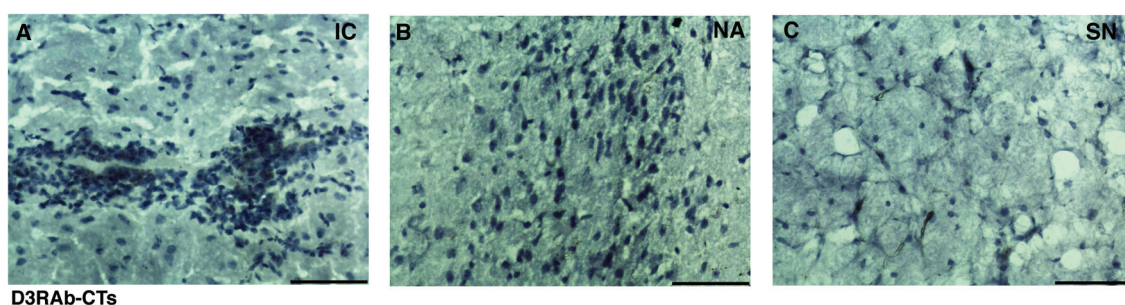


Figure 42. Nanoprobes targeted D3R brain regions. Three hours after intranasal administration of D3R-Ab-triskelia positive signals (black) from anti-D3R-Ab can be detected by IHC in D3R brain regions of non-perfused animals. Cell nuclei (blue) were stained with hematoxylin. The scale bar is 100 μ m (Vitaliano and Vitaliano 2008).

4.3.2. Qualitative Detection of Fluorescent D3R-Ab-Triskelia

In order to determine whether clathrin nanoplateforms with D3R-Abs could target D3Rs and remain stable in vivo, nanoparticles were modified with fluorescent tags (Vitaliano, Vitaliano et al. 2012). D3R-Ab-rhodamine-triskelia, D3R-Abs, rhodamine-triskelia, or saline, were administered intranasally in male SD rats (250–300 g) (n=4 per group).

Three hours after intranasal administration, positive signals from Alexa 488 anti-D3R-Ab (green) can be detected in D3R rat brain regions in rats that received D3R-Ab-triskelia, but not in control animals that received D3R-Abs or saline (Fig. 43). The punctate fluorescent deposits were mostly localized within discrete cellular structures. D3R-Ab-triskelia were identified in all D3R rat brain regions including the islands of Calleja (Fig. 43A), nucleus accumbens (Figure 43B), but not in the prefrontal cortex (Fig. 43C). In comparison, rhodamine-triskelia (red) (without targeting Abs) were identified in all rat brain regions, including the prefrontal cortex (Fig. 43I). Thus, fluorescent examination of D3R brain regions confirmed specific targeting of D3 receptors with D3R-Ab-triskelia.

In order to determine whether clathrin nanoplateforms with D3R-Abs could remain stable in vivo, nanoparticles were imaged with confocal microscopy. Confocal laser microscopy confirmed integrity and stability of the nanoprobes in the rat brain. For example, anti-D3R-Ab (Alexa 488, green, Fig. 44 A & D) and clathrin (rhodamine, red, Fig. 44 B & E) fluorescence co-localized in islands of Calleja (Fig. 44C) and nucleus accumbens (Fig. 44F). Nanoprobes were concentrated in D3R brain regions and had mostly cellular localization.

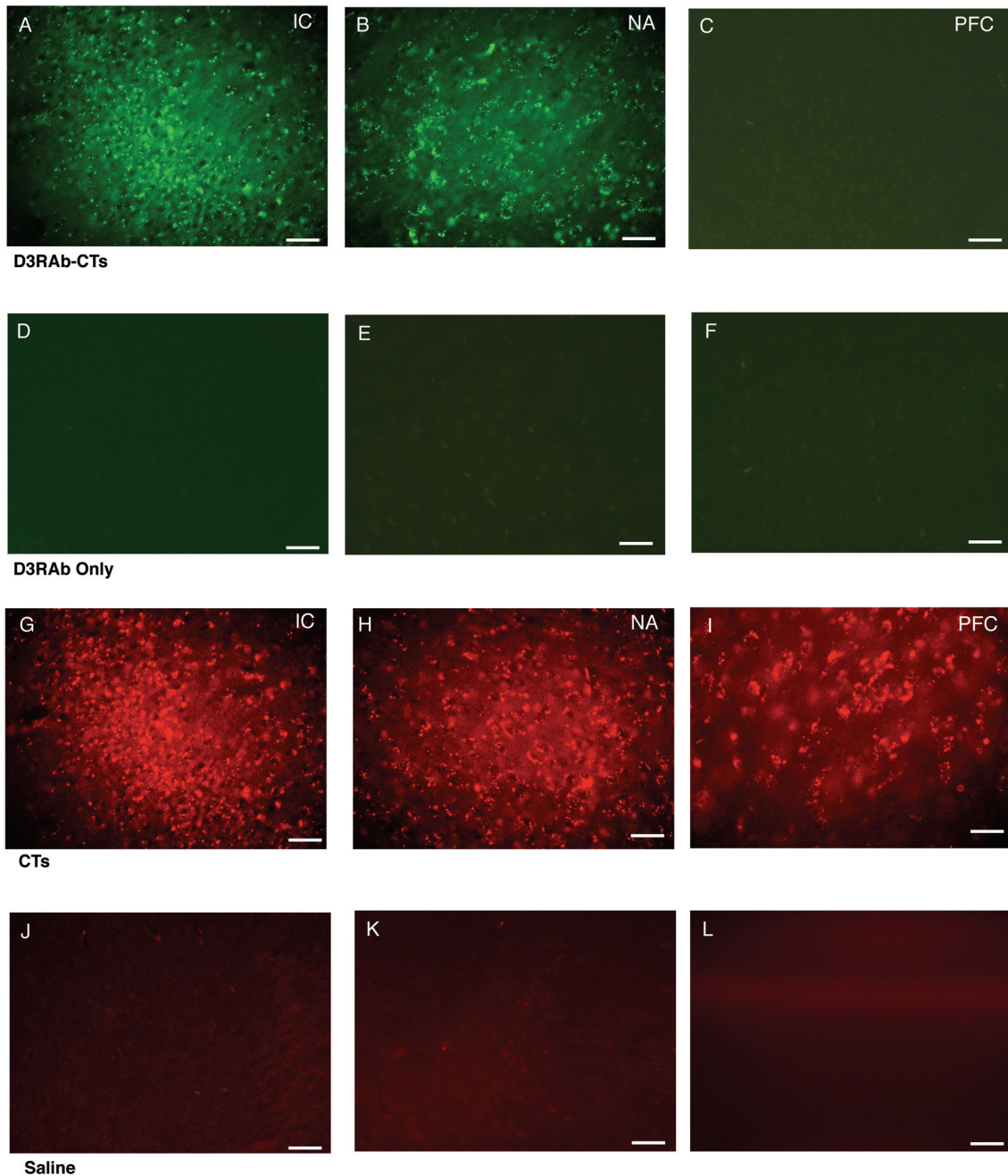


Figure 43. Fluorescent examination confirmed specific targeting of D3 receptors with nanoprobe: Anti-D3R-Ab immunofluorescence (Alexa 488, green) was detected in D3R brain regions of rats that received D3R-Ab nanoprobe: (A) islands of Calleja (IC) and (B) nucleus accumbens (NA); but not in the non-D3R region (C) the superficial layers of prefrontal cortex (PFC). Fluorescent signals from the anti-D3R-Abs were not detected in animals that only received D3R-Abs: (D) IC; (E) NA; and (F) PFC. Rhodamine-PEG-triskelia without targeting Abs (red) were observed in all brain regions of control animals: (G) IC; (H) NA; and (I) PFC. Punctuate fluorescent signals were not observed in animals that received saline (J, K, L). The scale bar is 50 μ m (Vitaliano and Vitaliano 2008).

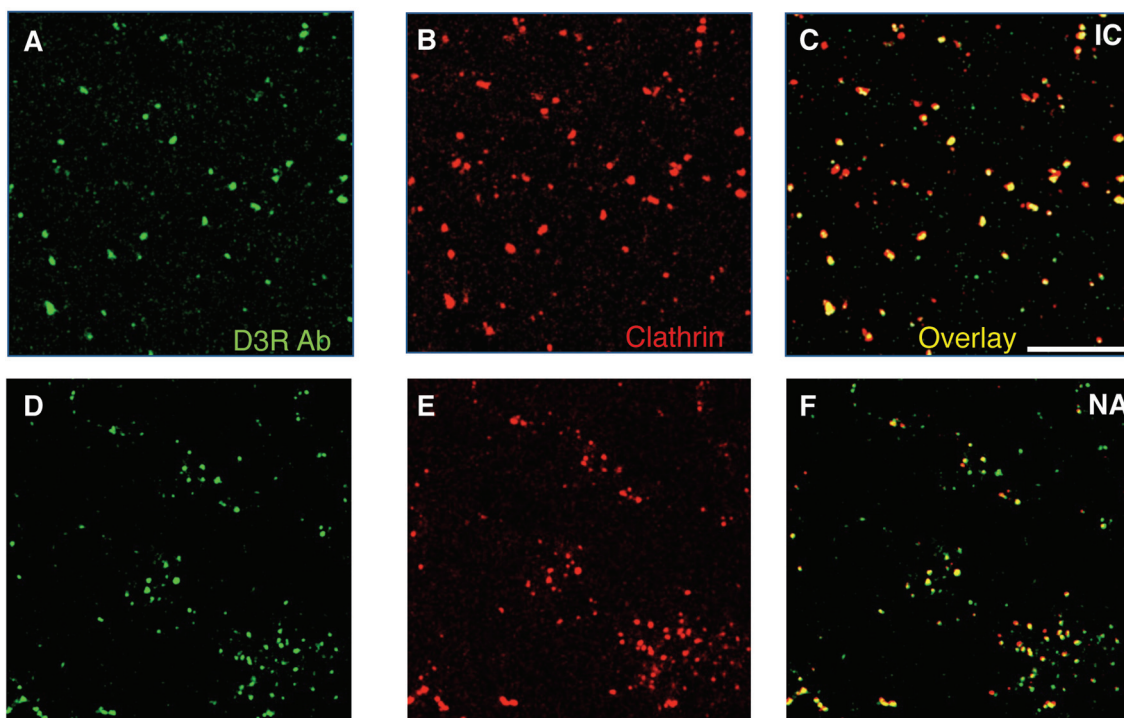


Figure 44. Confocal laser microscopy confirmed stability of nanoprobe in the rat brain. Anti-D3R-Ab immunofluorescence (Alexa 488, green) (A, D) and clathrin fluorescence (rhodamine, red) (B, E) were detected in D3R brain regions. Anti-D3R-Ab (Alexa 488, green) and clathrin (rhodamine, red) fluorescence co-localized (yellow) in the IC (C) and NA (F). The scale bar is 20 μm (Vitaliano and Vitaliano 2008).

4.3.3 Quantitative Detection of D3R-Ab-Triskelia in the CNS

Antibody was quantified in rat brain tissue by using Easy-Titer® Rabbit IgG Assay Kit (Pierce, Rockford, IL). Male Sprague-Dawley (SD) rats (250-300 g) (n=5 per group) received intranasally 64 $\mu\text{g}/\text{kg}$ of D3R-Ab-triskelia, or D3R-Ab (64 $\mu\text{g}/\text{kg}$) without triskelia or saline, and sacrificed 3 hours after intranasal delivery according to the published protocols (Gearhart, Middlemore et al. 2006).

The highest concentration of D3R-Ab-triskelia ($2,753 \pm 318$ ng per gram of tissue) was observed in the rat basal forebrain that included islands of Calleja and ventral pallidum (Fig. 45). D3R-Abs were also found in the nucleus accumbens ($1,028 \pm 235$ ng/g), striatum (358 ± 44 ng/g), hippocampus ($1,062 \pm 169$ ng/g), medial mammillary bodies (97 ± 4.4 ng/g) and substantia nigra/ ventral tegmental area (215 ± 56 ng/g). Low concentrations were detected in the cerebellum (84 ± 40 ng/g).

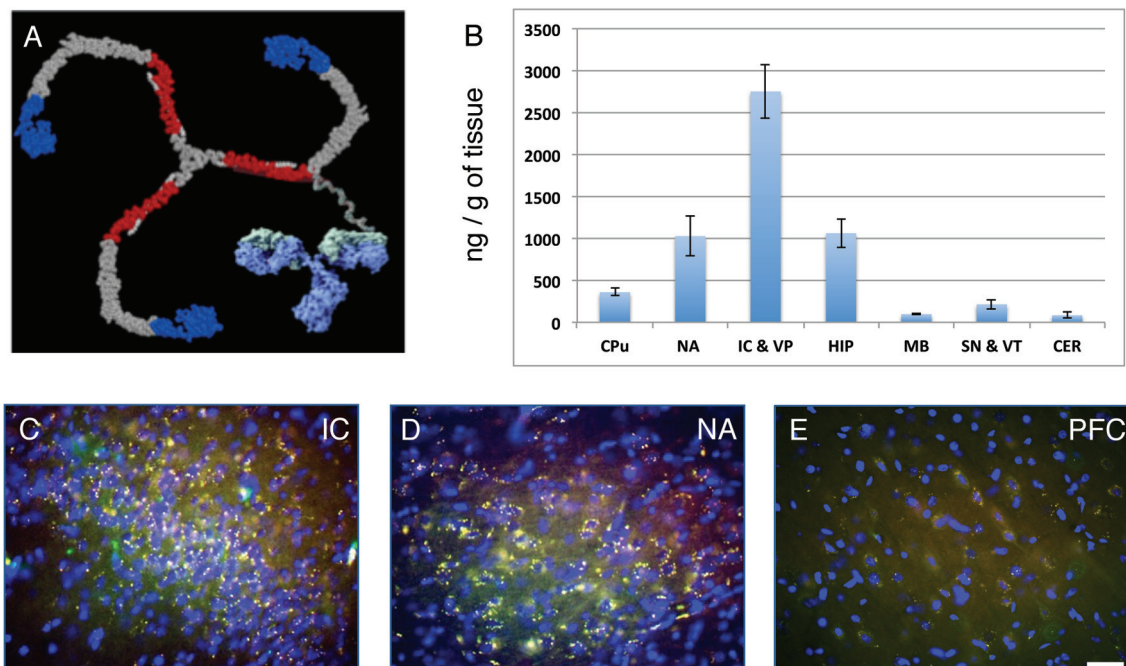


Figure 45. Plots of the in vivo brain distribution of D3R-Ab-triskelia in rats: Animals were sacrificed in groups of 5 at 180 min. post-intranasal administration. The mean dose (ng) of D3R-Ab-triskelia per gram of tissue is shown in the D3R brain regions (B): caudate/putamen (CPu), nucleus accumbens (NA), islands of Calleja (IC)/ ventral pallidum (VP), hippocampus (HIP), medial mammillary bodies (MB), substantia nigra (SN)/ ventral tegmental area (VT), and cerebellum (CER). D3R-Ab-nanopobes were not detected in the prefrontal cortex. D3R-Ab-triskelia (yellow) were also detected by immunofluorescence in D3R brain regions: (C) IC and (D) NA; but not in the non-D3R region (E) PFC. Cell nuclei (blue) were contra-stained with DAPI. The scale bar is 50 μm (Vitaliano and Vitaliano 2008).

D3R-Abs were not detected by assay in animals that received only D3R-Abs or saline. Also, D3R-Abs were not detected in the prefrontal cortex of animals that received D3Abs-CTs nanopobes (Figure 45E). Prefrontal cortex was used as a control region because it contains very low concentrations of D3R receptors (Le Foll, Wilson et al. 2014). These data indicated that D3RAb-nanoparticles remained functionally intact and targeted D3 brain receptors after intranasal delivery in rats. Also, there was no significant degradation of the D3RAb at the 3-hour time point, because the protein was detectable in brain homogenates by an anti-D3R-antibody in immunoassay.

4.4. Toxicity of D3RAb-triskelia

The fourth goal was to determine toxicity of intranasally administered D3RAb-triskelia in healthy rats. One hour after intranasal delivery and over a subsequent period of 2 hours each rat was examined every 30 minutes for lack of movement, ataxia, hunched posture, ruffled fur, hypothermia, dehydration, dyspnea, tachypnea, seizure and sustained rapid movement around the cage. Six rats continued to be examined every 24 h for 4 days. Histological studies were conducted in Sprague-Dawley rats (250-300 g) (n=6) four days after nanoprobe or saline administration. Rat brain tissues were processed, stained with hematoxylin and eosin, and compared using light microscopy. Careful monitoring of animals at different time points showed no clinical signs different from those of normal control rats. One rat in the study group and one rat in the control group experienced dyspnea and intranasal administration was briefly interrupted. Animals were able to recover quickly. Four days after nanoparticle administration no visible toxic effects were detected in the rat brains by histological studies (Fig. 46) (Vitaliano and Vitaliano 2008).

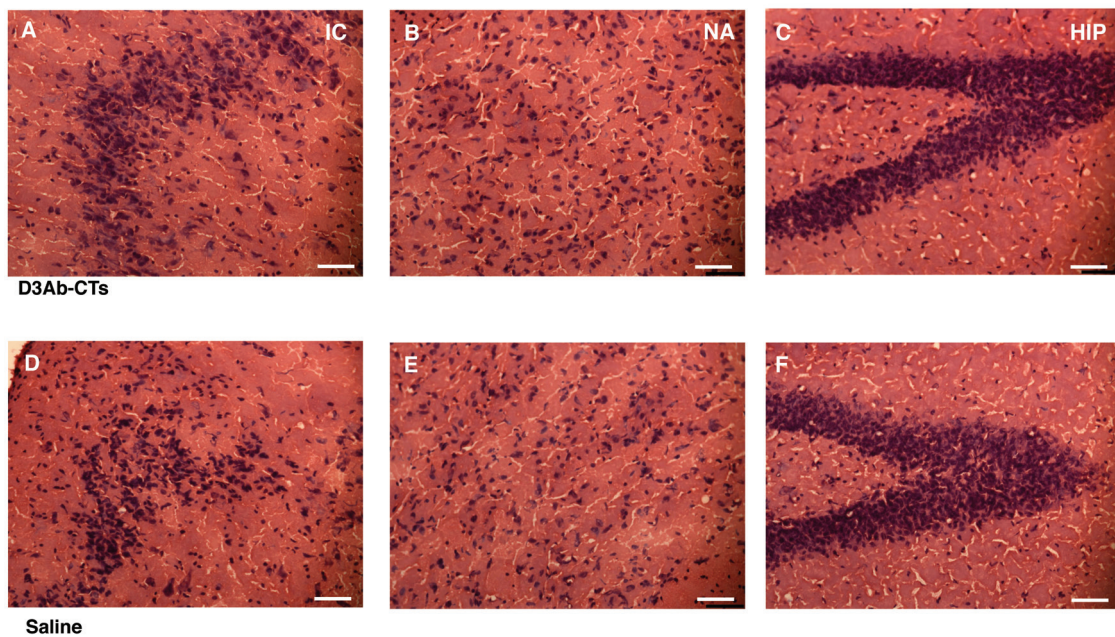


Figure 46. Nanoprobes were not neurotoxic: Four days after D3R-Ab-triskelia administration different brain sections (A) IC, (B) NA and (C) HIP were stained with hematoxylin and eosin and compared with control rat brain sections (D) IC, (E) NA and (F) HIP. No visible toxic effects were detected in the rat brains. The scale bar is 100.

5. DISCUSSION

The blood-brain barrier represents a major obstacle to development of new CNS therapeutics, impeding clinical use of promising neuropsychiatric drugs. CNS drug discovery is a difficult, complex and risky endeavor with high rates of attrition. Only 2% of small molecule CNS drug candidates (molecular weight <400 Da) can cross the blood brain barrier (BBB). Large molecules like antibodies have great potential for diagnosis and targeted treatment, but antibodies are effectively precluded from entering the brain, and the miniscule fraction that does (~ 0.1%) may take days to diffuse more than a few millimeters (Frank, Aboody et al. 2011). The development of new technologies for CNS imaging and drug delivery is a top priority goal of the National Institutes of Health (NIH) BRAIN Initiative.

Over the past 30 years, various protein-based nanoplatfoms such as dendrimers, nanogels, polymeric nanoparticles, liposomes, micelles, solid-lipid nanoparticles and Fullerenes, to name some, have been developed that show promise for imaging and also for delivery of different CNS therapies (Kobayashi and Brechbiel 2005, Manchester and Singh 2006, Gasco, Priano et al. 2009, Kabanov and Vinogradov 2009, Kozłowska, Foran et al. 2009, Maham, Tang et al. 2009, Mulder, Strijkers et al. 2009, Partha and Conyers 2009). While many diverse materials have been described and advanced as CNS drug carriers, clathrin, as a natural, non-toxic protein, offers important advantages. Indeed, nature has selected clathrin as its primary transporter for proteins, lipids, neurotransmitters, and some nutrients (Kirchhausen 2000, Pearse, Smith et al. 2000, Brodsky, Chen et al. 2001). Clathrin is the primary delivery vehicle responsible for transcytosis of large molecules like antibodies, hormones, growth factors at the BBB or nasal barrier (Gragera, Muniz et al. 1993, Omid, Campbell et al. 2003), but has never been tested as a nanoplatfom for transporting macromolecular proteins into the brain. Clathrin can move between neurons (Granseth, Odermatt et al. 2007), and is responsible for receptor-mediated endocytosis at the plasma membrane (Kirchhausen 2000, Pearse, Smith et al. 2000, Brodsky, Chen et al. 2001), but has never been used for delivery of therapeutic proteins inside cells. This thesis tested the hypothesis that clathrin, a protein that nature uses for transporting molecules across biological barriers and inside of cells, could serve as a vehicle to transport large molecules like antibodies and imaging agents into the brain, to target specific brain regions and penetrate cells. It further evaluated the feasibility of using a novel nanoplatfom for intranasal administration of macromolecular proteins across an intact BBB. Intranasal administration can bypass the blood-brain barrier and deliver therapeutically relevant concentrations of small proteins (<50 kDa), but not large proteins like antibodies (~150

kDa) directly to the brain (Lochhead and Thorne 2012). Brain delivery of proteins following intranasal administration has been previously demonstrated in rodents, non-human primates, and in humans (Lochhead and Thorne 2012). However, clathrin has never before been engineered for use as a macromolecular carrier for imaging or drug delivery, and dopamine antibodies have not been delivered noninvasively intranasally to the CNS.

Thus, as proof of principle this project first examined clathrin transport of imaging agents across BBB into the CNS to determine if it provided efficient CNS transport. The second phase of this research evaluated clathrin-mediated intranasal delivery of large molecules (e.g., dopamine-3 receptor antibodies) that cannot cross the BBB, to determine nose-to-brain transport in rats.

5.1. Clathrin Nanoparticles Exhibited Optimal Particle Sizes, Loading Efficiencies, Self-assembly Capabilities, and High Relaxivity

This study utilized a clathrin mono-unit (triskelion) with a radius of 17.7 nm. This measure compares well with other DLS studies of clathrin triskelion showing a Stokes radius of 17 to 18 nm (Ferguson, Prasad et al. 2006). An individual triskelion consists of three 190 kDa (1,675-residue) heavy chains, each bearing a single 25 kDa light chain (Kirchhausen 2000). A triskelion has an apparent native ability to enter cells (e.g., neurons) (Granseth, Odermatt et al. 2007). Thus, triskelia nanoplatfoms may offer significant potential in support of imaging of intracellular molecular markers and cell signaling pathways, for cellular tracking/imaging, and for intracellular delivery of drugs, genes and/or antisense oligonucleotides.

The first study goal was to create a method that would yield stable imaging nanoplatfoms that could provide enhanced imaging performance. A chelate ligand (DTPA-ITC) was attached to clathrin protein, and chelate to clathrin protein molar ratio was determined by using standard spectrophotometric methods (Pippin, Parker et al. 1992). Optimal DTPA-ITC loading for a single clathrin triskelion was 81. Saturation of clathrin binding sites resulted in a large number of metals (e.g., Gd^{+3}) attached to a single nanoparticle complex, which is important for different imaging and therapeutic modalities. At 0.47 T, Gd-DTPA-ITC-triskelia displayed a relaxivity of 16 $mM^{-1}s^{-1}$ per gadolinium ion and 1,166 $mM^{-1}s^{-1}$ per particle (Vitaliano, Vitaliano et al. 2012). Thus, triskelia exhibited 4 times higher ionic relaxivity and 291.5 times higher molecular relaxivity compared to Gd-DTPA. The molecular relaxivity was similar to relaxivity reported for some proteins

(e.g., albumin, fibrinogen, IgG) (Paajanen, Reisto et al. 1990), linear polymers (e.g., poly-L-lysine) (Schuhmann-Giampieri, Schmitt-Willich et al. 1991) and generation-5 dendrimers (Bryant, Brechbiel et al. 1999) that were covalently bound to Gd⁺³-DTPA.

Thus, a potent T₁ Gd-DTPA contrast agent was created using these novel nano-methods. However, a limitation was that nanoparticle characterizations were performed at 20 MHz. It is unclear whether similar relaxivities would be observed at other field strengths. Lower relaxivities were found for T₁ contrast agents at higher fields (Rohrer, Bauer et al. 2005, Noebauer-Huhmann, Szomolanyi et al. 2010). Further studies are needed to find optimal Gd-DTPA loading for clathrin-nanoplatfoms. Some studies showed longitudinal relaxivities increased initially with increasing Gd-DTPA/protein ratios, and reached a plateau at a particular Gd-DTPA/protein ratio (Nagaraja, Croxen et al. 2006). We reported T₁ measures, but T₂ measures should also be performed and an r_2/r_1 ratio estimated. In general, r_1 should be as large as possible, and r_2/r_1 ratio should be as close to 1 as possible in order for a nanoparticle to be used as a highly sensitive T₁ MRI contrast agent. In vitro experiments indicated that a clathrin-based CA could produce as much contrast as currently approved MRI contrast agents, but do so at much lower concentrations, which is important for minimizing Gd toxicity in clinical applications. More important, the addition of ligands or antibodies to the nanoplatfom may provide the specificity needed for molecular imaging. Further in-vivo MRI studies are required to determine minimal MRI-visible concentration and test stability, toxicity, biodistribution, and the general feasibility of these new nanoplatfoms for imaging.

5.2. Clathrin Triskelia Delivered Imaging Agents to the Brain after Intranasal and Intraperitoneal Administration

To determine if clathrin nanoplatfoms could enable in vivo, noninvasive delivery of imaging agents into the CNS, fluorescent-tagged triskelia were designed, and their utility for rat brain imaging tested. These qualitative studies provided first evidence that fluorescent-tagged clathrin nanoplatfoms were successfully delivered non-invasively into rat brain. Significantly, fluorescent clathrin triskelia crossed the BBB intraperitoneally and bypassed the BBB intranasally without enhancers or modifications, unlike other nanoparticle types (Bhaskar, Tian et al. 2010). Intranasal delivery of FITC-triskelia resulted in widespread brain distribution, as early as 30 min following intranasal administration (Figure 37). This rapid uptake indicated that intranasal administration of FITC-triskelia probably undergoes paracellular transport at the level of the olfactory epithelium. Transcellular or axonal mechanisms of nose-to-brain transport are unlikely

since they would require longer transit times to reach the brain (Graff and Pollack 2005). Also, clathrin triskelia quickly diffused throughout the rat brain. Moreover, the fluorescently labeled-nanoparticles appeared earlier in brain after intranasal delivery compared to intraperitoneal delivery, as evidenced by a greater number of fluorescent deposits visible at 30 min after I.N. administration (Figure 37). It was therefore decided that in the next phase a clathrin nanoparticle would be developed for intranasal transport of macromolecular proteins (e.g., antibodies) to the brain.

Both routes of delivery resulted in apparent cellular uptake of nanoparticles 90 minutes after delivery (Figures 35 & 36). The most likely mechanism involved in the intracellular uptake of clathrin triskelia is endocytosis. Clathrin can attach directly to adaptor proteins in cell membranes, but not lipids. Clathrin receptors on the cell surface have not been found and the exact mechanism of nanoparticle penetration into the cell needs to be elucidated. Moreover, the mechanism of clathrin transport through the BBB and nasal barrier is still unknown. Animal studies need to be conducted to clarify a mechanism of entry of clathrin nanoparticles into the CNS and into the cells.

5.3. D3R-Antibody-Triskelia Nanoprobes Have Optimal Particle Sizes and Loading Efficiencies

Conjugation of the D3R-Ab to clathrin triskelia resulted in particle sizes less than 60 nm, which is an optimal nanoparticle size for BBB penetration. The mean hydrodynamic radius of D3R-Ab-PEG-clathrin triskelia was 42.3 ± 14.8 nm (Fig. 38). Studies have estimated that molecules with a width of 38 - 64 nm may be transported through the fluid-filled pores of brain extracellular space (Thorne and Nicholson 2006). D3R-Ab-PEG-triskelia were about 25 nm larger than unmodified triskelia. D3R-Abs were about 10 nm in size and PEGs (MW 3,500 Da) were ~15 nm in size. Particles smaller than 20 nm were not observed after nanoparticle preparation. This result indicated that D3Rabs formed a stable and uniform complex with the clathrin triskelia and free antibodies were not present in the nanoparticle solution.

The immunoassay demonstrated that one molecule of D3Rab was attached to each clathrin triskelion. The number of PEGs conjugated to clathrin cysteine residues was also estimated spectrophotometrically with rhodamine-PEG-maleimide and confirmed by SDS PAGE (Fig. 39). One PEG molecule was attached to the reactive cysteine of the clathrin heavy chain. Intranasal administration of 50 μ l of this D3Rab nanoparticle preparation (0.318 mg/ml of Abs) resulted in a nominal dose of 16 μ g of Abs per rat.

Clathrin concentration in nanoparticle solution was 1.38 mg/ml and each rat received about 69 µg of modified clathrin triskelia.

5.4. D3RAb-Triskelia Remained Functionally Intact and Immunoreactive after Nanoparticle Preparation

D3RAb-CT nanoprobe integrity and immunoreactivity was determined after nanoparticle preparation by using Western Blot. The principle of this test was that only functionally intact D3RAb would be able to bind with high affinity and specificity to its D3 receptor in brain tissue homogenates. Results indicated that D3RAbs remained functionally intact following nanoparticle preparation and retained their biological activity. D3R-Ab-CTs nanoprobe immunoreacted specifically with two polypeptide bands (Fig. 40) that represented monomeric and tetrameric configurations of the D3 receptors respectively (Nimchinsky, Hof et al. 1997). The D3 synthetic peptide blocked D3RAb-nanoprobe binding to its receptor, which confirmed nanoprobe specificity.

5.5. D3RAb-Triskelia Nanoprobes Were Delivered to Targeted Brain Regions Following Intranasal Administration

Both qualitative and quantitative studies showed that D3R-Ab-CT nanoprobe were delivered to dopamine-3 brain regions following intranasal administration in rats. A previous study demonstrated delivery of D4R-Abs across the BBB after ultrasonic disruption, but D4R-Abs were only delivered to the sonicated brain region and brain concentrations were not reported (Kinoshita, McDannold et al. 2006). In contrast, D3R-Ab-CTs administered intranasally were able to diffuse throughout the brain and were discernible in regions distal to the olfactory bulbs. Also, D3R-Abs that were detected in D3R rat brain regions were sufficiently intact to be recognized by appropriate secondary antibodies.

As expected, the highest D3R-Ab-CTs concentrations were found in islands of Calleja, ventral pallidum and nucleus accumbens, as these regions are known to have the highest D3R density (Ariano and Sibley 1994, Bancroft, Morgan et al. 1998, Khan, Gutierrez et al. 1998, Diaz, Pilon et al. 2000, Stanwood, Artymyshyn et al. 2000). D3R-Ab-CTs were not detected qualitatively or quantitatively in non-D3R brain regions (e.g., superficial layers of the prefrontal cortex). Confocal laser microscopy confirmed integrity and stability of the nanoprobe in the rat brain as anti-D3R-Ab and clathrin fluorescence co-localized in D3R brain regions.

Interestingly, high D3R-Ab-CTs concentrations were also detected in the hippocampus. High D3R mRNA concentrations were previously found in hippocampus (Richtand, Kelsoe et al. 1995). These findings are inconsistent with results from *in vitro* autoradiography (Bancroft, Morgan et al. 1998) and some immunohistochemistry studies (Ariano and Sibley 1994), which show low D3 receptor densities in rat hippocampus. A key difference is that these studies used ligands or antibodies that only attached to the external epitopes of D3R without penetrating cells. However, this study used D3R-Abs that attached to the 3rd intracellular loop of D3R and could label receptors in the plasma membrane and cytoplasm (Khan, Gutierrez et al. 1998, Wolstencroft, Simic et al. 2007). Cytoplasmic D3Rs are shown to be abundant in the rat hippocampus (Wolstencroft, Simic et al. 2007).

Engineered clathrin-nanoplatfoms enabled D3R-Abs to penetrate cells, target the 3rd intracellular GPCR loop *in vivo* and bind to receptors in the cell membrane and cytoplasm. D3RAB-nanoparticles bind to D3 receptors within regions of the IC3 known to be motifs for regulation of D3 receptor trafficking pathways and signaling cascades. The segment of IC3 that binds to the D3RAB-nanoparticle is critical for D3 receptor function, and interacts with two proteins (parallemin and filamin-A) (Shioda, Takeuchi et al. 2010). These proteins regulate D3 receptor localization and signaling. Filamin-A anchors D3 receptors to the plasma membrane (Lin, Karpa et al. 2001), while paralemmin allows D3 receptors to couple to Gi proteins that inhibit cAMP (Basile, Lin et al. 2006). D3Rs can regulate cellular levels of cAMP in the hippocampus and are involved in long-term potentiation and memory formation (Swant 2006, 161, 2008, 492). D3R antagonists have been shown to improve cognitive functions in animals and humans (Nakajima, Gerretsen et al. 2013). Studies have also demonstrated that disruption of the interaction between dopamine D3 receptors and filamin-A can markedly reduce the number of D3 receptors in the cell membrane and inhibit receptor signaling (Li, Li et al. 2002). Therefore, D3RAB-CTs can be used to block D3R function that is enhanced in several psychiatric disorders like schizophrenia and drug addiction (Le Foll, Wilson et al. 2014). Therapeutic effects of D3RAB-CT nanoprobcs will be tested in future studies.

GPCR internal loops and their interacting proteins and signaling pathways are of particular interest as selective drug targets, but antibodies and peptides that interact with internal loops cannot be easily delivered to the CNS. For example, pepducins have been designed to penetrate cells and target the 3rd ICL of several GPCRs, but they cannot cross the BBB (Tressel, Koukos et al. 2011). Thus, clathrin nanoplatfoms may offer significant potential for bringing forward in time novel applications that are currently not considered feasible, and opening up new opportunities for drug discovery.

5.6. D3RAb-Triskelia Nanoprobes Were Delivered Highly-efficiently to the CNS and Remained Functionally Intact after Delivery

The CNS delivery of D3RAb-CTs was assessed quantitatively by using immunoassay. Immunoassay demonstrated that D3R-Ab protein integrity was conserved in brain tissue following intranasal administration. Intranasal delivery of D3R-Ab-CTs (64 $\mu\text{g}/\text{kg}$) resulted in relatively high concentrations of Abs in D3R-rich regions (e.g., $\sim 3 \mu\text{g}/\text{g}$ in islands of Calleja/ ventral pallidum). Moreover, delivery was efficient as this concentration represented a substantial portion of the administered dose (17.2% ID/g). One study demonstrated that intranasal delivery of antibodies (24 mg/kg) that were modified to avoid efflux from the CNS resulted in low brain concentrations (from 20 to 40 ng/g or 0.0003-0.0007 %ID/g) at the peak time point (Cooper, Ciambrone et al. 2013). In contrast, we delivered 375 times lower doses of Abs (64 $\mu\text{g}/\text{kg}$) to each rat intranasally via nanoparticles, and reported about 100 times higher concentrations in targeted brain regions (2,753 ng/g).

Antibodies have been delivered intranasally in some animal models with a compromised BBB (e.g., AD, stroke) (Lochhead and Thorne 2012), but not an intact BBB. One hour after induction of bilateral prefrontal photothrombosis in rats, intranasal administration of anti-glutamate antibody (250 $\mu\text{g}/\text{kg}$) improved retention of conditioned passive avoidance response (Romanova, Shakova et al. 2010). Moreover, intranasal delivery of the same Ab improved memory in rats that received injections of A β fragments (A β 25–35) into the nucleus basalis of Meynert (Gorbatov, Trekova et al. 2010). Anti-glutamate Abs were detected in the blood, but not the CNS. Furthermore, 5XFAD mice with A β plaques were treated intranasally twice a week for 8 weeks with a NU4 antibody (800 $\mu\text{g}/\text{kg}$) (Xiao, Davis et al. 2013). This treatment improved spatial memory, but reduced brain plaques in mice by only 28%. Therefore, only modest effects have been reported in removing A β from the CNS after intranasal delivery of Abs. Also, CNS concentrations of Abs were not reported in these studies, and therapeutic effects can be explained by “sinking” (Yu and Watts 2013) of CNS toxic molecules (e.g., A β or glutamate) into the vascular compartment and their removal from the vasculature. Moreover, fixed cellular molecular targets like CNS receptors have not been targeted with therapeutic antibodies using intranasal delivery.

BBB technologies for intravenous delivery of Abs required much larger doses of Abs (e.g., > 20 mg/kg) to deliver therapeutic CNS concentrations of Abs (Frank, Aboody et al. 2011). For example, 4 hours after ultrasound-induced BBB disruption and subsequent

intravenous administration of 20 mg/kg of Herceptin in mice, the mean Ab uptake in the sonicated brain tissue was about 0.5% ID/g (or 3 μ g/g) (Kinoshita, McDannold et al. 2006). Also, 48 hours after intravenous delivery of 20 mg/kg of a bispecific Ab that binds to TfR and BACE-1 (Yu, Zhang et al. 2011), the mean Ab uptake in the mouse brain was 0.57% ID/g. In comparison, the mean Ab uptake for monospecific anti-BACE-1 Ab was only 0.12% ID/g. Hence, intranasal delivery of clathrin-bound Abs may provide adequate concentrations (20 nM) in regions of interest using doses that are *300 times lower* than reported in previous BBB technology studies (Figure 47) (Frank, Aboody et al. 2011). Moreover, clathrin-conjugated antibodies can be detected at target sites throughout the brain within three-hours of administration rather than days. However, head-to-head comparisons are needed.

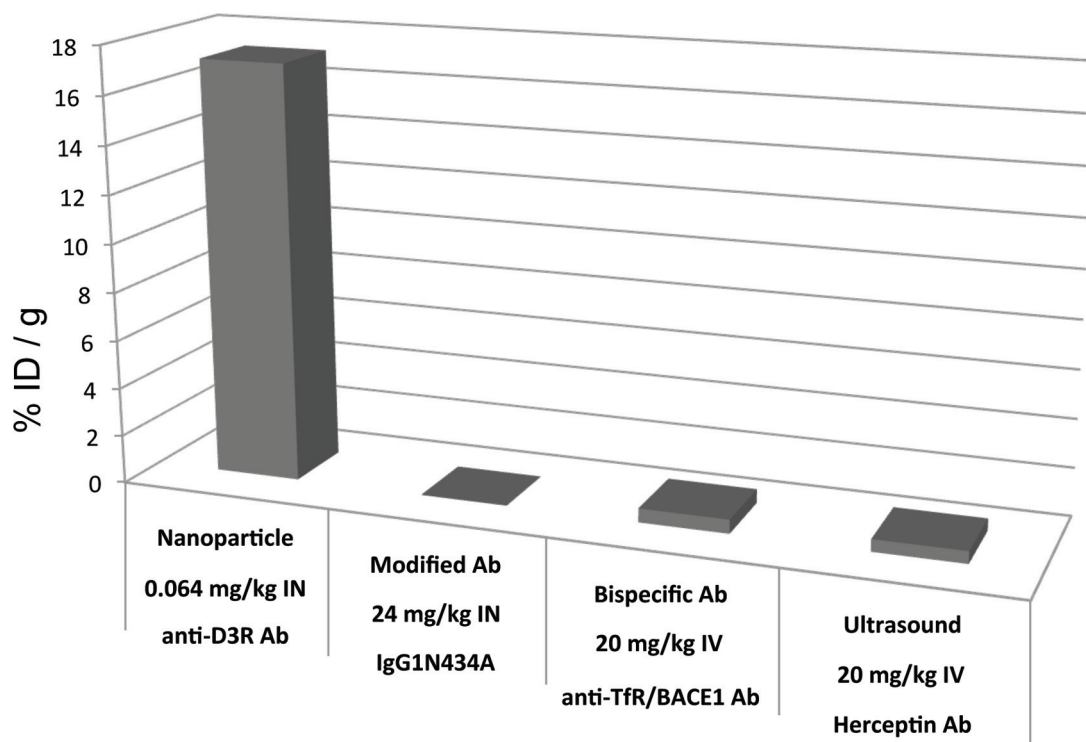


Figure 47. Comparisons of different methods for antibody delivery: Antibodies were given to animals intranasally with clathrin nanoparticles and resulted in the concentrations of 17.2 % of ID/g or 3 μ g/g in targeted brain regions. Other BBB technologies (e.g., modified Abs, bispecific Abs and ultrasonic delivery) delivered from 0.0007 % ID/g to 0.57 % ID /g of tissue (or 0.04 to 3.0 μ g/g) using 300 times higher doses.

6. CONCLUSION

This is the first report of dopamine Abs being successfully delivered *in vivo* noninvasively to the CNS in animals with an intact BBB. Intranasally administered D3R-Ab-clathrin-nanoparticles, but not D3R-Abs alone, can bypass the BBB; can rapidly diffuse throughout the CNS target regions with high D3R density; and can label D3 receptors in the cell membrane and cytoplasm. Thus, this study provides a new and detailed understanding and set of insights into the possibilities of utilizing clathrin protein as a novel nanotechnology for the transport of macromolecules that bypass the BBB and target specific cells. This technology is an improvement over existing BBB technologies and holds tremendous value for translational research, as it may enable antibodies to be used *in vivo* in a manner similar to conventional small ligands or pharmaceuticals, but with much greater specificity, intracellular efficacy, and reduced off-target side effects. Antibodies have great potential for diagnosis and targeted treatment of brain disorders. This nanotechnology holds promise for delivering antibodies to treat neurodegenerative disorders, to suppress neuroinflammation, infection or cancer growth, to regulate GPCR receptors, and to serve as nanoprobe for diagnosis and monitoring of cellular events.

To summarize, it was herein shown: **1)** A new nanotechnology method for CNS delivery of macromolecular proteins utilizing Clathrin bio-nanoparticles is feasible; **2)** Clathrin protein proved a small (~18 nm in size) and robust nanoplatfrom onto which multiple functional motifs could be added through chemical modifications of different amino acid residues; **3)** a single Clathrin triskelion can carry antibodies and imaging agents into the CNS; **4)** Clathrin nanoplatfroms can deliver different molecules that have high (e.g., D3R-Ab) and/or low (e.g., rhodamine) molecular weights, to specific brain regions inside targeted cells; **5)** Clathrin triskelia with drugs/ligands can cross or bypass the BBB and enter cells without enhancers or modifications, and **6)** Clathrin nanoprobe have potential for non-invasive CNS imaging and drug delivery. Results of this study should encourage further investigation into the use of clathrin triskelia as a new nanoplatfrom for molecular brain imaging and drug delivery.

7. REFERENCES

Abbott, N. J. (2013). "Blood-brain barrier structure and function and the challenges for CNS drug delivery." J Inherit Metab Dis **36**(3): 437-449.

Abbott, N. J., A. A. Patabendige, D. E. Dolman, S. R. Yusof and D. J. Begley (2010). "Structure and function of the blood-brain barrier." Neurobiol Dis **37**(1): 13-25.

Abbott, N. J., L. Ronnback and E. Hansson (2006). "Astrocyte-endothelial interactions at the blood-brain barrier." Nat Rev Neurosci **7**(1): 41-53.

Ahmed, M. and N. K. Cheung (2014). "Engineering anti-GD2 monoclonal antibodies for cancer immunotherapy." FEBS Lett **588**(2): 288-297.

Ahmed, M., D. W. Pan and M. E. Davis (2015). "Lack of in vivo antibody dependent cellular cytotoxicity with antibody containing gold nanoparticles." Bioconjug Chem **26**(5): 812-816.

Akunne, H. C., P. Towers, G. J. Ellis, D. Dijkstra, H. Wikstrom, T. G. Heffner, L. D. Wise and T. A. Pugsley (1995). "Characterization of binding of [3H]PD 128907, a selective dopamine D3 receptor agonist ligand, to CHO-K1 cells." Life Sci **57**(15): 1401-1410.

Alvarez, J. I., T. Katayama and A. Prat (2013). "Glial influence on the blood brain barrier." Glia **61**(12): 1939-1958.

Anderson, E. A., S. Isaacman, D. S. Peabody, E. Y. Wang, J. W. Canary and K. Kirshenbaum (2006). "Viral nanoparticles donning a paramagnetic coat: conjugation of MRI contrast agents to the MS2 capsid." Nano Lett **6**(6): 1160-1164.

Anderson, M. A., Y. Ao and M. V. Sofroniew (2014). "Heterogeneity of reactive astrocytes." Neurosci Lett **565**: 23-29.

Andras, I. E., H. Pu, M. A. Deli, A. Nath, B. Hennig and M. Toborek (2003). "HIV-1 Tat protein alters tight junction protein expression and distribution in cultured brain endothelial cells." J Neurosci Res **74**(2): 255-265.

Ariano, M. A. and D. R. Sibley (1994). "Dopamine receptor distribution in the rat CNS: elucidation using anti-peptide antisera directed against D1A and D3 subtypes." Brain Res **649**(1-2): 95-110.

Armulik, A., G. Genove, M. Mae, M. H. Nisancioglu, E. Wallgard, C. Niaudet, L. He, J. Norlin, P. Lindblom, K. Strittmatter, B. R. Johansson and C. Betsholtz (2010). "Pericytes regulate the blood-brain barrier." Nature **468**(7323): 557-561.

Artemov, D., Z. M. Bhujwala and J. W. Bulte (2004). "Magnetic resonance imaging of cell surface receptors using targeted contrast agents." Curr Pharm Biotechnol **5**(6): 485-494.

Attwell, D., A. M. Buchan, S. Charpak, M. Lauritzen, B. A. Macvicar and E. A. Newman (2010). "Glial and neuronal control of brain blood flow." Nature **468**(7321): 232-243.

Augustine, G. J., J. R. Morgan, C. A. Villalba-Galea, S. Jin, K. Prasad and E. M. Lafer (2006). "Clathrin and synaptic vesicle endocytosis: studies at the squid giant synapse." Biochem Soc Trans **34**(Pt 1): 68-72.

Baba, T., C. Rauch, M. Xue, N. Terada, Y. Fujii, H. Ueda, I. Takayama, S. Ohno, E. Farge and S. B. Sato (2001). "Clathrin-dependent and clathrin-independent endocytosis are differentially sensitive to insertion of poly (ethylene glycol)-derivatized cholesterol in the plasma membrane." Traffic **2**(7): 501-512.

Balda, M. S. and K. Matter (2009). "Tight junctions and the regulation of gene expression." Biochim Biophys Acta **1788**(4): 761-767.

Balin, B. J., R. D. Broadwell, M. Salzman and M. el-Kalliny (1986). "Avenues for entry of peripherally administered protein to the central nervous system in mouse, rat, and squirrel monkey." J Comp Neurol **251**(2): 260-280.

Balyasnikova, I. V., S. D. Ferguson, S. Sengupta, Y. Han and M. S. Lesniak (2010). "Mesenchymal stem cells modified with a single-chain antibody against EGFRvIII successfully inhibit the growth of human xenograft malignant glioma." PLoS One **5**(3): e9750.

Bancroft, G. N., K. A. Morgan, R. J. Flietstra and B. Levant (1998). "Binding of [3H] PD 128907, a putatively selective ligand for the D3 dopamine receptor, in rat brain: a receptor binding and quantitative autoradiographic study." Neuropsychopharmacology **18**(4): 305-316.

Banks, W. A. (2009). "Characteristics of compounds that cross the blood-brain barrier." BMC Neurol **9 Suppl 1**: S3.

Banks, W. A., B. Terrell, S. A. Farr, S. M. Robinson, N. Nonaka and J. E. Morley (2002). "Passage of amyloid beta protein antibody across the blood-brain barrier in a mouse model of Alzheimer's disease." Peptides **23**(12): 2223-2226.

Barani, I. J. and D. A. Larson (2015). "Radiation therapy of glioblastoma." Cancer Treat Res **163**: 49-73.

Bard, F., M. Fox, S. Friedrich, P. Seubert, D. Schenk, G. G. Kinney and T. Yednock (2012). "Sustained levels of antibodies against Aβ in amyloid-rich regions of the CNS following intravenous dosing in human APP transgenic mice." Exp Neurol **238**(1): 38-43.

Basile, M., R. Lin, N. Kabbani, K. Karpa, M. Kilimann, I. Simpson and M. Kester (2006). "Paralemmin interacts with D3 dopamine receptors: implications for membrane localization and cAMP signaling." Arch Biochem Biophys **446**(1): 60-68.

Battaglia, L., M. Gallarate, E. Peira, D. Chirio, I. Solazzi, S. M. Giordano, C. L. Gigliotti, C. Riganti and C. Dianzani (2015). "Bevacizumab loaded solid lipid nanoparticles prepared by the coacervation technique: preliminary in vitro studies." Nanotechnology **26**(25): 255102.

Bauer, H. C., I. A. Krizbai, H. Bauer and A. Traweger (2014). "'You Shall Not Pass'-tight junctions of the blood brain barrier." Front Neurosci **8**: 392.

Baumann, B. C., G. D. Kao, A. Mahmud, T. Harada, J. Swift, C. Chapman, X. Xu, D. E. Discher and J. F. Dorsey (2013). "Enhancing the efficacy of drug-loaded nanocarriers against brain tumors by targeted radiation therapy." Oncotarget **4**(1): 64-79.

Baust, T., C. Czupalla, E. Krause, L. Bourel-Bonnet and B. Hoflack (2006). "Proteomic analysis of adaptor protein 1A coats selectively assembled on liposomes." Proc Natl Acad Sci U S A **103**(9): 3159-3164.

Beeman, N., P. G. Webb and H. K. Baumgartner (2012). "Occludin is required for apoptosis when claudin-claudin interactions are disrupted." Cell Death Dis **3**: e273.

Begley, D. J. and M. W. Brightman (2003). "Structural and functional aspects of the blood-brain barrier." Prog Drug Res **61**: 39-78.

Bell, R. D., E. A. Winkler, A. P. Sagare, I. Singh, B. LaRue, R. Deane and B. V. Zlokovic (2010). "Pericytes control key neurovascular functions and neuronal phenotype in the adult brain and during brain aging." Neuron **68**(3): 409-427.

Bhaskar, S., F. Tian, T. Stoeger, W. Kreyling, J. M. de la Fuente, V. Grazu, P. Borm, G. Estrada, V. Ntziachristos and D. Razansky (2010). "Multifunctional Nanocarriers for diagnostics, drug delivery and targeted treatment across blood-brain barrier: perspectives on tracking and neuroimaging." Part Fibre Toxicol **7**: 3.

Bickel, U., S. Yamada and W. M. Pardridge (1994). "Synthesis and bioactivity of monobiotinylated DALDA: a μ-specific opioid peptide designed for targeted brain delivery." J Pharmacol Exp Ther **268**(2): 791-796.

Bidros, D. S. and M. A. Vogelbaum (2009). "Novel drug delivery strategies in neuro-oncology." Neurotherapeutics **6**(3): 539-546.

Bien-Ly, N., Y. J. Yu, D. Bumbaca, J. Elstrott, C. A. Boswell, Y. Zhang, W. Luk, Y. Lu, M. S. Dennis, R. M. Weimer, I. Chung and R. J. Watts (2014). "Transferrin receptor (TfR) trafficking determines brain uptake of TfR antibody affinity variants." J Exp Med **211**(2): 233-244.

Black, K. L., D. Yin, J. M. Ong, J. Hu, B. M. Konda, X. Wang, M. K. Ko, J. A. Bayan, M. R. Sacapano, A. Espinoza, D. K. Irvin and Y. Shu (2008). "PDE5 inhibitors enhance tumor permeability and efficacy of chemotherapy in a rat brain tumor model." Brain Res **1230**: 290-302.

Blasig, I. E., C. Bellmann, J. Cording, G. Del Vecchio, D. Zwanziger, O. Huber and R. F. Haseloff (2011). "Occludin protein family: oxidative stress and reducing conditions." Antioxid Redox Signal **15**(5): 1195-1219.

Boado, R. J., J. Z. Lu, E. K. Hui and W. M. Pardridge (2010). "IgG-single chain Fv fusion protein therapeutic for Alzheimer's disease: Expression in CHO cells and pharmacokinetics and brain delivery in the rhesus monkey." Biotechnol Bioeng **105**(3): 627-635.

Boado, R. J. and W. M. Pardridge (2009). "Comparison of blood-brain barrier transport of glial-derived neurotrophic factor (GDNF) and an IgG-GDNF fusion protein in the rhesus monkey." Drug Metab Dispos **37**(12): 2299-2304.

Boado, R. J. and W. M. Pardridge (2010). "Genetic engineering of IgG-glucuronidase fusion proteins." J Drug Target **18**(3): 205-211.

Boado, R. J., Q. H. Zhou, J. Z. Lu, E. K. Hui and W. M. Pardridge (2009). "Pharmacokinetics and Brain Uptake of a Genetically Engineered Bifunctional Fusion Antibody Targeting the Mouse Transferrin Receptor." Mol Pharm.

Bobo, R. H., D. W. Laske, A. Akbasak, P. F. Morrison, R. L. Dedrick and E. H. Oldfield (1994). "Convection-enhanced delivery of macromolecules in the brain." Proc Natl Acad Sci U S A **91**(6): 2076-2080.

Boileau, I., M. Guttman, P. Rusjan, J. R. Adams, S. Houle, J. Tong, O. Hornykiewicz, Y. Furukawa, A. A. Wilson, S. Kapur and S. J. Kish (2009). "Decreased binding of the D3 dopamine receptor-preferring ligand [11C]-(+)-PHNO in drug-naive Parkinson's disease." Brain **132**(Pt 5): 1366-1375.

Boileau, I., D. Payer, B. Chugani, D. Lobo, A. Behzadi, P. M. Rusjan, S. Houle, A. A. Wilson, J. Warsh, S. J. Kish and M. Zack (2013). "The D2/3 dopamine receptor in pathological gambling: a positron emission tomography study with [11C]-(+)-propyl-hexahydro-naphtho-oxazin and [11C]raclopride." Addiction **108**(5): 953-963.

Boileau, I., D. Payer, S. Houle, A. Behzadi, P. M. Rusjan, J. Tong, D. Wilkins, P. Selby, T. P. George, M. Zack, Y. Furukawa, T. McCluskey, A. A. Wilson and S. J. Kish (2012). "Higher binding of the dopamine D3 receptor-preferring ligand [11C]-(+)-propyl-hexahydro-naphtho-oxazin in methamphetamine polydrug users: a positron emission tomography study." J Neurosci **32**(4): 1353-1359.

Boockvar, J. A., A. J. Tsiouris, C. P. Hofstetter, I. Kovanlikaya, S. Fralin, K. Kesavabhotla, S. M. Seedial, S. C. Pannullo, T. H. Schwartz, P. Stieg, R. D. Zimmerman, J. Knopman, R. J. Scheff, P. Christos, S. Vallabhajosula and H. A. Riina (2011). "Safety and maximum tolerated dose of superselective intraarterial cerebral infusion of bevacizumab after osmotic blood-brain barrier disruption for recurrent malignant glioma. Clinical article." J Neurosurg **114**(3): 624-632.

Bouras, A., M. Kaluzova and C. G. Hadjipanayis (2015). "Radiosensitivity enhancement of radioresistant glioblastoma by epidermal growth factor receptor antibody-conjugated iron-oxide nanoparticles." J Neurooncol **124**(1): 13-22.

Bouthenet, M. L., E. Souil, M. P. Martres, P. Sokoloff, B. Giros and J. C. Schwartz (1991). "Localization of dopamine D3 receptor mRNA in the rat brain using in situ hybridization histochemistry: comparison with dopamine D2 receptor mRNA." Brain Res **564**(2): 203-219.

Braen, A. P., J. Perron, P. Tellier, A. R. Catala, G. Kolaitis and W. Geng (2010). "A 4-week intrathecal toxicity and pharmacokinetic study with trastuzumab in cynomolgus monkeys." Int J Toxicol **29**(3): 259-267.

Brodsky, F. M. (2012). "Diversity of clathrin function: new tricks for an old protein." Annu Rev Cell Dev Biol **28**: 309-336.

Brodsky, F. M., C. Y. Chen, C. Knuehl, M. C. Towler and D. E. Wakeham (2001). "Biological basket weaving: formation and function of clathrin-coated vesicles." Annu Rev Cell Dev Biol **17**: 517-568.

Brown, A. M. and B. R. Ransom (2007). "Astrocyte glycogen and brain energy metabolism." Glia **55**(12): 1263-1271.

Bryant, L. H., Jr., M. W. Brechbiel, C. Wu, J. W. Bulte, V. Herynek and J. A. Frank (1999). "Synthesis and relaxometry of high-generation (G = 5, 7, 9, and 10) PAMAM dendrimer-DOTA-gadolinium chelates." J Magn Reson Imaging **9**(2): 348-352.

Bullard, D. E., M. Bourdon and D. D. Bigner (1984). "Comparison of various methods for delivering radiolabeled monoclonal antibody to normal rat brain." J Neurosurg **61**(5): 901-911.

Burgess, A. and K. Hynynen (2014). "Drug delivery across the blood-brain barrier using focused ultrasound." Expert Opin Drug Deliv **11**(5): 711-721.

Bushong, E. A., M. E. Martone, Y. Z. Jones and M. H. Ellisman (2002). "Protoplasmic astrocytes in CA1 stratum radiatum occupy separate anatomical domains." J Neurosci **22**(1): 183-192.

Campbell, C. H., R. E. Fine, J. Squicciarini and L. H. Rome (1983). "Coated vesicles from rat liver and calf brain contain cryptic mannose 6-phosphate receptors." J Biol Chem **258**(4): 2628-2633.

Canovi, M., E. Markoutsas, A. N. Lazar, G. Pampalakis, C. Clemente, F. Re, S. Sesana, M. Masserini, M. Salmona, C. Duyckaerts, O. Flores, M. Gobbi and S. G. Antimisiaris (2011). "The binding affinity of anti-A β 1-42 MAb-decorated nanoliposomes to A β 1-42 peptides in vitro and to amyloid deposits in post-mortem tissue." Biomaterials **32**(23): 5489-5497.

Capsoni, S., S. Covaceuszach, G. Ugolini, F. Spirito, D. Vignone, B. Stefanini, G. Amato and A. Cattaneo (2009). "Delivery of NGF to the brain: intranasal versus ocular administration in anti-NGF transgenic mice." J Alzheimers Dis **16**(2): 371-388.

Capsoni, S., S. Giannotta and A. Cattaneo (2002). "Nerve growth factor and galantamine ameliorate early signs of neurodegeneration in anti-nerve growth factor mice." Proc Natl Acad Sci U S A **99**(19): 12432-12437.

Cattepoel, S., M. Hanenberg, L. Kulic and R. M. Nitsch (2011). "Chronic intranasal treatment with an anti-A β (30-42) scFv antibody ameliorates amyloid pathology in a transgenic mouse model of Alzheimer's disease." PLoS One **6**(4): e18296.

Chauhan, N. B., F. Davis and C. Xiao (2011). "Wheat germ agglutinin enhanced cerebral uptake of anti-A β antibody after intranasal administration in 5XFAD mice." Vaccine **29**(44): 7631-7637.

Chen, C. Y. and F. M. Brodsky (2005). "Huntingtin-interacting protein 1 (Hip1) and Hip1-related protein (Hip1R) bind the conserved sequence of clathrin light chains and thereby influence clathrin assembly in vitro and actin distribution in vivo." J Biol Chem **280**(7): 6109-6117.

Cheng, Y., W. Boll, T. Kirchhausen, S. C. Harrison and T. Walz (2007). "Cryo-electron tomography of clathrin-coated vesicles: structural implications for coat assembly." J Mol Biol **365**(3): 892-899.

Conner, S. D. and S. L. Schmid (2003). "Regulated portals of entry into the cell." Nature **422**(6927): 37-44.

Cooper, M. S., E. Sabbah and S. J. Mather (2006). "Conjugation of chelating agents to proteins and radiolabeling with trivalent metallic isotopes." Nat Protoc **1**(1): 314-317.

Cooper, P. R., G. J. Ciambone, C. M. Kliwinski, E. Maze, L. Johnson, Q. Li, Y. Feng and P. J. Hornby (2013). "Efflux of monoclonal antibodies from rat brain by neonatal Fc receptor, FcRn." Brain Res **1534**: 13-21.

Couch, J. A., Y. J. Yu, Y. Zhang, J. M. Tarrant, R. N. Fuji, W. J. Meilandt, H. Solanoy, R. K. Tong, K. Hoyte, W. Luk, Y. Lu, K. Gadkar, S. Prabhu, B. A. Ordonia, Q. Nguyen, Y. Lin, Z. Lin, M. Balazs, K. Scarce-Levie, J. A. Ernst, M. S. Dennis and R. J. Watts (2013). "Addressing safety liabilities of TfR bispecific antibodies that cross the blood-brain barrier." Sci Transl Med **5**(183): 183ra157, 181-112.

Crowther, R. A. and B. M. Pearse (1981). "Assembly and packing of clathrin into coats." J Cell Biol **91**(3 Pt 1): 790-797.

Dalkara, T. and L. Alarcon-Martinez (2015). "Cerebral microvascular pericytes and neurogliovascular signaling in health and disease." Brain Res **1623**: 3-17.

Daniels, T. R., E. Bernabeu, J. A. Rodriguez, S. Patel, M. Kozman, D. A. Chiappetta, E. Holler, J. Y. Ljubimova, G. Helguera and M. L. Penichet (2012). "The transferrin receptor and the targeted delivery of therapeutic agents against cancer." Biochim Biophys Acta **1820**(3): 291-317.

Datta, A., J. M. Hooker, M. Botta, M. B. Francis, S. Aime and K. N. Raymond (2008). "High relaxivity gadolinium hydroxypyridonate-viral capsid conjugates: nanosized MRI contrast agents." J Am Chem Soc **130**(8): 2546-2552.

Davson, H., B. Zlokovic, L. Rakic and M. Segal (1993). An Introduction to the Blood-brain Barrier Macmillan.

De Keyser, J., J. P. Mostert and M. W. Koch (2008). "Dysfunctional astrocytes as key players in the pathogenesis of central nervous system disorders." J Neurol Sci **267**(1-2): 3-16.

De Rosa, R., A. A. Garcia, C. Braschi, S. Capsoni, L. Maffei, N. Berardi and A. Cattaneo (2005). "Intranasal administration of nerve growth factor (NGF) rescues recognition memory deficits in AD11 anti-NGF transgenic mice." Proc Natl Acad Sci U S A **102**(10): 3811-3816.

del Burgo, L. S., R. M. Hernandez, G. Orive and J. L. Pedraz (2014). "Nanotherapeutic approaches for brain cancer management." Nanomedicine **10**(5): 905-919.

Deli, M. A. (2009). "Potential use of tight junction modulators to reversibly open membranous barriers and improve drug delivery." Biochim Biophys Acta **1788**(4): 892-910.

Dell'Angelica, E. C., J. Klumperman, W. Stoorvogel and J. S. Bonifacino (1998). "Association of the AP-3 adaptor complex with clathrin." Science **280**(5362): 431-434.

Desai, B. S., A. J. Monahan, P. M. Carvey and B. Hendey (2007). "Blood-brain barrier pathology in Alzheimer's and Parkinson's disease: implications for drug therapy." Cell Transplant **16**(3): 285-299.

Dhuria, S. V., L. R. Hanson and W. H. Frey, 2nd (2010). "Intranasal delivery to the central nervous system: mechanisms and experimental considerations." J Pharm Sci **99**(4): 1654-1673.

Diaz, J., D. Levesque, C. H. Lammers, N. Griffon, M. P. Martres, J. C. Schwartz and P. Sokoloff (1995). "Phenotypical characterization of neurons expressing the dopamine D3 receptor in the rat brain." Neuroscience **65**(3): 731-745.

Diaz, J., C. Pilon, B. Le Foll, C. Gros, A. Triller, J. C. Schwartz and P. Sokoloff (2000). "Dopamine D3 receptors expressed by all mesencephalic dopamine neurons." J Neurosci **20**(23): 8677-8684.

Diaz, R. J., P. Z. McVeigh, M. A. O'Reilly, K. Burrell, M. Bebenek, C. Smith, A. B. Etame, G. Zadeh, K. Hynynen, B. C. Wilson and J. T. Rutka (2014). "Focused ultrasound delivery of Raman nanoparticles across the blood-brain barrier: potential for targeting experimental brain tumors." Nanomedicine **10**(5): 1075-1087.

Diaz-Flores, L., R. Gutierrez, J. F. Madrid, H. Varela, F. Valladares, E. Acosta, P. Martin-Vasallo and L. Diaz-Flores, Jr. (2009). "Pericytes. Morphofunction, interactions and pathology in a quiescent and activated mesenchymal cell niche." Histol Histopathol **24**(7): 909-969.

Djupesland, P. G., J. C. Messina and R. A. Mahmoud (2014). "The nasal approach to delivering treatment for brain diseases: an anatomic, physiologic, and delivery technology overview." Ther Deliv **5**(6): 709-733.

Doolittle, N. D., K. Jahnke, R. Belanger, D. A. Ryan, R. W. Nance, Jr., C. A. Lacy, R. M. Tyson, M. Haluska, N. A. Hedrick, C. Varallyay and E. A. Neuwelt (2007). "Potential of chemo-immunotherapy and radioimmunotherapy in relapsed primary central nervous system (CNS) lymphoma." Leuk Lymphoma **48**(9): 1712-1720.

Doolittle, N. D., M. E. Miner, W. A. Hall, T. Siegal, E. Jerome, E. Osztie, L. D. McAllister, J. S. Bubalo, D. F. Kraemer, D. Fortin, R. Nixon, L. L. Muldoon and E. A. Neuwelt (2000). "Safety and efficacy of a multicenter study using intraarterial chemotherapy in conjunction with osmotic opening of the blood-brain barrier for the treatment of patients with malignant brain tumors." Cancer **88**(3): 637-647.

Drake, M. T. and L. M. Traub (2001). "Interaction of two structurally distinct sequence types with the clathrin terminal domain beta-propeller." J Biol Chem **276**(31): 28700-28709.

Drake, M. T., Y. Zhu and S. Kornfeld (2000). "The assembly of AP-3 adaptor complex-containing clathrin-coated vesicles on synthetic liposomes." Mol Biol Cell **11**(11): 3723-3736.

Edeling, M. A., C. Smith and D. Owen (2006). "Life of a clathrin coat: insights from clathrin and AP structures." Nat Rev Mol Cell Biol **7**(1): 32-44.

Elliott, P. J., N. J. Hayward, M. R. Huff, T. L. Nagle, K. L. Black and R. T. Bartus (1996). "Unlocking the blood-brain barrier: a role for RMP-7 in brain tumor therapy." Exp Neurol **141**(2): 214-224.

Emerich, D. F., P. Snodgrass, R. Dean, M. Agostino, B. Hasler, M. Pink, H. Xiong, B. S. Kim and R. T. Bartus (1999). "Enhanced delivery of carboplatin into brain tumours with intravenous Cereport (RMP-7): dramatic differences and insight gained from dosing parameters." Br J Cancer **80**(7): 964-970.

Fan, C. H., C. Y. Ting, H. L. Liu, C. Y. Huang, H. Y. Hsieh, T. C. Yen, K. C. Wei and C. K. Yeh (2013). "Antiangiogenic-targeting drug-loaded microbubbles combined with focused ultrasound for glioma treatment." Biomaterials **34**(8): 2142-2155.

Feldman, G. J., J. M. Mullin and M. P. Ryan (2005). "Occludin: structure, function and regulation." Adv Drug Deliv Rev **57**(6): 883-917.

Feng, B., K. Tomizawa, H. Michiue, S. Miyatake, X. J. Han, A. Fujimura, M. Seno, M. Kirihata and H. Matsui (2009). "Delivery of sodium borocaptate to glioma cells using immunoliposome conjugated with anti-EGFR antibodies by ZZ-His." Biomaterials **30**(9): 1746-1755.

Ferguson, M. L., K. Prasad, D. L. Sackett, H. Boukari, E. M. Lafer and R. Nossal (2006). "Conformation of a clathrin triskelion in solution." Biochemistry **45**(18): 5916-5922.

Filosa, J. A., H. W. Morrison, J. A. Iddings, W. Du and K. J. Kim (2015). "Beyond neurovascular coupling, role of astrocytes in the regulation of vascular tone." Neuroscience.

Fotin, A., Y. Cheng, P. Sliz, N. Grigorieff, S. C. Harrison, T. Kirchhausen and T. Walz (2004). "Molecular model for a complete clathrin lattice from electron cryomicroscopy." Nature **432**(7017): 573-579.

Frank, R. T., K. S. Aboody and J. Najbauer (2011). "Strategies for enhancing antibody delivery to the brain." Biochim Biophys Acta **1816**(2): 191-198.

Frank, R. T., M. Edmiston, S. E. Kendall, J. Najbauer, C. W. Cheung, T. Kassa, M. Z. Metz, S. U. Kim, C. A. Glackin, A. M. Wu, P. J. Yazaki and K. S. Aboody (2009). "Neural stem cells as a novel platform for tumor-specific delivery of therapeutic antibodies." PLoS One **4**(12): e8314.

Frank, R. T., J. Najbauer and K. S. Aboody (2010). "Concise review: stem cells as an emerging platform for antibody therapy of cancer." Stem Cells **28**(11): 2084-2087.

Fujita, M., B. S. Lee, N. M. Khazenzon, M. L. Penichet, K. A. Wawrowsky, R. Patil, H. Ding, E. Holler, K. L. Black and J. Y. Ljubimova (2007). "Brain tumor tandem targeting using a combination of monoclonal antibodies attached to biopoly(beta-L-malic acid)." J Control Release **122**(3): 356-363.

Gabathuler, R. (2010). "Approaches to transport therapeutic drugs across the blood-brain barrier to treat brain diseases." Neurobiol Dis **37**(1): 48-57.

Gasco, M. R., L. Priano and G. P. Zara (2009). "Chapter 10 - Solid lipid nanoparticles and microemulsions for drug delivery The CNS." Prog Brain Res **180**: 181-192.

Gearhart, D. A., M. L. Middlemore and A. V. Terry (2006). "ELISA methods to measure cholinergic markers and nerve growth factor receptors in cortex, hippocampus, prefrontal cortex, and basal forebrain from rat brain." J Neurosci Methods **150**(2): 159-173.

Giannini, A. J., R. H. Loiselle, B. H. Graham and D. J. Folts (1993). "Behavioral response to buspirone in cocaine and phencyclidine withdrawal." J Subst Abuse Treat **10**(6): 523-527.

Ginovart, N., M. Willeit, P. Rusjan, A. Graff, P. M. Bloomfield, S. Houle, S. Kapur and A. A. Wilson (2007). "Positron emission tomography quantification of [¹¹C]-(+)-PHNO binding in the human brain." J Cereb Blood Flow Metab **27**(4): 857-871.

Girod, J., L. Fenart, A. Regina, M. P. Dehouck, G. Hong, J. M. Scherrmann, R. Cecchelli and F. Roux (1999). "Transport of cationized anti-tetanus Fab'2 fragments across an in vitro blood-brain barrier model: involvement of the transcytosis pathway." J Neurochem **73**(5): 2002-2008.

Goncalves, A., A. F. Ambrosio and R. Fernandes (2013). "Regulation of claudins in blood-tissue barriers under physiological and pathological states." Tissue Barriers **1**(3): e24782.

Gonzalez, A. M. and D. R. Sibley (1995). "[³H]7-OH-DPAT is capable of labeling dopamine D2 as well as D3 receptors." Eur J Pharmacol **272**(1): R1-3.

Gorbatov, V. Y., N. A. Trekova, V. G. Fomina and T. V. Davydova (2010). "Antiamnestic effects of antibodies to glutamate in experimental Alzheimer's disease." Bull Exp Biol Med **150**(1): 23-25.

Gouin, S. and F. M. Winnik (2001). "Quantitative assays of the amount of diethylenetriaminepentaacetic acid conjugated to water-soluble polymers using isothermal titration calorimetry and colorimetry." Bioconjug Chem **12**(3): 372-377.

Graff, C. L. and G. M. Pollack (2005). "Nasal drug administration: potential for targeted central nervous system delivery." J Pharm Sci **94**(6): 1187-1195.

Graff-Guerrero, A., R. Mizrahi, O. Agid, H. Marcon, P. Barsoum, P. Rusjan, A. A. Wilson, R. Zipursky and S. Kapur (2009). "The dopamine D2 receptors in high-affinity state and D3 receptors in schizophrenia: a clinical [¹¹C]-(+)-PHNO PET study." Neuropsychopharmacology **34**(4): 1078-1086.

Graff-Guerrero, A., L. Redden, W. Abi-Saab, D. A. Katz, S. Houle, P. Barsoum, A. Bhathena, R. Palaparthi, M. D. Saltarelli and S. Kapur (2010). "Blockade of [¹¹C](+)-PHNO binding in human subjects by the dopamine D3 receptor antagonist ABT-925." Int J Neuropsychopharmacol **13**(3): 273-287.

Graff-Guerrero, A., M. Willeit, N. Ginovart, D. Mamo, R. Mizrahi, P. Rusjan, I. Vitcu, P. Seeman, A. A. Wilson and S. Kapur (2008). "Brain region binding of the D2/3 agonist [¹¹C](+)-PHNO and the D2/3 antagonist [¹¹C]raclopride in healthy humans." Hum Brain Mapp **29**(4): 400-410.

Gragera, R. R., E. Muniz and R. Martinez-Rodriguez (1993). "Molecular and ultrastructural basis of the blood-brain barrier function. Immunohistochemical demonstration of Na⁺/K⁺ ATPase, alpha-actin, phosphocreatine and clathrin in the capillary wall and its microenvironment." Cell Mol Biol (Noisy-le-grand) **39**(8): 819-828.

Granseth, B., B. Odermatt, S. J. Royle and L. Lagnado (2007). "Clathrin-mediated endocytosis: the physiological mechanism of vesicle retrieval at hippocampal synapses." J Physiol **585**(Pt 3): 681-686.

Gross, G., K. Wicke and K. U. Drescher (2013). "Dopamine D(3) receptor antagonism-still a therapeutic option for the treatment of schizophrenia." Naunyn Schmiedebergs Arch Pharmacol **386**(2): 155-166.

Grossi, P. M., H. Ochiai, G. E. Archer, R. E. McLendon, M. R. Zalutsky, A. H. Friedman, H. S. Friedman, D. D. Bigner and J. H. Sampson (2003). "Efficacy of intracerebral microinfusion of trastuzumab in an athymic rat model of intracerebral metastatic breast cancer." Clin Cancer Res **9**(15): 5514-5520.

Gupta, B. and V. P. Torchilin (2007). "Monoclonal antibody 2C5-modified doxorubicin-loaded liposomes with significantly enhanced therapeutic activity against intracranial human brain U-87 MG tumor xenografts in nude mice." Cancer Immunol Immunother **56**(8): 1215-1223.

Gurevich, E. V., Y. Bordelon, R. M. Shapiro, S. E. Arnold, R. E. Gur and J. N. Joyce (1997). "Mesolimbic dopamine D3 receptors and use of antipsychotics in patients with schizophrenia. A postmortem study." Arch Gen Psychiatry **54**(3): 225-232.

Gurevich, E. V. and J. N. Joyce (1999). "Distribution of dopamine D3 receptor expressing neurons in the human forebrain: comparison with D2 receptor expressing neurons." Neuropsychopharmacology **20**(1): 60-80.

Hadjipanayis, C. G., R. Machaidze, M. Kaluzova, L. Wang, A. J. Schuette, H. Chen, X. Wu and H. Mao (2010). "EGFRvIII antibody-conjugated iron oxide nanoparticles for magnetic resonance imaging-guided convection-enhanced delivery and targeted therapy of glioblastoma." Cancer Res **70**(15): 6303-6312.

Hall, H., C. Halldin, D. Dijkstra, H. Wikstrom, L. D. Wise, T. A. Pugsley, P. Sokoloff, S. Pauli, L. Farde and G. Sedvall (1996). "Autoradiographic localisation of D3-dopamine receptors in the human brain using the selective D3-dopamine receptor agonist (+)-[3H] PD 128907." Psychopharmacology (Berl) **128**(3): 240-247.

Haseloff, R. F., S. Dithmer, L. Winkler, H. Wolburg and I. E. Blasig (2015). "Transmembrane proteins of the tight junctions at the blood-brain barrier: structural and functional aspects." Semin Cell Dev Biol **38**: 16-25.

Hawkins, B. T. and T. P. Davis (2005). "The blood-brain barrier/neurovascular unit in health and disease." Pharmacol Rev **57**(2): 173-185.

Hdeib, A. and A. E. Sloan (2011). "Convection-enhanced delivery of ¹³¹I-chTNT-1/B mAB for treatment of high-grade adult gliomas." Expert Opin Biol Ther **11**(6): 799-806.

Heidbreder, C. A. and A. H. Newman (2010). "Current perspectives on selective dopamine D(3) receptor antagonists as pharmacotherapeutics for addictions and related disorders." Ann N Y Acad Sci **1187**: 4-34.

Herroelen, L., J. P. De Backer, N. Wilczak, A. Flamez, G. Vauquelin and J. De Keyser (1994). "Autoradiographic distribution of D3-type dopamine receptors in human brain using [3H]7-hydroxy-N,N-di-n-propyl-2-aminotetralin." Brain Res **648**(2): 222-228.

Herve, F., N. Ghinea and J. M. Scherrmann (2008). "CNS delivery via adsorptive transcytosis." AAPS J **10**(3): 455-472.

Heuser, J. E., J. H. Keen, L. M. Amende, R. E. Lippoldt and K. Prasad (1987). "Deep-etch visualization of 27S clathrin: a tetrahedral tetramer." J Cell Biol **105**(5): 1999-2009.

Holman, D. W., R. S. Klein and R. M. Ransohoff (2011). "The blood-brain barrier, chemokines and multiple sclerosis." Biochim Biophys Acta **1812**(2): 220-230.

Hopkins K, Chandler C, Eatough J, Moss T, Kemshead JT. (1998) "Direct injection of 90Y MoAbs into glioma tumor resection cavities leads to limited diffusion of the radioimmunoconjugates into normal brain parenchyma: a model to estimate absorbed radiation dose." Int J Radiat Oncol Biol Phys. **40**(4):835-44

Hu, J., J. Y. Ljubimova, S. Inoue, B. Konda, R. Patil, H. Ding, A. Espinoza, K. A. Wawrowsky, C. Patil, A. V. Ljubimov and K. L. Black (2010). "Phosphodiesterase type 5 inhibitors increase Herceptin transport and treatment efficacy in mouse metastatic brain tumor models." PLoS One **5**(4): e10108.

Hui, E. K., R. J. Boado and W. M. Pardridge (2009). "Tumor necrosis factor receptor-IgG fusion protein for targeted drug delivery across the human blood-brain barrier." Mol Pharm **6**(5): 1536-1543.

Huppert, J., D. Closhen, A. Croxford, R. White, P. Kulig, E. Pietrowski, I. Bechmann, B. Becher, H. J. Luhmann, A. Waisman and C. R. Kuhlmann (2010). "Cellular mechanisms of IL-17-induced blood-brain barrier disruption." FASEB J **24**(4): 1023-1034.

Hynynen, K., N. McDannold, N. A. Sheikov, F. A. Jolesz and N. Vykhodtseva (2005). "Local and reversible blood-brain barrier disruption by noninvasive focused ultrasound at frequencies suitable for trans-skull sonications." Neuroimage **24**(1): 12-20.

Ikemoto, S. (2007). "Dopamine reward circuitry: two projection systems from the ventral midbrain to the nucleus accumbens-olfactory tubercle complex." Brain Res Rev **56**(1): 27-78.

Illum, L. (2003). "Nasal drug delivery--possibilities, problems and solutions." J Control Release **87**(1-3): 187-198.

Jackson, A. P. (1993). "The isolation of clathrin-coated vesicles and purification of their protein components." Methods Mol Biol **19**: 83-96.

Jaime-Perez, J. C., L. N. Rodriguez-Romo, O. Gonzalez-Llano, A. Chapa-Rodriguez and D. Gomez-Almaguer (2009). "Effectiveness of intrathecal rituximab in patients with acute lymphoblastic leukaemia relapsed to the CNS and resistant to conventional therapy." Br J Haematol **144**(5): 794-795.

Jain, R. K. (1989). "Delivery of novel therapeutic agents in tumors: physiological barriers and strategies." J Natl Cancer Inst **81**(8): 570-576.

Jansson, B. and E. Bjork (2002). "Visualization of in vivo olfactory uptake and transfer using fluorescein dextran." J Drug Target **10**(5): 379-386.

Jin, A. J., K. Prasad, P. D. Smith, E. M. Lafer and R. Nossal (2006). "Measuring the elasticity of clathrin-coated vesicles via atomic force microscopy." Biophys J **90**(9): 3333-3344.

Johanson, C. E., J. A. Duncan, E. G. Stopa and A. Baird (2005). "Enhanced prospects for drug delivery and brain targeting by the choroid plexus-CSF route." Pharm Res **22**(7): 1011-1037.

Jordao, J. F., C. A. Ayala-Grosso, K. Markham, Y. Huang, R. Chopra, J. McLaurin, K. Hynynen and I. Aubert (2010). "Antibodies targeted to the brain with image-guided focused ultrasound reduces amyloid-beta plaque load in the TgCRND8 mouse model of Alzheimer's disease." PLoS One **5**(5): e10549.

Jordao, J. F., E. Thevenot, K. Markham-Coultes, T. Scarcelli, Y. Q. Weng, K. Xhima, M. O'Reilly, Y. Huang, J. McLaurin, K. Hynynen and I. Aubert (2013). "Amyloid-beta plaque reduction, endogenous antibody delivery and glial activation by brain-targeted, transcranial focused ultrasound." Exp Neurol **248**: 16-29.

Joyce, J. N. (2001). "Dopamine D3 receptor as a therapeutic target for antipsychotic and antiparkinsonian drugs." Pharmacol Ther **90**(2-3): 231-259.

Joyce, J. N. and M. J. Millan (2007). "Dopamine D3 receptor agonists for protection and repair in Parkinson's disease." Curr Opin Pharmacol **7**(1): 100-105.

Kabanov, A. V. and S. V. Vinogradov (2009). "Nanogels as pharmaceutical carriers: finite networks of infinite capabilities." Angew Chem Int Ed Engl **48**(30): 5418-5429.

Kaluzova, M., A. Bouras, R. Machaidze and C. G. Hadjipanayis (2015). "Targeted therapy of glioblastoma stem-like cells and tumor non-stem cells using cetuximab-conjugated iron-oxide nanoparticles." Oncotarget **6**(11): 8788-8806.

Karow, M. (2013). "Mountaineering pericytes--a universal key to tissue repair?" Bioessays **35**(9): 771-774.

Kateb, B., K. Chiu, K. L. Black, V. Yamamoto, B. Khalsa, J. Y. Ljubimova, H. Ding, R. Patil, J. A. Portilla-Arias, M. Modo, D. F. Moore, K. Farahani, M. S. Okun, N. Prakash, J. Neman, D. Ahdoot, W. Grundfest, S. Nikzad and J. D. Heiss (2010). "Nanoplatforms for constructing new approaches to cancer treatment, imaging, and drug delivery: What should be the policy?" Neuroimage.

Katsuno, T., K. Umeda, T. Matsui, M. Hata, A. Tamura, M. Itoh, K. Takeuchi, T. Fujimori, Y. Nabeshima, T. Noda, S. Tsukita and S. Tsukita (2008). "Deficiency of zonula occludens-1 causes embryonic lethal phenotype associated with defected yolk sac angiogenesis and apoptosis of embryonic cells." Mol Biol Cell **19**(6): 2465-2475.

Kean, T. J., P. Lin, A. I. Caplan and J. E. Dennis (2013). "MSCs: Delivery Routes and Engraftment, Cell-Targeting Strategies, and Immune Modulation." Stem Cells Int **2013**: 732742.

Keen, J. H., M. C. Willingham and I. H. Pastan (1979). "Clathrin-coated vesicles: isolation, dissociation and factor-dependent reassociation of clathrin baskets." Cell **16**(2): 303-312.

Khan, Z. U., A. Gutierrez, R. Martin, A. Penafiel, A. Rivera and A. De La Calle (1998). "Differential regional and cellular distribution of dopamine D2-like receptors: an immunocytochemical study of subtype-specific antibodies in rat and human brain." J Comp Neurol **402**(3): 353-371.

Kinoshita, M., N. McDannold, F. A. Jolesz and K. Hynynen (2006). "Noninvasive localized delivery of Herceptin to the mouse brain by MRI-guided focused ultrasound-induced blood-brain barrier disruption." Proc Natl Acad Sci U S A **103**(31): 11719-11723.

Kirchhausen, T. (2000). "Clathrin." Annu Rev Biochem **69**: 699-727.

Kirchhausen, T., W. Boll, A. van Oijen and M. Ehrlich (2005). "Single-molecule live-cell imaging of clathrin-based endocytosis." Biochem Soc Symp(72): 71-76.

Kirchhausen, T., S. C. Harrison and J. Heuser (1986). "Configuration of clathrin trimers: evidence from electron microscopy." J Ultrastruct Mol Struct Res **94**(3): 199-208.

Kirchhausen, T., D. Owen and S. C. Harrison (2014). "Molecular structure, function, and dynamics of clathrin-mediated membrane traffic." Cold Spring Harb Perspect Biol **6**(5): a016725.

Kobayashi, H. and M. W. Brechbiel (2005). "Nano-sized MRI contrast agents with dendrimer cores." Adv Drug Deliv Rev **57**(15): 2271-2286.

Kocsis, E., B. L. Trus, C. J. Steer, M. E. Bisher and A. C. Steven (1991). "Image averaging of flexible fibrous macromolecules: the clathrin triskelion has an elastic proximal segment." J Struct Biol **107**(1): 6-14.

Konrad, M., A. Schaller, D. Seelow, A. V. Pandey, S. Waldegger, A. Lesslauer, H. Vitzthum, Y. Suzuki, J. M. Luk, C. Becker, K. P. Schlingmann, M. Schmid, J. Rodriguez-Soriano, G. Ariceta, F. Cano, R. Enriquez, H. Juppner, S. A. Bakkaloglu, M. A. Hediger, S. Gallati, S. C. Neuhaus, P. Nurnberg and S. Weber (2006). "Mutations in the tight-junction gene claudin 19 (CLDN19) are associated with renal magnesium wasting, renal failure, and severe ocular involvement." Am J Hum Genet **79**(5): 949-957.

Kotova, S., K. Prasad, P. D. Smith, E. M. Lafer, R. Nossal and A. J. Jin (2010). "AFM visualization of clathrin triskelia under fluid and in air." FEBS Lett **584**(1): 44-48.

Kozłowska, D., P. Foran, P. MacMahon, M. J. Shelly, S. Eustace and R. O'Kennedy (2009). "Molecular and magnetic resonance imaging: The value of immunoliposomes." Adv Drug Deliv Rev **61**(15): 1402-1411.

Kreuter, J. (2004). "Influence of the surface properties on nanoparticle-mediated transport of drugs to the brain." J Nanosci Nanotechnol **4**(5): 484-488.

Kroll, R. A. and E. A. Neuwelt (1998). "Outwitting the blood-brain barrier for therapeutic purposes: osmotic opening and other means." Neurosurgery **42**(5): 1083-1099; discussion 1099-1100.

Kucherianu, V. G., G. N. Kryzhanovskii, V. S. Kudrin, V. V. Iurasov, E. V. Nikushkin and I. V. Zhigal'tsev (1999). "[Effect of acidic fibroblast growth factor on experimental parkinsonism and levels of dopamine and its metabolites in the striatum of mice of various ages]." Biull Eksp Biol Med **127**(5): 502-505.

Kuesters, G. M. and R. B. Campbell (2010). "Conjugation of bevacizumab to cationic liposomes enhances their tumor-targeting potential." Nanomedicine (Lond) **5**(2): 181-192.

Kumagai, A. K., J. B. Eisenberg and W. M. Pardridge (1987). "Absorptive-mediated endocytosis of cationized albumin and a beta-endorphin-cationized albumin chimeric peptide by isolated brain capillaries. Model system of blood-brain barrier transport." J Biol Chem **262**(31): 15214-15219.

Kurihara, A. and W. M. Pardridge (1999). "Imaging brain tumors by targeting peptide radiopharmaceuticals through the blood-brain barrier." Cancer Res **59**(24): 6159-6163.

Kutlu, C., A. S. Cakmak and M. Gumusderelioglu (2014). "Double-effective chitosan scaffold-PLGA nanoparticle system for brain tumour therapy: in vitro study." J Microencapsul **31**(7): 700-707.

Lampson, L. A. (2011). "Monoclonal antibodies in neuro-oncology: Getting past the blood-brain barrier." MAbs **3**(2): 153-160.

Landwehrmeyer, B., G. Mengod and J. M. Palacios (1993). "Differential visualization of dopamine D2 and D3 receptor sites in rat brain. A comparative study using in situ hybridization histochemistry and ligand binding autoradiography." Eur J Neurosci **5**(2): 145-153.

Landwehrmeyer, B., G. Mengod and J. M. Palacios (1993). "Dopamine D3 receptor mRNA and binding sites in human brain." Brain Res Mol Brain Res **18**(1-2): 187-192.

Le Foll, B., G. Collo, E. A. Rabiner, I. Boileau, E. Merlo Pich and P. Sokoloff (2014). "Dopamine D3 receptor ligands for drug addiction treatment: update on recent findings." Prog Brain Res **211**: 255-275.

Le Foll, B., J. Diaz and P. Sokoloff (2003). "Increased dopamine D3 receptor expression accompanying behavioral sensitization to nicotine in rats." Synapse **47**(3): 176-183.

Le Foll, B., H. Frances, J. Diaz, J. C. Schwartz and P. Sokoloff (2002). "Role of the dopamine D3 receptor in reactivity to cocaine-associated cues in mice." Eur J Neurosci **15**(12): 2016-2026.

Le Foll, B., J. C. Schwartz and P. Sokoloff (2003). "Disruption of nicotine conditioning by dopamine D(3) receptor ligands." Mol Psychiatry **8**(2): 225-230.

Le Foll, B., A. A. Wilson, A. Graff, I. Boileau and P. Di Ciano (2014). "Recent methods for measuring dopamine D3 receptor occupancy in vivo: importance for drug development." Front Pharmacol **5**: 161.

Le Roy, C. and J. L. Wrana (2005). "Clathrin- and non-clathrin-mediated endocytic regulation of cell signalling." Nat Rev Mol Cell Biol **6**(2): 112-126.

Levant, B. (1998). "Differential distribution of D3 dopamine receptors in the brains of several mammalian species." Brain Res **800**(2): 269-274.

Levesque, D., J. Diaz, C. Pilon, M. P. Martres, B. Giros, E. Souil, D. Schott, J. L. Morgat, J. C. Schwartz and P. Sokoloff (1992). "Identification, characterization, and localization of the dopamine D3 receptor in rat brain using 7-[3H]hydroxy-N,N-di-n-propyl-2-aminotetralin." Proc Natl Acad Sci U S A **89**(17): 8155-8159.

Li, M., C. Li, P. Weingarten, J. R. Bunzow, D. K. Grandy and Q. Y. Zhou (2002). "Association of dopamine D(3) receptors with actin-binding protein 280 (ABP-280)." Biochem Pharmacol **63**(5): 859-863.

Lin, R., K. Karpa, N. Kabbani, P. Goldman-Rakic and R. Levenson (2001). "Dopamine D2 and D3 receptors are linked to the actin cytoskeleton via interaction with filamin A." Proc Natl Acad Sci U S A **98**(9): 5258-5263.

Lindahl, P., B. R. Johansson, P. Leveen and C. Betsholtz (1997). "Pericyte loss and microaneurysm formation in PDGF-B-deficient mice." Science **277**(5323): 242-245.

Liu, W. Y., Z. B. Wang, L. C. Zhang, X. Wei and L. Li (2012). "Tight junction in blood-brain barrier: an overview of structure, regulation, and regulator substances." CNS Neurosci Ther **18**(8): 609-615.

Liu, X. F., J. R. Fawcett, R. G. Thorne, T. A. DeFor and W. H. Frey, 2nd (2001). "Intranasal administration of insulin-like growth factor-I bypasses the blood-brain barrier and protects against focal cerebral ischemic damage." J Neurol Sci **187**(1-2): 91-97.

Liu, X. F., J. R. Fawcett, R. G. Thorne and W. H. Frey, 2nd (2001). "Non-invasive intranasal insulin-like growth factor-I reduces infarct volume and improves neurologic function in rats following middle cerebral artery occlusion." Neurosci Lett **308**(2): 91-94.

Lochhead, J. J. and R. G. Thorne (2012). "Intranasal delivery of biologics to the central nervous system." Adv Drug Deliv Rev **64**(7): 614-628.

Lockman, P. R., R. J. Mumper, M. A. Khan and D. D. Allen (2002). "Nanoparticle technology for drug delivery across the blood-brain barrier." Drug Dev Ind Pharm **28**(1): 1-13.

Lu, H., S. Demny, Y. Zuo, W. Rea, L. Wang, S. I. Chefer, D. B. Vaupel, Y. Yang and E. A. Stein (2010). "Temporary disruption of the rat blood-brain barrier with a monoclonal antibody: a novel method for dynamic manganese-enhanced MRI." Neuroimage **50**(1): 7-14.

Ma, Y. P., M. M. Ma, S. Ge, R. B. Guo, H. J. Zhang, W. H. Frey, 2nd, G. L. Xu and X. F. Liu (2007). "Intranasally delivered TGF-beta1 enters brain and regulates gene expressions of its receptors in rats." Brain Res Bull **74**(4): 271-277.

Maezawa, S. and T. Yoshimura (1990). "Assembly of clathrin molecules on liposome membranes: a possible event necessary for induction of membrane fusion." Biochem Biophys Res Commun **173**(1): 134-140.

Maham, A., Z. Tang, H. Wu, J. Wang and Y. Lin (2009). "Protein-based nanomedicine platforms for drug delivery." Small **5**(15): 1706-1721.

Manchester, M. and P. Singh (2006). "Virus-based nanoparticles (VNPs): platform technologies for diagnostic imaging." Adv Drug Deliv Rev **58**(14): 1505-1522.

Marchi, N., L. Angelov, T. Masaryk, V. Fazio, T. Granata, N. Hernandez, K. Hallene, T. Diglaw, L. Franic, I. Najm and D. Janigro (2007). "Seizure-promoting effect of blood-brain barrier disruption." Epilepsia **48**(4): 732-742.

Mariano, C., I. Palmela, P. Pereira, A. Fernandes, A. S. Falcao, F. L. Cardoso, A. R. Vaz, A. R. Campos, A. Goncalves-Ferreira, K. S. Kim, D. Brites and M. A. Brito (2013). "Tricellulin expression in brain endothelial and neural cells." Cell Tissue Res **351**(3): 397-407.

Martins, T., S. Baptista, J. Goncalves, E. Leal, N. Milhazes, F. Borges, C. F. Ribeiro, O. Quintela, E. Lendoiro, M. Lopez-Rivadulla, A. F. Ambrosio and A. P. Silva (2011). "Methamphetamine transiently increases the blood-brain barrier permeability in the hippocampus: role of tight junction proteins and matrix metalloproteinase-9." Brain Res **1411**: 28-40.

Mason, C. W., H. E. Hassan, K. P. Kim, J. Cao, N. D. Eddington, A. H. Newman and P. J. Voulalas (2010). "Characterization of the transport, metabolism, and pharmacokinetics of the dopamine D3 receptor-selective fluorenyl- and 2-pyridylphenyl amides developed for treatment of psychostimulant abuse." J Pharmacol Exp Ther **333**(3): 854-864.

Matsui, W. and T. Kirchhausen (1990). "Stabilization of clathrin coats by the core of the clathrin-associated protein complex AP-2." Biochemistry **29**(48): 10791-10798.

Matuskey, D., J. D. Gallezot, B. Pittman, W. Williams, J. Wanyiri, E. Gaiser, D. E. Lee, J. Hannestad, K. Lim, M. Q. Zheng, S. F. Lin, D. Labaree, M. N. Potenza, R. E. Carson, R. T. Malison and Y. S. Ding (2014). "Dopamine D(3) receptor alterations in cocaine-dependent humans imaged with [(1)(1)C](+)PHNO." Drug Alcohol Depend **139**: 100-105.

Mehta, A. I., A. M. Brufsky and J. H. Sampson (2013). "Therapeutic approaches for HER2-positive brain metastases: circumventing the blood-brain barrier." Cancer Treat Rev **39**(3): 261-269.

Menon, D., C. S. Karyekar, A. Fasano, R. Lu and N. D. Eddington (2005). "Enhancement of brain distribution of anticancer agents using DeltaG, the 12 kDa active fragment of ZOT." Int J Pharm **306**(1-2): 122-131.

Miele, A. E., P. J. Watson, P. R. Evans, L. M. Traub and D. J. Owen (2004). "Two distinct interaction motifs in amphiphysin bind two independent sites on the clathrin terminal domain beta-propeller." Nat Struct Mol Biol **11**(3): 242-248.

Miller, G. (2002). "Drug targeting. Breaking down barriers." Science **297**(5584): 1116-1118.

Mills, I. G. (2007). "The interplay between clathrin-coated vesicles and cell signalling." Semin Cell Dev Biol **18**(4): 459-470.

Mirzadeh, S., M. W. Brechbiel, R. W. Atcher and O. A. Gansow (1990). "Radiometal labeling of immunoproteins: covalent linkage of 2-(4-isothiocyanatobenzyl) diethylenetriaminepentaacetic acid ligands to immunoglobulin." Bioconjug Chem **1**(1): 59-65.

Mogg, K., B. P. Bradley, B. O'Neill, M. Bani, E. Merlo-Pich, A. Koch, E. T. Bullmore and P. J. Nathan (2012). "Effect of dopamine D(3) receptor antagonism on approach responses to food cues in overweight and obese individuals." Behav Pharmacol **23**(5-6): 603-608.

Morgan, J. R., K. Prasad, W. Hao, G. J. Augustine and E. M. Lafer (2000). "A conserved clathrin assembly motif essential for synaptic vesicle endocytosis." J Neurosci **20**(23): 8667-8676.

Morgan, P., P. H. Van Der Graaf, J. Arrowsmith, D. E. Feltner, K. S. Drummond, C. D. Wegner and S. D. Street (2012). "Can the flow of medicines be improved? Fundamental pharmacokinetic and pharmacological principles toward improving Phase II survival." Drug Discov Today **17**(9-10): 419-424.

Morissette, M., M. Goulet, R. Grondin, P. Blanchet, P. J. Bedard, T. Di Paolo and D. Levesque (1998). "Associative and limbic regions of monkey striatum express high levels of dopamine D3 receptors: effects of MPTP and dopamine agonist replacement therapies." Eur J Neurosci **10**(8): 2565-2573.

Morrison, E. E. and R. M. Costanzo (1992). "Morphology of olfactory epithelium in humans and other vertebrates." Microsc Res Tech **23**(1): 49-61.

Mortensen, J. H., M. Jeppesen, L. Pilgaard, R. Agger, M. Duroux, V. Zachar and T. Moos (2013). "Targeted antiepidermal growth factor receptor (cetuximab) immunoliposomes enhance cellular uptake in vitro and exhibit increased accumulation in an intracranial model of glioblastoma multiforme." J Drug Deliv **2013**: 209205.

Mugnaini, M., L. Iavarone, P. Cavallini, C. Griffante, B. Oliosi, C. Savoia, J. Beaver, E. A. Rabiner, F. Micheli, C. Heidbreder, A. Andorn, E. Merlo Pich and M. Bani (2013). "Occupancy of brain dopamine D3 receptors and drug craving: a translational approach." Neuropsychopharmacology **38**(2): 302-312.

Mulder, W. J., G. J. Strijkers, G. A. van Tilborg, D. P. Cormode, Z. A. Fayad and K. Nicolay (2009). "Nanoparticulate assemblies of amphiphiles and diagnostically active materials for multimodality imaging." Acc Chem Res **42**(7): 904-914.

Muldoon, L. L., S. J. Lewin, E. Dosa, D. F. Kraemer, M. A. Pagel, N. D. Doolittle and E. A. Neuwelt (2011). "Imaging and therapy with rituximab anti-CD20 immunotherapy in an animal model of central nervous system lymphoma." Clin Cancer Res **17**(8): 2207-2215.

Musolino, A., L. Ciccolallo, M. Panebianco, E. Fontana, D. Zanoni, C. Bozzetti, M. Michiara, E. M. Silini and A. Ardizzoni (2011). "Multifactorial central nervous system recurrence susceptibility in patients with HER2-positive breast cancer: epidemiological and clinical data from a population-based cancer registry study." Cancer **117**(9): 1837-1846.

Mustacchi, G., L. Biganzoli, P. Pronzato, F. Montemurro, M. Dambrosio, M. Minelli, L. Molteni and L. Scaltriti (2015). "HER2-positive metastatic breast cancer: a changing scenario." Crit Rev Oncol Hematol **95**(1): 78-87.

Nagaraja, T. N., R. L. Croxen, S. Panda, R. A. Knight, K. A. Keenan, S. L. Brown, J. D. Fenstermacher and J. R. Ewing (2006). "Application of arsenazo III in the preparation and characterization of an albumin-linked, gadolinium-based macromolecular magnetic resonance contrast agent." J Neurosci Methods **157**(2): 238-245.

Nakajima, S., P. Gerretsen, H. Takeuchi, F. Caravaggio, T. Chow, B. Le Foll, B. Mulsant, B. Pollock and A. Graff-Guerrero (2013). "The potential role of dopamine D(3) receptor neurotransmission in cognition." Eur Neuropsychopharmacol **23**(8): 799-813.

Narendran, R., M. Slifstein, O. Guillin, Y. Hwang, D. R. Hwang, E. Scher, S. Reeder, E. Rabiner and M. Laruelle (2006). "Dopamine (D2/3) receptor agonist positron emission tomography radiotracer [¹¹C]-(+)-PHNO is a D3 receptor preferring agonist in vivo." Synapse **60**(7): 485-495.

Nathan, P. J., B. V. O'Neill, K. Mogg, B. P. Bradley, J. Beaver, M. Bani, E. Merlo-Pich, P. C. Fletcher, B. Swirski, A. Koch, C. M. Dodds and E. T. Bullmore (2012). "The effects of the dopamine D(3) receptor antagonist GSK598809 on attentional bias to palatable food cues in overweight and obese subjects." Int J Neuropsychopharmacol **15**(2): 149-161.

Neisewander, J. L., R. A. Fuchs, L. T. Tran-Nguyen, S. M. Weber, G. P. Coffey and J. N. Joyce (2004). "Increases in dopamine D3 receptor binding in rats receiving a cocaine challenge at various time points after cocaine self-administration: implications for cocaine-seeking behavior." Neuropsychopharmacology **29**(8): 1479-1487.

Nel, A., T. Xia, L. Madler and N. Li (2006). "Toxic potential of materials at the nanolevel." Science **311**(5761): 622-627.

Neuwelt, E., N. J. Abbott, L. Abrey, W. A. Banks, B. Blakley, T. Davis, B. Engelhardt, P. Grammas, M. Nedergaard, J. Nutt, W. Pardridge, G. A. Rosenberg, Q. Smith and L. R. Drewes (2008). "Strategies to advance translational research into brain barriers." Lancet Neurol **7**(1): 84-96.

Neuwelt, E. A. (2004). "Mechanisms of disease: the blood-brain barrier." Neurosurgery **54**(1): 131-140; discussion 141-132.

Neuwelt, E. A., P. A. Barnett, K. E. Hellstrom, I. Hellstrom, C. I. McCormick and F. L. Ramsey (1994). "Effect of blood-brain barrier disruption on intact and fragmented monoclonal antibody localization in intracerebral lung carcinoma xenografts." J Nucl Med **35**(11): 1831-1841.

Neuwelt, E. A., H. D. Specht, P. A. Barnett, S. A. Dahlborg, A. Miley, S. M. Larson, P. Brown, K. F. Eckerman, K. E. Hellstrom and I. Hellstrom (1987). "Increased delivery of tumor-specific monoclonal antibodies to brain after osmotic blood-brain barrier modification in patients with melanoma metastatic to the central nervous system." Neurosurgery **20**(6): 885-895.

Nico, B. and D. Ribatti (2012). "Morphofunctional aspects of the blood-brain barrier." Curr Drug Metab **13**(1): 50-60.

Niewoehner, J., B. Bohrmann, L. Collin, E. Urich, H. Sade, P. Maier, P. Rueger, J. O. Stracke, W. Lau, A. C. Tissot, H. Loetscher, A. Ghosh and P. O. Freskgard (2014). "Increased brain penetration and potency of a therapeutic antibody using a monovalent molecular shuttle." Neuron **81**(1): 49-60.

Nimchinsky, E. A., P. R. Hof, W. G. Janssen, J. H. Morrison and C. Schmauss (1997). "Expression of dopamine D3 receptor dimers and tetramers in brain and in transfected cells." J Biol Chem **272**(46): 29229-29237.

Ningaraj, N. S., M. Rao, K. Hashizume, K. Asotra and K. L. Black (2002). "Regulation of blood-brain tumor barrier permeability by calcium-activated potassium channels." J Pharmacol Exp Ther **301**(3): 838-851.

Ningaraj, N. S., U. T. Sankpal, D. Khaitan, E. A. Meister and T. S. Vats (2009). "Modulation of K_{Ca} channels increases anticancer drug delivery to brain tumors and prolongs survival in xenograft model." Cancer Biol Ther **8**(20): 1924-1933.

Nitta, T., M. Hata, S. Gotoh, Y. Seo, H. Sasaki, N. Hashimoto, M. Furuse and S. Tsukita (2003). "Size-selective loosening of the blood-brain barrier in claudin-5-deficient mice." J Cell Biol **161**(3): 653-660.

Noebauer-Huhmann, I. M., P. Szomolanyi, V. Juras, O. Kraff, M. E. Ladd and S. Trattnig (2010). "Gadolinium-based magnetic resonance contrast agents at 7 Tesla: in vitro T₁ relaxivities in human blood plasma." Invest Radiol **45**(9): 554-558.

O'Driscoll, M. C., S. B. Daly, J. E. Urquhart, G. C. Black, D. T. Pilz, K. Brockmann, M. McEntagart, G. Abdel-Salam, M. Zaki, N. I. Wolf, R. L. Ladda, S. Sell, S. D'Arrigo, W. Squier, W. B. Dobyns, J. H. Livingston and Y. J. Crow (2010). "Recessive mutations in the gene encoding the tight junction protein occludin cause band-like calcification with simplified gyration and polymicrogyria." Am J Hum Genet **87**(3): 354-364.

Ohshima-Hosoyama, S., H. A. Simmons, N. Goecks, V. Joers, C. R. Swanson, V. Bondarenko, R. Velotta, K. Brunner, L. D. Wood, R. H. Hruban and M. E. Emborg (2012). "A monoclonal antibody-GDNF fusion protein is not neuroprotective and is associated with proliferative pancreatic lesions in parkinsonian monkeys." PLoS One **7**(6): e39036.

Olivier, J. C. (2005). "Drug transport to brain with targeted nanoparticles." NeuroRx **2**(1): 108-119.

Omidi, Y., L. Campbell, J. Barar, D. Connell, S. Akhtar and M. Gumbleton (2003). "Evaluation of the immortalised mouse brain capillary endothelial cell line, b.End3, as an in vitro blood-brain barrier model for drug uptake and transport studies." Brain Res **990**(1-2): 95-112.

Paajanen, H., T. Reisto, I. Hemmila, M. Komu, P. Niemi and M. Kormanen (1990). "Proton relaxation enhancement of albumin, immunoglobulin G, and fibrinogen labeled with Gd-DTPA." Magn Reson Med **13**(1): 38-43.

Paganelli, M., X. Stephenne, A. Gilis, E. Jacquemin, A. Henrion Caude, M. Girard, E. Gonzales, N. Revencu, R. Reding, C. Wanty, F. Smets and E. M. Sokal (2011). "Neonatal ichthyosis and sclerosing cholangitis syndrome: extremely variable liver disease severity from claudin-1 deficiency." J Pediatr Gastroenterol Nutr **53**(3): 350-354.

Palmieri, D., J. L. Bronder, J. M. Herring, T. Yoneda, R. J. Weil, A. M. Stark, R. Kurek, E. Vega-Valle, L. Feigenbaum, D. Halverson, A. O. Vortmeyer, S. M. Steinberg, K. Aldape and P. S. Steeg (2007). "Her-2 overexpression increases the metastatic outgrowth of breast cancer cells in the brain." Cancer Res **67**(9): 4190-4198.

Pardridge, W. M. (2005). "The blood-brain barrier: bottleneck in brain drug development." NeuroRx **2**(1): 3-14.

Pardridge, W. M. (2007). "Blood-brain barrier delivery." Drug Discov Today **12**(1-2): 54-61.

Pardridge, W. M., U. Bickel, J. Buciak, J. Yang and A. Diagne (1994). "Enhanced endocytosis and anti-human immunodeficiency virus type 1 activity of anti-rev antibodies after cationization." J Infect Dis **169**(1): 55-61.

Pardridge, W. M. and R. J. Boado (2012). "Reengineering biopharmaceuticals for targeted delivery across the blood-brain barrier." Methods Enzymol **503**: 269-292.

Pardridge, W. M., D. Triguero, J. Buciak and J. Yang (1990). "Evaluation of cationized rat albumin as a potential blood-brain barrier drug transport vector." J Pharmacol Exp Ther **255**(2): 893-899.

Park, E. J., Y. Z. Zhang, N. Vykhodtseva and N. McDannold (2012). "Ultrasound-mediated blood-brain/blood-tumor barrier disruption improves outcomes with trastuzumab in a breast cancer brain metastasis model." J Control Release **163**(3): 277-284.

Partha, R. and J. L. Conyers (2009). "Biomedical applications of functionalized fullerene-based nanomaterials." Int J Nanomedicine **4**: 261-275.

Patil, A. and G. V. Sherbet (2015). "Therapeutic approach to the management of HER2-positive breast cancer metastatic to the brain." Cancer Lett **358**(2): 93-99.

Paxinos, G. and C. Watson (1998). The Rat Brain in Stereotaxic Coordinates, Academic Pres.

Payer, D. E., A. Behzadi, S. J. Kish, S. Houle, A. A. Wilson, P. M. Rusjan, J. Tong, P. Selby, T. P. George, T. McCluskey and I. Boileau (2014). "Heightened D3 dopamine receptor levels in cocaine dependence and contributions to the addiction behavioral phenotype: a positron emission tomography study with [11C]-+-PHNO." Neuropsychopharmacology **39**(2): 311-318.

Pearse, B. M. (1976). "Clathrin: a unique protein associated with intracellular transfer of membrane by coated vesicles." Proc Natl Acad Sci U S A **73**(4): 1255-1259.

Pearse, B. M., C. J. Smith and D. J. Owen (2000). "Clathrin coat construction in endocytosis." Curr Opin Struct Biol **10**(2): 220-228.

Perissinotti, A. J. and D. J. Reeves (2010). "Role of intrathecal rituximab and trastuzumab in the management of leptomeningeal carcinomatosis." Ann Pharmacother **44**(10): 1633-1640.

Piggott, M. A., E. F. Marshall, N. Thomas, S. Lloyd, J. A. Court, E. Jaros, D. Costa, R. H. Perry and E. K. Perry (1999). "Dopaminergic activities in the human striatum: rostrocaudal gradients of uptake sites and of D1 and D2 but not of D3 receptor binding or dopamine." Neuroscience **90**(2): 433-445.

Pilla, M., S. Perachon, F. Sautel, F. Garrido, A. Mann, C. G. Wermuth, J. C. Schwartz, B. J. Everitt and P. Sokoloff (1999). "Selective inhibition of cocaine-seeking behaviour by a partial dopamine D3 receptor agonist." Nature **400**(6742): 371-375.

Pippin, C. G., T. A. Parker, T. J. McMurry and M. W. Brechbiel (1992). "Spectrophotometric method for the determination of a bifunctional DTPA ligand in DTPA-monoclonal antibody conjugates." Bioconjug Chem **3**(4): 342-345.

Proescholdt, M. G., B. Hutto, L. S. Brady and M. Herkenham (2000). "Studies of cerebrospinal fluid flow and penetration into brain following lateral ventricle and cisterna magna injections of the tracer [¹⁴C]inulin in rat." Neuroscience **95**(2): 577-592.

Pugsley, T. A., M. D. Davis, H. C. Akunne, R. G. MacKenzie, Y. H. Shih, G. Damsma, H. Wikstrom, S. Z. Whetzel, L. M. Georgic, L. W. Cooke and et al. (1995). "Neurochemical and functional characterization of the preferentially selective dopamine D3 agonist PD 128907." J Pharmacol Exp Ther **275**(3): 1355-1366.

Quaegebeur, A., I. Segura and P. Carmeliet (2010). "Pericytes: blood-brain barrier safeguards against neurodegeneration?" Neuron **68**(3): 321-323.

Rabiner, E. A., M. Slifstein, J. Nobrega, C. Plisson, M. Huiban, R. Raymond, M. Diwan, A. A. Wilson, P. McCormick, G. Gentile, R. N. Gunn and M. A. Laruelle (2009). "In vivo quantification of regional dopamine-D3 receptor binding potential of (+)-PHNO: Studies in non-human primates and transgenic mice." Synapse **63**(9): 782-793.

Rakovic, D. and D. Uskokovic (2010). Biomaterials. Belgrade, Institute of Technical Sciences SASA & MRS Serbia.

Ramakrishnan, M., T. M. Wengenack, K. K. Kandimalla, G. L. Curran, E. J. Gilles, M. Ramirez-Alvarado, J. Lin, M. Garwood, C. R. Jack, Jr. and J. F. Poduslo (2008). "Selective contrast enhancement of individual Alzheimer's disease amyloid plaques using a polyamine and Gd-DOTA conjugated antibody fragment against fibrillar Aβ42

for magnetic resonance molecular imaging.” Pharm Res **25**(8): 1861-1872.

Ransom, C. B. and H. Sontheimer (2001). “BK channels in human glioma cells.” J Neurophysiol **85**(2): 790-803.

Rapoport, S. I., W. R. Fredericks, K. Ohno and K. D. Pettigrew (1980). “Quantitative aspects of reversible osmotic opening of the blood-brain barrier.” Am J Physiol **238**(5): R421-431.

Raymond, S. B., L. H. Treat, J. D. Dewey, N. J. McDannold, K. Hynynen and B. J. Bacskai (2008). “Ultrasound enhanced delivery of molecular imaging and therapeutic agents in Alzheimer’s disease mouse models.” PLoS One **3**(5): e2175.

Reavill, C., S. G. Taylor, M. D. Wood, T. Ashmeade, N. E. Austin, K. Y. Avenell, I. Boyfield, C. L. Branch, J. Cilia, M. C. Coldwell, M. S. Hadley, A. J. Hunter, P. Jeffrey, F. Jewitt, C. N. Johnson, D. N. Jones, A. D. Medhurst, D. N. Middlemiss, D. J. Nash, G. J. Riley, C. Routledge, G. Stemp, K. M. Thewlis, B. Trail, A. K. Vong and J. J. Hagan (2000). “Pharmacological actions of a novel, high-affinity, and selective human dopamine D(3) receptor antagonist, SB-277011-A.” J Pharmacol Exp Ther **294**(3): 1154-1165.

Regina, A., M. Demeule, S. Tripathy, S. Lord-Dufour, J. C. Currie, M. Iddir, B. Annabi, J. P. Castaigne and J. E. Lachowicz (2015). “ANG4043, a novel brain-penetrant peptide-mAb conjugate, is efficacious against HER2-positive intracranial tumors in mice.” Mol Cancer Ther **14**(1): 129-140.

Ribatti, D., B. Nico and E. Crivellato (2011). “The role of pericytes in angiogenesis.” Int J Dev Biol **55**(3): 261-268.

Richtand, N. M., J. R. Kelsoe, D. S. Segal and R. Kuczenski (1995). “Regional quantification of D1, D2, and D3 dopamine receptor mRNA in rat brain using a ribonuclease protection assay.” Brain Res Mol Brain Res **33**(1): 97-103.

Riina, H. A., J. F. Fraser, S. Fralin, J. Knopman, R. J. Scheff and J. A. Boockvar (2009). “Superselective intraarterial cerebral infusion of bevacizumab: a revival of interventional neuro-oncology for malignant glioma.” J Exp Ther Oncol **8**(2): 145-150.

Rohrer, M., H. Bauer, J. Mintorovitch, M. Requardt and H. J. Weinmann (2005). “Comparison of magnetic properties of MRI contrast media solutions at different magnetic field strengths.” Invest Radiol **40**(11): 715-724.

Romanova, G. A., F. M. Shakova, V. Y. Gorbatov, Y. N. Kvashennikova and T. V. Davydova (2010). “Effect of antibodies to glutamate on retention of conditioned passive avoidance response in rats with ischemic injury of the prefrontal cortex.” Bull Exp Biol Med **149**(3): 289-292.

Rose, J. S., M. Branchey, L. Wallach and L. Buydens-Branchey (2003). "Effects of buspirone in withdrawal from opiates." Am J Addict **12**(3): 253-259.

Royle, S. J., N. A. Bright and L. Lagnado (2005). "Clathrin is required for the function of the mitotic spindle." Nature **434**(7037): 1152-1157.

Royle, S. J. and L. Lagnado (2003). "Endocytosis at the synaptic terminal." J Physiol **553**(Pt 2): 345-355.

Ryoo, H. L., D. Pierrotti and J. N. Joyce (1998). "Dopamine D3 receptor is decreased and D2 receptor is elevated in the striatum of Parkinson's disease." Mov Disord **13**(5): 788-797.

Saitou, M., Y. Ando-Akatsuka, M. Itoh, M. Furuse, J. Inazawa, K. Fujimoto and S. Tsukita (1997). "Mammalian occludin in epithelial cells: its expression and subcellular distribution." Eur J Cell Biol **73**(3): 222-231.

Sakane, T., S. Yamashita, N. Yata and H. Sezaki (1999). "Transnasal delivery of 5-fluorouracil to the brain in the rat." J Drug Target **7**(3): 233-240.

Sampson, J. H., G. Akabani, A. H. Friedman, D. Bigner, S. Kunwar, M. S. Berger and K. S. Bankiewicz (2006). "Comparison of intratumoral bolus injection and convection-enhanced delivery of radiolabeled antitenascin monoclonal antibodies." Neurosurg Focus **20**(4): E14.

Sandoval, K. E. and K. A. Witt (2008). "Blood-brain barrier tight junction permeability and ischemic stroke." Neurobiol Dis **32**(2): 200-219.

Sarin, H., A. S. Kanevsky, S. H. Fung, J. A. Butman, R. W. Cox, D. Glen, R. Reynolds and S. Auh (2009). "Metabolically stable bradykinin B2 receptor agonists enhance transvascular drug delivery into malignant brain tumors by increasing drug half-life." J Transl Med **7**: 33.

Schmid, S. L., A. K. Matsumoto and J. E. Rothman (1982). "A domain of clathrin that forms coats." Proc Natl Acad Sci U S A **79**(1): 91-95.

Schnyder, A. and J. Huwyler (2005). "Drug transport to brain with targeted liposomes." NeuroRx **2**(1): 99-107.

Schoen, A. P., D. T. Schoen, K. N. Huggins, M. A. Arunagirinathan and S. C. Heilshorn (2011). "Template engineering through epitope recognition: a modular, biomimetic strategy for inorganic nanomaterial synthesis." J Am Chem Soc **133**(45): 18202-18207.

Schreibelt, G., G. Kooij, A. Reijkerkerk, R. van Doorn, S. I. Gringhuis, S. van der Pol, B. B. Weksler, I. A. Romero, P. O. Couraud, J. Piontek, I. E. Blasig, C. D. Dijkstra, E. Ronken and H. E. de Vries (2007). "Reactive oxygen species alter brain endothelial tight junction dynamics via RhoA, PI3 kinase, and PKB signaling." *FASEB J* **21**(13): 3666-3676.

Schuhmann-Giampieri, G., H. Schmitt-Willich, T. Frenzel, W. R. Press and H. J. Weinmann (1991). "In vivo and in vitro evaluation of Gd-DTPA-polylysine as a macromolecular contrast agent for magnetic resonance imaging." *Invest Radiol* **26**(11): 969-974.

Schummers, J., H. Yu and M. Sur (2008). "Tuned responses of astrocytes and their influence on hemodynamic signals in the visual cortex." *Science* **320**(5883): 1638-1643.

Searle, G., J. D. Beaver, R. A. Comley, M. Bani, A. Tziortzi, M. Slifstein, M. Mugnaini, C. Griffante, A. A. Wilson, E. Merlo-Pich, S. Houle, R. Gunn, E. A. Rabiner and M. Laruelle (2010). "Imaging dopamine D3 receptors in the human brain with positron emission tomography, [¹¹C]PHNO, and a selective D3 receptor antagonist." *Biol Psychiatry* **68**(4): 392-399.

Segal, D. M., C. T. Moraes and D. C. Mash (1997). "Up-regulation of D3 dopamine receptor mRNA in the nucleus accumbens of human cocaine fatalities." *Brain Res Mol Brain Res* **45**(2): 335-339.

Shioda, N., Y. Takeuchi and K. Fukunaga (2010). "Advanced research on dopamine signaling to develop drugs for the treatment of mental disorders: proteins interacting with the third cytoplasmic loop of dopamine D2 and D3 receptors." *J Pharmacol Sci* **114**(1): 25-31.

Shupliakov, O. and L. Brodin (2010). "Recent insights into the building and cycling of synaptic vesicles." *Exp Cell Res* **316**(8): 1344-1350.

Shvedova, A. A., V. E. Kagan and B. Fadeel (2010). "Close encounters of the small kind: adverse effects of man-made materials interfacing with the nano-cosmos of biological systems." *Annu Rev Pharmacol Toxicol* **50**: 63-88.

Simard, M. and M. Nedergaard (2004). "The neurobiology of glia in the context of water and ion homeostasis." *Neuroscience* **129**(4): 877-896.

Sirotkin, H., B. Morrow, B. Saint-Jore, A. Puech, R. Das Gupta, S. R. Patanjali, A. Skoultschi, S. M. Weissman and R. Kucherlapati (1997). "Identification, characterization, and precise mapping of a human gene encoding a novel membrane-spanning protein from the 22q11 region deleted in velo-cardio-facial syndrome." *Genomics* **42**(2): 245-251.

Slepnev, V. I. and P. De Camilli (2000). "Accessory factors in clathrin-dependent synaptic

vesicle endocytosis.” Nat Rev Neurosci **1**(3): 161-172.

Smith, A. J. (2015). “New horizons in therapeutic antibody discovery: opportunities and challenges versus small-molecule therapeutics.” J Biomol Screen **20**(4): 437-453.

Smith, M. W. and M. Gumbleton (2006). “Endocytosis at the blood-brain barrier: from basic understanding to drug delivery strategies.” J Drug Target **14**(4): 191-214.

Sofroniew, M. V. and H. V. Vinters (2010). “Astrocytes: biology and pathology.” Acta Neuropathol **119**(1): 7-35.

Sokoloff, P., J. Diaz, B. Le Foll, O. Guillin, L. Leriche, E. Bezard and C. Gross (2006). “The dopamine D3 receptor: a therapeutic target for the treatment of neuropsychiatric disorders.” CNS Neurol Disord Drug Targets **5**(1): 25-43.

Sokoloff, P., B. Giros, M. P. Martres, M. L. Bouthenet and J. C. Schwartz (1990). “Molecular cloning and characterization of a novel dopamine receptor (D3) as a target for neuroleptics.” Nature **347**(6289): 146-151.

Spangler, R., N. L. Goddard, N. M. Avena, B. G. Hoebel and S. F. Leibowitz (2003). “Elevated D3 dopamine receptor mRNA in dopaminergic and dopaminoceptive regions of the rat brain in response to morphine.” Brain Res Mol Brain Res **111**(1-2): 74-83.

Staley, J. K. and D. C. Mash (1996). “Adaptive increase in D3 dopamine receptors in the brain reward circuits of human cocaine fatalities.” J Neurosci **16**(19): 6100-6106.

Stanwood, G. D., R. P. Artymyshyn, M. P. Kung, H. F. Kung, I. Lucki and P. McGonigle (2000). “Quantitative autoradiographic mapping of rat brain dopamine D3 binding with [(125)I]7-OH-PIPAT: evidence for the presence of D3 receptors on dopaminergic and nondopaminergic cell bodies and terminals.” J Pharmacol Exp Ther **295**(3): 1223-1231.

Stemmler, H. J., M. Schmitt, A. Willems, H. Bernhard, N. Harbeck and V. Heinemann (2007). “Ratio of trastuzumab levels in serum and cerebrospinal fluid is altered in HER2-positive breast cancer patients with brain metastases and impairment of blood-brain barrier.” Anticancer Drugs **18**(1): 23-28.

Sumbria, R. K., E. K. Hui, J. Z. Lu, R. J. Boado and W. M. Pardridge (2013). “Disaggregation of amyloid plaque in brain of Alzheimer’s disease transgenic mice with daily subcutaneous administration of a tetravalent bispecific antibody that targets the transferrin receptor and the Aβ amyloid peptide.” Mol Pharm **10**(9): 3507-3513.

Takei, K., V. Haucke, V. Slepnev, K. Farsad, M. Salazar, H. Chen and P. De Camilli (1998). “Generation of coated intermediates of clathrin-mediated endocytosis on protein-free liposomes.” Cell **94**(1): 131-141.

ter Haar, E., S. C. Harrison and T. Kirchhausen (2000). "Peptide-in-groove interactions link target proteins to the beta-propeller of clathrin." Proc Natl Acad Sci U S A **97**(3): 1096-1100.

ter Haar, E., A. Musacchio, S. C. Harrison and T. Kirchhausen (1998). "Atomic structure of clathrin: a beta propeller terminal domain joins an alpha zigzag linker." Cell **95**(4): 563-573.

Thorne, R. G., C. R. Emory, T. A. Ala and W. H. Frey, 2nd (1995). "Quantitative analysis of the olfactory pathway for drug delivery to the brain." Brain Res **692**(1-2): 278-282.

Thorne, R. G. and W. H. Frey, 2nd (2001). "Delivery of neurotrophic factors to the central nervous system: pharmacokinetic considerations." Clin Pharmacokinet **40**(12): 907-946.

Thorne, R. G. and C. Nicholson (2006). "In vivo diffusion analysis with quantum dots and dextrans predicts the width of brain extracellular space." Proc Natl Acad Sci U S A **103**(14): 5567-5572.

Thorne, R. G., G. J. Pronk, V. Padmanabhan and W. H. Frey, 2nd (2004). "Delivery of insulin-like growth factor-I to the rat brain and spinal cord along olfactory and trigeminal pathways following intranasal administration." Neuroscience **127**(2): 481-496.

Tosi, G., R. A. Fano, L. Bondioli, L. Badiali, R. Benassi, F. Rivasi, B. Ruozi, F. Forni and M. A. Vandelli (2011). "Investigation on mechanisms of glycopeptide nanoparticles for drug delivery across the blood-brain barrier." Nanomedicine (Lond) **6**(3): 423-436.

Tressel, S. L., G. Koukos, B. Tchernychev, S. L. Jacques, L. Covic and A. Kuliopulos (2011). "Pharmacology, biodistribution, and efficacy of GPCR-based pepducins in disease models." Methods Mol Biol **683**: 259-275.

Triguero, D., J. B. Buciak, J. Yang and W. M. Pardridge (1989). "Blood-brain barrier transport of cationized immunoglobulin G: enhanced delivery compared to native protein." Proc Natl Acad Sci U S A **86**(12): 4761-4765.

Tsukita, S. and M. Furuse (1998). "Overcoming barriers in the study of tight junction functions: from occludin to claudin." Genes Cells **3**(9): 569-573.

Tziortzi, A. C., G. E. Searle, S. Tzimopoulou, C. Salinas, J. D. Beaver, M. Jenkinson, M. Laruelle, E. A. Rabiner and R. N. Gunn (2011). "Imaging dopamine receptors in humans with [¹¹C]-(+)-PHNO: dissection of D3 signal and anatomy." Neuroimage **54**(1): 264-277.

Umeda, K., J. Ikenouchi, S. Katahira-Tayama, K. Furuse, H. Sasaki, M. Nakayama, T. Matsui, S. Tsukita, M. Furuse and S. Tsukita (2006). "ZO-1 and ZO-2 independently

determine where claudins are polymerized in tight-junction strand formation.” Cell **126**(4): 741-754.

Umeda, K., T. Matsui, M. Nakayama, K. Furuse, H. Sasaki, M. Furuse and S. Tsukita (2004). “Establishment and characterization of cultured epithelial cells lacking expression of ZO-1.” J Biol Chem **279**(43): 44785-44794.

Van Itallie, C. M., A. S. Fanning, J. Holmes and J. M. Anderson (2010). “Occludin is required for cytokine-induced regulation of tight junction barriers.” J Cell Sci **123**(Pt 16): 2844-2852.

van Tellingen, O., B. Yetkin-Arik, M. C. de Gooijer, P. Wesseling, T. Wurdinger and H. E. de Vries (2015). “Overcoming the blood-brain tumor barrier for effective glioblastoma treatment.” Drug Resist Updat **19**: 1-12.

van Woensel, M., N. Wauthoz, R. Rosiere, K. Amighi, V. Mathieu, F. Lefranc, S. W. van Gool and S. de Vleeschouwer (2013). “Formulations for Intranasal Delivery of Pharmacological Agents to Combat Brain Disease: A New Opportunity to Tackle GBM?” Cancers (Basel) **5**(3): 1020-1048.

Vengeliene, V., F. Leonardi-Essmann, S. Perreau-Lenz, P. Gebicke-Haerter, K. Drescher, G. Gross and R. Spanagel (2006). “The dopamine D3 receptor plays an essential role in alcohol-seeking and relapse.” FASEB J **20**(13): 2223-2233.

Vigers, G. P., R. A. Crowther and B. M. Pearse (1986). “Three-dimensional structure of clathrin cages in ice.” EMBO J **5**(3): 529-534.

Vitaliano, F. and G. Vitaliano (2008). “Smart bio-nanoparticle elements “ US Patent 7393924

Vitaliano, G. D., F. Vitaliano, J. D. Rios, P. F. Renshaw and M. H. Teicher (2012). “New clathrin-based nanoplatfoms for magnetic resonance imaging.” PLoS One **7**(5): e35821.

Wang, C. H., S. H. Chiou, C. P. Chou, Y. C. Chen, Y. J. Huang and C. A. Peng (2011). “Photothermolysis of glioblastoma stem-like cells targeted by carbon nanotubes conjugated with CD133 monoclonal antibody.” Nanomedicine **7**(1): 69-79.

Wang, F., X. Jiang and W. Lu (2003). “Profiles of methotrexate in blood and CSF following intranasal and intravenous administration to rats.” Int J Pharm **263**(1-2): 1-7.

Wang, W., W. Sivakumar, S. Torres, N. Jhaveri, V. P. Vaikari, A. Gong, A. Howard, E. B. Golden, S. G. Louie, A. H. Schonthal, F. M. Hofman and T. C. Chen (2015). “Effects of convection-enhanced delivery of bevacizumab on survival of glioma-bearing animals.” Neurosurg Focus **38**(3): E8.

Warren, K., R. Jakacki, B. Widemann, A. Aikin, M. Libucha, R. Packer, G. Vezina, G. Reaman, D. Shaw, M. Krailo, C. Osborne, J. Cehelsky, D. Caldwell, J. Stanwood, S. M. Steinberg and F. M. Balis (2006). "Phase II trial of intravenous lobradimil and carboplatin in childhood brain tumors: a report from the Children's Oncology Group." Cancer Chemother Pharmacol **58**(3): 343-347.

Wattenhofer, M., A. Reymond, V. Falcicola, A. Charollais, D. Caille, C. Borel, R. Lyle, X. Estivill, M. B. Petersen, P. Meda and S. E. Antonarakis (2005). "Different mechanisms preclude mutant CLDN14 proteins from forming tight junctions in vitro." Hum Mutat **25**(6): 543-549.

Weyerbrock, A., S. Walbridge, R. M. Pluta, J. E. Saavedra, L. K. Keefer and E. H. Oldfield (2003). "Selective opening of the blood-tumor barrier by a nitric oxide donor and long-term survival in rats with C6 gliomas." J Neurosurg **99**(4): 728-737.

Wicki, A., D. Witzigmann, V. Balasubramanian and J. Huwyler (2015). "Nanomedicine in cancer therapy: challenges, opportunities, and clinical applications." J Control Release **200**: 138-157.

Winkler, E. A., R. D. Bell and B. V. Zlokovic (2011). "Central nervous system pericytes in health and disease." Nat Neurosci **14**(11): 1398-1405.

Wolak, D. J. and R. G. Thorne (2013). "Diffusion of macromolecules in the brain: implications for drug delivery." Mol Pharm **10**(5): 1492-1504.

Wolburg, H., S. Noell, K. Wolburg-Buchholz, A. Mack and P. Fallier-Becker (2009). "Agrin, aquaporin-4, and astrocyte polarity as an important feature of the blood-brain barrier." Neuroscientist **15**(2): 180-193.

Wolstencroft, E. C., G. Simic, N. thi Man, I. Holt, T. Lam le, P. R. Buckland and G. E. Morris (2007). "Endosomal location of dopamine receptors in neuronal cell cytoplasm." J Mol Histol **38**(4): 333-340.

Wu, G., R. F. Barth, W. Yang, S. Kawabata, L. Zhang and K. Green-Church (2006). "Targeted delivery of methotrexate to epidermal growth factor receptor-positive brain tumors by means of cetuximab (IMC-C225) dendrimer bioconjugates." Mol Cancer Ther **5**(1): 52-59.

Wu, G., W. Yang, R. F. Barth, S. Kawabata, M. Swindall, A. K. Bandyopadhyaya, W. Tjarks, B. Khorsandi, T. E. Blue, A. K. Ferketich, M. Yang, G. A. Christoforidis, T. J. Sferra, P. J. Binns, K. J. Riley, M. J. Ciesielski and R. A. Fenstermaker (2007). "Molecular targeting and treatment of an epidermal growth factor receptor-positive glioma using boronated cetuximab." Clin Cancer Res **13**(4): 1260-1268.

Xiao, C., F. J. Davis, B. C. Chauhan, K. L. Viola, P. N. Lacor, P. T. Velasco, W. L. Klein and N. B. Chauhan (2013). "Brain transit and ameliorative effects of intranasally delivered anti-amyloid-beta oligomer antibody in 5XFAD mice." J Alzheimers Dis **35**(4): 777-788.

Xu, H. L., L. Mao, S. Ye, C. Paisansathan, F. Vetri and D. A. Pelligrino (2008). "Astrocytes are a key conduit for upstream signaling of vasodilation during cerebral cortical neuronal activation in vivo." Am J Physiol Heart Circ Physiol **294**(2): H622-632.

Xu, J., P. J. Kausalya, D. C. Phua, S. M. Ali, Z. Hossain and W. Hunziker (2008). "Early embryonic lethality of mice lacking ZO-2, but Not ZO-3, reveals critical and nonredundant roles for individual zonula occludens proteins in mammalian development." Mol Cell Biol **28**(5): 1669-1678.

Yang, W., R. F. Barth, G. Wu, T. Huo, W. Tjarks, M. Ciesielski, R. A. Fenstermaker, B. D. Ross, C. J. Wikstrand, K. J. Riley and P. J. Binns (2009). "Convection enhanced delivery of boronated EGF as a molecular targeting agent for neutron capture therapy of brain tumors." J Neurooncol **95**(3): 355-365.

Yang, W., G. Wu, R. F. Barth, M. R. Swindall, A. K. Bandyopadhyaya, W. Tjarks, K. Tordoff, M. Moeschberger, T. J. Sferra, P. J. Binns, K. J. Riley, M. J. Ciesielski, R. A. Fenstermaker and C. J. Wikstrand (2008). "Molecular targeting and treatment of composite EGFR and EGFRvIII-positive gliomas using boronated monoclonal antibodies." Clin Cancer Res **14**(3): 883-891.

Yarnitsky, D., Y. Gross, A. Lorian, A. Shalev, I. Lamensdorf, R. Bornstein, S. Shorer, A. Mayevsky, K. P. Patel, N. J. Abbott and W. G. Mayhan (2004). "Blood-brain barrier opened by stimulation of the parasympathetic sphenopalatine ganglion: a new method for macromolecule delivery to the brain." J Neurosurg **101**(2): 303-309.

Yarnitsky, D., Y. Gross, A. Lorian, A. Shalev, S. Shorer, T. Tanaka, K. Ayajiki, M. Fujimiya and T. Okamura (2004). "Increased BBB permeability by parasympathetic sphenopalatine ganglion stimulation in dogs." Brain Res **1018**(2): 236-240.

Ybe, J. A., N. Ruppel, S. Mishra and E. VanHaaften (2003). "Contribution of cysteines to clathrin trimerization domain stability and mapping of light chain binding." Traffic **4**(12): 850-856.

Yoshimura, T., K. Kameyama, S. Maezawa and T. Takagi (1991). "Skeletal structure of clathrin triskelion in solution: experimental and theoretical approaches." Biochemistry **30**(18): 4528-4534.

Yu, Y. J., J. K. Atwal, Y. Zhang, R. K. Tong, K. R. Wildsmith, C. Tan, N. Bien-Ly, M. Hersom, J. A. Maloney, W. J. Meilandt, D. Bumbaca, K. Gadkar, K. Hoyte, W. Luk, Y. Lu, J. A. Ernst, K. Scarce-Levie, J. A. Couch, M. S. Dennis and R. J. Watts (2014).

“Therapeutic bispecific antibodies cross the blood-brain barrier in nonhuman primates.” Sci Transl Med **6**(261): 261ra154.

Yu, Y. J. and R. J. Watts (2013). “Developing therapeutic antibodies for neurodegenerative disease.” Neurotherapeutics **10**(3): 459-472.

Yu, Y. J., Y. Zhang, M. Kenrick, K. Hoyte, W. Luk, Y. Lu, J. Atwal, J. M. Elliott, S. Prabhu, R. J. Watts and M. S. Dennis (2011). “Boosting brain uptake of a therapeutic antibody by reducing its affinity for a transcytosis target.” Sci Transl Med **3**(84): 84ra44.

Zagouri, F., T. N. Sargentanis, R. Bartsch, A. S. Berghoff, D. Chrysikos, E. de Azambuja, M. A. Dimopoulos and M. Preusser (2013). “Intrathecal administration of trastuzumab for the treatment of meningeal carcinomatosis in HER2-positive metastatic breast cancer: a systematic review and pooled analysis.” Breast Cancer Res Treat **139**(1): 13-22.

Zarrilli, R., R. E. Lippoldt, H. Edelhoch and P. K. Nandi (1985). “The stability and transitions of tryptic-digested clathrin.” Arch Biochem Biophys **241**(1): 22-27.

Zhou, Q. H., A. Fu, R. J. Boado, E. K. Hui, J. Z. Lu and W. M. Pardridge (2011). “Receptor-mediated abeta amyloid antibody targeting to Alzheimer’s disease mouse brain.” Mol Pharm **8**(1): 280-285.

Zhu, Y., M. T. Drake and S. Kornfeld (2001). “Adaptor protein 1-dependent clathrin coat assembly on synthetic liposomes and Golgi membranes.” Methods Enzymol **329**: 379-387.

Zhu, Y., L. M. Traub and S. Kornfeld (1999). “High-affinity binding of the AP-1 adaptor complex to trans-golgi network membranes devoid of mannose 6-phosphate receptors.” Mol Biol Cell **10**(3): 537-549.

Zlokovic, B. V., D. S. Skundric, M. B. Segal, M. N. Lipovac, J. B. Mackic and H. Davson (1990). “A saturable mechanism for transport of immunoglobulin G across the blood-brain barrier of the guinea pig.” Exp Neurol **107**(3): 263-270.

Zonta, M., M. C. Angulo, S. Gobbo, B. Rosengarten, K. A. Hossmann, T. Pozzan and G. Carmignoto (2003). “Neuron-to-astrocyte signaling is central to the dynamic control of brain microcirculation.” Nat Neurosci **6**(1): 43-50.

8. BIOGRAPHY

Dr. Vitaliano received her M.D. and M.S. degrees from the Belgrade University School of Medicine. In 1991 she received a prestigious NIH Fogarty Fellowship and came to the United States. From 1994 until 2002 Dr. Vitaliano was leading a multidisciplinary team at VXM Technologies in Boston. She was a PI for an NIH-funded project and developed a first-ever standardized software test to diagnose Attention Deficit Hyperactivity Disorder (ADHD) early in preschool children. Her software was standardized and used in three Boston-area hospitals and in a number of public and private preschools and day care centers. Her team also developed a new type of distributed artificial neural network for medical applications that was based on Arthur Eddington's "structuralist" approach to the acquisition of knowledge, and also Piaget's cognitive theory of development.

Dr. Vitaliano's contributions at VXM (now, ExQor Tech) also lead to the development of a Clathrin-based programmable nanoplatform. She developed clathrin-based intelligent nano-scale biosensors, biomolecular nanorobots, nanolasers, imaging tools, and drug delivery systems and has 4 issued patents in these areas and 6 more patents pending. She was managing different nanotechnology related research projects funded by industry and/or the U.S. Government and VXM's customers include the U.S. Navy, U.S. Air Force, etc. She served as an expert in bio-nanotechnology at the US President's Innovation and Technology Advisory Committee (PITAC, The White House) and for various journals, on NIH review panels, NIDA, NARSAD and DOD conferences.

Dr. Vitaliano completed her residency training in psychiatry at Tufts University in Boston and continued her academic career at Mclean Hospital, Harvard Medical School. She is a board certified psychiatrist and Director of Brian Imaging Nanotechnology Group (BING). Dr. Vitaliano is a principal investigator on NIH and other grants and is developing brain imaging and drug delivery nanotechnologies for neuropsychiatric disorders.

Прилог 1.

Изјава о ауторству

Потписани-а: Гордана Станојевић - Виталиано

Изјављујем

да је докторска дисертација под насловом

Нова нанотехнологија на бази клатрина за пренос великих протеинских молекула у централни нервни систем

- резултат сопственог истраживачког рада,
- да предложена дисертација у целини ни у деловима није била предложена за добијање било које дипломе према студијским програмима других високошколских установа,
- да су резултати коректно наведени и
- да нисам кршио/ла ауторска права и користио интелектуалну својину других лица.

У Београду, 18.12.2015.

Потпис докторанда

Гордана Станојевић-
Виталиано

Прилог 2.

Изјава о истоветности штампане и електронске верзије докторског рада

Име и презиме аутора Гордана Станојевић – Виталиано

Студијски програм: Неуронауке и биоинжењерство

Наслов рада: Нова нанотехнологија на бази клатрина за пренос великих протеинских молекула у централни нервни систем

Ментори: проф. др. Слободан Малобабић и проф. др. Дејан Раковић

Потписани/а: Гордана Станојевић – Виталиано

Изјављујем да је штампана верзија мог докторског рада истоветна електронској верзији коју сам предао/ла за објављивање на порталу **Дигиталног репозиторијума Универзитета у Београду**.

Дозвољавам да се објаве моји лични подаци везани за добијање академског звања доктора наука, као што су име и презиме, година и место рођења и датум одбране рада.

Ови лични подаци могу се објавити на мрежним страницама дигиталне библиотеке, у електронском каталогу и у публикацијама Универзитета у Београду

У Београду, 18.12.2015

Потпис докторанда

*Гордана Станојевић-
Виталиано*

Прилог 3.

Изјава о коришћењу

Овлашћујем Универзитетску библиотеку „Светозар Марковић“ да у Дигитални репозиторијум Универзитета у Београду унесе моју докторску дисертацију под насловом:

Нова нанотехнологија на бази клатрина за пренос великих протеинских молекула у централни нервни систем

која је моје ауторско дело.

Дисертацију са свим прилозима предао/ла сам у електронском формату погодном за трајно архивирање.

Моју докторску дисертацију похрањену у Дигитални репозиторијум Универзитета у Београду могу да користе сви који поштују одредбе садржане у одабраном типу лиценце Креативне заједнице (Creative Commons) за коју сам се одлучио/ла.

1. Ауторство
2. Ауторство - некомерцијално
3. Ауторство – некомерцијално – без прераде
4. Ауторство – некомерцијално – делити под истим условима
5. Ауторство – без прераде
6. Ауторство – делити под истим условима

(Молимо да заокружите само једну од шест понуђених лиценци, кратак опис лиценци дат је на полеђини листа).

Напомена: Ова докторска дисертација подлеже ауторским правима у Америци и не може слободно да се користи.

Потпис докторанда

Ђорѓана Станојевић
Ђукић

У Београду, 18.12.2015.